Heat Metering with Glycol-Water-Mixtures

vorgelegt von
M. Sc.
Sebastian Baack

an der Fakultät V - Verkehrs- und Maschinensysteme
der Technischen Universität Berlin
zur Erlangung des akademischen Grades

Doktor der Ingenieurwissenschaften
-Dr.-Ing.-

genehmigte Dissertation

Promotionsausschuss:

Vorsitzender:	Prof. Dr.-Ing. Henning Jürgen Meyer
1. Gutachter:	Prof. Dr.-Ing. Paul Uwe Thamsen
2. Gutachter:	Prof. Dr.-Ing. Stefan Frank
3. Gutachter:	Dr. rer. nat. Peter Lau

Tag der wissenschaftlichen Aussprache: 27. November 2019

Berlin 2020

meiner Familie gewidmet

Danksagung

Ich möchte mich für die Unterstützung bedanken, die ich während der Realisierung der vorliegenden Arbeit erhielt.

Besonderer Dank gebührt Herr Prof. Dr.-Ing. Paul Uwe Thamsen vom Fachgebiet für Fluidsystemdynamik der Technischen Universität Berlin für die Betreuung und Begutachtung meiner Arbeit. Ebenfalls danken möchte ich Dr. rer. nat. Peter Lau für die unermüdliche Arbeit als Zweitgutachter und Betreuer, die zahlreich geführten Diskussionen sowie hilfreichen Anmerkungen.

Die Arbeit ist im Rahmen meiner Tätigkeit als wissenschaftlicher Mitarbeiter im Fachbereich 7.5 “Wärme und Vakuum” der Physikalisch-Technischen Bundesanstalt in Berlin entstanden. Bei meinen Kollegen, die diese Arbeit mit ihrem Fachwissen, Engagement und tatkräftiger Unterstützung bereicherten, möchte ich mich ebenfalls herzlich bedanken. Bei fachlichen, metrologischen und wissenschaftlichen Fragen seien vor allem den Herren Dr.-Ing Jürgen Rose, Dr.-Ing. Jonas Steinbock, Dr.-Ing. Markus Juling sowie Dr. rer. nat. Thomas Lederer für Rat und Tat gedankt. Für tatkräftige Unterstützung bei anlagentechnischen Problemstellungen sowie der Durchführung von Messungen möchte ich mich vor allem bei den Herren Bastian Peetz, Andreas Wilke, Joshua Leonhardt, Konstantin Richter, Kai Biebrach und Rico Biedermann bedanken. Auch Kollegen anderer Fachbereiche und Arbeitsgruppen der PTB gilt mein Dank, inbesondere für die Hilfsbereitschaft bei der Durchführung von Messungen physikalischer Eigenschaften, der koordinatenmesstechnischen Bestimmung der Kolbendimensionen sowie der Fertigung und Montage des volumetrischen Prüfstands: Herr Dr. Sarge, Herr Dr. Henning Wolf, Herr Dr. Volker Wilkens, Herr Jürgen Hirsch, Herr Axel Kuhn, Herr Helmar Spaeth, Herr Klaus Schwericke und Herr Dirk Trepte.

Im Bekanntenkreis möchte ich mich bei Herrn Humphrey Spoor für zahlreiche Diskussionen und fachliche Ratschläge zum Thema und bei Frau Sarah Schmidt für die sprachliche Korrekturlesung bedanken.

Bei den Mitgliedern des gemeinschaftlichen Forschungsprojektes, dem Verband der deutschen Wasser- und Wärmezählerindustrie e.V. (VDDW) und der Arbeitsgemeinschaft Heiz- und Wasserkostenverteilung e.V. (ARGE Heiwako), in dessen Rahmen diese Arbeit realisiert wurde, möchte ich mich ebenfalls bedanken.

Nicht zuletzt bedanke ich mich natürlich bei meiner Familie für immer währenden moralischen Rückhalt. Insbesondere meiner Frau Jenny und meinem Sohn Jakob danke ich für stete Motivation.

Abstract

Due to its physical properties, glycol-water-mixtures cause typical heat meters to measure with increased deviations. Both the volume flow measurement and the fluid's heat coefficient are affected. For the determination of the exchanged energy, for example in cooling or solar thermal installations, heat meters which are suitable for commonly used glycol-based heat conveying media are necessary. A joint project of the Physikalisch-Technische Bundesanstalt (PTB), the Verband der deutschen Wasser- und Wärmezählerindustrie e.V. (VDDW) and the Arbeitsgemeinschaft Heiz- und Wasserkostenverteilung e.V. (ARGE Heiwako) aims at gathering data and developing procedures to introduce heat meters for glycol-water-mixtures into legal metrology.

In a first step, the heat transfer and flow properties for a selection of 4 glycol-based media are investigated. Traceable investigations of the physical properties density $\rho(T)$, kinematic viscosity $\nu(T)$ and specific heat capacity $c_p(T)$ of the investigated fluids partially show deviations of up to 18 % from the manufacturer's data. Heat coefficients for glycol-based fluids are calculated with an expanded uncertainty of 1.5 % (k=2). Furthermore, preliminary investigations indicate that a review of the stability of the heat conveying medium under conditions of use (degradation) is necessary. After performing accelerated laboratory degradation procedures, heat transfer properties partially change to varying degrees (up to 5 %), depending on the glycol base. As the transferability to field conditions is currently not possible, further measurements with improved measuring instruments and in-field data acquisition is planned to confirm the experiments and further explore the field of degradation.

The second step includes the determination of the specific medium's influence on the flow measurement of heat meters. Therefore, a new volumetric testing facility at PTB's laboratories is designed, built and validated. It has an expanded uncertainty (k=2) between 0.017 % and 0.36 %, based on the flow rate and temperature. Results of five mass-market suitable flowmeter types like ultrasonic and impeller flowmeters partially show maximum deviations that are multiple times bigger than current maximum permitted deviations (-45 % to 30 % for ultrasonic sensors; -8 % to 7 % for impeller flow sensors). However, after applying medium-specific corrections to the sensor, the results improve drastically (± 2 %), indicating that a legal use of those sensors in near future is possible. More sophisticated sensors like Coriolis or Electromagnetic flow sensors measure within a narrow deviation range below ± 1 %.

Further investigations include the evaluation of in-field use of glycol-based media as well as possible challenges and testing procedures for legal metrology purposes. Restrictions may arise due to uncertainties in the specific fluid's composition and stability in the field. Testing and calibration of glycol-applicable sensors with water appears feasible and will be investigated further on.

Zusammenfassung

Die von Wasser abweichenden physikalischen Eigenschaften von Glykol-Wasser-Gemischen bewirken erhöhte Abweichungen bei Wärmemengenzählern. Dabei sind sowohl die Messung des Volumenstroms als auch der für die Wärmemenge maßgebende Wärmekoeffizient betroffen. Eine Vielzahl von Kühl- oder Solarthemie-Anlagen sind für die Abrechnung ausgetauschter Energie auf Sensoren angewiesen, welche für gebräuchliche glykolbasierte Wärmeträger einsetzbar sind. Ein Gemeinschaftsprojekt der Physikalisch-Technischen Bundesanstalt (PTB), dem Verband der deutschen Wasser- und Wärmezählerindustrie e.V. (VDDW) und der Arbeitsgemeinschaft Heiz- und Wasserkostenverteilung e.V. (ARGE Heiwako) hat das Ziel, Grundlagen zu schaffen und Verfahren zu entwickeln, um Wärmemengenzähler für Glykol-Wasser-Gemische in das gesetzliche Messwesen einzuführen.

In einem ersten Schritt werden die Fluideigenschaften von 4 glykolbasierten Medien untersucht. Dabei zeigen die rückgeführten Messungen der Dichte $\rho(T)$, der kinematischen Viskosität $\nu(T)$ und der spezifischen Wärmekapazität $c_p(T)$ teilweise Abweichungen von bis zu 18 % von Herstellerangaben. Aus den gewonnenen Daten werden Wärmekoeffizienten mit einer erweiterten Messunsicherheit von 1,5 % (k=2) für eine Auswahl von 4 Wärmeträgern auf Glykolbasis berechnet. Darüberhinaus wird die Stabilität der Fluide unter Betriebsbedingungen (Alterung) untersucht. Mithilfe von beschleunigten Labortests wird ermittelt, dass sich teilweise Änderung der Wärmeträgereigenschaften um 5 % ergeben. Da die Übertragbarkeit beschleunigter Alterungsversuche im Labor auf reale Bedingungen im Feld derzeit nicht möglich ist, sind weitere Experimente sowie Probenentnahmen aus dem Feld zur Vertiefung des Kenntnisstands zum Thema Alterung geplant.

Der zweite Schritt beinhaltet die Untersuchung des Mediumeinflusses auf die Volumenstrommessung. Dafür wurde ein nach dem Verdränger-Prinzip arbeitetender Prüfstand konstruiert, erbaut und validiert. Dieser hat eine erweiterte Messunsicherheit, welche je nach Temperatur und Durchfluss zwischen 0,017 % und 0,36 % (k=2) liegt. Die Ergebnisse von fünf massenmarkttauglichen Geräten auf Ultraschall- und Flügelradbasis ergeben teilweise Abweichungen, welche weit oberhalb derzeitig zulässiger Fehlergrenzen liegen (-45 % bis 30 % für Ultraschallzähler; -8 % bis 7 % für Flügelradzähler). Nach medienspezifischen Korrekturen zeigen diese Zähler deutlich niedrigere Abweichungen (bis zu ± 2 %), sodass ein gesetzlich geregelter Einsatz dieser Sensoren in naher Zukunft realistisch erscheint. Sensoren nach dem Coriolis- und Elektromagnetischen Prinzip messen den Durchfluss innerhalb von ± 1 %.

Weitere Untersuchungen beinhalten die Einschätzung des Feldeinsatzes von Glykol-Wasser-Gemischen sowie mögliche Herausforderungen und Testmöglichkeitenim im Rahmen des gesetzlichen Messwesens. Einschränkungen sind aufgrund von Unsicherheiten in der Fluidzusammensetzung sowie -stabilität denkbar. Das Testen, Kalibrieren und Prüfen der korrigierten Volumensensoren mit Wasser erscheint möglich, wird jedoch weiter untersucht.

Contents

List of Figures

List of Tables

Nomenclature

A	area in m^2/temperature tolerance class
AA	temperature tolerance class
A_{ideal}	ideal cross-sectional area in m^2
approx.	approximately
ARGE	Arbeitsgemeinschaft Heiz- und Wasserkostenverteilung e.V.
ASTM	American Society for Testing and Materials
α_i	respective angle in °
α_{LM}	thermal expansion of Length Measurement System in K^{-1}
α_P	thermal expansion of piston material in K^{-1}
B	temperature tolerance class
B_i	magnetic flux density in T
β	thermal expansion coefficient in K^{-1}
β_C	thermal expansion coefficient in cylinder in K^{-1}
β_{CV}	thermal expansion coefficient in connecting volume in K^{-1}
C	temperature tolerance class
c	speed of sound in m s^{-1}
CAD	Computer Aided Design
c_i	sensitivity coefficient
CMM	coordinate measuring machine
c_p	specific heat capacity at constant pressure in $J/(kg \cdot K)$
contr.	contribution
CY	cylinder
D	diameter in m
D_E	distance between the electrodes in m
D_{ref}	reference diameter of displacement body in m
D_p	measured Piston diameter in m
$\Delta\varphi$	phase difference in rad
Δt	period of time in s

ΔT	temperature difference in K
$\Delta\rho_C^{if}$	density difference in the container in kg/m³
$\Delta\rho_{CV}^{if}$	density difference in the connecting volume during a measurement in kg/m³
ΔV_C^{if}	volume displaced by the piston in m³
ΔV_{CV}^{if}	change of the connecting volume during a measurement in m³
degr.	degraded
distr.	distribution
DN	nominal diameter of pipe
η	dynamic viscosity in Pa · s
E	electrode
e.g.	for example
EFM	electromagnetic flowmeter
EG	ethane-1,2-diol /ethylene glycol
EMPA	German acronym for "Eidgenössische Materialprüfungs- und Forschungsanstalt" - Swiss Federal Laboratories for Materials Science and Technology
f	frequency in Hz
F	power source
FC	field coil
F_C	coriolis force in N
FVR	fluid viscosity ratio
FVV	German acronym for "Forschungsvereinigung Verbrennungskraftmaschinen" - Research Association for Combustion Engines e.V.
G	planetary gear
GUM	Guide to the Expression of Uncertainty in Measurement
H	enthalpy in J
h	hour
h_f	specific enthalpy in feed in J/kg
h_i	specific enthalpy in J/kg
h_r	specific enthalpy in return in J/kg
HZP	Haushaltszählerprüfstand

K	bulk modulus in Pa
k	heat coefficient in $J/(m^3 \cdot K)$
k_E	device-specific constant
$k=2$	coverage factor of 2; regarding expanded measurement uncertainty
κ	compressibility factor of medium in Pa^{-1}
κ_C	compressibility factor of the medium inside the cylinder in Pa^{-1}
κ_{CV}	compressibility factor of the medium inside the connecting volume in Pa^{-1}
ν	kinematic viscosity in $m^2 \cdot s^{-1}$
l	litre
l/h	litres per hour
L	distance between a transmitter in m
LSC	least square circle
m	meter
M	motor
max.	maximum
m_c	mass in rotating system in kg
$\dot{m}$	mass flow in $kg \cdot s^{-1}$
μm	micrometer
min	minimum
mK	milliKelvin
mm	millimetre
m^2	square meter
m^3	cubic meter
MPa	megapascal
MPE	maximum permissible error
MUT	meter under test
$\mu S/cm$	conductivity
n	rotational speed in $rad \cdot s^{-1}$
n.d.	not determined

p_C^f	final pressure inside the cylinder in Pa
p_C^{fill}	filling pressure in Pa
p_C^i	initial pressure inside the cylinder in Pa
p_{CV}^f	final pressure inside the connecting volume in Pa
p_{CV}^i	initial pressure inside the connecting volume in Pa
$\tilde{p}_{MUT}$	average pressure measurement at the Meter under Test in Pa
Pa	pascal
$\%$	percent
pH	logarithmic scale for acidity or basicity
P_{ideal}	ideal pressure in Pa
PG	propane-1,2-diol /propylene glycol
ppm	parts per million
Pt100	platinum resistance thermometer with nominal resistance of 100 Ohm
Pt500	platinum resistance thermometer with nominal resistance of 500 Ohm
Pt1000	platinum resistance thermometer with nominal resistance of 1000 Ohm
PTB	Physikalisch-Technische Bundesanstalt
ρ	density in $kg \cdot m^{-3}$
ρ_C^f	final density inside the cylinder in $kg \cdot m^{-3}$
ρ_C^i	initial density inside the cylinder in $kg \cdot m^{-3}$
ρ_{CV}^f	final density inside the connecting volume in $kg \cdot m^{-3}$
ρ_{CV}^i	initial density inside the connecting volume in $kg \cdot m^{-3}$
$\tilde{\rho}_{MUT}$	averaged density at the Meter under Test in $kg \cdot m^{-3}$
ρ_{ref}	reference density in $kg \cdot m^{-3}$
Q	heat output in J
$\dot{Q}$	heat flow in $J \cdot s^{-1}$
q_i	lower flow limit in $m^3 \cdot s^{-1}$
q_p	nominal flow in $m^3 \cdot s^{-1}$
q_s	upper flow limit in $m^3 \cdot s^{-1}$
ν_s	specific volume in $m^3 \cdot kg^{-1}$

v_m	mean flow velocity in m · s^{-1}
r	radial position in mm
R	radius in m
Re	Reynolds number
Rr	receiver
RTD	resistance thermometer
r_m	mean radius of impeller blade in m
S	spindle
s_{ref}	distance measurement uncertainty of linear scale in m
s_A	uncertainty of angle between linear scale and displacement body in m
s_{ideal}	ideal travelled distance in m
s_{LM}	uncertainty influences on linear scale in m
s_{meas}	measured value without angle correction in m
s_0	measured value in m
s_R	uncertainty caused by resolution of linear scale in m
spec.	specific
St. Dev.	standard deviation
St. U.	standard uncertainty
Tr	transmitter
T_C^{fill}	filling temperature in K
T_{ideal}	ideal temperature in K
T_{ref_LM}	ideal temperature in K
T_{ref_P}	ideal temperature in K
t_-	propagation time extension in s
t_+	propagation time shortening in s
Θ	temperature in °C
Θ_f	temperature in feed in °C
Θ_r	temperature in return in °C
ϑ_i	temperature readout in °C

ϑ_C^f	final temperature in cylinder in °C
ϑ_C^i	initial temperature in cylinder in °C
ϑ_{CV}^f	final temperature in connecting volume in °C
ϑ_{CV}^i	initial temperature in connecting volume in °C
ϑ_m	temperature measured in °C
$\tilde{\vartheta}_{MUT}$	averaged temperature at the Meter under Test in °C
$\sum t_i$	transit time sum in °C
U	voltage in °C
$U_{\vartheta A}$	uncertainty due to ambient temperature
$U_{\vartheta w}$	uncertainty caused by linearisation errors of the control unit
U_C	uncertainty of the calibration
U_F	uncertainty associated with heat conduction errors
U_{LT}	uncertainty due to long term behaviour of the sensor
$u(x_i)$	input uncertainty
u_m	circumferential speed in rad · s^{-1}
U_{Th}	uncertainty caused by thermoelectric voltage
VDDW	Verband der deutschen Wasser- und Wärmezählerindustrie e.V.
v_F	velocity inside Coriolis sensor in m · s^{-1}
VGP	Volumetrischer Glykol-Prüfstand
Vol.	volume
v_m	mean flow velocity in m · s^{-1}
$\dot{V}$	volume flow in m^3 · s^{-1}
V_C	volume inside the cylinder in m^3
V_C^f	final volume inside the cylinder in m^3
V_C^i	initial volume inside the cylinder in m^3
V_{CV}	connecting volume in m^3
V_{CV}^f	final volume inside the connecting volume in m^3
V_{CV}^i	initial volume inside the connecting volume in m^3
V_{ideal}	ideal displaced volume in m^3

V_{MUT}	volume that passed the meter under test in m^3
V_{MUT}	volume that passed the meter under test in m^3
V_G^{fill}	gas volume at filling pressure in m^3
V_G^{op}	gas volume at initial operating pressure in m^3
V_{ref}	reference volume in m^3
w	local flow velocity in $m \cdot s^{-1}$
w_{vol}	volumetric flow velocity in $m \cdot s^{-1}$
x	position in m
X_A	distance between length measurement with and without angle error in m
X_i	input quantity
x_i	input estimate
Y	measurand
y	estimate of measurand

1. Introduction

Due to its favourable physical properties, water is the preferred heat conveying medium in various technical applications. However, the use of media other than water is necessary if, for example in the case of solar thermal energy or in cooling circuits, application temperatures below the freezing point of water occur. Common antifreeze solutions are water-glycol mixtures based on propane-1,2-diol or ethane-1,2-diol (also known as propylene glycol, PG and ethylene glycol, EG). Their flow and heat transfer properties, which differ from water, have a direct influence on the behaviour of heat metering devices, manifesting in the flow measuring sensor as well as the calculation unit. Thus, thermal energy measurements with mixes of water and glycol are currently not subject to legal verification which leads to the state that they are currently non-approvable. Meters measuring these fluids are therefore not type approved. This leads to the situation, that either the provider and consumer negotiate with a handshake, knowing that the error of heat metering increases when glycol-water-mixtures are in use, or the measurement takes place in a water cycle. The losses due to the heat exchanger are then economically shared between provider and consumer [1]. As heat generation starts to shift towards renewable sources, the number of systems using water-glycol mixtures like solar plants, geothermal plants or heat pumps increases. Improved volume flow sensor technology can help to raise the efficiency of those systems and ensure the fair determination between consumer and provider according to legal standardisation.

Investigations on impeller flowmeters with multiple EG-water mixtures showed that measurement deviations are increasing with higher glycol content. Ranges of increased relative deviations are shifting to higher flow rates [2]. Since the largest deviations generally occur in the minimum flow range as well as in the transition region between laminar and turbulent flow, the shifting of the error curve into regions of higher flow rates is critical. Over the years, new heat meters have been developed and refined to meet the increased requirements in the transition area between laminar and turbulent flow. Comprehensive measurements by March compared flowmeters based on different measuring principles. Some impeller meters as well as a magnetic-inductive flow sensor were found to be suitable whereas turbine meters and ultrasonic flowmeters proved unsuitable [3]. March's investigations of calculating units showed relative measurement deviations regarding thermal energy of up to 20 % [4]. However, the same calculating units showed mainly good results after correcting relevant parameters [4].

Adunka [5] and Spoor [6] calculated heat coefficients for selected glycol compounds based on manufacturer's data on density and specific heat capacity. Depending on the quality of the manufacturer's specifications, the uncertainty of the calculated heat coefficient varies. As product specifications generally do not provide information either on the measurement uncertainty of data or the source, heat coefficients and the resulting calculation of thermal energy based on manufacturer data can be considered critically.

A problem which was not taken into account within the framework of the above-mentioned research activities is the degradation of the glycol-water-mixture under thermal load, as observed practically in solar thermal systems. At temperatures above the limit of the antifreeze fluids, chemical-physical changes of the fluid occur, which can lead to flocculation or even clumping of pipes or fittings [7]. If the flow or heat transfer properties change under these conditions, it has a direct influence on the measurement technique which must be investigated.

The aforementioned aspects of glycol-induced influences on volume flow sensors and thermal energy calculations affect heat metering directly. To minimize uncertainty of heat metering sensors and subsequently allow its legal use, emphasis must be put on investigations regarding these aspects.

1.1 Objective

This work was realised within a joint project of the Physikalisch-Technische Bundesanstalt (PTB), the Verband der deutschen Wasser- und Wärmezählerindustrie e.V. (VDDW) and the Arbeitsgemeinschaft Heiz- und Wasserkostenverteilung e.V. (ARGE Heiwako). The basic objective of this work is the collection of data and the development of procedures to officially allow the use of heat meters with glycol-water-mixtures for consumption calculations according to recognized rules of technology.

This results in two essential components of the investigations:

1. Determination of the necessary heat coefficients and the physical properties of selected heat conveying media as the basis for further investigations. In addition, the stability of these properties should include the case of aging.
2. Determination of the effects caused by investigated media on q_p 1.5 volume measurement sensors based on measurements in a specially designed test rig at the PTB.

1.2 Structure

Following chapter 2 deals with fundamentals regarding heat metering as well as glycol-water-mixtures, their decisive properties and the application-related conditions they are exposed to. In chapter 3, results of thermophysical property investigations as well as effects of degradation are presented. Chapter 4 is about the volumetric test rig including its features and its measurement uncertainty budget. In chapter 5, results of volume flow measurements are shown. Chapter 6 contains the author's view on perspectives and restrictions of heat metering with glycol-water-mixtures while chapter 7 summarises the results of this work and gives an outlook of possible future steps.

2. Fundamentals

This chapter deals with fundamentals concerning heat metering including measurements of volume flow, temperature difference and property-based enthalpy change calculations. Furthermore, information regarding the measuring fluid glycol-water-mixture and the conditions it is exposed to in certain applications are presented. At last, the stability of glycols as well as methods to determine it are considered.

2.1 Measuring Thermal Energy

Heat metering is of great importance for technical, economic and environmental reasons. On the one hand, correctly measured data increases the efficiency of heat supply systems (and thus reduce their fuel consumption). On the other hand, it ensures a fair determination and distribution of heating costs between provider and consumer.

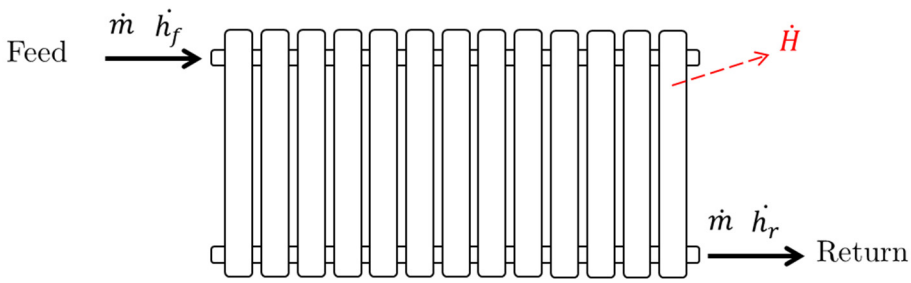

Figure 2.1: Principle of measuring thermal energy of a heating system

The principle of measuring thermal energy can be described by using the example of the above shown stationary heating system. During a period of time Δt, a mass flow $\dot{m}$ of a heat conveying medium enters the meter through the feed and an equal mass flow leaves it through the return. As the heat Q is submitted by the heater to the surrounding air, the specific enthalpy h_i of the medium decreases between feed and return as it cools down. The measurement of thermal energy which is fed to a consumer is based on the enthalpy difference. Thus, the specific enthalpy of the heat medium in feed h_f and return h_r are compared.

$$Q = \int_{t_0}^{t_1} \dot{m} \cdot \Delta h \cdot dt \tag{1}$$

Since the measurement of the enthalpy change is not directly possible, the relation of enthalpy and specific heat capacity at constant pressure $c_p(\Theta)$ for incompressible fluids is used:

$$\Delta h = c_p(\Theta) \cdot (\Theta_f - \Theta_r). \tag{2}$$

As the volume flow is easier to measure compared to mass flow, the volume flow $\dot{V}$ and the flow and return temperatures Θ_f and Θ_r are measured. The heat output Q is finally calculated using the pressure- and temperature-dependent heat coefficient k, which is a function of the specific heat capacity at constant pressure $c_p(\Theta)$ and the density $\rho(\Theta)$ of the heat conveying

medium for feed and return. Thus, following technical working equation can be given for a heat meter [8]:

$$Q = k(p, \Theta_f, \Theta_r) \cdot (\Theta_f - \Theta_r) \cdot V \tag{3}$$

Accordingly, a heat meter basically consists of three functional groups responsible for:

1. Temperature Measurement (in feed and return)
2. Volume Flow Measurement
3. Measuring Change in Enthalpy,

which could be subject to medium-related influences. A brief introduction of those functional groups and the respective glycol-induced impacts is given in following chapters.

2.1.1 Temperature Measurement

To determine the temperature difference between feed and return, industrial platinum resistance thermometers and measuring resistors are widely used. Based on the temperature dependence of the electrical resistance of platinum, the temperature is determined by inserting the sensor set into the flow of the feed and the return flow. The platinum resistance thermometers are classified into tolerance classes (AA, A, B, C) specifying allowed temperature tolerance values and temperature ranges of validity [9]. For heat meters, temperature sensors of at least tolerance class B are recommended [10]. Typical nominal resistances for industrial use are Pt100, Pt500 and Pt1000, a nominal resistance of 100 Ohm at a temperature of 0 °C has the designation Pt100. [11]

Regarding glycol-water-mixtures, the thermophysical properties, which deviate from water and probably have an impact on temperature sensors, should be considered. Nau and Leitgen have addressed the problem identifying thermal conductivity errors during their investigations, which can have a negative effect on the determination of heat quantity, especially at low temperature differences between the supply and the return flow. While a maximum permissible error of 2 % is allowed for ΔT=3 K [10], the isolated influence of thermal conductivity errors of glycol-water-mixtures cause deviations of up to 0.53 % at ΔT=3 K compared to water [12]. Further influences can be associated with the response time of temperature sensors [13]. However, since the temperatures are measured in feed and return flow to determine the temperature difference, those thermal conductivity and timing deviations occur at both installation positions. Thus, the effect glycol-based fluids have on the measurement of temperature differences is supposed to have a minor impact on heat metering.

2.1.2 Volume Flow Measurement

The volume sensor determines the flow rate of the heat carrier. It can be based on a series of measurement principles resulting in a vast variety of differently sophisticated sensor types which are able to measure the flow rate of a likewise vast variety of media such as water, fuel, gas, multiphase substances, solids or even cryogenics like liquid helium [14]. Conventional

methods are, for example, direct volume sensors such as the oval wheel meter, indirect volume sensors such as the impeller flowmeter or sensors which do not require any moving parts such as the ultrasonic or electromagnetic flowmeter.

Based on the dimensions of the solar or cooling system, a sensor has to be chosen, which on the one hand delivers reliable measurements and on the other hand is economically reasonable. According to [15] and [16], the larger the solar system's capacity, the smaller the investment costs for volume flow sensors compared to costs for the whole system. For smaller scale applications with glycol-based heat carrier fluids such as household solar thermal energy systems, sensors which are comparatively inexpensive while having a wide measuring range are preferred for economic reasons. This applies particularly to the impeller flowmeters in single and multi-jet design as well as ultrasonic meters. This work mainly focusses on those two volume sensor types (size: DN 15) and their capabilities of dealing with varying fluids.

Bigger scale industrial or scientific applications may require more advanced (and usually more expensive) sensor types like electromagnetic flowmeters or Coriolis flowmeters to gain supposedly more reliable results. Thus, those flow sensor types will be included, too.

2.1.2.1 Impeller Flowmeter

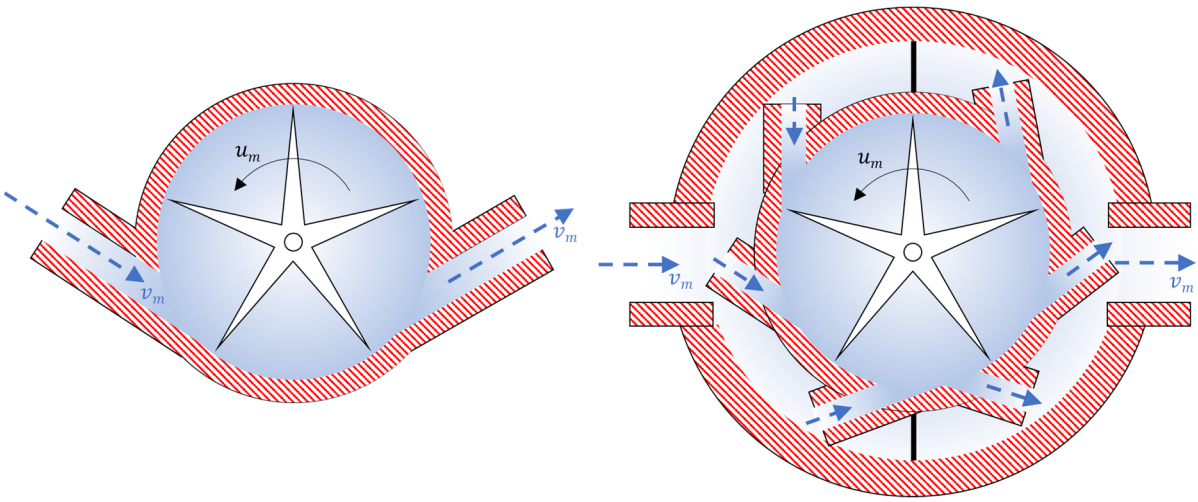

Figure 2.2: Principle sketch of impeller flowmeter types

The impeller flowmeter in single-jet design (cf. Figure 2.2, left) is probably the simplest design of a volume sensor. The fluid flows through an inflow channel tangentially onto the impeller, drives the latter, and leaves the measuring section through an outflow channel. The circumferential speed u_m of the impeller, which is read out via impulses or a counter, represents a characteristic mean flow velocity v_m of the fluid according to [17]:

$$v_m = u_m \cdot \cot \alpha \tag{4}$$

with the setting angle of the blade α. The circumferential speed u_m can be written as:

$$u_m = 2 \cdot \pi \cdot n \cdot r_m \tag{5}$$

with n as the rotational speed and r_m as the mean radius of the blade.

$$\dot{V} = (2 \cdot \pi \cdot r_m \cdot A \cdot \cot \alpha) \cdot n \tag{6}$$

The term in parentheses including the cross-section area A states, that for a simplified, frictionless assumption the flow rate is proportional to the rotational speed [17]. However, realistic assumptions lead to a correction factor, which includes dependencies of viscosity, density and flow velocity as well as an instrument constant. This factor must be investigated through volumetric calibration due to the measuring section's complex flow conditions [17]. The relationship between flow rate and rotational speed can be adjusted by baffle ribs and bypass throttling [18] or by adjustments of the inflow channel [19] or the impeller blades.

This type of sensor is particularly sensitive to disturbances in the inlet and outlet flow of the sensor as the flow profile of the tube flow almost corresponds to the flow profile of the inflow channel and accordingly has a direct influence on the inflow of the impeller [20].

Multi-jet impeller meters, on the other hand, consist of several inlet channels, which lead the flow on the impeller at several points making it less sensitive to bearing friction and flow disturbances. Though the improved bearing friction behaviour is accompanied by higher pressure losses and a worsened starting behaviour [11]. Corresponding to the single-jet design, the aforementioned adjustments to the multi-jet sensor lead to similar results.

Typical applications of turbine-type flowmeters are domestic water supply systems. However, other fluids like natural gas, diesel, fuels and heating oil are commonly used measuring fluids, too. Prior investigations with impeller or turbine flowmeters in use with glycol [3] or oil [21] stated that error curves are highly dependent on the fluids flow velocity, viscosity and density.

2.1.2.2 Ultrasonic Flowmeter

Typical ultrasonic flowmeters are usually either based on the principle of *transit time difference* (cf. Figure 2.3) or *phase difference* (cf. Figure 2.4). If a transmitter Tr sends an acoustic wave through a moving fluid, the propagation time of the sound is either extended (t_-; if the sound has been sent against the direction of flow) or shortened (t_+; as the sound propagates with the direction of flow, depending on the direction of the fluid). If a sound wave is emitted (or reflected) in and/or against the direction of the flow, the average flow velocity v_m can be deduced from the *transit time difference* Δt, the transit time sum $\sum t_i$ and knowledge of the distance L between a transmitter Tr and a receiver Rr.

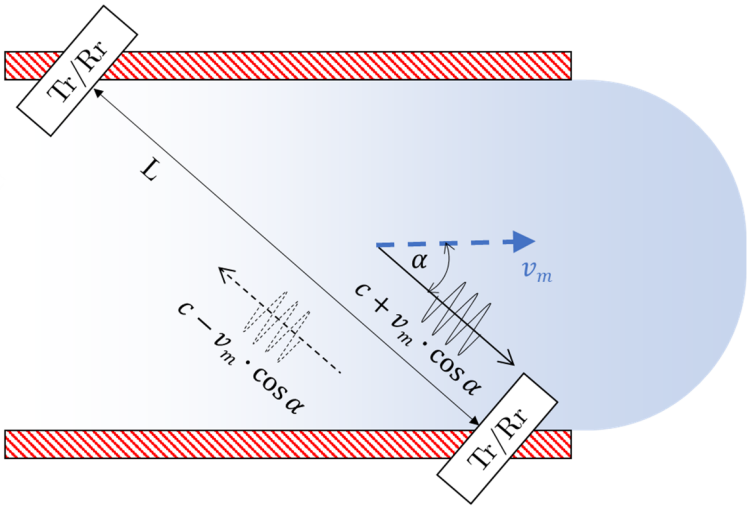

Figure 2.3: Transit time difference principle

$$t_+ = \frac{L}{c + v_m \cdot \cos\alpha} \tag{7}$$

$$t_- = \frac{L}{c - v_m \cdot \cos\alpha} \tag{8}$$

The difference $\Delta t = t_- - t_+$ and sum $\sum t_i = t_- + t_+$ can be calculated [17] to:

$$v_m = \frac{\Delta t}{(\sum t_i)^2} \cdot \frac{2L}{\cos\alpha}. \tag{9}$$

This principle allows the flow velocity to be approximatively calculated without the knowledge of the current speed of sound c of the measured medium, making it interesting for media where c is unknown. Apart from that, the speed of sound c can be obtained by summing up the transit times resulting in following formula:

$$c = \frac{2L}{\sum t_i} \tag{10}$$

As the speed of sound c is generally very high compared to the mean flow velocity v_m (e.g. c~1480 m/s in water, v_m ~1-10 m/s), limitations occur at low flow velocities and short distances between the transducers as time difference measurements have a corresponding growing influence.

Another way of measuring flow velocity is based on *phase difference* measuring. If a sound wave is transmitted through a pipe, its wavelength changes depending on the flow direction of the medium passed. If two ultrasound pulses are transmitted (in downstream direction and upstream direction), the downstream wavelength is elongated while the upstream wavelength is shortened resulting in a phase shift between both wavelengths. A phase detector detects the phase difference $\Delta\varphi$ which is then used to determine the flow velocity of the passing fluid for a frequency f and a distance $L \cdot \cos\alpha$ [17].

$$v_m = \frac{\Delta\varphi \cdot c^2}{4 \cdot \pi \cdot f \cdot \cos\alpha \cdot L} \tag{11}$$

This method is highly dependent on the speed of sound c, which weighs in to the power of two. Thus, results must be continually corrected, as c is highly temperature-dependent.

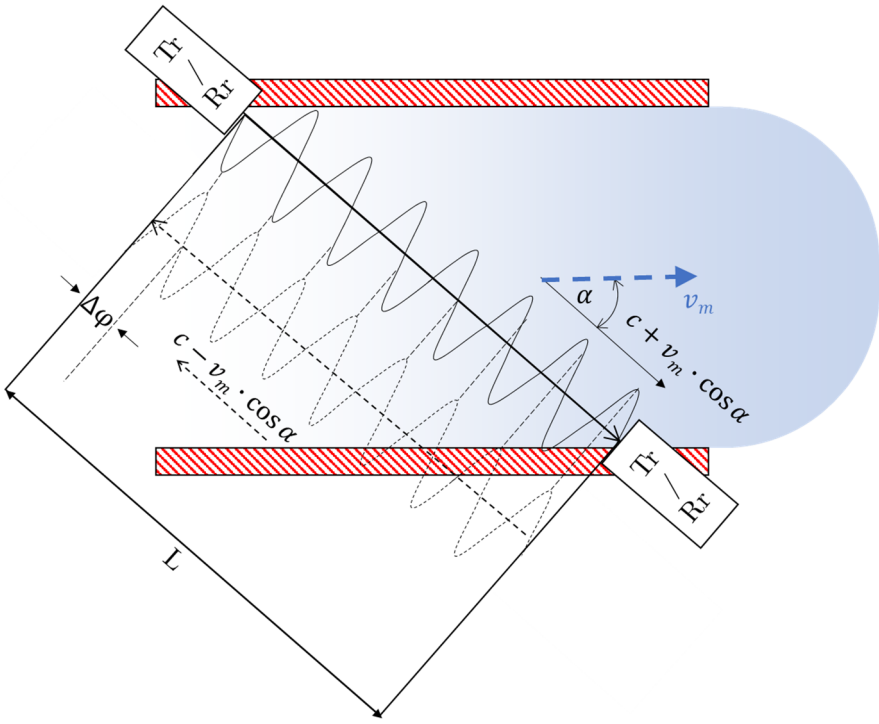

Figure 2.4: Phase difference principle

As this static principle doesn't require moving parts, ultrasonic flowmeters interfere less with the tube flow resulting in modest pressure losses and high reliability, but are strongly dependent on the flow profile, especially in single beam design [20]. Due to upstream fittings like valves, bends and junctions, the flow conditions can strongly differ from the fully developed turbulent profile as secondary, swirl or vortex flow develops [20]. Gas cavities can affect performance [11] and transducer pockets can cause systematic influences on the velocity measurements [22]. More expensive multi-beam designs, which average velocity along several paths, are subsequently less sensitive to the flow profile [23].

As mentioned above, prior investigations [3] concluded that ultrasonic flowmeters (calibrated for water) turned out to be unsuitable for measuring glycol-water-mixtures due to the change in physical properties which led to increased deviations. However, recent developments in sensor technology led to sensors which either apply correction factors for a special glycol-based fluid [24] or sensors which can deduce fluid partial concentrations of several glycols based on sound speed and temperature measurements (in limited temperature intervals of already known mixtures)[25]. Sensor manufacturers declare increased maximum deviations in comparison with water, for example $\pm$ 10 % [26] and $\pm$ 6 % [27]. However, the corresponding manufacturer's data of the fluids may have to be considered critical as partly large deviations between manufacturer's data and traceable measurements occurred [28]. Nevertheless, the innovation afford behind those systems can be highlighted positively.

2.1.2.3 Electromagnetic Flowmeter

For conductive fluids, electromagnetic flowmeters (EFM) can be applied. This type of sensor is based on the principle of electromagnetic induction. A magnetic field of (idealised) magnetic flux density B_i is generated throughout the entire tube cross section by a field coil FC (cf. Figure 2.5). Orthogonal to the magnetic field, electrodes E are placed in an insulated tube to measure the voltage. Without flow (1.) the electrically charged particles of the conductive fluid are distributed uniformly and disorderly inside the tube cross-section; no voltage is measured between the electrodes.

At flow state (2.), the conductive fluid is moved causing the magnetic field to exert the Lorentz force on the charged particles. As the positive particles are separating from the negative particles; an induced voltage can be measured. The measured voltage U is directly proportional to the mean flow velocity v of the medium to be measured; the higher the flow velocity v_m, the higher the voltage U between the two electrodes. Following idealised equation can be used, where D_E is the distance between the electrodes and k is a device-specific constant $0.9 \leq k \leq 1.0$, which includes imperfections in the magnetic field and the flow profile inside the sensor [17].

$$\Delta U = k \cdot B_i \cdot D_E \cdot v_m \tag{12}$$

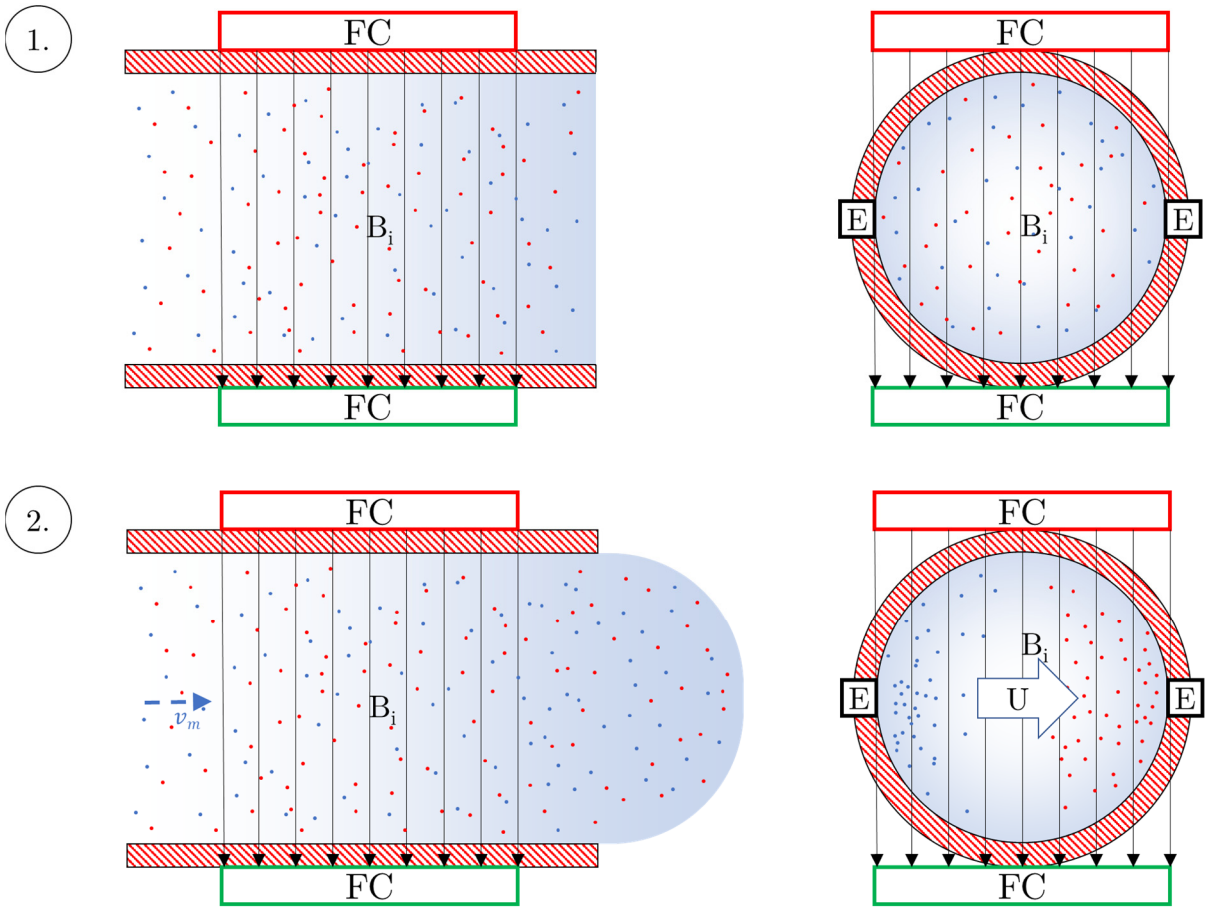

Figure 2.5: Electromagnetic flowmeter principle

More precise equations for EFMs include weighing functions as described in [29] and [30].

Obviously, the electromagnetic flowmeter requires conductive fluids, e.g. >5 µS/cm (depending on device) or >200 µS/cm for testing according to [31]. While fluid pressure, temperature and viscosity play a minor role for most purposes [32], those conditions can have an impact on more challenging applications. Electromagnetic flowmeters are, to a certain amount, dependent on upstream flow conditions [33], density changes due to pressurised gas amounts inside the measuring fluid water [34] and temperature influences [34]. Nevertheless, due to its favourable flow measuring properties, the electromagnetic flowmeter is used in a variety of sophisticated applications including intercomparison measurements [33], as master meters [35] and in glycol-based process analytics [36].

Compared to the measuring principles that have been introduced before, this type of sensor is less dependent on fluid properties and therefore supposed to measure usually applied glycol-water-mixtures regardless of their composition. As this type of sensor can be associated with higher investment costs, its use may be limited to larger scale systems.

2.1.2.4 Coriolis Flowmeter

This type of sensor makes use of a force that is experienced by a mass m_c which moves at a velocity v_F in a rotating system driven by an angular velocity ω, namely Coriolis force F_C.

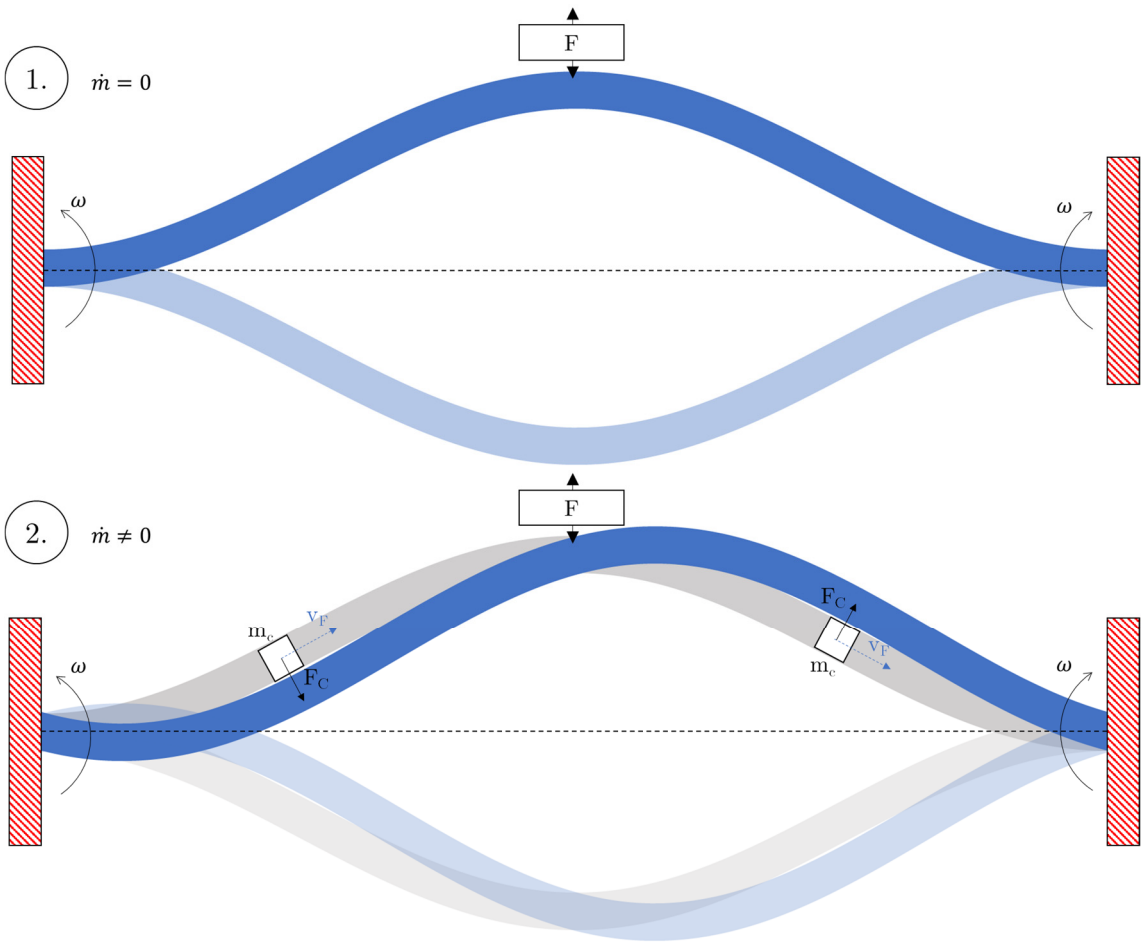

Figure 2.6: Coriolis flowmeter principle

The flowmeter works according to Figure 2.6. A power source F (e.g. an electromagnet) periodically oscillates a pipe section which is fixed at both ends. Ideally, the tube section and the medium inside is induced according to its natural frequency. Without flow (1.), the motion sensors near the flow inlet and outlet detect an even and symmetrical oscillation.

In the case of flow (2.), the medium's F_C causes the inlet part of the tube to lag the vibration and the outlet part of the tube to lead the vibration. Thus, motion sensors will measure a phase shift $\Delta\varphi$ between the inlet and outlet position.

$$\Delta\varphi = k \cdot \dot{m} \tag{13}$$

The phase shift $\Delta\varphi$ is proportional to the mass flow $\dot{m}$ and a device-specific constant k which includes the measuring tube section's spring stiffness, the length as well as the distance between the motion detectors [17]. A further feature is the use of the frequency to measure the density of the measuring fluid; the denser the fluid, the lower the frequency.

As Coriolis flowmeters measure the whole mass of a fluid flowing through the measuring section, they are relatively insensitive to fluid properties and nearly independent on the flow profile [32]. Coriolis flowmeters have been successfully used as a scientific transfer standard between water and mineral oils [37] underlining their capability of measuring different media with minimal measuring uncertainty.

More demanding tasks with actively disturbed flow profiles, however, lead to deviations [33]. Further disadvantages of the Coriolis flowmeter are the sensitivity to external vibrations (pumps, motors), which could affect measuring signals as well as debris inside the measuring section, which could change the measuring section's vibration behaviour.

To meter the heat supply e.g. of a household solar system, this sensor type is regarded to be an uneconomic investment to justify its strengths measuring various media in severe conditions [14]. However, larger scale applications as well as scientific institutions performing calibrations may be more suitable for devices of that quality. Consequently, a Coriolis flowmeter is used for the test rig described in chapter 4 performing numerous tasks.

2.1.3 Measuring Change in Enthalpy

Regardless of the quality of volume flow measurements, the calculation of the measured medium's enthalpy change has a direct influence on the determination of heat. Therefore, the quality as well as the reliability of the decisive heat coefficient k plays an important role.

As aforementioned, the heat coefficient k is calculated using thermodynamic properties of the desired heat conveying medium. Water as a widely used technical medium has been subject to numerous scientific investigations. Thus, its properties can be determined using various sources [38], [39]. For scientific applications, the IAPWS-95 ("IAPWS Formulation 1995 for the Thermodynamic Properties of Ordinary Water Substance for General and Scientific Use") is generally preferred. However, since industry applications often require "computation-friendly"

calculations, a simplified method has been formulated known as the IAPWS-IF97 ("IAPWS Industrial Formulation 1997 for the Thermodynamic Properties of Water and Steam"). The differences between those two formulations are small for most purposes as calculated values (according to IAPWS-IF97) of the specific volume ν_s and specific isobar heat capacity c_p in a pressure range between 0.1 MPa and 1.0 MPa and a temperature range between 0 °C and 100 °C are supposed to have an uncertainty of ± 0.003 % (ν) and ±0.2 % (c_p), respectively [40]. Standardisation refers to the IAPWS-IF97 to calculate heat coefficients for water based on equations of state [10] with:

$$k(p, \theta_f, \theta_r) = \frac{1}{v_s} \cdot \frac{h_f - h_r}{\theta_f - \theta_r}, \tag{14}$$

where $k(p, \theta_f, \theta_r)$ is the pressure and temperature dependent heat coefficient, $\nu_s(\Theta)$ is the specific volume and h_i and Θ_i are the respective specific enthalpy and temperature values for feed and return flow.

For numerous coolants based on glycol-water-mixtures with varying inhibitors and ratios, a more simplistic way of determining k must be applied since the data pool of relevant physical properties is rather small. The change in enthalpy for approximately incompressible media like water or glycol can be described using the specific heat capacity at constant pressure $c_p(\Theta)$ and the temperature change between inlet and outlet. The heat coefficient is determined from the average specific heat capacity $c_p(\Theta)$ and density $\rho(\Theta)$ of the heat conveying fluid [41] for feed flow k_f and return flow k_r. Thus, those physical properties, or more precisely the differences of the physical properties between a specific glycol-water mixture and water play an important role for enthalpy change calculations.

$$k_f = \frac{\rho(\theta_f)}{\Delta\Theta} \cdot \int_{\theta_f}^{\theta_r} c_p(\Theta) d\Theta \tag{15}$$

$$k_r = \frac{\rho(\theta_r)}{\Delta\Theta} \cdot \int_{\theta_f}^{\theta_r} c_p(\Theta) d\Theta \tag{16}$$

Concerning physical properties of typical glycols and their influence on heat metering, cf. Chapter 2.3. Concerning the applicability of the simplified way to calculate the heat coefficient k, cf. Chapter 3.4.

2.2 Applications of Glycol-based Heat Conveying Fluids

In this chapter, fields of application and the resulting typical application conditions for glycol-water-mixtures are presented. This chapter mainly focusses on small scale solar and cooling applications, but also shows examples from other fields of use.

2.2.1 Solar Heating

The term "solar thermal energy" describes the conversion of solar radiation into heat as applied in a wide variety of solar thermal systems. In principle, all solar thermal systems are based on absorbing a part of the solar radiation and converting it into heat through a collector. This heat is transported to a heat conveying medium which makes the heat energy usable for the final consumer.

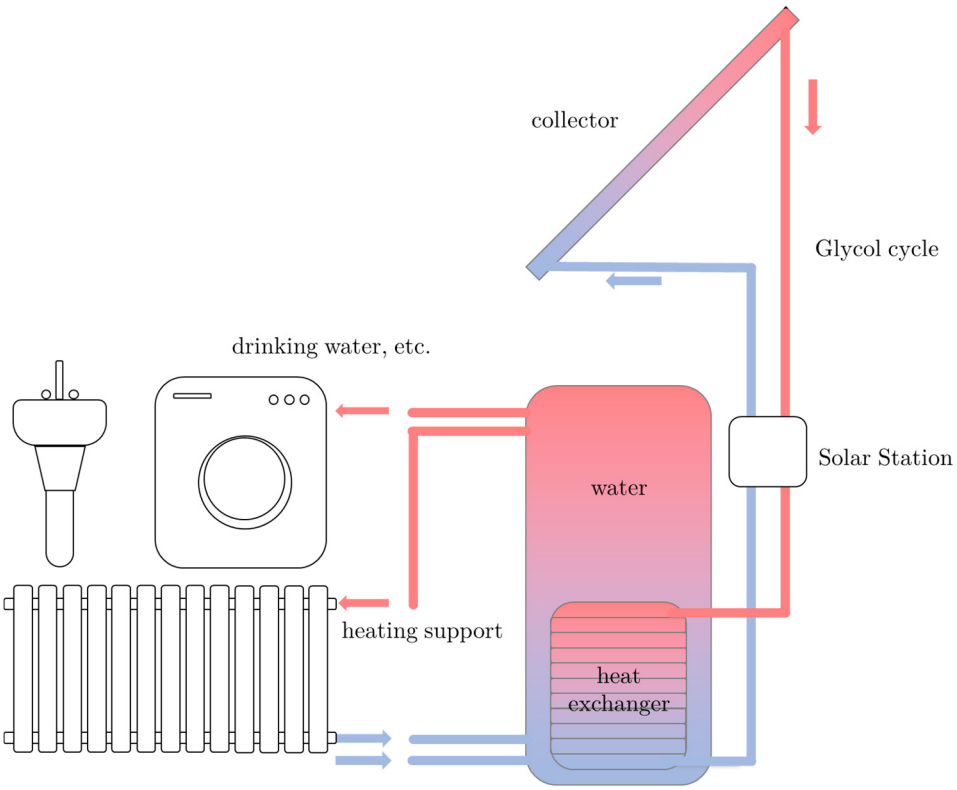

Figure 2.7: solar system scheme

Depending on the application requirements, water, air, oil, salts or water-glycol mixtures are used as heat conveying media. In flat-plate collectors and vacuum tube collectors as the most commonly used solar thermal systems in Central Europe, glycol-water-mixtures are applied as heat conveying media. Those mixtures resist temperatures below 0 °C and protect the system against corrosion. Using a flat collector system (cf. Figure 2.7), typical operating conditions are presented. A flat collector (top) is connected to the supply pipe (blue) and return pipe (red). The cold medium is pumped into the collector where it is heated by solar radiation. From the collector, it is conveyed to the storage reservoir in which it transfers parts of its heat to the water via a heat exchanger. The cooled medium then continues its path back to the collector, while the water can be used, for example, for heating and domestic appliances or for fresh water supply. Operating temperatures in flat plate collectors of around 80 °C to 90 °C are common. In vacuum tube collectors, considerably higher temperatures occur.

Two common solar system concepts for one- or two-family houses are solar systems for exclusive heating of drinking water and combined solar systems for the heating of drinking water as well as heating support. For the dimensioning of both plant concepts, there are rules of thumb which are briefly presented in two examples:

- For a system for the exclusive use of drinking water, the collector area is estimated to be 1.0 - 1.5 m² per person. For a presumed 4-person household, a collector area of 6 m² can be selected accordingly. The storage volume can be calculated according to [42] with 100 l per person which leads to a storage volume of 400 l.
- For a combi-installation for drinking water heating and heating support, neclecting important structural features like the roof direction and inclination, the cable management and the insulation of the house are neglected, a collector area of 0.8 - 1.0 m² is recommended for 10 m² of living space. For an average single-family house with 150 m² of floor-heated living space, a collector area of 15 m² can be installed [42]. There are different concepts for storage, but the most common is a combi storage tank. Its volume is determined according to the rule "50-100 l per m² collector area" [42]. For a collector with a surface area of 15 m², a tank of 1000 l volume can be used.

Three different operating states are differentiated for domestic solar systems. The "high-flow" principle describes a volume flow of 30 l/h - 50 l/h or more per m² collector area. [43] The rapid flow of the heat conveying medium results in a low temperature spread of 10 - 15 K between collector and solar storage. The low temperature level of the collector is advantageous as it increases the collector efficiency due to lower heat losses. In addition, the turbulent pipe flow allows an improved heat transport inside the heat exchanger. However, a higher power consumption of the circulating pump and the resulting higher operating costs and the slower heating of the storage tank are disadvantageous.

In contrast, "low-flow" systems operate at a flow rate of 10 - 15 l/h per m² of collector area. The heat carrier lasts longer in the collector and experiences a faster rise in temperature, just like the collector itself [44]. Accordingly, the temperature spread between collector and solar storage is increased, which means that heating of the storage tank is accelerated. As a result, hot water can be removed more quickly. Another advantage is lower operating costs due to low pump speeds. Disadvantages are higher heat losses occurring at high collector temperatures and losses during heat transport at the heat exchanger due to laminar flow [45].

"Matched-flow" systems adapt the volume flow variably, depending on the solar irradiation, and are consequently more flexible with regard to changing weather conditions as they combine advantages of both the high and low-flow systems [46]. However, the system is associated with higher acquisition costs for more complex control technology or an additional solar pump. That's why it is less common than the first two systems.

The theoretical flow range can be specified as follows by means of example systems and the operating states presented.

Table 2.1: Examples of possible flow ranges depending on the solar system's dimension and operating conditions

	High Flow	Low Flow	Matched Flow
6 m^2 collector surface area for drinking water heating	180 - 300+ l/h	60 - 90 l/h	60 - 300+ l/h
15 m^2 collector surface area for drinking water heating and heating	450 - 750+ l/h	150 - 225+ l/h	150 - 750+ l/h

Thus, for usual flat-plate installations, volume flow below 60 l/h should not occur. In fact, flow rates below 100 l/h are assumed to be very uncommon as pumps for solar systems usually have operating points at higher flow rates (depending on delivery pressure). High flow systems are supposed to be the most widespread systems. Thus, flow rate for solar systems is assumed to range above 100 l/h.

Solar thermal systems of larger size and subsequently higher flow rates will be shortly introduced in 2.2.3, though typical conditions remain comparable.

2.2.2 Cooling

The process of cooling aims to establish a temperature below ambient temperature. In a physical formulation, cooling of a system means to withdraw heat of a system. The cooling industry offers a wide field of applications which play a major role nowadays, e.g.:

- preservation of food
- air conditioning
- process cooling
- medical technology
- heat pumps
- district cooling
- drying systems
- refrigerated containers

The principle of common cooling processes is based on cyclic compression and expansion of a primary refrigerant, which leads to cyclic phase changes between liquid and gas state of this medium. The related change of the medium's enthalpy is used to withdraw heat of a secondary coolant, which can then be applied for the above-mentioned tasks.

Popular secondary coolants are water, air, oils and soles, water being the desired medium of choice. The variety of applications results in a range of different conditions like temperature range of media, flow range and temperature differences between feed and return. If the temperature of the coolant drops below or near freezing temperatures of water, an antifreeze agent must be mixed to the water to lower its freezing point. Widely used agents are based on

non-toxic PG and toxic EG, which are applied according to their physical properties and their toxicity (cf. 2.3.1). Depending on the mixing ratio, those glycol-based coolants can be deployed at temperatures between approx. -50 °C and approx. 15 °C. Of course, those media can be used at higher temperatures, but the superior fluid properties of water make that impractical.

As temperature differences of coolant circuits are relatively low (e.g. $\Delta T=6$ K for systems with temperature levels of 12 °C/18 °C, 6 °C/12 °C or -3 °C/3 °C), the flow rate is correspondingly high in order to withdraw thermal energy from the system in a sufficient quantity and to allow turbulent flow, which improves heat transfer coefficients between the fluid and heat exchanger [47]. Thus, flow measurements can be carried out primarily at higher flow rates of 800 l/h (and above) and temperatures below ~20 °C.

2.2.3 Additional Applications

Following applications feature conditions regarding their heat carrier fluids that are comparable to the previously mentioned applications. In fact, a lot of the upcoming technical facilities apply parts of both the cooling and the solar thermal system displaying the potential to successfully combine both techniques.

Near Surface Geothermal Energy

This renewable energy source energy makes use of thermal energy which is stored in the soil near the surface. In a primary circle, a fluid of low temperature (e.g. a mixture of water and EG) is circulated through the ground where it receives thermal energy. A generally applied heat pump then uses the fluid's increased temperature to raise the temperature of a secondary consumer (like heating systems of houses). Depending on the technique of heat exchanging (borehole heat exchanger vs. heat collector), its corresponding depth (~100 m vs. ~1.5 m) and the outside air temperature, occurring temperatures of the fluid inside the primary circle are between ~18 °C and -6 °C [48].

Solar District/Local Heating

As a solar thermal system's heat production may exceed the owner's demand, the surplus of heat can be used to supply nearby consumers. Larger-scale solar systems supply heat through a heat exchanger to a preheating cycle, which either feeds thermal energy to consuming residential units belonging to the local heat network or a storage tank [36]. Similar industrial applications include solar process heat systems, which feed thermal energy to power industrial processes in sectors like e.g. food and beverages, paper or chemicals. As the demand for heat is usually more constant throughout a season in industrial applications than in domestic applications, the conditions to use a solar system may be favourable [49].

Geo-Solar Heat Storage

As the heat demand in Middle-European households is subject to seasonal changes, the demand of heat rises during winter time while the biggest output of solar heating systems occurs during

summer. A system to seasonally store the excess heat of the summer period to make it available for winter can help to reduce additionally needed fossil energy. Based on borehole heat exchangers, a fluid (e.g. a mixture of ethylene glycol and water) either stores or extracts thermal energy to or from the underground, depending on the season [50].

~

What unites all those additional applications are flow rates, that are rather high (especially) for cooling purposes while temperature levels are rather low compared to the isolated thermal solar system. However, as the general purpose of glycol in a mixture with water is the antifreeze protection, that aspect is not completely unexpected. What may be more important is the assumption that heat metering of glycol-based fluids becomes more important for increasing heating/cooling system sizes. The bigger the thermal energy, the bigger the losses due to incorrect measurements. At the same time, investment costs for heat meters decrease compared to the investments for the whole heating/cooling system. That makes more sophisticated (and possibly more reliable) sensor types interesting.

2.3 Thermophysical Properties of Glycol-Water-Mixtures

This chapter gives an overview of glycol-based heat conveying media and lists their decisive properties concerning heat metering (cf. Table 2.2). As PG and EG are widely used among coolants, this chapter focusses on these two fluids and water. Note that PG and EG are not used in pure concentration but are mixed in several concentrations with water according to the heat carrier's operating conditions.

Table 2.2: Selection of physical properties of pure glycols compared to water at 20 °C and atmospheric pressure

	Water	PG	EG
c_p / kJ/(kg · K)	approx. 4.18 [38]	approx. 2.46 [51]	approx. 2.4 [52]
ρ / kg/m³	approx. 998 [38]	approx. 1036 [53]	approx. 1115 [54]
ν / mm²/s	approx. 1 [38]	approx. 61 [51]	approx. 20 [55]
c / m/s	approx. 1482 [38]	approx. 1523 [53]	approx. 1666 [56]

The differences of the specific heat capacity c_p and the density ρ of the glycols compared to water lead to incorrect heat coefficients, which must be determined for correct enthalpy change results. The higher kinematic viscosity ν of PG and EG has an influence on the flow properties of the fluids and therefore also on the volume flow measurement. Compared to EG, the specific heat capacity of PG is 2.5 % higher while the density is 7 % lower. The flow properties of ethylene glycol appear more advantageous than those of 1,2-propylene glycol due to the significantly lower viscosity.

As the speed of sound c is linked to other fluid properties and ultrasonic flowmeters partly rely on the speed of sound, the fluid's speed of sound is included in the above shown table. For

pure PG, the speed of sound is ~2.8 % higher than that of water while the speed of sound in EG is 12.4 % higher than that of water.

2.3.1 Overview of Heat Conveying Media based on Glycol

As shown, the field of applications offers a variety of different working conditions. Accordingly, the European antifreeze market consists of more than 40 products mainly based on PG and EG, including concentrates and prefabricated ready-to-use products. Due to the corrosive properties of pure glycol, it is common to all of them, that additives (so-called inhibitors) and buffer substances are added to protect metallic parts of the system from corrosion and to counteract chemical reactions in the fluid (especially acid formation). Each manufacturer supplies its products with a special inhibitor package in solid or liquid form which is adapted to the given operating conditions (e.g. max. or min. temperatures, metal materials, phase transitions). Table 2.3 shows the composition of a conventional concentrated solar medium [57].

Table 2.3: Ingredients of an exemplary commercially available heat conveying medium concentrate

Component	Percent by weight	Function
propane-1,2-diol	92 - 94	frost protection
salts of organic acids	3 - 4	protection for ferrous metals
silicates	< 1	protection for aluminium
triazole	< 0.2	protection for non-ferrous metal
borax	1.0 – 1.5	alkali-reserve
potassium hydroxide	< 1	neutraliser
water	3 - 4	solvent for inhibitors
stabilisers, dyes	0.1 – 0.3	hardness stabiliser/labelling

Since ethylene glycol is poisonous, it cannot be used as a heat carrier in a solar thermal system for domestic use or in the food industry to avoid health risks. In contrast, the food-safe fluid PG can safely be used in solar plants.

To get an overview of commercially available heat conveying media without going beyond the scope of this work, the following selection of four products was put together:

1. Tyfocor L is a concentrate based on PG, which can be used in the food and drinking water sector as cooling brine or as heat conveying medium. Depending on concentration, frost protection down to -50 °C can be ensured. According to the manufacturer, the maximum operating temperature is 170 °C. At temperatures above 200 ° C, chemical changes occur which can endanger solar system safety.
2. Tyfocor LS is a ready-to-use mixture based on PG which has been specially designed for use as a heat carrier in solar thermal installations with high thermal loads. As a

finished product, it should not be further diluted and provides frost protection down to -28 °C. Tyfocor LS also has a maximum application temperature of 170 °C, chemical changes may occur above 200 °C.

3. Antifrogen N is a concentrate based on EG for industrial applications such as technical cooling systems, heat pump systems and hot water heaters. Depending on concentration, frost protection down to -50 °C can be ensured permanently. The maximum application temperature is 150 °C.
4. Antifrogen Sol HT, which is based on higher boiling glycol, is a ready-to-use mixture which can be used in solar systems with a higher thermal load. It provides frost protection down to a temperature of -23 ° C. Although the boiling point of the glycol used is about 270 °C, a maximum application temperature of 200 °C is recommended.

Thus, there are two ready-to-use products specifically developed for solar thermal applications and one frost protection concentrate based on PG and EG, respectively represented in the measuring program. Those fluids will be put to test in terms of physical properties as well as flow rate measurements. Obviously, four fluids (and further concentrate ratios) cannot fully represent the whole range of available glycol-based heat carrier fluids. But as ratios of PG and EG and their respective inhibitors inside the heat carrier media are assumed to be comparable, the selection should still provide a rough idea how other fluids act from a heat metering perspective.

The following chapters give a short introduction of essential fluid properties and their respective influence on heat metering.

2.3.2 Density

Knowledge of the density $\rho(\Theta)$ gives insights into the behaviour of a liquid including flow characteristics (Re), its behaviour as a heat carrier (heat coefficient k) and information regarding its composition. The density of PG and EG is higher than the density of water. Accordingly, typical mixtures of these media with water have a higher density than water. As the uncertainty of density measurements is relatively low (for water: ~0.01 kg/m³), maintenance measurements based on $\rho(\Theta)$ are convenient to check mixtures for decomposition. Since the considerably temperature-dependant density can be linked to other fluid properties, it is of special interest for monitoring.

Referred to flow and heat metering, the density plays an important role as the measurement of the actual variable of interest, the mass flow is generally more elaborate than the measurement of volume flow. The mass relates to the volume of a fluid through density.

2.3.3 Specific Heat Capacity

As stated in 2.1.3, the change in specific enthalpy Δh of a fluid between feed and return cannot be measured directly. As liquids are approximately incompressible, $c_p(\Theta)$ can be used to measure Δh according to:

$$\Delta h = c_p(\Theta) \cdot (\Theta_f - \Theta_r). \tag{2}$$

In conjunction with the density of the liquid, $c_p(\Theta)$ is the foundation for enthalpy change calculations. Thus, the measurement uncertainty of $c_p(\Theta)$ directly influences the uncertainty of the heat metering device. Unfortunately, the quantity $c_p(\Theta)$ is relatively difficult to measure. State of the art measurements of liquids and in the desired temperature range provide data with a measurement uncertainty of approx. 1.0 % [58], even though lower values of 0.3 % uncertainty, based on another principle of calorimeter, are claimed [59].

The heat capacity $c_p(\Theta)$ of usual antifreeze agents is lower than that of water making it less attractive as a heat carrier or coolant.

2.3.4 Kinematic Viscosity

The viscosity is a measure of a fluid's resistance to deformation due to friction between its molecules. The higher the fluid's viscosity, the higher its resistance to deformation. Divided by the density, the dynamic viscosity $\eta(\Theta)$ gives the kinematic viscosity $\nu(\Theta)$. Applied to pipe flow, the kinematic viscosity characterises the fluid's flow behaviour in relation to its flow velocity and the pipe dimensions. The dimensionless Reynolds number Re is of special interest for flow measuring, as its predictions regarding flow state and flow profile of the measuring fluid play an important role for most flow sensors, almost regardless of their principle.

Antifreeze agents, especially those based on PG, exhibit a significantly higher viscosity than water leading to laminar flow state at flow rates for which water would be in turbulent flow state (cf. chapter 3.5). Especially flowmeters, which are highly dependent on the flow profile, produce incorrect measurements, if the fluid switch from water to glycol-water-mixture is not considered as shown later.

2.3.5 Speed of Sound

The speed of sound $c(\Theta)$ of a medium enables, similarly to its density, numerous statements regarding fluid characteristics. It can be used as a bridging function between state functions which allows to calculate linked physical properties [60]. As the speed of sound is comparably temperature dependent and relatively easy to measure, it can be used to determine the temperature for certain applications where other industrial temperature measurements are difficult. Further applications could include the identifying of changes in liquid composition.

There are numerous flowmeters making use of ultrasound; several of them are highly dependent on $c(\Theta)$ for the accuracy of its measurements. A data base of $c(\Theta)$ of different fluids could

improve ultrasonic flow measurements by enabling sensors to measure not “only” the correct volume flow but potentially other quantities of interest.

2.4 Degradation of Glycol-Water-Mixtures

The term "aging" or "degradation" broadly describes chemo-physical changes in the glycol-water-mixture which can occur by numerous different causes. The strongest influences on the process of aging are high temperatures and the presence of oxygen and/or metals [61]. Thus, temperature-induced degradation is assumed to predominantly occur in solar thermal systems and not in cooling applications.

Stagnation temperatures are typically above 200 °C in a flat collector (above 270 °C in vacuum tube collectors) and subsequently above the maximum permissible operating temperatures of glycol-water-mixtures [62]. Depending on the stagnation behaviour of the system (emptying behaviour and construction of the collector field, remaining non-vaporised liquid residues, system pressure), a portion of the medium is exposed to higher temperatures than can be tolerated [63]. The glycols are split into more or less known decomposition products during complex chemical reactions [64]. According to Rossiter, these include inter alia Carbonic acids, strongly smelling aldehydes, hardly water-soluble chemical compounds such as esters, ethers and salts. These constituents can occasionally lead to caking, sticking, clumping and clogging, which are insoluble and, in the worst case, require the exchange of entire plant components. Stichel [65] adds that overheating can also render specific inhibitors ineffective, so that corrosive damage occurs at the collector circuit. Acids that form during degradation are neutralised by buffer substances in the solar fluid. If these buffer substances are consumed below a critical reserve alkalinity below 10% [66], the pH-level can go down to the acid range below 7. In this case, accelerated corrosion can also occur without oxygen [67].

The presence of oxygen is a minor issue if the solar systems is properly installed. However, it is conceivable that during stagnation standstill, the safety valves respond, and solar fluid exits during an increase of vapor pressure in the solar circuit above the safety limits (typically above 6 bar). During cooling, vacuum is created in the system, so that air is sucked into the system. During thermal load, the aging processes of the glycols are then accelerated under the influence of oxygen.

Materials predominantly used for solar thermal systems include metals such as copper, steel, stainless steel and aluminium, which may also be constructed in mixed installations. Each prefabricated solar fluid contains a corresponding inhibitor package, which protects the above metals from corrosion by forming inhibitory surface layers. In the case of high thermal loads, some of these inhibitors may be rendered unusable, whereby the metals are exposed to the corrosion attack of the heat conveying medium without protection.

It becomes obvious that the combination of temperature, oxygen presence and metals installed in mixed installations can lead to degradation of glycol-based fluids and thus to failure of their

functions. Laboratory testing of those influences has been done in the hope to quantify occurring changes inside the medium at field applications.

2.4.1 Test Methods

There are several methods and standard tests, which deal with the aging of glycol-water-mixtures, but usually with a focus on the corrosion behaviour. Stichel carried out experiments with 1,2-propylene and ethylene glycol-based heat conveying fluids in 1997, which were based on various test methods (ASTM D 1384, EMPA test, ASTM D 4340, FVV hot test, rotating cylinder test, crevice corrosion test). In general, the metal alloys (copper, brass, steel, stainless steel, aluminium) commonly used in heating and solar systems were subjected to a gravimetric (or optical) test of the material loss due to corrosion under thermal load and oxygen influence.

The tests showed that all commercially available heat conveying media meet the corrosion protection requirements excellently under most operating conditions in heating and cooling circuits such as solar systems. Failures occur only in the presence of narrow gaps (e.g. seals, deposits, welds) [65] and high temperatures ~135 °C [68]. Following, the test methods recommended by Stichel will be briefly presented. Meanwhile it should be considered that those tests represent a reliable assessment of the inhibitory effect of heat carriers but are *poorly reproducible* and are *not assumed to fully reproduce* aging processes in real solar systems!

ASTM D1384:

In this most frequently used method for testing the efficiency of inhibitors, metal samples (conductive or insulated from each other) are exposed to the test medium at temperatures of 90 °C and air supply of 100 ml/min for a duration of 14 days. After a follow-up treatment (pickling) of the metals, the specific mass losses are evaluated. The results from Stichel showed that all ready-to-use heat conveying media caused negligibly small mass losses, which were accordingly well inhibited. However, the measured values spread, which raises questions about the reproducibility [69].

Crevice corrosion test:

Like ASTM D1384, metal samples are immersed into a test medium, but these are fixed by plastic plates with a sloped surface to create a gap. Over a period of 28 days, the medium is heated daily to 90 °C for 10 hours and allowed to cool down to room temperature. The final optical evaluation of the corrosion reveals a weakness of the prefabricated heat conveying fluids. Apart from copper materials, clear signs of crevice corrosion were evident in all metals [65].

Rotating cylinder test:

In this test, cylindrical metal samples are rotated at a speed of 500 rpm in the fluid, whereby the flow of the heat carrier is simulated. At constant temperatures of 80 ° C and without active air intake, the test takes 7 days before the mass losses of the metal samples are determined.

Again, the measured values of the mass loss significantly spread, but show the effectiveness of the inhibitor properties of the prefabricated glycol-water-mixtures [65].

~

The test methods presented so far offer the opportunity to examine heat carriers under normal operating conditions, while the temperatures which are especially critical for aging are lying at temperatures above 200 °C or even 300 °C. In this area, the heat carrier can age within hours, including darkening of the medium, lowering of the pH-level and the formation of insoluble residues [57]. Hafner simulated the processes in a collector during stagnation with the heat carriers Antifrogen L and Antifrogen Sol HT at cyclically changing temperatures between 120 °C and 315 °C including copper contact and flow influence. Investigations included values such as the inhibitor concentration, the reserve alkalinity, the pH-level, the density and the concentration of copper in the mixture. After 47 days or more than 2700 heating cycles, the stated values for Antifrogen Sol HT changed as follows [70]:

- inhibitor concentration: dropped to 25 %
- reserve alkalinity: dropped to 33 %
- pH-level: dropped from 8.2 to 7.0
- density: drop from 1.0647 kg/m³ to 1.0616 kg/m³ (~0.3 %)
- concentration of copper in the mixture: $<$ 1 ppm (from 0 ppm)

Clogging of the metal surface and the technical failure of the additives could accordingly be prevented. However, the comparison of the fluid samples of the laboratory test with practice-loaded samples does not reveal any correlation due to sample variances. In addition, only copper has been experimented with, whereas a solar system is usually a mixed installation. From a heat metering standpoint, the drop of density can be seen critical, as a change in density could be caused by a change of water ratio. That, in turn, would lead to changing physical properties and thus have an impact on heat metering those fluids.

2.4.2 Field Samples

Hiller [71] investigated the effects of temperature, pressure and exposure time on a solar fluid (Tyfocor LS) by collecting data in solar systems of different sizes and collector types (flat plate and vacuum tube). The data included values of density, which can be used to detect changes in concentration. While two solar systems caused no signs of density changes of the solar fluid, two systems showed small changes (flat plate system: density drop by 0.2 % due to adding of water; vacuum tube system: density rise by 0.09 % due to fractional evaporation caused by minimal leaks). While those changes in density appear small, their cause, the change of water concentration, could have led to an error on heat metering those fluids.

Dimitrova [72] collected data from fluids applied in in-field systems and compared them to laboratory testing data. Apart from slight optical changes of the medium, no density changes

could be detected though stagnation occurred in the solar system, where the measuring fluid Tyfocor L has been applied in.

Thus, while a series of laboratory and field tests investigated the corrosion behaviour of glycol-water-mixtures under thermal and oxidative stress, there hasn't been developed a method to determine the aging and maximum operating time of a solar fluid regarding its fluid properties (heat capacity, density - though density data is often investigated, viscosity).

The aging of the fluid is strongly dependent on the conditions it is exposed to, determined by the nature and structure of the solar circuit [61]. According to Haller and Vogelsanger, relevant parameters are [61]:

- stagnation temperature
- frequency and duration of stagnation
- system pressure
- emptying behaviour of the collector field
- metals the system's components are made of
- presence of oxygen in the system

Accordingly, the lifetime of the glycol-water-mixture is not dependent solely on the fluid properties but also on the properties of the fluid in a specific solar system. As laboratory testing usually focusses on procedures to describe a wide range of applications, the specific solar system may not be fully displayable by laboratory testing. Nevertheless, in order to determine possible changes of physical properties that have an influence on heat metering, two (slightly adjusted) methods were applied with the aim to investigate degradation in solar fluids. They are presented in Chapter 3.8.

3. Results of Thermophysical Property Investigations

As stated above, the knowledge of certain physical properties of a fluid has an impact on heat metering which manifests on enthalpy change calculations (specific heat capacity, density) or on volume flow measurements (viscosity, density, speed of sound). All tests have been carried out in PTB-laboratories of different divisions and departments.

For the investigation of the thermophysical properties, the concentrates Tyfocor L and Antifrogen N were mixed with water as instructed by the manufacturer while the ready-to-use fluids Tyfocor LS and Antifrogen Sol HT were examined undiluted (cf. Table 3.1). The mixtures were prepared with a volumetric flask with a relative expected uncertainty of 0.1 % (k=2) regarding volume fraction between concentrate and water. The corresponding uncertainty of glycol concentration of ready-to-use mixtures is unknown but assumed to be ≤ 1 %. The minimum concentrations of 20 vol.- % antifreeze concentrate for Antifrogen N and 25 vol.-% for Tyfocor L are due to corrosion protection and ensure frost protection for temperatures as low as -10 °C. The widely used 40 % mixtures of Antifrogen N and Tyfocor L allow frost protection for temperatures as low as -25 °C and -21 °C, respectively.

Table 3.1: Selection of mixtures tested

Name	Vol.-% of spec. Fluid	Antifreeze protection [°C]
Tyfocor LS	100 (undiluted)	-28
Antifrogen Sol HT	100 (undiluted)	-23
Tyfocor L	25	-10
	30	-14
	35	-17
	40	-21
Antifrogen N	20	-10
	25	-13
	30	-16
	35	-20
	40	-25

Depending on the test setup and the mixture slight deviations from the desired measuring range between -20 °C and 100 °C can occur. Thus, some density and viscosity measurements could only be carried out at maximum temperatures of 90 °C to 95 °C due to the "open" design of the measuring devices. Some mixtures were studied at temperatures above -20 °C as they already began to freeze at lower temperatures.

3.1 Density

The density tests were carried out by Dr. Henning Wolf, Head of PTB Working Group 3.32 “Properties of liquids” with an expanded measurement uncertainty of 0.05 kg/m³ (k=2). The measurements have been carried out with an Anton Paar DMA 5000 M, which is based on frequency measurements of an oscillating U-tube (likewise to 2.1.2.4). The fluids have been degassed prior to the tests (and compared to samples which were not degassed) and corrected for potential changes in density.

Before going into more detail about the individual heat carriers, the following overview compares the fluids regarding their density. Therefore, the ready-to-use-mixes are compared with concentrates mixed according to a 40:60 ratio (concentrate: water). The higher-boiling glycol-based Antifrogen Sol HT has the highest density, followed by Antifrogen N (EG) and the PG-based Tyfocor L and Tyfocor LS.

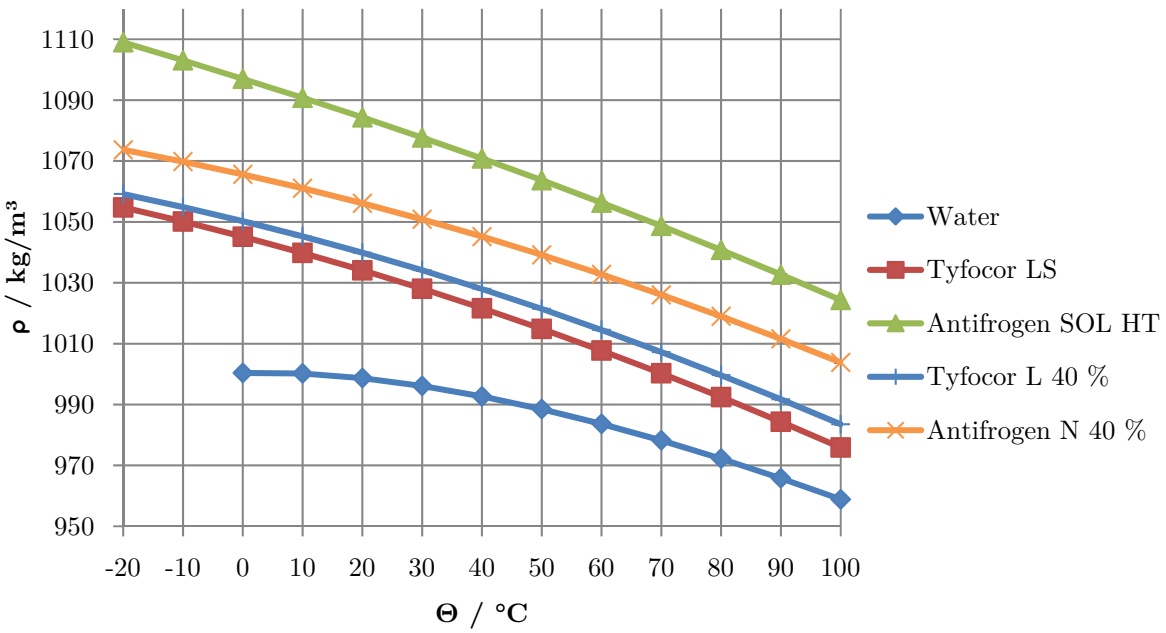

Figure 3.1: Comparison of densities *ρ(Θ)* of a selection of heat media

At a temperature of 20 °C, the density of Tyfocor LS is ~3.8 % higher, the density of Tyfocor L 40 % is ~4.5 % higher, the density of Antifrogen Sol HT is ~9.1 % higher while the values of density of Antifrogen N 40 % are ~6.1 % higher in comparison with water. Thus, the values differ noticeably between the fluids and water but also among each other. Compared to water, the density values of the tested fluids are higher and more temperature-dependent as they all decrease with rising temperatures (Tyfocor LS: -7.5 %, Tyfocor L 40 %: -7.1 %, Antifrogen Sol HT: -7.6 %, Antifrogen N 40 %: -6.5 % compared to water: ~4.2 % in the considered temperature region).

The deviations of the manufacturer's data to the measured values (cf. Figure 3.2) of Tyfocor LS amount to -0.15 % at the lower temperature limit and 0.15 % at the upper temperature limit.

The manufacturer's data of Tyfocor L 40 % lie up to approx. 0.12 % below the measured values in the temperature range between -20 °C and 75 °C; above these temperatures they deviate by up to 0.15 %. For Antifrogen Sol HT, the deviations of the manufacturer's specifications are between 0.28 % and 0.15 % below the measured values. The largest deviations from the manufacturer's data are existent for Antifrogen N 40 % with deviations of between -0.2 % and -0.4 %, depending on the temperature.

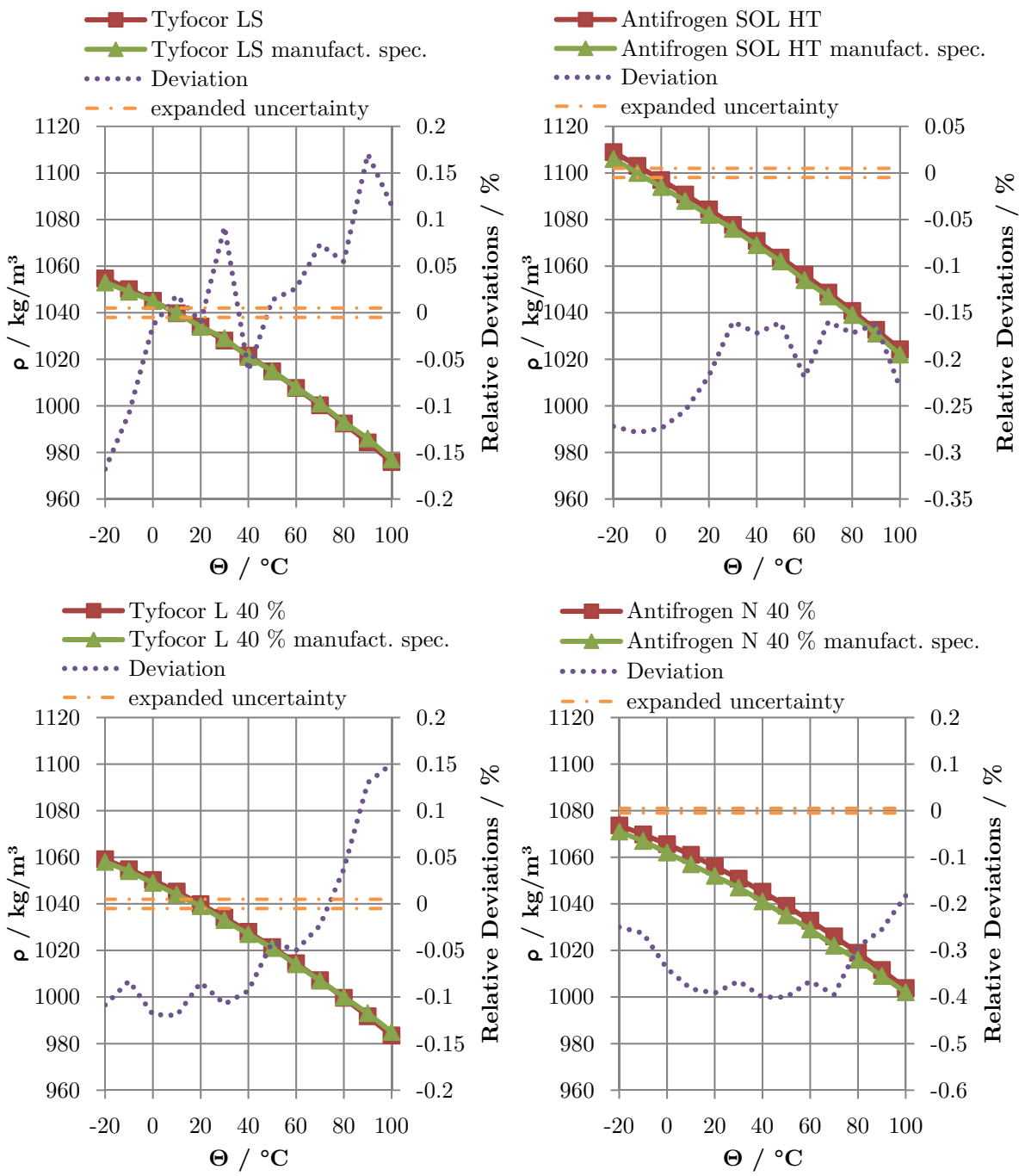

Figure 3.2: Density *ρ(Θ)* of fluids measured and according to manufacturer's data

In summary, it can be stated that based on their relative deviations, the manufacturer's specifications of the density are barely sufficient for in-field use (cf. 3.7). As the density is a

comparably good-to-measure quantity with a low measurement uncertainty it can be, inter alia, used to detect changes of the fluid concentration in field or to calculate other fluid properties. By taking the example of Antifrogen N 40 % at 20 °C, the density according to the manufacturer is 1052 kg/m³, whereas the measured density is 1056.14 kg/m³. According to the measured data, 1052 kg/m³ would fit to a mixing ratio of 37 % to 38 % Tyfocor L instead of 40 %. Thus, in field density measurements and ultimately the manufacturer's data sets of density must meet high requirements to reliably detect changes of concentration. Including the measured deviations to manufacturer's data, it is recommended to validate the fluid's density prior to its use. Further density data is presented in Appendix 4.

3.2 Specific Heat Capacity

The calorimetric tests were done in PTB Working Group 1.44 "Caloric Quantities" by Dr. Stefan Sarge with an extended measurement uncertainty of 1.5 % (k=2; cf. error bars in Figure 3.3). The principle of differential scanning calorimetry (DSC) was used to measure the specific heat capacity at constant pressure $c_p(\Theta)$; this method does not measure absolute but relative values (relative to a calibration fluid), which must be converted to absolute ones [58].

Before the specific heat capacities of the mixtures are shown in detail, Figure 3.3 is used to present the measured values of the ready-to-use mixtures in comparison to the concentrates in a 40 % mixture and water as well as the concentrates in the indicated mixing ratios.

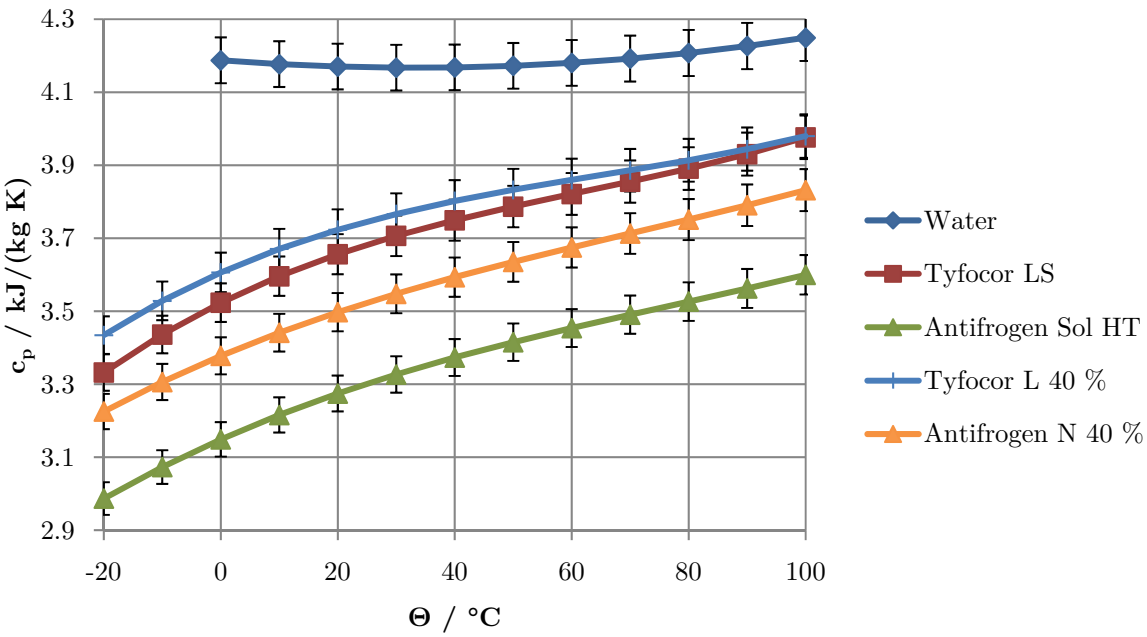

Figure 3.3: Comparison of specific heat capacities $c_p(\Theta)$ of a selection of heat media

Tyfocor L and Tyfocor LS have the highest specific heat capacity of the four media (except water). Both heat carriers are based on PG, the differences in the measured values can be explained with slightly different proportions of water on the one hand and with the influence of the substance's additives on the other hand. While in Tyfocor L anti-corrosive inhibitors on

a solid basis were used, Tyfocor LS was mixed with high-temperature liquid inhibitors which, in the case of high stagnation temperatures, should evaporate together with the liquid and prevent crystalline residues. As expected, Antifrogen N, based on EG, shows a lower specific heat capacity compared to Tyfocor L/LS. Antifrogen Sol HT has the lowest specific heat capacity. At a temperature of 20 °C, in comparison with water, the values of c_p of Tyfocor LS are ~12 % lower, the values of c_p of Tyfocor L 40 % are ~11% lower, the values of c_p of Antifrogen Sol HT are ~21 % lower while the values of c_p of Antifrogen N 40 % are ~16 % lower. Thus, the differences are substantial between the fluids and water but also among each other. Compared to water the values of the tested fluids are considerably more temperature-dependent as they all substantially increase with rising temperatures (Tyfocor LS: ~19 %, Tyfocor L 40 %: ~16 %, Antifrogen Sol HT: ~21 %, Antifrogen N 40 %: 19 % compared to water: ~1.5 % in the considered temperature region).

Explanation of Figure 3.4: For each fluid, the graph shows the values of the specific heat capacity (left vertical axis) of a commercially available glycol-water-mixture according to the manufacturer specifications (green) and laboratory measured values (red) as a function of the temperature. The violet dotted line indicates the percentage deviation of the manufacturer's data (right vertical axis) in relation to the measured value. The specific heat capacity of Tyfocor LS shows negative deviations of up to 3 % compared to the manufacturer's specifications at temperatures below 0 °C which is supposedly uninteresting for solar thermal energy but may be decisive for cooling applications. Apart from that, the value shows deviations of up to 2 % above the value stated by the manufacturer (and just above the extended measurement uncertainty). The measured specific heat capacity of Antifrogen Sol HT differs widely from the manufacturer's specifications, amounting to differences of up to +5 % at low temperatures (-20 °C) and approx. 7 % at high temperatures (100 °C). For Tyfocor L in a 40 % solution, the deviations of the measured values to the manufacturer's data are mostly within the extended measurement uncertainty at the examined temperature range. More data for further Tyfocor L mixtures can be found in Appendix 2. The manufacturer's specifications of c_p of Antifrogen N 40 % differ by approx. 3 % - 7 % in the temperature range below 0 °C and up to -2 % in the upper temperature range of the measured values. More data for further Antifrogen N 40 % mixtures can be found in Appendix 2.

It becomes obvious that ignoring the change of specific heat capacity between different fluids leads to corresponding errors in enthalpy change calculations. That applies to differences between the respective fluid to water but also to other fluids. An exception are the PG-based fluids Tyfocor L 40 % and Tyfocor LS, where most measured values lie within the expanded measurement uncertainty of 1.5 %. Another point of interest are the deviations between measured values and manufacturer specifications. Their influence manifests directly on heat coefficient definition. Thus, enthalpy change calculations based on manufacturer data would partly lead to deviations of up to 6 % - 7 %.

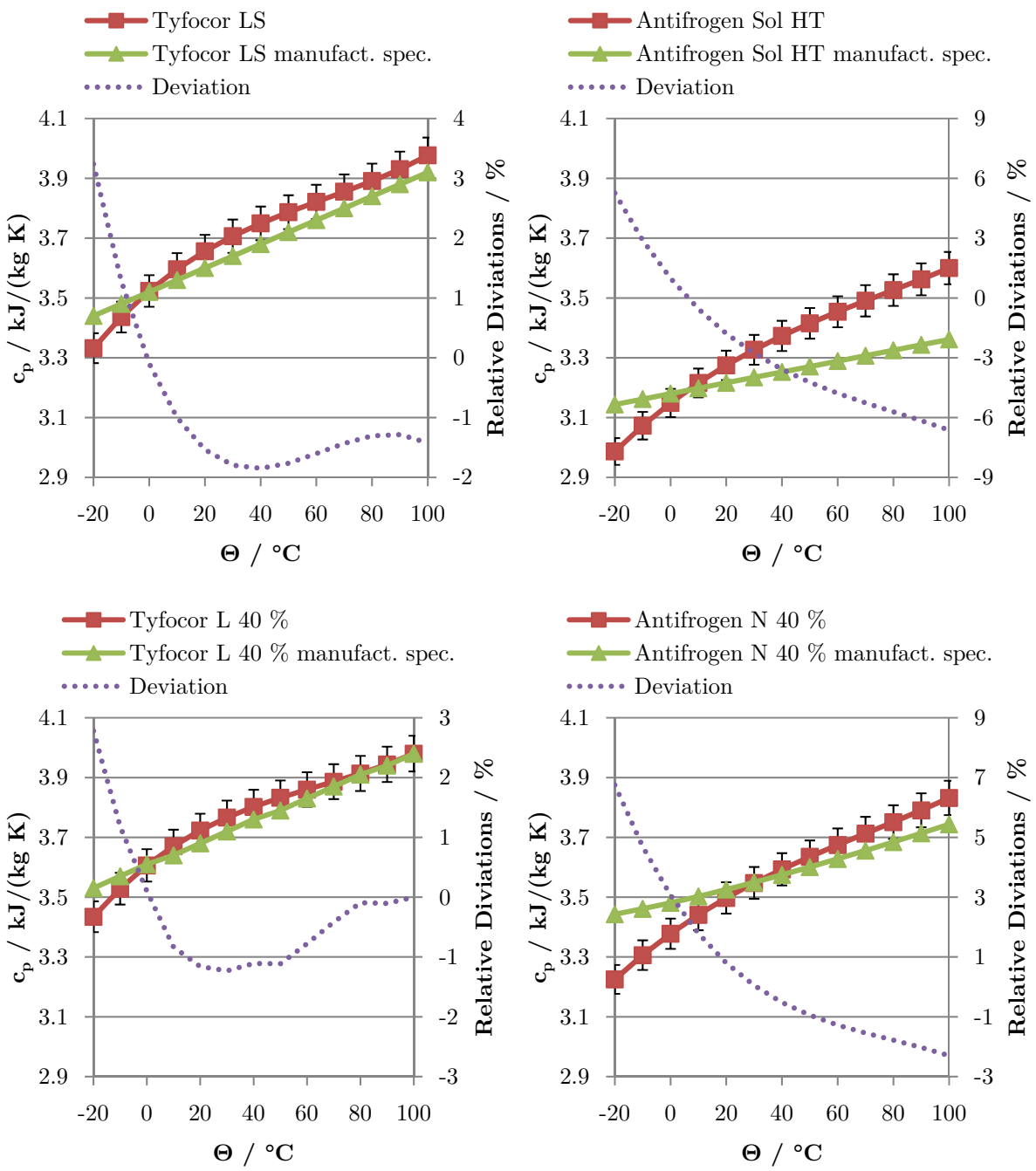

Figure 3.4: Specific heat capacity $c_p(\Theta)$ of fluids measured and according to manufacturer's data

3.3 Kinematic Viscosity

The viscosity investigations have been done by Dr. Henning Wolf, Head of PTB Working Group 3.32 "Properties of liquids", applying an Anton Paar SVM 3000. The principle of measurement is based on motor torque measurements of a rotating fluid-filled cup according to ASTM 7042 [73].

A comparison of the kinematic viscosity $\nu(\Theta)$ of investigated fluids (with a measurement uncertainty: 1 %, k=2) shows how much the viscosity varies in comparison with water but also in comparison between glycol-based fluids (cf. Figure 3.5). Especially in the temperature range

below 20 °C the differences are considerable, in the temperature range above 20 °C the values approach those of the water. The higher-boiling Antifrogen Sol HT has the highest viscosity (maximum value: 84 mm²/s at -20 °C), followed by Tyfocor LS (maximum value: 62 mm²/s at -20 °C) and Tyfocor L (maximum value: 48 mm²/s at -20 °C) based on 1,2-propylene glycol. Antifrogen N 40 %, based on ethylene glycol, shows as expected the lowest kinematic viscosity (maximum value: 17 mm²/s at -20 °C) and thus the best flow properties of the investigated media. Critical for volume flow measurement is the viscosity's temperature dependency of the media. While the kinematic viscosity of water increases by approx. 500 % at a temperature change from 100 °C to 5 °C, the increase of the glycol-based media amounts to approx. 1450 % (Tyfocor LS, Antifrogen Sol HT), 1280 % (Tyfocor L 40 %) and 830 % (Antifrogen N 40 %), respectively. Further viscosity data can be found in Appendix 5, foll.

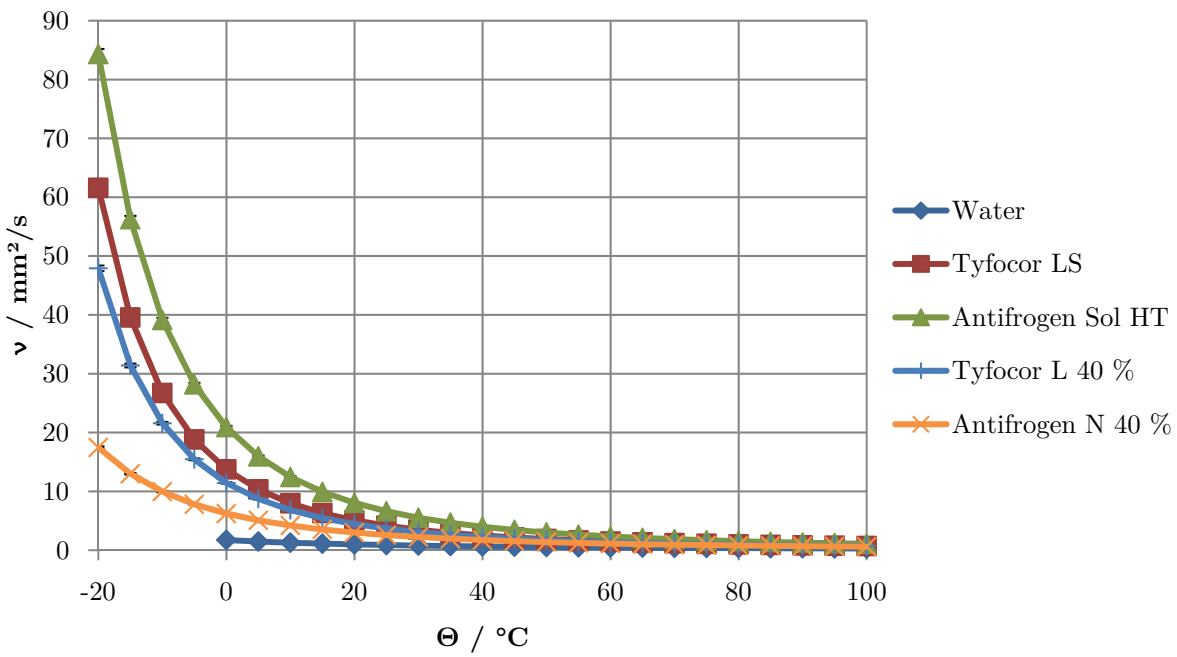

Figure 3.5: Kinematic viscosity *ν(Θ)* of investigated fluids

Since the viscosity of the samples reaches very high values, especially in the temperature range below 0 °C, the measured values displayed in Figure 3.6 are presented once more in logarithmic scale. The values of the percentage deviations (right vertical axis), however, are not displayed logarithmically. In the case of the ready-to-use-mixture Tyfocor LS, deviations as high as 5 % and -18 % occur between manufacturer's data and measured values. The manufacturer's data from the measured values to the manufacturer's specifications appear to deviate particularly in the temperature range between 60 °C and 80 °C, since the measured values apart of these outliers deviate rather by ± 5 % from the measured value. A similar outlier can be found in the manufacturer's data from Antifrogen Sol HT. However, the deviations in the case are more in the range between 6 % and 8 % below the measured values, whereas the outlier drops to 0.35 %. The values of the kinematic viscosity of Tyfocor L 40 % are below the values of Tyfocor LS, which indicates small differences in the water content of the mixtures and/or for the effect

of the inhibitors used on the viscosity of the heat conveying medium. The deviations of the manufacturer's data vary between 6 % and -4 %. Antifrogen N 40 % has variations between 4 % and 9 % above the measured values regarding the manufacturer's specifications, which have maximum values especially in the lowest and highest temperature areas of the measuring range. While deviations of viscosity from manufacturer's data to measured values appear comparably high, their influence on heat metering is only indirect and manifests in flow profile differences between the fluids (cf. chapter 3.5). Obviously, that would affect flow sensors which are especially depending on the flow profile.

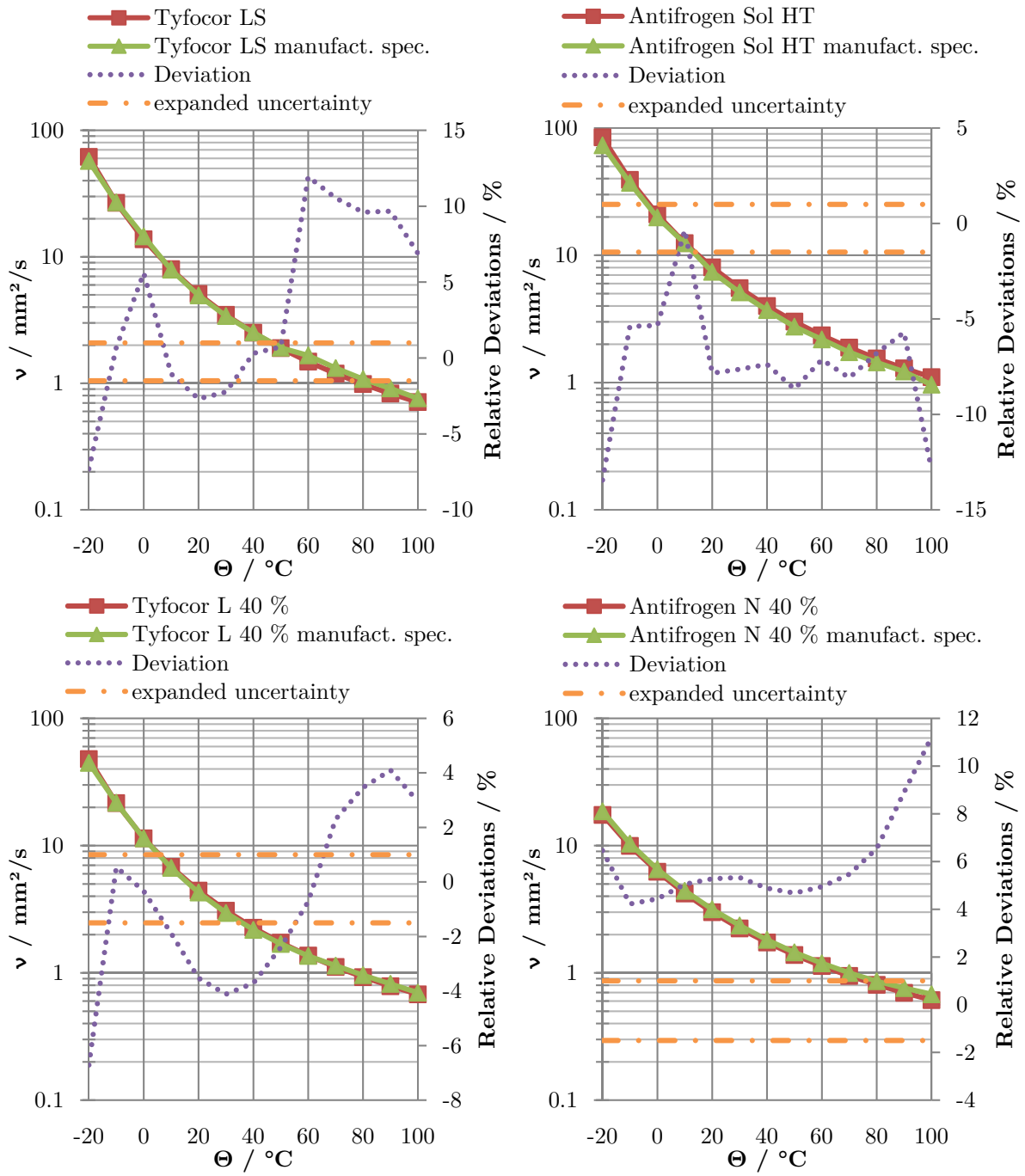

Figure 3.6: Kinematic viscosity *ν(Θ)* of fluids measured and according to manufacturer's data

3.4 Heat Coefficient k

The calculation of the heat coefficients was carried out according to the simplified form already presented above for the measurement in feed flow k_f and return flow k_r according to:

$$k_f = \frac{\rho(\theta_f)}{\Delta\Theta} \cdot \int_{\theta_f}^{\theta_r} c_p(\Theta) d\Theta \tag{15}$$

$$k_r = \frac{\rho(\theta_r)}{\Delta\Theta} \cdot \int_{\theta_f}^{\theta_r} c_p(\Theta) d\Theta \tag{16}$$

The values of $\rho(\Theta)$ and $c_p(\Theta)$ are given as polynomial functions of Θ calculated from the measured data (cf. Appendix 1).

Before looking at the results of investigated fluids, the applicability of using the simplified form to calculate k_i must be controlled. The easiest way of doing this is to compare calculated k-values for water based on the method proposed in EN 1434 and on the method used in this work. Data basis for the latter method are values of specific heat capacity and density according to IAPWS-IF97 [40].

Figure 3.7 shows the deviations between both methods for a temperature range of 0 °C to 100 °C and atmospheric pressure, where the value according to EN 1434 is set to be the putative true value. The differences between both methods tend to be lower than 0.05 %, which is well within the expanded measurement uncertainty of k, according to EN 1434. Thus, the simplified method proves applicable for the following calculations.

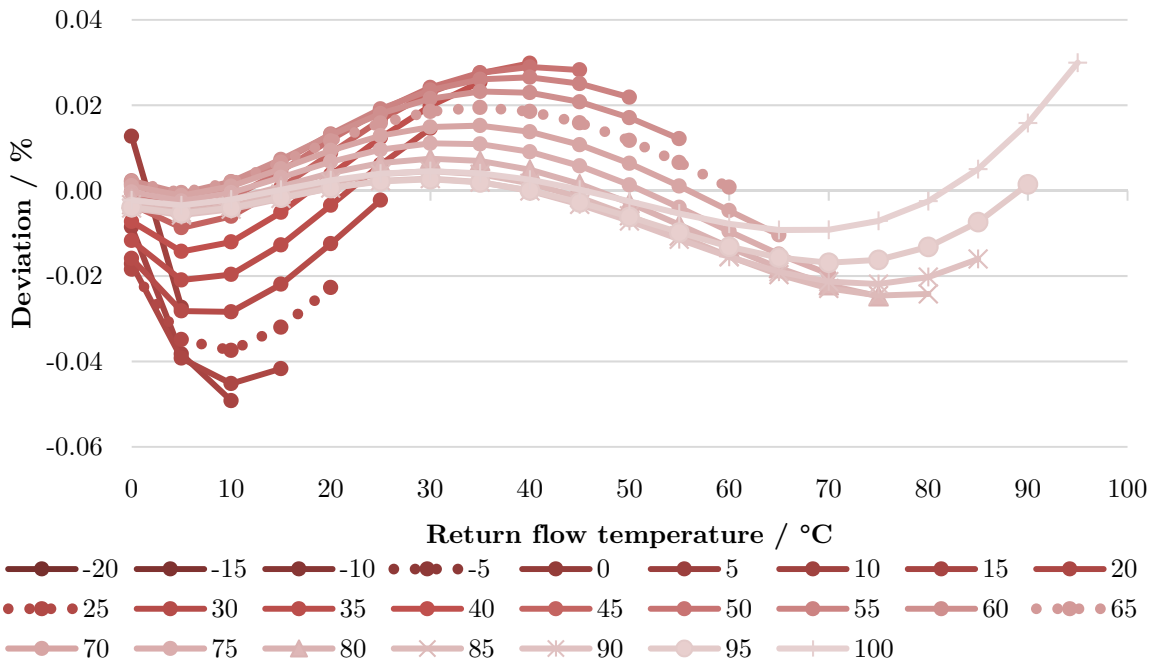

Figure 3.7: Differences between k, calculated based on EN 1434 and simplified method

Figure 3.8 gives an overview of calculated heat coefficients for the investigated fluids at feed temperatures of 10 °C (dashed lines) and 85 °C (solid lines), when measured in return flow. It shows proportions between heat coefficients of water (blue) to glycol-based fluids (orange: Tyfocor L 40 %, red: Tyfocor LS, green: Antifrogen N 40 %, grey: Antifrogen Sol HT) based on two examples (blue and red brackets). For tables of calculated heat coefficients of all investigated fluids, cf. Appendix 11, foll. Overall, the more pronounced temperature dependency of k of glycol-based fluids in comparison with water is noticeable which could be expected as the respective density and specific heat capacity of glycol-based fluids show a more pronounced temperature-dependency, as well. Especially at low temperatures, the heat coefficients of glycol-based fluids differ from water but also from each other. At high temperatures, however, the heat coefficient differences are less pronounced. Between the PG- and EG-based mixtures, differences are approx. 2 % or less at the upper temperature limit.

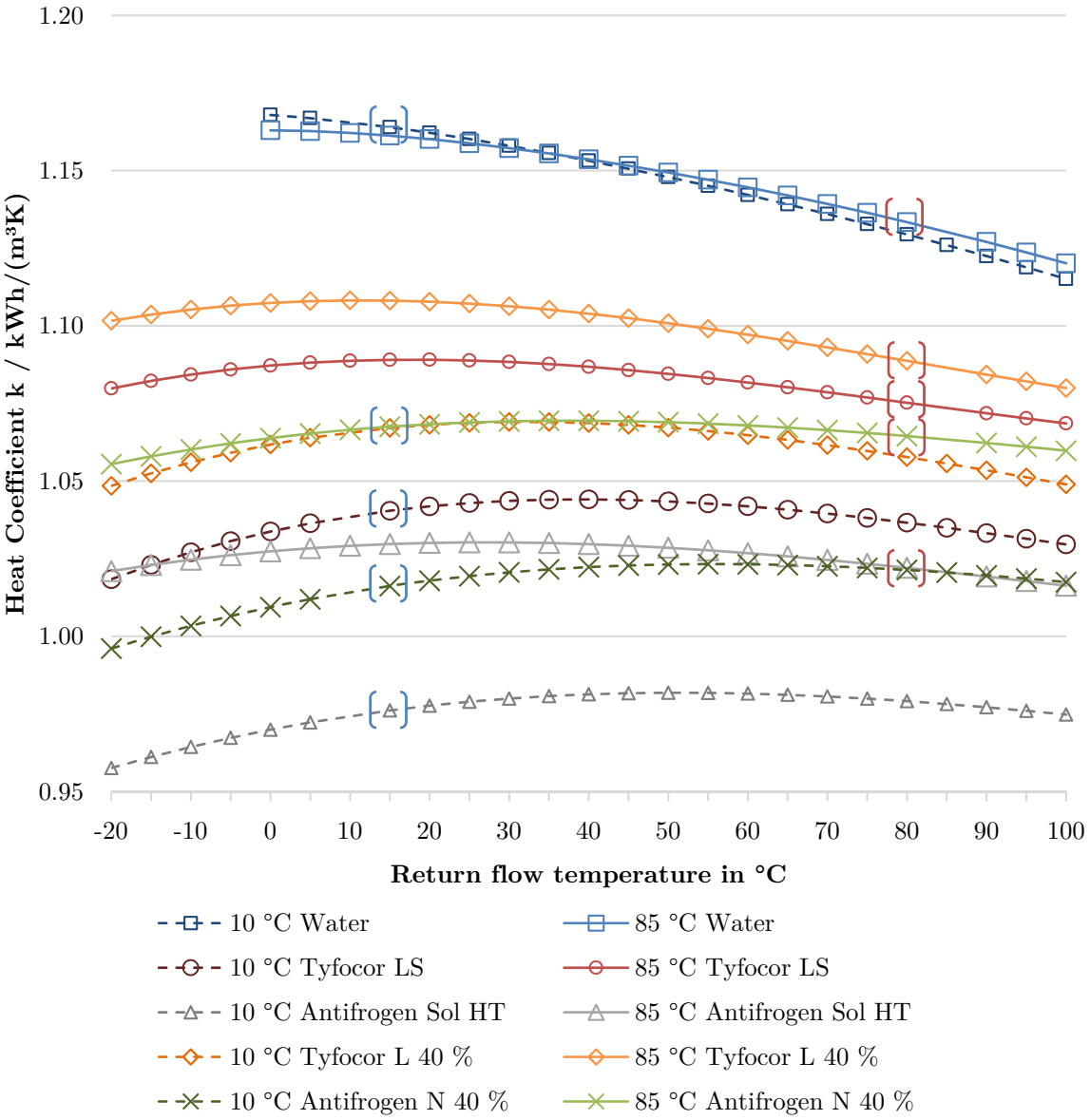

Figure 3.8: Overview of k values of investigated fluids

By including the aforementioned examples, the temperature-related deviations between the calculated heat coefficients become more obvious: To give an example from the lower temperature part with a feed temperature of 10 °C and a return temperature of 15 °C (blue brackets [ ]), the heat coefficient *k:*

- for water is 1.164 kWh/m³K,
- for Tyfocor L 40 %, *k* is 1.067 kWh/m³K (deviations to water are -8.3 %),
- for Tyfocor LS, *k* is 1.040 kWh/m³K (-10.7 %),
- for Antifrogen N 40 %, *k* is 1.016 kWh/m³K (-12.7 %),
- and for Antifrogen Sol HT, *k* is 0.976 kWh/m³K (-16.2 %).

To give an example from the upper temperature application with a feed temperature of 85 °C and a return temperature of 80 °C (red brackets [ ]), the heat coefficient *k:*

- for water is 1.133 kWh/m³K,
- for Tyfocor L 40 %, *k* is 1.089 kWh/m³K (deviation to water: -3.9 %),
- for Tyfocor LS, *k* is 1.075 kWh/m³K (-5.1 %),
- for Antifrogen N 40 %, *k* is 1.065 kWh/m³K (-6.0 %),
- and for Antifrogen Sol HT, *k* is 1.022 kWh/m³K (-9.8 %).

Note that these deviations would directly affect the heat measurement of the heat meter, if *k*-values of water would be applied. The uncertainty of the heat coefficient is directly influenced by the measurement uncertainty of its input values $c_p(\Theta)$, $\rho(\Theta)$, the uncertainty of its composition and the temperature measurement in feed and return. For an idealised temperature measurement and neglecting composition uncertainties, the biggest contribution to the uncertainty of the heat coefficient (U=1.5 %, k=2) arises from the uncertainty of the specific heat capacity whereas the influence of the density measurement uncertainty is almost negligible. However, for field conditions the uncertainty of the heat coefficient rises based on influences which are briefly discussed in chapter 6.4 and Appendix 10.

3.5 Flow Conditions

This chapter focusses mainly on the dimensionless Reynolds number *Re* and the theoretical flow state of heat conveying media at a few selected flow rates. Flow sensors are preferably calibrated with the medium it will later operate with to assure accurate results [74]. The accuracy of some flow sensors can be related to *Re* which gives the opportunity to calibrate with a fluid different to the operating fluid. Thus, knowledge of *Re* allows predictions of the performance of some sensor types. The calculation of *Re* was done according to the equation:

$$Re = \frac{d \cdot v}{\nu} \tag{17}$$

with *Re* being based on the pipe diameter *d*, the fluid velocity *v* and the kinematic viscosity ν, which was determined by measurement. The Reynolds number indicates which flow regime prevails inside the pipe cross-section, laminar or turbulent. Thus, it is crucial for a volume

sensor's performance, as most sensors are highly dependent on the velocity profile of the measuring medium. Fully established laminar flow leads to a parabolic-shaped profile, where the velocity in the middle of the pipe has its maximum but is gradually decreasing to zero towards the wall. It states at $Re < 2320$ [75] and predicts a flow profile where the mean volumetric flow velocity is half the maximum velocity at the pipe's central axis. Above $Re = 2320$ vortices can lead to disturbances of the laminar flow profile while the turbulent flow profile may still be far from developed. This transient area is especially critical for flow sensors as its velocity contribution is hard to predict. Turbulent velocity profiles show a more even distribution of fluid velocity throughout the pipe to abruptly decrease to zero near the wall. A fully developed turbulent flow state can be assumed at $Re > 10000$. The corresponding factor between mean velocity and maximum velocity in the pipe centre is considerably higher than at laminar flow state (usually between ~ 0.8 and 0.9).

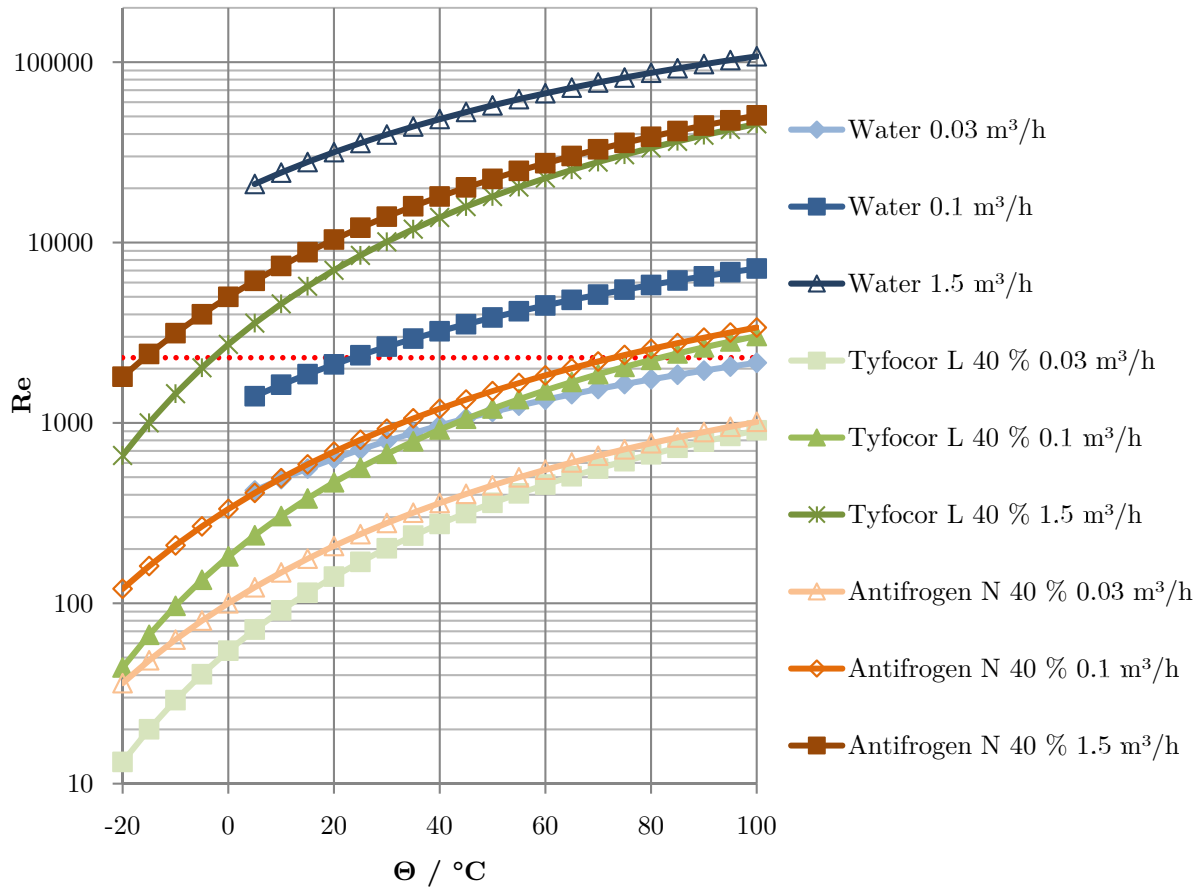

Figure 3.9: Comparison of Re of investigated fluids at different flow rates

Explanation of Figure 3.9: The red dashed line indicates the critical Reynolds number 2320 which represents the upper boundary of laminar flow state. Above this number, the transition range to turbulent flow begins, which should be completely turbulent at $Re = 10000$, depending on the condition of the piping and the constancy of the flow velocity. The following examples cover the flow characteristics for a DN 15 pipe (with $d = 17.3$ mm) at different flow rates. It should be noted that flow channels of sensors for DN 15 piping should be considerably smaller

in diameter than 17.3 mm. That would lead to higher Reynolds numbers and subsequently to turbulent flow shifting to lower flow rates than shown (turbulent flow with its more even distributed flow velocity is typically preferred inside the measuring section). However, the graph aims to give a comparison of flow states of PG-based Tyfocor L 40 %, EG-based Antifrogen N 40 % and water at corresponding flow rates. Find the Re-comparison of further fluids in Appendix 8.

At a flow rate of 30 l/h the considered fluids (including water) are in laminar condition over the entire temperature range. It is also noticeable that, apart from water, Antifrogen N 40 % has the highest Reynolds number, followed by Tyfocor L 40 %. At a flow rate of 100 l/h water is above Re_{crit} for the temperature range above ~25 °C while Antifrogen N 40 % reaches Re_{crit} at a temperature > 75 °C and Tyfocor L 40 % at a temperature > 85 °C.

For a flow rate of 1500 l/h it can be noted that the glycol-based fluids are at laminar or transient flow state at a temperature below approx. -5 °C to become turbulent at higher temperatures. Cooling applications may be subject to critical laminar to transient flow states while (solar) heating applications are all at least in the transition region between laminar and turbulent flow.

To sum it up, there are at least four crucial problems affecting the performance of a flow sensor in use with glycol:

1. The region of laminar and transient flow state is shifted to higher flow rates depending on the fluid's respective viscosity. This point is especially critical as turbulent flow state is generally preferred inside the measuring section and influences of laminar flow state are straightened out with correction factors during calibration.

2. Due to a more temperature-sensitive viscosity, the factor between lowest and highest Reynolds number in relation to a certain flow range increases compared to water when glycol-water-mixtures are in use. Thus, less predictable transient flow state regions increase, too.

3. The differences of properties between ethylene-, propylene- and higher boiling glycols as well as inhibitor composition and water ratios lead to deviating Reynolds numbers between those glycol-based fluids. Calibration for a special medium may be necessary if a certain measurement uncertainty is required.

4. Even at turbulent flow state the flow velocity profile is affected by the fluid in use as the viscosity influences that region, too. The relation between mean velocity and maximum velocity inside the pipe especially affects sensors which are highly flow profile dependent.

Subsequently, a sensor which was calibrated with water to be applied in glycol-based fluids faces at least those four influences on its performance. To give an example, a simple theoretical approach to include a fully developed turbulent flow profile [76] is presented in Figure 3.10.

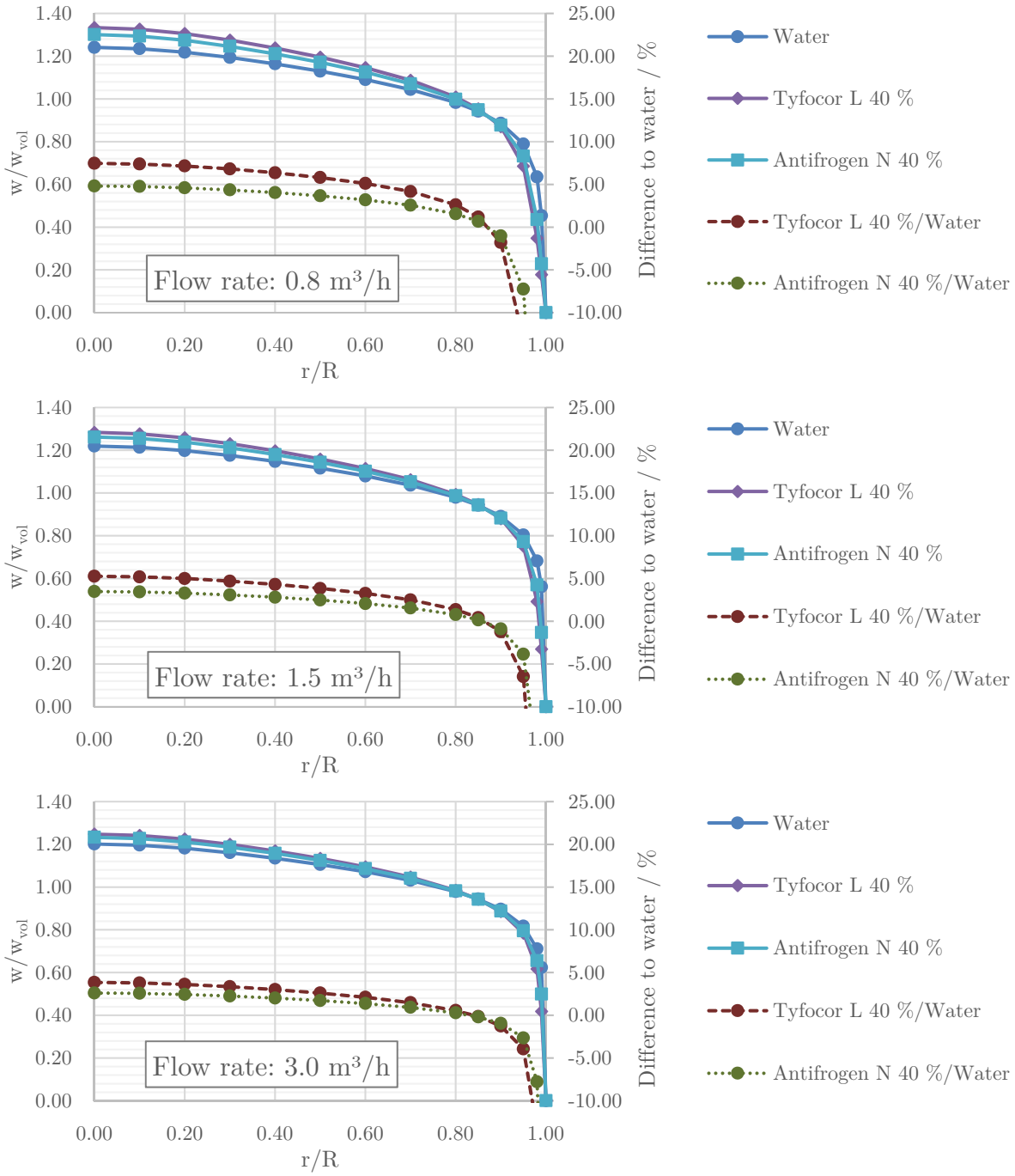

Figure 3.10: Theoretical turbulent flow profile for water and other glycol-based fluids

It gives the dimensionless factor of the local flow velocity w to the volumetric flow velocity w_{vol} depending on the radial pipe position r/R with R=4 mm at 20 °C medium temperature for three different turbulent flow rates $\dot{V}$= 0.8 m³/h, 1.5 m³/h and 3.0 m³/h. The right vertical axis gives the change of local flow velocity of the respective medium in % compared to that of water. To give an example: At a flow rate of 0.8 m³/h, water (blue solid line) exhibits a factor

of 1.24 between local flow velocity in the centre and volumetric velocity. In comparison, Tyfocor L 40 % (purple solid line) shows a corresponding factor of 1.33. That leads to an overestimation of ~7.5 % (red dotted line) between Tyfocor L 40 % and water and correspondingly ~5 % for Antifrogen N 40 % compared to water at this position. Apart from the area near the pipe wall, local velocities will be overestimated throughout the pipe's cross sectional. That is also evident for flow rates of 1.5 m^3/h and 3.0 m^3/h and the other fluid shown, though less pronounced. Subsequently, flow rate measurements could lead to differing overestimations, if no calibration-based corrections to a certain fluid or fluid group were applied. That would lead to noticeable positive errors of volume flow, depending on the measurement principle and the medium in use.

Note that a fully developed flow profile shouldn't be expected inside the volume sensor's measuring section due to disturbances arising from the tubing or design of the measuring section. Nevertheless, the approach of including a theoretical flow profile may give qualitatively useful predictions of the sensor performance. Cf. Appendix 9 for theoretical flow profile of the other investigated fluids.

3.6 Speed of Sound

In a first step, the measurements were carried out by Dr. Volker Wilkens, head of the PTB Working Group 1.62 "Ultrasonics". Due to the open construction of the measuring device, the measurements could only be carried out for temperatures of 4 °C to 50 °C due to evaporation of the water content within the mixtures. The measurements have a measurement uncertainty (k=2) of approx. 0.1 % (At present, a test rig is in use which allows measurements at higher temperatures and above ambient pressure).

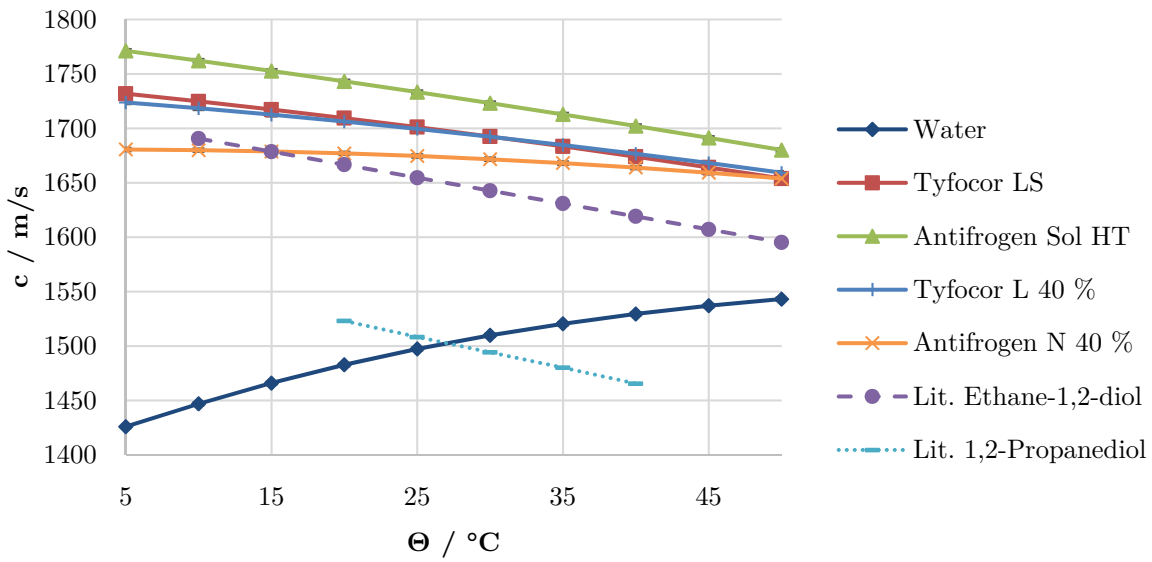

Figure 3.11: Comparison of *c(Θ)*

The speed of sound *c(Θ)* of the investigated mixtures is presented in Figure 3.11. They are compared with the values of water and literature values of EG [56] and PG [53]. The speed of sound of the glycol-based fluids differs greatly from water. The values of water lie between approx. 1420 m/s and approx. 1545 m/s [39] in the investigated temperature range, whereby the speed of sound increases for a rising temperature. The speed of sound of the other heat carrier fluids decreases with increasing temperature from approx. 1770 m/s to 1650 m/s, substantially above the sound velocity of water. Antifrogen Sol HT has the highest speed of sound, followed by the mixtures based on PG, Tyfocor LS and Tyfocor L 40 %, and ultimately EG-based Antifrogen N 40 %. There are slight differences in *c(Θ)* between PG-based fluids Tyfocor LS and Tyfocor L 40 % as *c(Θ)* of Tyfocor LS lies above *c(Θ)* of Tyfocor L 40 % at 5 °C to fall below Tyfocor L 40 % at temperatures above 30 °C. The source of this behaviour could be a different ratio of PG between the fluids but also the use of liquid inhibitors in Tyfocor LS while Tyfocor L relies on solid inhibitors.

The influence of volume fraction of water and PG-based Tyfocor L is shown in Figure 3.12. As expectable, *c(Θ)* decreases in this temperature and fraction-range with increasing water content. At low temperatures, the differences become more pronounced than at high temperatures. Noteworthy is the maximum of *c(Θ)* for the 25 %-mixture between 26 °C and 28 °C and the maximum of *c(Θ)* for the 30 %-mixture between 7 °C and 10 °C. Thus, the corresponding maximum value of *c(Θ)* shifts to lower temperatures as the content of Tyfocor L increases. The almost constant behaviour of *c(Θ)* of Tyfocor L 25 % between 20 °C and 33 °C offers interesting calibration possibilities for temperature-critical applications.

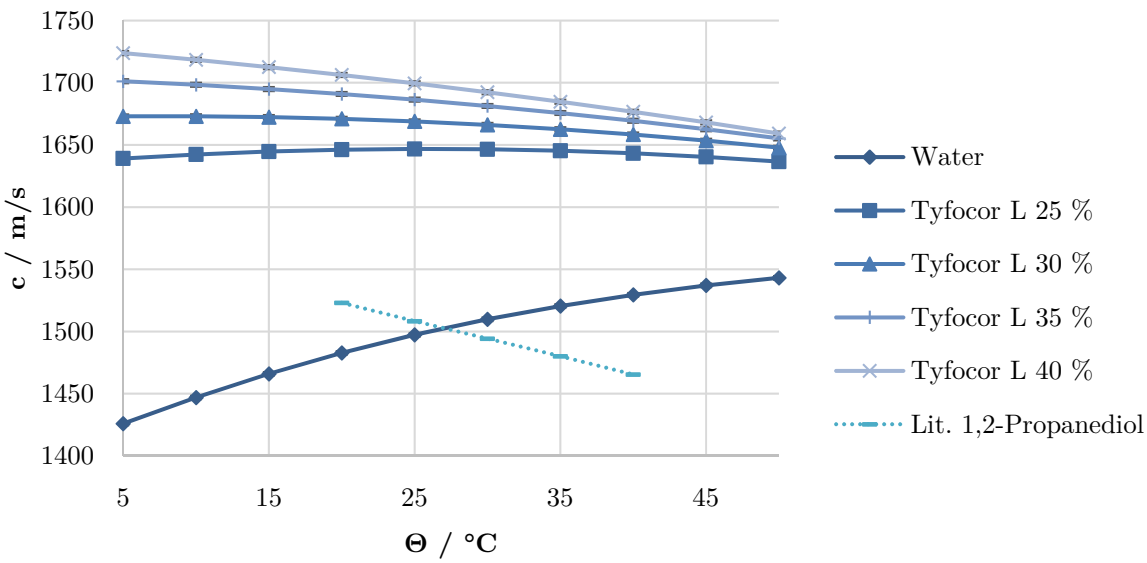

Figure 3.12: Comparison of *c(Θ)*for PG-based Tyfocor L depending on volume fraction

The influence of volume fraction of water and EG-based Antifrogen N is shown Figure 3.13. Again, *c(Θ)* decreases in this temperature and fraction-range with increasing water content. The temperature dependency, however, is less pronounced than the temperature dependency

of Tyfocor L. Again, there is a maximum of *c(Θ)* for the 25 %-mixture, this time around 40 °C, a maximum of *c(Θ)* for the 30 %-mixture at around 34 °C and a maximum of *c(Θ)* for the 35 %-mixture at around 18 °C. Comparable to Tyfocor L, the corresponding maximum value of *c(Θ)* shifts to lower temperatures as the content of Antifrogen N increases. Due to almost constant behaviour of *c(Θ)* of Antifrogen N 30 % and 35 % over a wide temperature area, there may be calibration possibilities for temperature-critical applications.

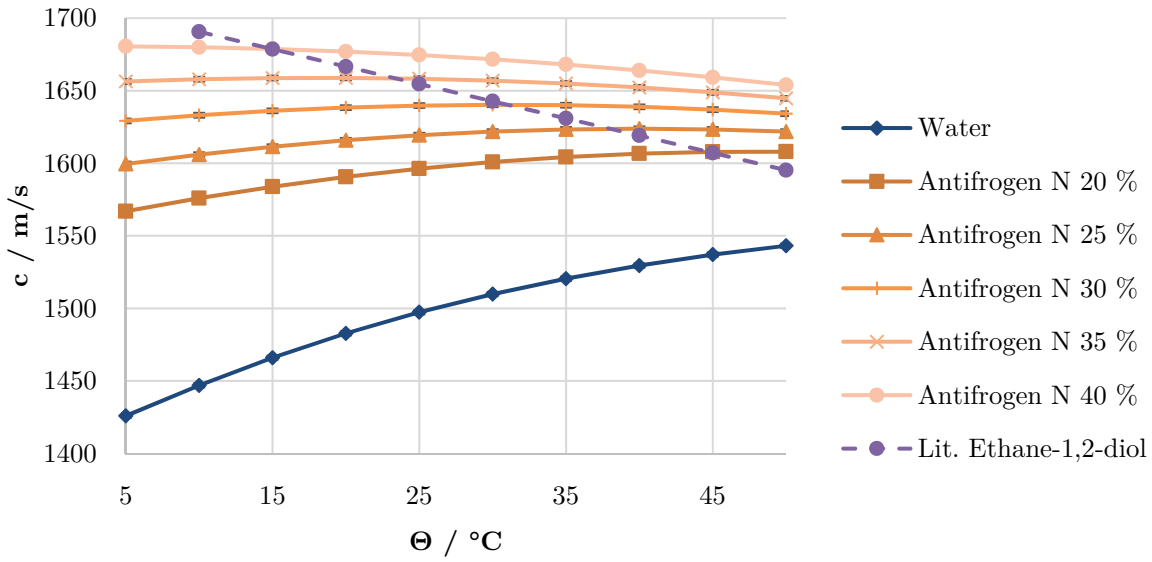

Figure 3.13: Comparison of *c(Θ)*for EG-based Antifrogen N depending on volume fraction

The speed of sound *c(Θ)* of a medium enables numerous statements regarding fluid characteristics. In this case, the data of speed of sound was used (along with the fluid's density) to determine the fluid's bulk modulus K and thereby the compressibility κ according to [77]:

$$\kappa = \frac{1}{K} \tag{18}$$

with

$$K = c^2 \cdot \rho \tag{19}$$

The compressibility κ is an especially useful quantity to describe influences of pressure changes on a fluid's specific volume v_s or density ρ (cf. 4.2.2). Figure 3.14 shows the κ-values of Tyfocor L 40 %, Tyfocor LS, Antifrogen Sol HT and Antifrogen N 40 % compared to water between 5 °C and 50 °C. Noticeable is the higher compressibility of water (from ~4.2E^{-10} Pa^{-1} to ~4.9E^{-10} Pa^{-1}) compared to the investigated fluids (~3.0 E^{-10} Pa^{-1} to ~3.5E^{-10} Pa^{-1}). Furthermore, while the compressibility of water decreases with increasing temperature, the compressibility of the other fluids increases while also being less temperature-dependent.

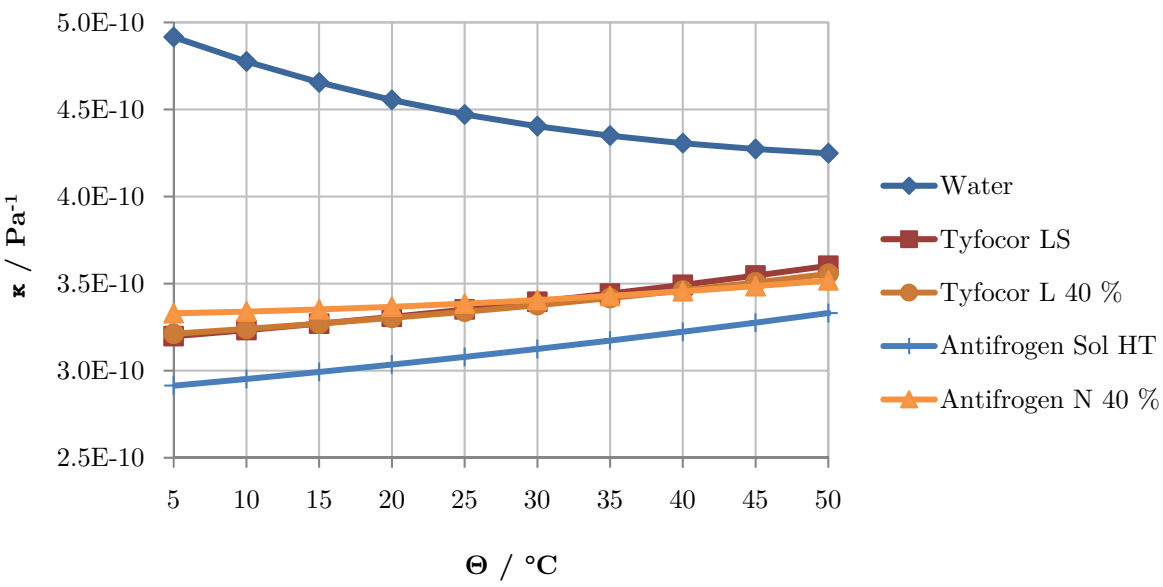

Figure 3.14: Compressibility factors of glycol-based fluids and water

3.7 Thermophysical Properties - Summary

Most fluids showed deviations of their manufacturer data to traceable measurements that are unacceptable high if legal metering with the fluid is intended. Especially heat capacity and density measurements are critical, as erroneous data directly influences heat metering (through enthalpy change calculations) if the user relies on manufacturer data. The viscosity data provided by manufacturer data sheets partly showed high deviations as well. However, those deviations influence the result only indirectly as the measuring fluid's flow profile is dependent on its viscosity. The consequence is the urgency for the end user to measure the respective property at certified laboratories to gain reliable measuring data of the fluid in use. That point is in accordance with the respective fluid's manufacturers who usually recommend independent investigations of fluid properties in their product specifications.

Table 3.2: Fluid properties in dependence of mixing ratio at 20 °C

Ratio [%]	Tyfocor L				Antifrogen N			
Property	c_p	ν	ρ	c	c_p	ν	ρ	c
Unit	kJ/(kgK)	mm²/s	kg/m³	m/s	kJ/(kgK)	mm²/s	kg/m³	m/s
20	-	-	-	-	3.90	1.76	1028.12	1590.60
25	3.96	2.56	1025.01	1646.17	3.81	1.99	1034.98	1615.87
30	3.91	3.09	1030.41	1671.00	3.70	2.28	1042.23	1638.34
35	3.83	3.71	1035.35	1690.97	3.60	2.61	1049.11	1658.83
40	3.72	4.44	1039.88	1706.26	3.50	3.00	1056.14	1676.97

Reliable fluid data of heat capacity, density, viscosity and speed of sound gives following opportunities:

1. The enthalpy change of a heating system with the medium in use can be calculated.

2. The density can be used to control the medium's glycol concentration and subsequently can be used to detect changes of the medium. Table 3.2 gives an overview of measured properties in dependence of volume fraction at a temperature of 20 °C, including density values. For example: If the ratio of the concentrate inside the respective fluid changes by 5 % from 40 % to 35 %, the density of Tyfocor L changes by ~4.5 kg/m³ (or ~0.43 %) while the density of Antifrogen N changes by ~7 kg/m³ (or ~0.66 %).

3. Knowledge of viscosity allows qualitative predictions of the flow sensor's behaviour when used in media other than the calibration medium.

4. Knowledge of the speed of sound and/or density of the respective fluid may provide the user with valuable information on fluid composition, the concentration of the respective composition and other linked physical properties.

3.8 Results of Degradation Methods

After a basis of property data for glycol-based fluids has been formed throughout the previous chapters, the aim of this chapter is to compare data of unused fluids to fluids which have been in use in order to determine a possible influence of degradation on heat metering.

As mentioned in 2.4, there is a variety of tests which aim at characterising a coolant's capability to maintain its anti-corrosive properties while degradation occurs. From a heat metering perspective, corrosion protection properties of heat conveying media under aging processes play an important but still secondary role compared to flow and heat transfer properties. The modification of the values of density, specific heat capacity and viscosity should be investigated after artificially accelerated aging to deduce the stability of the measuring fluid. Considering the above-described test methods and their results, following methods were developed to investigate the aging of glycol-water-mixtures as comprehensively as possible.

3.8.1 Method 1 - Conditions of Use

Based on ASTM D 1384 [78], method 1 can be described as a simple, fast-to-implement setup for determining the aging under operating temperatures of up to 90 °C. Each heat carrier is filled in a measuring glass in a recommended concentration (concentrates Tyfocor L and Antifrogen N in 40 % volume fraction, the ready-to-use mixtures undiluted) in a measuring glass and equipped with a metal samples package consisting of copper, brass, steel and aluminium. The fluid is held at a temperature of 90 °C for a period of 14 days while being stirred and actively supplied with air. The medium is cooled to room temperature in a two-day rhythm to measure the pH values and to perform optical tests.

During the procedure while performing the optical tests, a slight reduction of the filling level attracted attention. Although active return cooling is part of the test setup, evaporation (more crucial: fractional evaporation) cannot be ruled out.

3.8.2 Method 2 - Stagnation

Method 2 is intended to qualitatively simulate degradation under stagnation conditions. The heating of the fluid is waived here - instead, it is aged at a pressure of 3.0 MPa and an oxygen atmosphere in an autoclave. A similar method is widely used for organic substances like oils and lubricants to make predictions about their long-term stability [79].

As mentioned above, the presence of oxygen plays a major role during degradation processes. By increasing the pressure, the number of oxygen molecules inside a constant volume increases leading to accelerated chemical reactivity. Unfortunately, the experiments have to be carried out at ambient temperature due to the lack of appropriate technical equipment.

Before the measurements of density, specific heat capacity and viscosity are presented, it is noted that the recorded pH values do not allow any conclusions to be drawn on aging. The pH values remained largely constant corresponding with the findings of earlier investigations. That can be traced back to the action of the alkaline buffer substances which buffer the formation of organic acids.

3.8.3 Density

The density measurements were done likewise to chapter 3.1 using the same measurement setup and applying the same preparatory treatment. Due to its comparably low measurement uncertainty, the density is projected to be a good value to check the respective fluid for changes in composition or degradation.

After examining the first results of the density measurements, the suspicion that Method 1 may be inadequate to examine a fluid concerning changes of certain physical properties due to fractional evaporation, is supposed to hold true. The density values of all investigated fluids increased significantly indicating that fractional evaporation of water occurred.

While the decomposition seems to be pronounced differently among the tested fluids, the author supposes Degradation Method 1 to be little meaningful. Therefore, considering that former investigations applied far more harsh conditions to the media without changes of density (cf. 2.4), the results of Method 1 will be excluded from this chapter.

Figure 3.15 shows the density of the four investigated fluids, unused (red) and artificially degraded (blue) as well as the change and expanded measurement uncertainty of density in percent (violet points; orange dotted line, right vertical axis). Degradation Method 2 seems to have other influences than expected. Apart from Tyfocor LS, which shows only slight negative changes outside the measurement uncertainty at the lower end of the temperature range, all fluids show a varying pronounced drop in density. The density of Tyfocor LS slightly changes

between -0.33 kg/m³ and +0.05 kg/m³, the last value being within the measurement uncertainty. While the density values lie within measurement uncertainty above 0 °C, the values drop at lower temperatures below 0 °C. With Antifrogen Sol HT, the density drops by -0.45 kg/m³ to -0.92 kg/m³. Highest deviations occur as the temperature decreases. Tyfocor L 40 % exhibits changes from -0.35 kg/m³ to -0.75 kg/m³ showing a comparable behaviour to Antifrogen Sol HT. The density of Antifrogen N 40 % decreases by -1.96 kg/m³ to -3.27 kg/m³, with the largest changes in density again occurring especially in the negative temperature range. As the density of water is lower than the density of the respective base fluid glycol, a fractional evaporation of water is not reasonable.

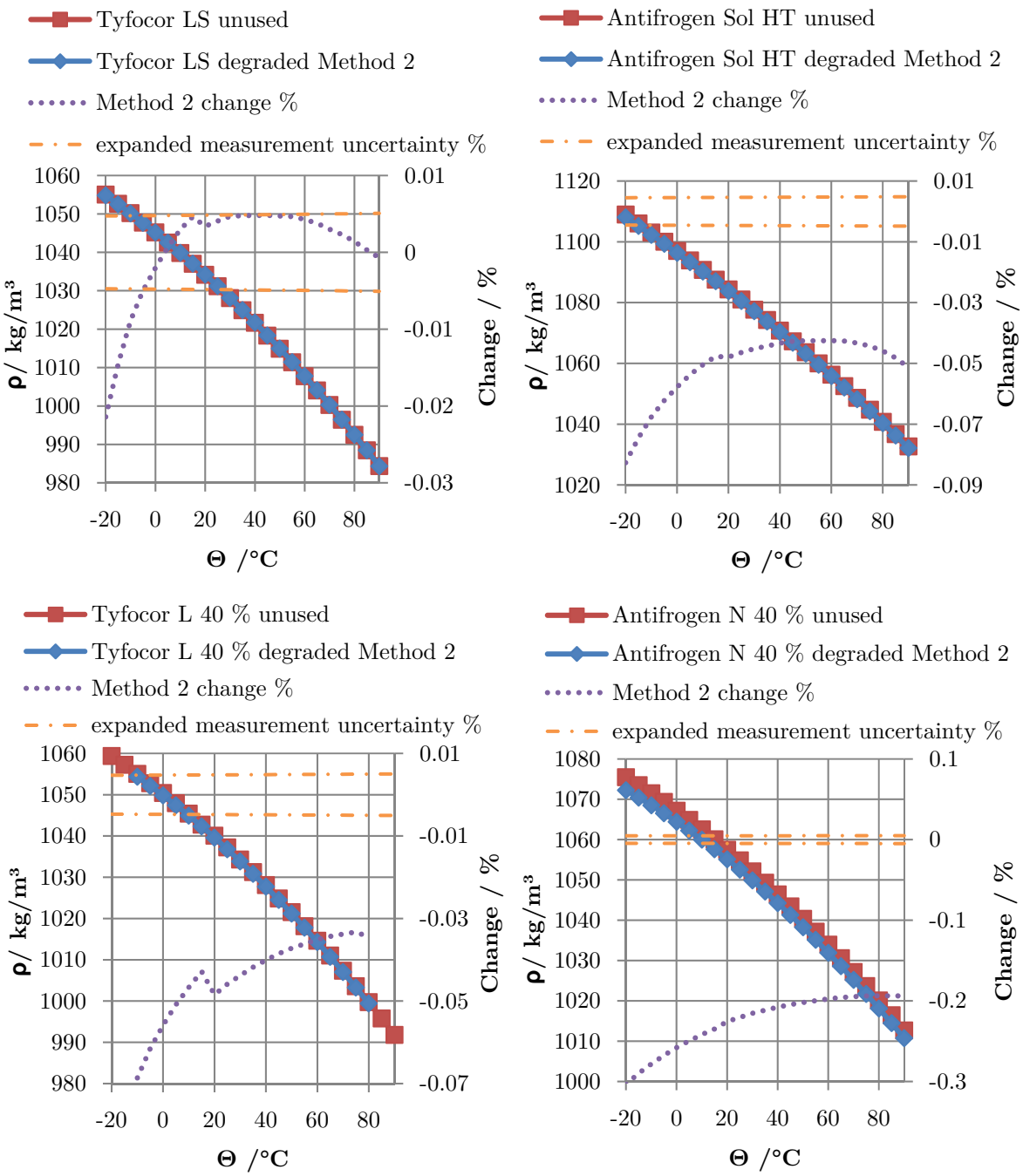

Figure 3.15: Comparison of *ρ(Θ)* of the fluids; unused and artificially degraded

3.8.4 Specific Heat Capacity

The investigations were done in a temperature range between -20 °C and 105 °C at atmospheric pressure. The investigated glycol-water-mixtures show individually more or less pronounced changes in the specific heat capacity after the artificially induced aging process, whereby the expanded measurement uncertainty of 1.5 % (k=2) should be considered.

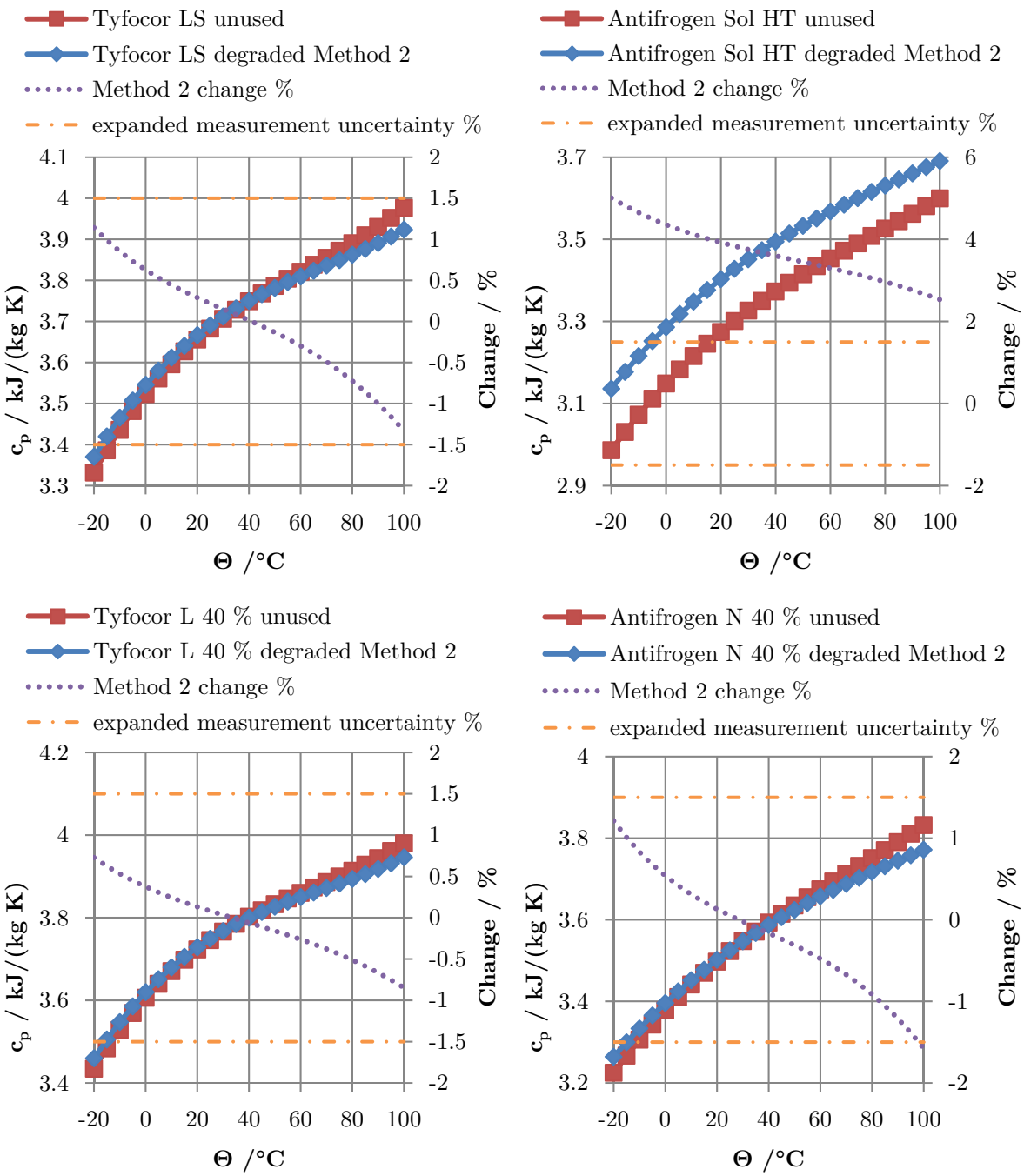

Figure 3.16: Comparison of $c_p(\Theta)$ of the fluids; unused and artificially degraded

Figure 3.16 shows the respective values of the specific heat capacity (left vertical axis) of a commercially available glycol-water-mixture in unused state (red) and in aged state (blue) as

a function of temperature. The purple dotted line indicates the percentage change of the measured values (right vertical axis) after aging in relation to the original value.

The ready-to-use Tyfocor LS, based on 1,2-propylene glycol, shows moderate changes of the measured values within the expanded uncertainty, which are characterised by an increase of the specific heat capacity up to approx. 1 % (at -20 °C) in a temperature range below 40 °C and a steady decrease of the specific heat capacity up to approx. 1.5 % (at 105 °C) in the temperature range above 40 °C.

Antifrogen Sol HT shows the largest changes of the specific heat capacity of all investigated water-glycol mixtures. Depending on the temperature, the values increase by 2.3 % to 4.8 %, whereby the maximum changes occur in the low-temperature range of the higher-boiling glycol-based heat carrier and then steadily decrease. This fluid is the only one of the investigated media to consistently show higher measured values over the entire measuring range and thus improved heat transfer properties, which are also beyond the specified measurement uncertainty of the tests.

The 1,2-propylene glycol-based Tyfocor L shows similarly to the ready-mixed Tyfocor LS slight changes in the c_p measurements, which, however, are all within the extended measurement uncertainty. At low temperatures (below approximately 35 °C) c_p increases by approx. 0.7 % (at -20 °C) to steadily drop above this temperature to a value of approx. -1.0 % (at 105 °C) below the original state.

The c_p curve of Antifrogen N 40 %, based on ethylene glycol, behaves similarly to that of the heat conveying fluids Tyfocor L and Tyfocor LS. Below a temperature of about 30 °C the values rise after the aging procedure. Above this temperature they steadily decrease. However, the changes are a bit higher with a maximum of +1.2 % (at -20 °C) and -1.8 % (at 105 °C) - thus the measured values are on the verge of extended measurement uncertainty.

In summary, it can be noted that the measured values of the specific heat capacity of three aged media have a comparable function curve (which may be associated with the uncertainty of the measurement). Compared to the heat carrier in the new state, the increase of the curves is flatter but starts at a higher output value. The values for Tyfocor L, Tyfocor LS and Antifrogen N are almost entirely within or just above the stated measurement uncertainty and should therefore be used with caution.

Apart from that, the measured values of Antifrogen Sol HT indicate a change of the fluid's heat carrier properties which is unexpected since this fluid is intended to serve in high-temperature conditions.

3.8.5 Dynamic Viscosity

In contrast to the measurements shown above the dynamic viscosity is shown to rule out possible degradation-induced density changes affecting the kinemtic viscosity. It slightly

changes for the most part (cf. Figure 3.17) with only one medium exhibiting constant deviations outside of the measurement uncertainty.

For the fluids Tyfocor LS and Antifrogen Sol HT, all measured changes in viscosity are predominantly within the measurement uncertainty.

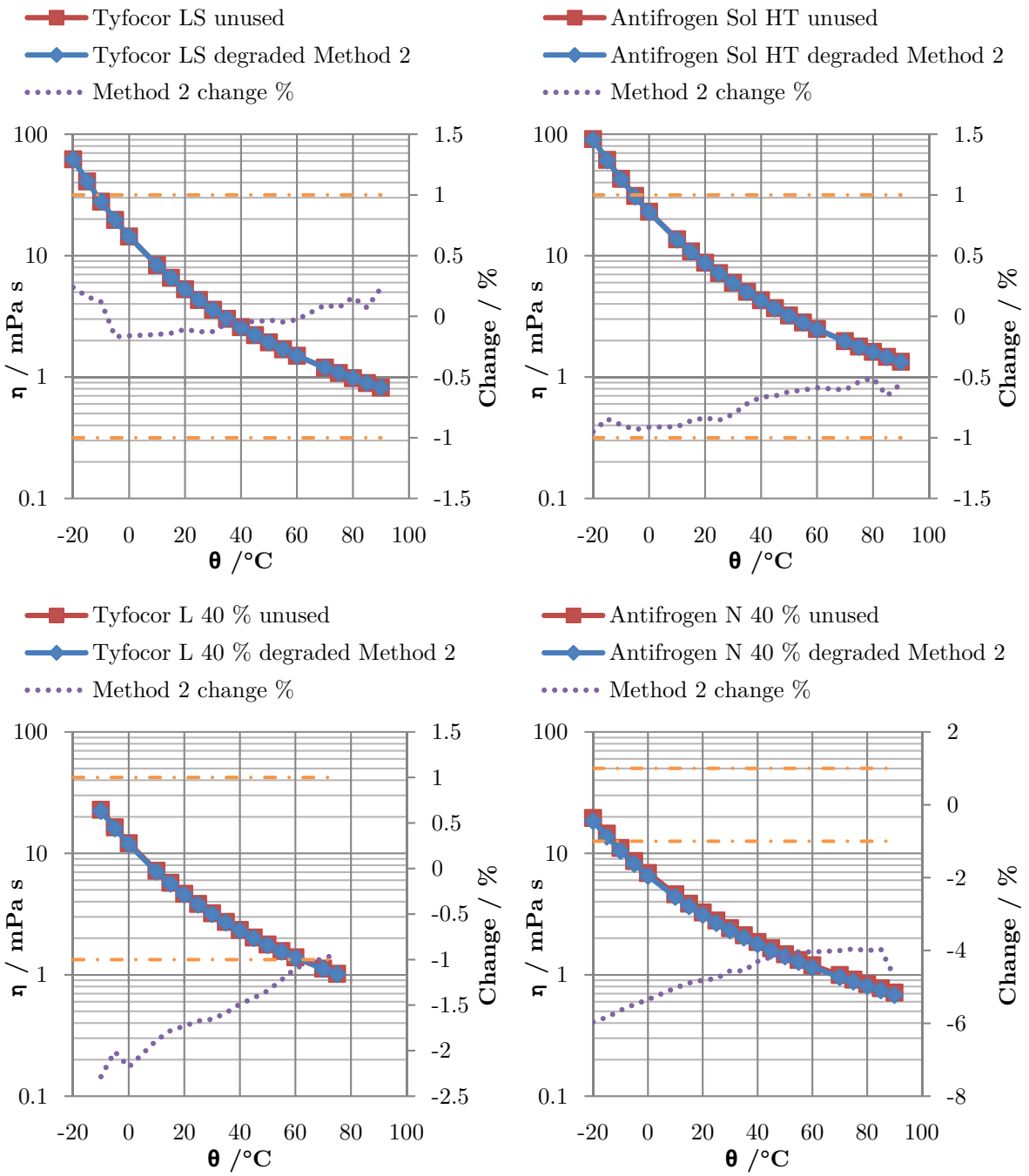

Figure 3.17: Comparison of $\eta(\Theta)$ of the fluids; unused and artificially degraded

Only at the upper limit of the temperature range, larger deviations occur which are more likely to be due to handling problems of the measuring fluid than to causes of aging (if the handling problems are somehow linked to the process of degradation is unclear). The changes of η of Tyfocor L 40 % lie slightly outside measurement uncertainty with changes between -1 % and

-2.3 %. In contrast, the viscosity of Antifrogen N 40 % decreases after aging by -4 % to -6 %, whereby the flow characteristics are improved in this case.

In summary, all but one fluid (Tyfocor LS) tend to decrease their viscosity during the degradation process.

3.8.6 Heat Coefficient *k*

According to the changes in the specific heat capacity and density, the values of the heat coefficient also vary. Since the change in density plays a minor role compared to the change in specific heat capacity, especially the latter is the main influence of degradation-induced heat coefficients changes. The investigations of the specific heat capacity showed signs of aging of different characteristics (cf. Figure 3.16). In the case of Antifrogen Sol HT, significant property changes in the form of an increase in the specific heat capacity by approx. 2.3 % to 4.8 % has been apparent. However, the other fluids showed changes in specific heat capacity, which were either within the extended uncertainty of measurement or just barely exceeding it. Therefore, the change of those heat coefficients is within the measurement uncertainty or just above it, too. Thus, the consideration of the change in the heat coefficient is limited only to Antifrogen Sol HT. For documentation purposes the respective coefficients for the other media can be found in Appendix 33. The calculation of the heat coefficients was carried out as already described in 3.4, but with adapted coefficients of the polynomials of the specific heat capacity and density.

A look at the relative changes of the heat coefficients reveals that they increased by 2.5 % to 4.6 % depending on the flow and return temperatures. Thus, the heat transfer properties change for the better in the case of Antifrogen Sol HT. The heat transfer properties of the other heat transfer mediums investigated showed changes of the values all being within the uncertainty of measurement.

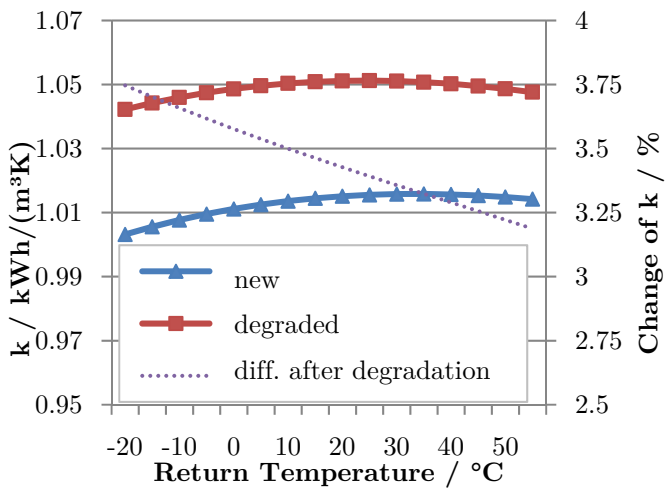

		Antifrogen Sol HT - new	Antifrogen Sol HT - degraded
$c_p(\Theta)$	c_{p0}	3.14889204	3.2861384
	c_1	0.00711891	0.00660667
	c_2	-4.5691E-05	-4.1251E-05
	c_3	1.9596E-07	1.5664E-07
$\rho(\Theta)$	ρ_0	1097.00874	1096.37019
	b_1	-0.61389887	-0.60516453
	b_2	-0.00080809	-0.00102967
	b_3	-6.1945E-06	-3.5296E-06
	b_4	3.0176E-08	2.4245E-08
	b_5	3.8336E-22	-7.2648E-11

Figure 3.18: Comparison of k of Antifrogen Sol HT at a feed temperature of 60 °C measured in return flow, new and after degradation in %

3.8.7 Remarks concerning Degradation Experiments

Prior investigations and the methods performed in this work showed that the applied accelerated degradation experiments of glycol-water mixtures are either subject to instable process-related changes in fluid composition (Method 1) or/and the transferability to in-field applications is currently not given (Method 2). The produced data's usability is questionable either way.

Collecting data from real life solar installations may be more promising to increase the reliability of data and to enable to draw conclusions on long-term in field behaviour. The outcome of a corresponding campaign should depend on following assumptions.

A statistically relevant number of systems has to be investigated. Those systems should either be subject to comparable conditions (irradiation, inclination, built-up) or categorised into sub groups with different conditions (flat plate/ vacuum tube collectors) to draw conclusions from monitored conditions (process temperature, pressure, flow rate). The medium or media in use have to possess the same composition before being filled into the system. It may be preferable to use a specific fluid coming from one batch to reduce manufacturing influences on its composition. The fluid properties have to be reliably measured prior to filling and repeatedly during a timespan of years. In that regard, a standard procedure to "draw off specimen" has to be applied to reduce sampling influences like demixing and re-filling errors.

A campaign of this scope may raise questions regarding its costs and its duration, but its outcome would bring reliable information on the desired real-life fluid stability.

4. The Volumetric Test Rig

For the testing of flow sensors in water, test rigs which are metrologically based on gravimetric measurements have widely been used. A pump conveys the measuring fluid located in a storage container through a measuring section which consists of one or more meters under test, then through one or more master meters to be ultimately fed through a diverter either to the balance container or back to the storage container. Assuming an approximately constant temperature during the measuring process and applying density and buoyancy corrections, the target volume can be determined by weighing and then be compared with the actual volume of the meter under test. A similar standard measuring device is a reservoir of which the volume is approximately known through incremental filling, which is filled instead of the weighing container. However, temperature differences and a limited resolution play a significant role.

The test stands presented are generally designed for maximum temperatures of 90 °C [80]. If flow sensors are projected to be tested or calibrated above these temperatures, closed systems are necessary. The use of a volume standard in the form of a displacement body enables to achieve very low measurement uncertainties (relative to the test stand) even at higher temperatures.

The author designed a volumetric test bench at the PTB which, based on the principle of volumetric displacement, allows the measurement of flow sensors with glycol-water-mixtures under usual operating conditions of on-roof solar flat plate systems as well as cooling systems.

4.1 General Description

The principle of volumetric displacement is based on a body which is guided into a container at a defined speed to displace a fluid contained therein. Alternatively, it is displaced by the medium if the displacer is not actively driven. The more precisely both the volume and the travelled distance of the displacer can be determined, the lower is the measurement uncertainty of the displaced volume.

This principle is particularly applicable to piston normals which are used, for example, to calibrate gas and liquid flow sensors of different sizes. For example, a bell-piston prover device used at PTB for the calibration of gas measuring devices allows to trace a volume flow with a relative uncertainty of 0.06 % [81] while a pipe prover-based calibration method used at the PTB to calibrate a test facility for flow sensors has a reported standard uncertainty of down to 0.005 % [82].

The test rig named VGP ("Volumetrischer Glykol Prüfstand" - volumetric glycol test rig), which was built within the scope of this work, will be explained in the sketch shown in Figure 4.1. The centrepiece of the test rig is a cylindric displacement body (PI=piston), which is driven into a containment (CY=cylinder) by a ball screw (S) and conveys the measuring fluid (blue) through the measuring section into a second compensating tank (R1). The test rig is

mainly designed double-walled (red hatched) to ensure thermal heating of the measuring section via thermal circuit (TC) by the thermal bath (TB). The pressure of approx. 0.1 MPa to 0.5 Mpa is provided via the compensating tank (R2) through the in-house compressed air supply (AS). Built-in sensors include a length measurement system (LM) for the travelled distance of the piston, a conductivity sensor (LF) and multiple temperature and pressure sensors (T, P).

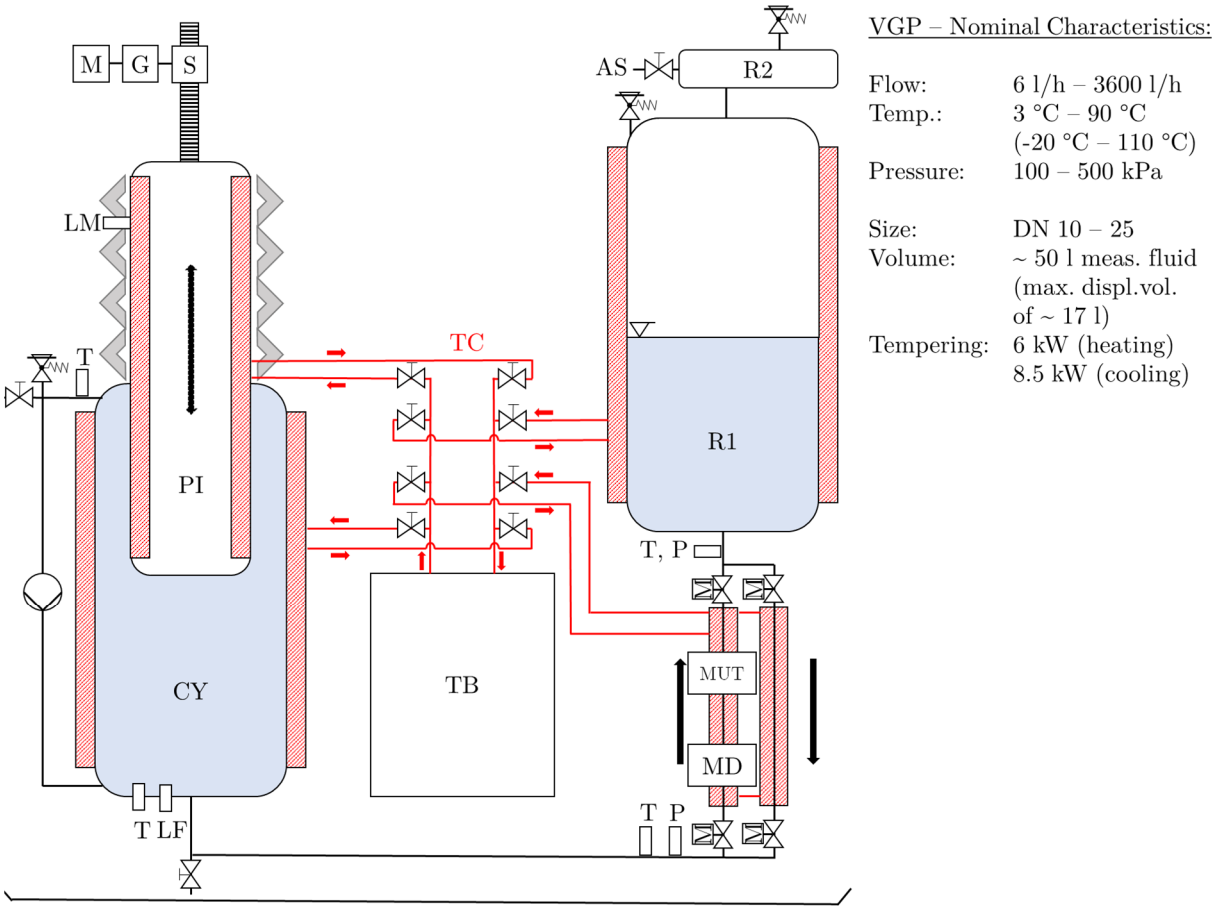

Figure 4.1: Nominal characteristics and schematic sketch of the test rig

The test rig allows flow rates between 6 l/h and 3600 l/h and currently a fluid temperature between 3 °C and 90 °C (with an option to expand to -20 °C and 110 °C). The pressure can be varied between 100 kPa and 500 kPa. Sensor sizes of DN 10 to DN 25 can be built-in.

To describe the VGP in its entirety may exceed the scope of this work (for more information on the facility and its construction, cf. [83]). Thus, the essential components of the test bench are presented in Figure 4.2. The feed of the displacer or “piston” (3) is of special relevance since it has a direct effect on the generated volume flow (constancy, repeatability, uncertainty). For the drive of the piston, a ball screw (1) is used, which allows the feed to be largely backlash-free and is suitable for continuous use due to its advantageous friction properties. The spindle is driven by a servomotor (M) with planetary gear (G), which allows the drive of low speeds and thus the generation of low volume flow with improved stick slip behaviour. The total ratio

of motor speed to spindle speed is i = 28 (planetary gear - 1:4, spindle - 1:7). A feed of 10 mm is performed per spindle revolution. The cylinder (4) is the storage tank of the fluid prior and during the measurement. The heating or cooling of the test stand is realised with double-walled components. Therefore, the cylinder, the displacer, the compensating tank and parts of the measuring section are double-walled. The respective double-walled section of the test rig is filled with a thermal oil which in turn is tempered in a bath thermostat (TB). The heat transport to the measuring fluid happens through the pipe wall which separates both thermal oil and measuring fluid. To establish a uniform fluid temperature inside the cylinder, on the one hand, the displacer is cycled up and down and on the other hand, the cylinder consists of a circulating pump. As the fluid is repeatedly moved in and out of the cylinder, the rest of the test rig including its measurement section is tempered as well.

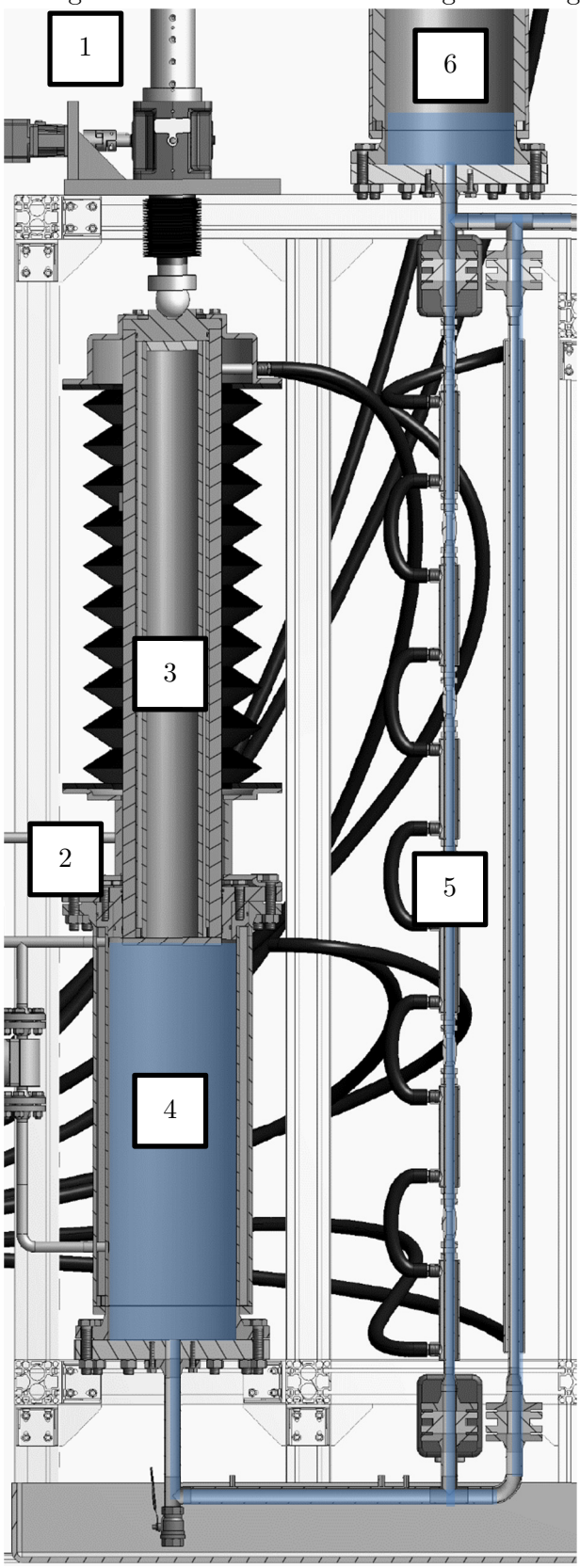

Figure 4.2: Sectional view of the test rig (blue: measuring fluid)

The sealing between the displacer and the storage tank is realised with a wiper seal. If the starting criteria is met for a measurement, the piston is guided into the cylinder at the desired feed rate which causes the measuring medium (blue) to be displaced into the measurement section (5).

It passes through the Master-Coriolis (MD) and reaches the meter under test (MUT) in the measuring section. The fluid is then displaced into the compensating tank (6) above the measuring section at which the system pressure is applied.

In the case of measurements below 0 °C or generally at low temperatures, during the displacement of the piston from the cylinder, surfaces with low temperature would be exposed. A type of protective chamber (2)

can be provided for condensation and icing protection. In principle, it consists of chamber parts which are connected to the displacer and a bellow which permits a gas-tight, axial movement and allows filling with nitrogen or actively dried air and thus prevents frost formation by means of atmospheric moisture.

The test rig can perform both the standing start/stop and flying start/stop method. Former method 'standing start/stop' is the simpler one and can be used for high as well as low accuracy measurements and is preferred for sensors which measure exact quantities of liquid, e.g. batch meters [74]. The latter method 'flying start/stop' is commonly used to forego a change of flowrate through the MUT during measurement. Here, a main source of uncertainty are errors related to timing problems.

4.2 Measurement Principle

The task to compare the volume displaced by the piston to the volume passed at the MUT may appear simple, but there are several factors that can have an influence on the measurement. During a measurement, the conservation of mass between piston and MUT applies. Thus, mass displaced by the piston equals mass flown through the MUT. Since the comparison between the volume that got displaced by the piston and the volume that passed the MUT is desired, the measuring fluid's density is of interest. To be more accurate, the ratio between the fluid's density at the piston and the fluid's density at the MUT is of interest as differences in temperature and pressure between those locations result in differing densities. Thus, the volume displaced by the piston wouldn't equal the volume that passed the meter.

This chapter focusses on the establishment of a working equation for a volume measurement performed by the test rig. In chapter 4.2.1, the volume of the piston at reference conditions is introduced. The correction of this reference volume due to conditions that differ from reference conditions during a measurement is shown in chapter 4.2.2 resulting in the introduction of the model of the volumetric test rig. It is the foundation for measurement uncertainty considerations as described in chapter 4.3.1. The considerations in following chapters are especially inspired by a detailed NIST Special Publication on flowmeter calibrations with piston provers by Pope et al. [84].

4.2.1 Reference Conditions

Based on the principle of volumetric displacement, an ideal generated volume can be described with

$$V_{ideal} = s_{ideal} A_{ideal} \tag{20}$$

where V_{ideal} is the ideal volume displaced by the displacement body with a cross sectional area A_{ideal} multiplied by its travelled distance s_{ideal}. For conditions that differ from ideal conditions p_{ideal} and ϑ_{ideal}, the cross section (in this case: a function of the piston's diameter D_P; $\frac{\pi}{4} D_P^2$) as well as the distance travelled (in this case: the distance measured by a length measurement

system s_{LM}) may change due to thermal expansion or pressure related load of the respective material. One way of dealing with that problem would be to perform sophisticated measurements of those values to characterise the system for all occurring conditions. Another way is the measurement of displacer dimensions at reference conditions ϑ_{ref} and p_{ref}, and the correction of condition-related changes using

$$D_{ref} = D_P\left(1 + \alpha_P\left(\vartheta_{ideal} - \vartheta_{ref\_P}\right)\right), \tag{21}$$

$$s_{ref} = s_{LM}\left(1 + \alpha_{LM}\left(\vartheta_{ideal} - \vartheta_{ref\_LM}\right)\right), \tag{22}$$

where α_P is the thermal expansion coefficient of the piston material and α_{LM} is the thermal expansion coefficient of the length measurement system. The influence of pressure stress on the displacement body's dimensions is supposed to be neglectable at a maximum pressure change of 0.4 MPa inside the system. Dimensions of the displacer have been measured at a reference temperature ϑ_{ref_P} of 20 °C (± 0.2 °C). The calibration certificate of the length measurement system states a reference temperature ϑ_{ref_LM} of 20 °C (± 1.0 °C). The respective temperature uncertainties have to be included.

For those reference conditions, the volume could theoretically be calculated from the reference diameter D_{ref} and the reference distance s_{ref}. However, dimensional measurements could also be affected by influences other than thermophysical conditions. Incorrect alignment (which can result in an erroneous angle) between linear scale and piston has an influence as well as the resolution of the linear scale. Subsequently, corrections must be applied according to:

$$s_{LM} = s_0(1 - s_A) + s_R \tag{23}$$

The term s_{LM} includes the measurement uncertainty caused by the linear scale's specifications s_0, the possible error of angle between linear scale and the piston's movement axis s_A and by the measuring system's resolution s_R.

The linear scale's uncertainty regarding length measurements s_0 as well as its resolution is taken from the manufacturer's calibration certificate while the angle between linear scale and piston is generously estimated to be 0.5 °.

$$s_0 = s_{meas} \pm E_{lin} \tag{24}$$

Note that an angle α between linear scale and piston that deviates from 0 ° leads to a real distance s_{real}, that is shorter than the measured distance s_0 (cf. Figure 4.3). The difference between s_0 and s_{real} is the distance X_A. The value of s_A is projected to be within 0 and X_A.

Thus, by applying the cos-function to the angle α between piston and linear scale, the estimated value of s_A is calculated according to:

$$s_A = \frac{X_A}{2} \pm \frac{X_A}{2} \tag{25}$$

with

$$X_A = s_0 - \cos\alpha\, s_0. \tag{26}$$

Following uncertainty influence caused by the linear scale's resolution must be considered.

$$s_R = 0 \pm 0.5\ \mu m \tag{27}$$

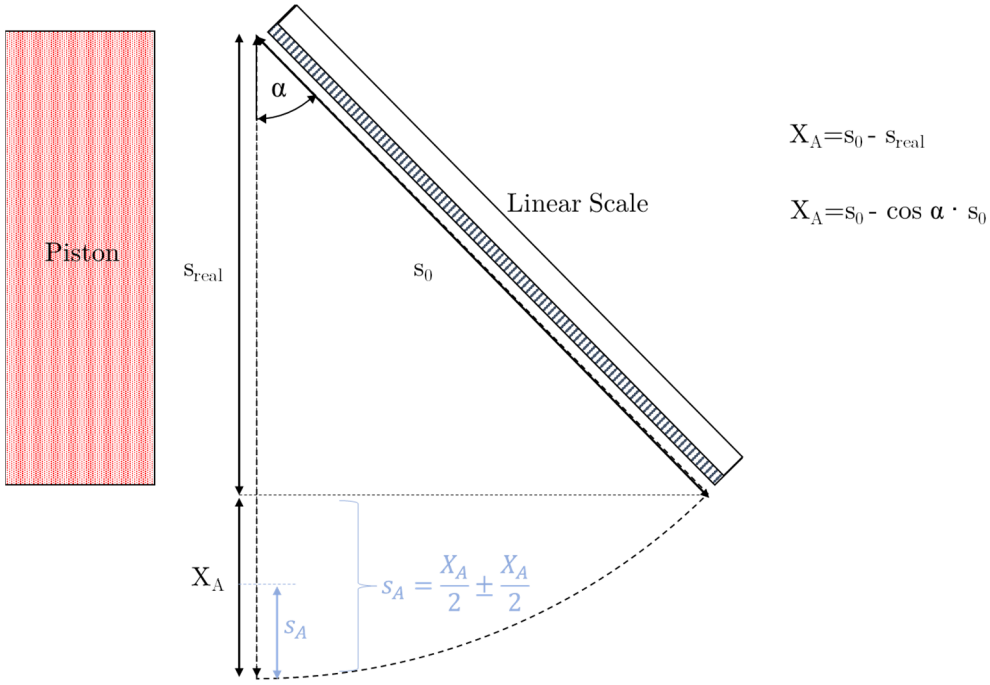

Figure 4.3: Influence of the angle α on the distance measurement (angle is exaggerated)

With equations (21), (22) and (23), the displaced volume of the piston V_{ref} can be expressed with:

$$V_{ref} = \left[s_0(1 - s_A)\left(1 + \alpha_{LM}\left(\vartheta_{ideal} - \vartheta_{ref\_LM}\right)\right) + s_R\right] \cdot \left[D_P\left(1 + \alpha_P\left(\vartheta_{ideal} - \vartheta_{ref\_P}\right)\right)\right]^2 \frac{\pi}{4}, \tag{28}$$

if the VGP is operated at reference conditions. Since the aim of this test rig is to compare the volume generated by the piston to the volume that passes the MUT, V_{ref} only equals V_{MUT} if:

- the fluid temperature inside the whole test rig equals reference temperature ϑ_{ref_P},
- the fluid pressure inside the whole test rig equals p_{ref},
- the ambient temperature equals reference temperature ϑ_{ref_LM}, and
- no leakage exists.

In practice, those reference conditions can never be fully realised. The pressure inside the VGP cannot be maintained at ambient pressure to prevent cavitation inside the tubing and to overcome pressure loss. Differing temperatures are required for this test rig. The absence of gaseous portions inside the fluid is not guaranteed, nor is the leakage of measuring fluid. Leakage of fluid can be observed through a sight glass situated above the piston sealing and through pressure changes during measurements. Stable pressure values and/or optical control

of the sealing leads to the assumption that the leak during a single measurement or during a usual series of measurements can be neglected. Although bigger gas bubbles can be detected due to noise generation, a circulating pump is used, a gas separator is employed, and the fluid is cycled prior to a measurement, the absence of smaller bubbles cannot be guaranteed. A dimensional analysis of possible areas of the test rig where bubbles could remain leads to the assumption that its volume would be up to ~0.3 ml.

4.2.2 Corrections for Conditions differing from Reference Conditions

When operating conditions occur that differ from reference conditions, they impact not only the volume displaced by the piston (due to dimensional changes) but also the rest of the test rig's piping between piston and MUT and the medium which is displaced (due to changes in density). They can be categorised according to [84] into

- reference condition effects,
- gradient effects and
- mass storage effects inside the volume between the piston and the MUT.

The corrections for *reference condition effects* Ref_i must be applied if the fluid temperature differs from ϑ_{ref_P}, the room temperature differs from ϑ_{ref_LM} and the fluid pressure differs from p_{ref}. Both the displacer volume and the fluid's density are affected. Changes of the displacer volume can be determined according to equations (21) and (22) while changes in density are assigned with

$$\rho = \rho_{ref}\left(1 + \kappa(p - p_{ref}) - \beta(\vartheta - \vartheta_{ref})\right) \tag{29}$$

where κ is the respective fluid's isothermal compressibility factor and β is the fluid's thermal expansion coefficient. The compressibility κ can be derived from the medium's density $\rho(\Theta)$ and speed of sound $c(\Theta)$ while the thermal expansion β can be derived from the medium's density $\rho(\Theta)$:

$$\kappa = \frac{1}{K} \tag{18}$$

with

$$\mathrm{K} = c^2\rho \tag{19}$$

$$\beta = -\frac{1}{\rho}\left(\frac{\delta\rho}{\delta\vartheta}\right) \tag{30}$$

Gradient effects $Grad_i$ are triggered by temperature and pressure differences between the fluid displaced by the piston inside the container and the fluid that passes the MUT resulting in differing densities at those positions. Heat transport between the fluid and the test rig's ambience can cause differences in fluid temperature while pressure differences are caused by pressure loss inside the tubing due to wall friction and installations or by hydrostatic pressure. By measuring the temperature and pressure at the piston (inside the container) and at the

MUT, those gradient effects can be corrected with the aid of equation (29) and the conservation of mass. Accordingly, the volume that passed the MUT equals the volume that got displaced by the piston multiplied by the density ratio between piston and MUT.

Furthermore, *mass storage effects* MS_i arise from temporal density changes of the fluid inside the connecting volume V_{CV} between container and MUT as well as the "dead volume" inside the cylinder V_C^f and dimensional changes of the piping due to thermal expansion. As the temperature and pressure inside the connecting volume change during a measurement, the fluid's density of this volume as well as the connecting volume's pipe dimensions are affected. That holds true for the "dead volume" inside the cylinder which is the volume that remains inside the container while the piston strokes. That may lead to the effect that the mass leaving the cylinder doesn't equal the mass passing the MUT. For example, if the temperature of the dead volume increases during a measurement, its density decreases causing a higher mass to reach the MUT than displaced by the piston. Mass storage can be corrected with equation (29) and dimensional corrections in accord with equation (21).

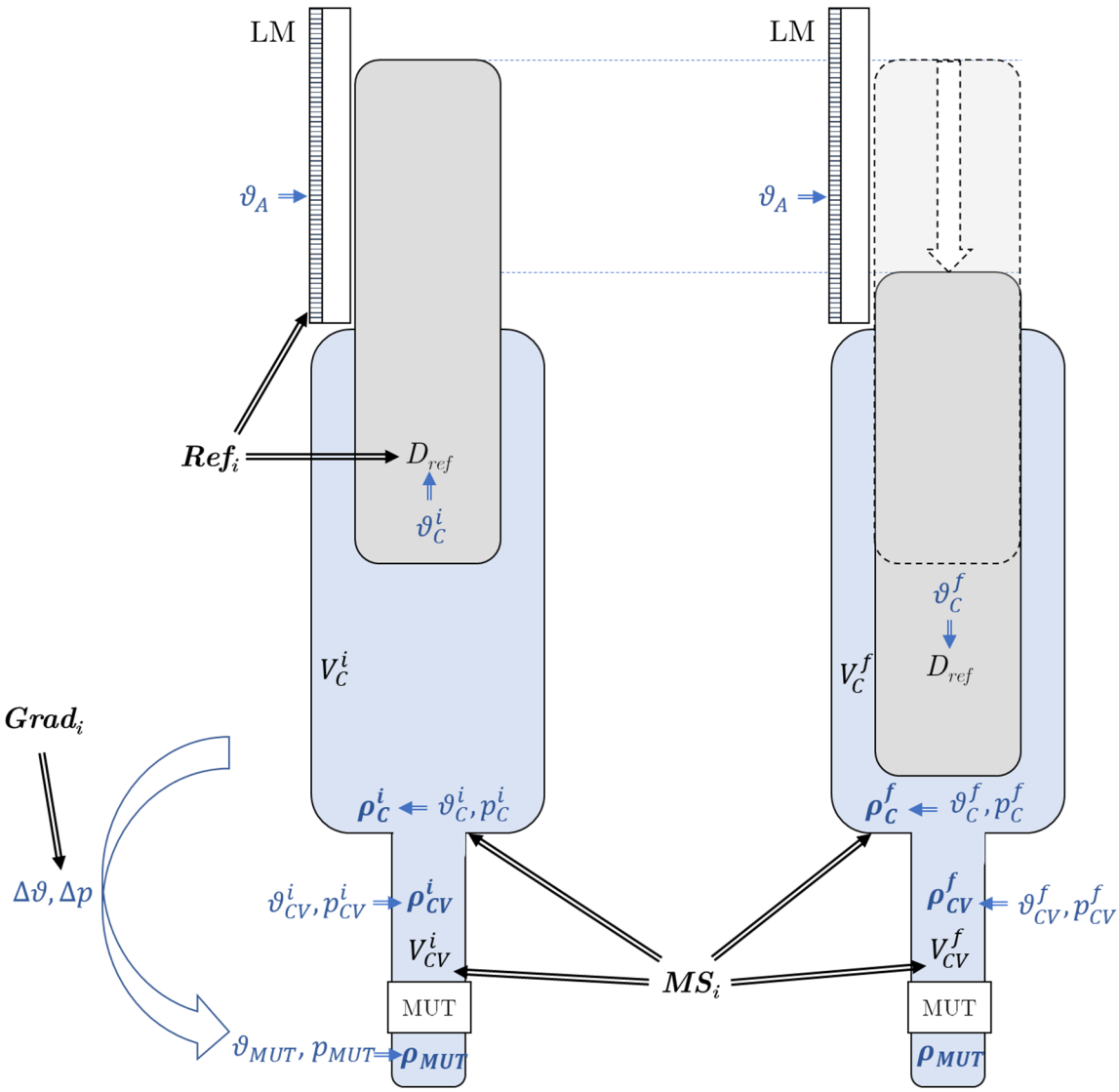

Figure 4.4: Influences on the test rig between the start (left) and stop (right) of a measurement

Figure 4.4 gives an overview of the effects the test rig and its components are exposed to at the start (left) and end (right) of a measurement cycle. As mentioned in chapter 4.2, mass displaced by the piston is compared to the mass flown trough the MUT. Thus, to compare a volume displaced with the volume flown through the MUT, the respective densities must be considered. For a measurement, the considered fluid volume consists of the fluid volume inside the cylinder V_C and the fluid volume inside the connecting volume V_{CV}. As the piston is driven from its initial position to its final position, it causes the volume inside the cylinder to decrease from its initial volume V_C^i to its final volume V_C^f. In addition, the fluid volume inside the connecting pipes may change from V_{CV}^i to V_{CV}^f. By multiplying the respective temperature and pressure dependent densities ρ_C^i , ρ_C^f, ρ_{CV}^i and ρ_{CV}^f, the corresponding mass flown through the MUT m_{MUT} can be calculated according to:

$$m_{MUT} = \left(V_C^i \rho_C^i - V_C^f \rho_C^f\right) + \left(V_{CV}^i \rho_{CV}^i - V_{CV}^f \rho_{CV}^f\right) \tag{31}$$

Using the method of adding and subtracting $V_C^f \rho_C^i$ and $V_{CV}^f \rho_{CV}^i$ to the right side of equation (31) as shown in [85], m_{MUT} can be calculated with

$$\begin{aligned} m_{MUT} &= \Big(V_C^i \rho_C^i - V_C^f \rho_C^f + \left(V_C^f \rho_C^i - V_C^f \rho_C^i\right)\Big) \\ &\qquad + \Big(V_{CV}^i \rho_{CV}^i - V_{CV}^f \rho_{CV}^f + \left(V_{CV}^f \rho_{CV}^i - V_{CV}^f \rho_{CV}^i\right)\Big) \\ &= \Big(\left(V_C^i \rho_C^i - V_C^f \rho_C^i\right) + \left(V_C^f \rho_C^i - V_C^f \rho_C^f\right)\Big) \\ &\qquad + \Big(\left(V_{CV}^i \rho_{CV}^i - V_{CV}^f \rho_{CV}^i\right) + \left(V_{CV}^f \rho_{CV}^i - V_{CV}^f \rho_{CV}^f\right)\Big). \end{aligned} \tag{32}$$

With $V_C^i - V_C^f = \Delta V_C^{if}$ as the volume displaced by the piston and $V_{CV}^i - V_{CV}^f = \Delta V_{CV}^{if}$ as the change of the connecting volume during a measurement and $\rho_C^i - \rho_C^f = \Delta\rho_C^{if}$ as the density difference in the container and $\rho_{CV}^i - \rho_{CV}^f = \Delta\rho_{CV}^{if}$ as the density difference in the connecting volume during a measurement, following equation can be used:

$$m_{MUT} = \Delta V_C^{if} \rho_C^i + V_C^f \Delta\rho_C^{if} + \Delta V_{CV}^{if} \rho_{CV}^i + V_{CV}^f \Delta\rho_{CV}^{if} \tag{33}$$

To get V_{MUT}, m_{MUT} must be divided by $\tilde{\rho}_{MUT}$, which is the averaged density at the MUT:

$$V_{MUT} = \frac{\Delta V_C^{if}\ \rho_C^i}{\tilde{\rho}_{MUT}} + \frac{V_C^f \Delta\rho_C^{if}}{\tilde{\rho}_{MUT}} + \frac{\Delta V_{CV}^{if} \rho_{CV}^i}{\tilde{\rho}_{MUT}} + \frac{V_{CV}^f \Delta\rho_{CV}^{if}}{\tilde{\rho}_{MUT}} \tag{34}$$

The volume displaced by the piston (or the difference between initial and final volume inside the cylinder) ΔV_C^{if} can be described with the piston's reference volume at reference conditions V_{ref} (cf. equation (28)), which leads to:

$$V_{MUT} = \frac{V_{ref}\ \rho_C^i}{\tilde{\rho}_{MUT}} + \frac{V_C^f \Delta\rho_C^{if}}{\tilde{\rho}_{MUT}} + \frac{\Delta V_{CV}^{if} \rho_{CV}^i}{\tilde{\rho}_{MUT}} + \frac{V_{CV}^f \Delta\rho_{CV}^{if}}{\tilde{\rho}_{MUT}} \tag{35}$$

It becomes obvious that the volume at the MUT V_{MUT} is depending on 9 variables C_i which will be discussed briefly:

V_{ref}: The reference volume is subject to *reference condition effects* that affect the dimension of the displacement body and the length measurement. It is accordingly corrected using equations (21) and (22).

$$C_1 = V_{ref}\ \left(1 + 2\alpha_P\left(\vartheta_C^i - \vartheta_{ref\_p}\right) + \alpha_{LM}\left(\vartheta_A - \vartheta_{ref\_LM}\right)\right)$$

ρ_C^i: The initial density in the cylinder is subject to *reference condition effects*. It is corrected using the respective physical laws described in equation (29).

$$C_2 = \left(1 + \kappa\left(p_C^i - p_{ref}\right) - \beta_C\left(\vartheta_C^i - \vartheta_{ref}\right)\right)$$

$\tilde{\rho}_{MUT}$: The averaged density at the MUT is subject to *reference condition* and *gradient effects*. It is corrected using the respective physical laws described in equation (29).

$$C_3 = \left(1 + \kappa\left(\tilde{p}_{MUT} - p_{ref}\right) - \beta_{CV}\left(\tilde{\vartheta}_{MUT} - \vartheta_{ref}\right)\right)$$

V_C^f: The dead volume inside the cylinder is subject to *reference condition effects*, likewise to V_{ref}. It is corrected with equations (21) and (22).

$$C_4 = \left(V_C^i\ \left(1 + 3\alpha_P\left(\vartheta_C^i - \vartheta_{ref\_p}\right)\right) - V_{ref}\ \left(1 + 2\alpha_P\left(\vartheta_C^i - \vartheta_{ref\_p}\right) + \alpha_{LM}\left(\vartheta_C^i - \vartheta_{ref\_LM}\right)\right)\right)$$

$\Delta\rho_C^{if}$: The density inside the cylinder during a measurement is subject to *mass storage effects* that occur inside the cylinder. It is corrected using the respective physical laws described in equation (29).

$$C_5 = \left(\left(1 + \kappa\left(p_C^i - p_{ref}\right) - \beta_C\left(\vartheta_C^i - \vartheta_{ref}\right)\right) - \left(1 + \kappa\left(p_C^f - p_{ref}\right) - \beta_C\left(\vartheta_C^f - \vartheta_{ref}\right)\right)\right)$$

ΔV_{CV}^{if}: The change of the connecting volume during a measurement is subject to temperature-induced dimensional changes of the piping. It is corrected using equations (21) and (22).

$$C_6 = \left(V_{CV}^i\ \left(1 + 3\alpha_{CV}\left(\vartheta_{CV}^i - \vartheta_{ref}\right)\right) - V_{CV}^i\ \left(1 + 3\alpha_{CV}\left(\vartheta_{CV}^f - \vartheta_{ref\_p}\right)\right)\right)$$

ρ_{CV}^i: The initial density inside the connecting volume is subject to *mass storage effects* that occur inside the connecting volume. It is corrected using the respective physical laws described in equation (29).

$$C_7 = \left(1 + \kappa\left(p_{CV}^i - p_{ref}\right) - \beta_{CV}\left(\vartheta_{CV}^i - \vartheta_{ref}\right)\right)$$

V_{CV}^f: The connecting volume is subject to *reference condition effects* that occur inside the connecting volume. It can be corrected using the respective physical laws described in equation (21).

$$C_8 = \left(V_{CV}^i\ \left(1 + 3\alpha_{CV}\left(\vartheta_{CV}^f - \vartheta_{ref}\right)\right)\right)$$

$\Delta\rho_{CV}^{if}$: The density change in the connecting volume during a measurement is subject to *mass storage effects*. It is corrected using the respective physical laws described in equation (29).

$$C_9 = \left(\left(1 + \kappa\left(p_{CV}^i - p_{ref}\right) - \beta_{CV}\left(\vartheta_{CV}^i - \vartheta_{ref}\right)\right) - \left(1 + \kappa\left(p_{CV}^f - p_{ref}\right) - \beta_{CV}\left(\vartheta_{CV}^f - \vartheta_{ref}\right)\right)\right)$$

Based on equation (35), equation (36) represents the simplified model for the volumetric test rig VGP without leakage and gas inside the relevant volume.

$$V_{MUT} = \frac{C_1 \cdot C_2}{C_3} + \frac{C_4 \cdot C_5}{C_3} + \frac{C_6 \cdot C_7}{C_3} + \frac{C_8 \cdot C_9}{C_3} \tag{36}$$

As stated above, the absence of gaseous volume inside the measurement section of the test rig cannot be guaranteed, though arrangements of prevention have been made. Dimensional analysis yields a remaining gas volume V_G of up to 0.3 ml (or 19 ppm for a displaced volume of 15.7 l) after filling the test rig, which could be subject to pressure and temperature changes resulting in an contribution to the volume. It is supposed that this volume of gas is situated at the upper part of the cylinder and remains there during a measurement.

Three cases have to be considered: Case (I) describes the change of volume due to a differing pressure from the pressure during filling. Case (II) describes the change of the volume due to measurement temperatures that differ from the temperature during filling. Case (III) describes the change of volume during a measurement.

(I): As the temperature inside the cylinder remains approximately constant during the pressurisation of the system, the temperature influence is neglected. For an ideal gas at constant temperature, the volume V_G is solely depending on the pressure ratio between filling pressure and operating pressure inside the cylinder according to

$$V_G^{op} = V_G^{fill}\left(p_A / p_C^i\right) \tag{37}$$

with V_G^{op} and V_G^{fill} being the gas volume at initial operating pressure and filling pressure, respectively, and p_A being the ambient pressure during filling and p_C^i being the initial operating pressure inside the cylinder.

(II): The test rig operates at various temperatures. While the temperature is free to choose, the operating pressure is usually remained approximately constant between differing temperatures. Thus, the initial measurement gas volume V_G^i is solely depending on the temperature ratio between (ambient) filling temperature T_A and initial measurement temperature T_C^i according to:

$$V_G^i = V_G^{op}\left(T_C^i / T_A\right) \tag{38}$$

(III): The initial measurement pressure and temperature is reached. The change of temperature inside the cylinder is low during a measurement, so the temperature influence is neglected. For an ideal gas at constant temperature, the volume V_G is again solely depending on the pressure ratio between initial pressure and final pressure inside the cylinder according to:

$$V_G^f = V_G^i(p_C^i/p_C^f) \tag{39}$$

with V_G^f and V_G^i being the final and initial volume of gas, respectively, and p_C^i being the initial pressure and p_C^f being the final pressure inside the cylinder during a measurement.

As the gas volume is supposed to remain inside the cylinder during a measurement, its contribution to the volume that passes the MUT is subject to the initial cylinder temperature (having an influence on the size of V_G^i), the cylinder pressure change during a measurement (having an influence on the volume change of V_G^i) and the piston stroke length (manifesting in the ratio of gas volume to overall displaced volume). Thus, during a measurement, only the change of V_G^i to V_G^f (ΔV_G) directly contributes to the volume at the MUT. A combination of equations (37), (38) and (39) leads to:

$$\Delta V_G = V_G^f - V_G^i = \left(V_G^{fill}\left(\frac{p_A}{p_C^i}\right)\left(\frac{T_C^i}{T_A}\right)\left(\frac{p_C^i}{p_C^f}\right)\right) - \left(V_G^{fill}\left(\frac{p_A}{p_C^i}\right)\left(\frac{T_C^i}{T_A}\right)\right). \tag{40}$$

$$\Delta V_G = C_{10}$$

As V_G^f solely differs from V_G^i in terms of the ratio of initial and final pressure inside the cylinder and the pressure strictly rises during the measurement, the figure of ΔV_G is negative. Thus, V_G decreases during a measurement which leads to the effect that less volume of fluid reaches the MUT than displaced by the piston.

That effect (simplified with the variable C_{10}) can be added to Equation (36) which leads to equation (41). It is the basis for measurement uncertainty considerations as described in chapter 4.3.9.

$$V_{MUT} = \frac{C_1 \cdot C_2}{C_3} + \frac{C_4 \cdot C_5}{C_3} + \frac{C_6 \cdot C_7}{C_3} + \frac{C_8 \cdot C_9}{C_3} + C_{10} \tag{41}$$

4.3 Measurement Uncertainty

If the result of a measurement of a physical quantity is reported, its quality should preferably be characterised to provide the result with a reliability that allows their comparison with other values or standards [86]. According to the guide to the expression of uncertainty in measurements (GUM) [86], a measurand Y is a function f of n input quantities X_i.

$$Y = f(X_1, X_2, \dots, X_n) \tag{42}$$

Its input quantities X_1, X_2, ..., X_n can be categorised as Type A quantities (values x_i and their respective uncertainties $u(x_i)$ are statistically evaluated) and Type B quantities (values x_i and their uncertainties $u(x_i)$ are estimated by other means). If the estimate of a measurand Y is denoted by y using input estimates x_i for the quantities X_i, the output estimate is given by

$$y = f(x_1, x_2, \dots, x_n). \tag{43}$$

The impact of the uncertainty $u(x_i)$ of an input value x_i on the estimated value y is calculated through partial differentiation of the model function of y with its input values (cf. equation (44)). The determined sensitivity coefficients c_i are multiplied with their input uncertainties $u(x_i)$, squared and summed according to equation (45) to receive the combined variance $u^2(y)$. Note, that this simple form is valid only if variables x_i are uncorrelated (which is assumed in this work). The square root of the combined variance $u^2(y)$ gives the standard measurement uncertainty $u(y)$.

$$c_i = \frac{\partial y}{\partial x_i} \tag{44}$$

$$u^2(y) = \sum_{i=1}^{n} (c_i u(x_i))^2 \tag{45}$$

$$u(y) = \sqrt{\sum_{i=1}^{n} (c_i u(x_i))^2} \tag{46}$$

The standard measurement uncertainty shown in equation (46) describes a confidence level of ~68.27 % if the resulting probability distribution is a normal one. With a coverage factor $k=2$, the expanded measurement uncertainty yields a level of confidence of ~95.45 %, which is recommended in practice [87].

4.3.1 Model of Uncertainty

In accordance with 4.2 and especially equation (41), this chapter introduces the model of uncertainty for the volume that passed the MUT, V_{MUT}. Its input quantities und uncertainties listed below will be discussed in following chapters:

- reference volume V_{ref} consisting of piston dimensions and length measurement
- cylinder volume V_C and connecting volume V_{CV}
- temperature measurements at the cylinder ϑ_C, the connecting volume ϑ_{CV}, at the MUT $\tilde{\vartheta}_{MUT}$ and of the ambience ϑ_{Amb}
- pressure measurements at the cylinder p_C, the connecting volume p_{CV} and at the MUT $\tilde{p}_{MUT}$
- thermal expansion coefficients of the piston material α_{LP} and length measuring system α_{LM}
- thermal expansion coefficients in the cylinder β_C and in the connecting volume β_{CV} of the respective medium in use
- compressibility factor in the cylinder κ_C and in the connecting volume κ_{CV} of the respective medium in use
- the influence of a probable gaseous volume inside the system V_G.

4.3.2 Reference Volume

There are three commonly used methods to determine the volume of a volumetric prover, the

- water draw method [88],
- a flowmeter used as transfer standard [88] or
- dimensional measurements of the displacer and its length measurement system [89].

The method used in this work focusses on the traceable determination of the dimensions of the displacer and of its distance travelled to generate a volume. Accordingly, special attention has been paid to the manufacturing (grinding, honing) of the displacement body as well as the measurement of its dimensions.

4.3.2.1 Piston Diameter

The uncertainty of the piston diameter consists of individual uncertainties regarding the measurement system (specifications, calibration, temperature dependency, repeatability and resolution) as well as the piston's shape imperfections (angular and along the axis).

To determine the shape of the displacer with high resolution, the cylindrical body was measured by 36 angular positions (resulting in 10 ° steps between each position) along the circumference at 18 positions along the axis of displacement, each position having a distance of 50 mm to the next axis position (between x = 34 mm and x = 884 mm; cf. Figure 4.5).

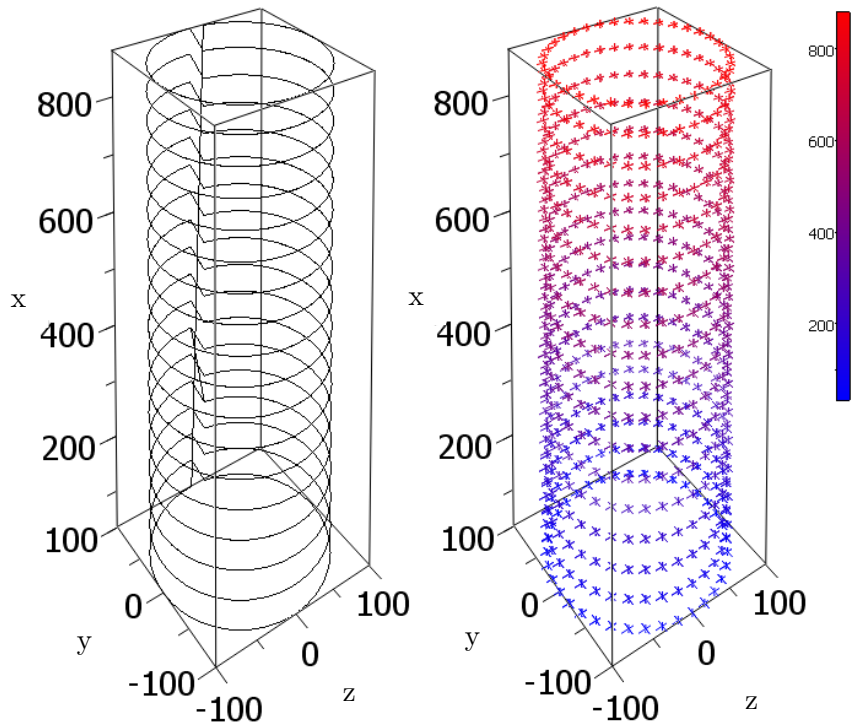

Figure 4.5: Measuring grid / point cloud from measured data (not to scale)

The general procedure of the diameter calculations in this work are:

- the use of raw measured data to detect form errors (due to imperfect manufacturing),

- applying a circle fit for each measuring plane based on its measured points to calculate its ideal diameter,
- determining the Piston Diameter D_P by averaging the plane's fitted diameters $D_{Pl\,i}$.

The measurements were carried out at the PTB, Department 5.3, with a coordinate measuring machine (CMM) using a mechanical stop detection system (LEITZ Infinity 12.10.7) at a reference temperature of 20 °C (± 0.2 °C). Under those conditions, the regularly calibrated CMM has a standard uncertainty of 0.5 µm (0.3 µm + L/1000) for each distance measurement of L < 200 mm. The cylinder was supported at two positions with one of the supporting points being within the measuring range. Accordingly, two measurement sets were carried out, the support point being shifted during the second set, so that the missing diameters could also be determined. A positive side effect is the presence of two data sets for most positions. To give an example of the CMM's repeatability between first and second set: A total of 576 radii could be calculated for each set of raw data with 504 radii being measured twice. Of those 504 radii, a comparison of the values measured at the respective positions between first and second set yields maximum deviations lower than 0.8 µm. Deviations between diameters calculated based on raw data at the respective positions were lower than 0.7 µm. Thus, it is assumed that a combination of both data sets to calculate the diameter of the piston is valid.

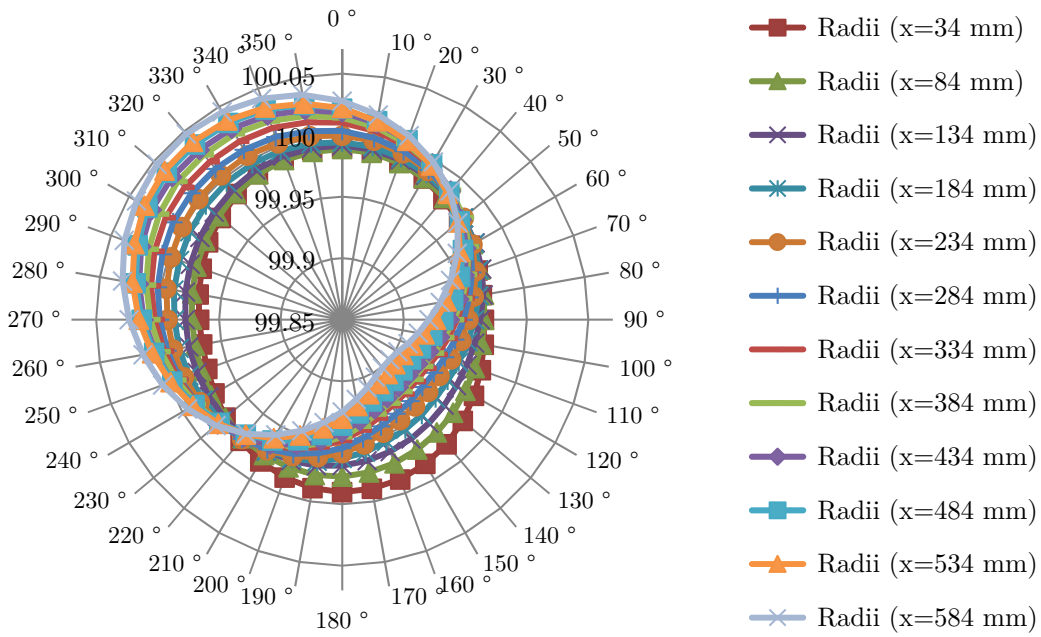

Figure 4.6: Radii calculated from raw data points for 36 angular positions. Radial axes range from 99.85 mm (centre) to 100.05 mm; scaled ~500:1

Radii calculated from raw measurement data points (x_i, x_i, z_i) of the first set for 36 angular positions are presented in Figure 4.6 for the relevant x-values from 34 mm to 584 mm (with values for x=184 mm and x=234 mm taken from the second set of measurements). Note, that the radial axes [mm] are scaled ~500:1 to make deviations visible. Recognisable is a centre shift of the radii towards the upper left corner for increasing x-axis values as well as slight differences

from a perfect circle shape throughout the measured range. The respective raw diameters can be calculated by summing up opposing radii.

However, to calculate the volume of a body, its cross-sectional area is of interest. For an ideal cylinder, the cross-sectional area is solely depending on its ideal circle shape formed by an ideal diameter or radius. As observed in Figure 4.6, the shape of the respective circles along the x-axis is not ideal (neither along the x-axis nor along its angular position). Subsequently, a circle fit must be applied to the measured data for any given measuring plane along the x-axis.

A common way to fit an idealised circle is to average all measured raw diameters as shown in [89] and [90]. This method includes all angular and longitudinal form imperfections of the body to calculate an ideal diameter. However, the result does not include insights on the centre of each circle fit.

As the cross-sectional area is of interest, in this work the respective diameters of the measuring planes along the piston's displacement axis were determined according to the LSC (least square circle) method [91]. Thus, the raw measured points are considered to be in an equilibrium to calculate an ideal circle from their error squares. Benefits of this method include the knowledge of the ideal circle's centre and the correction of form errors arising from imperfect manufacturing of the piston (cf. Figure 4.7).

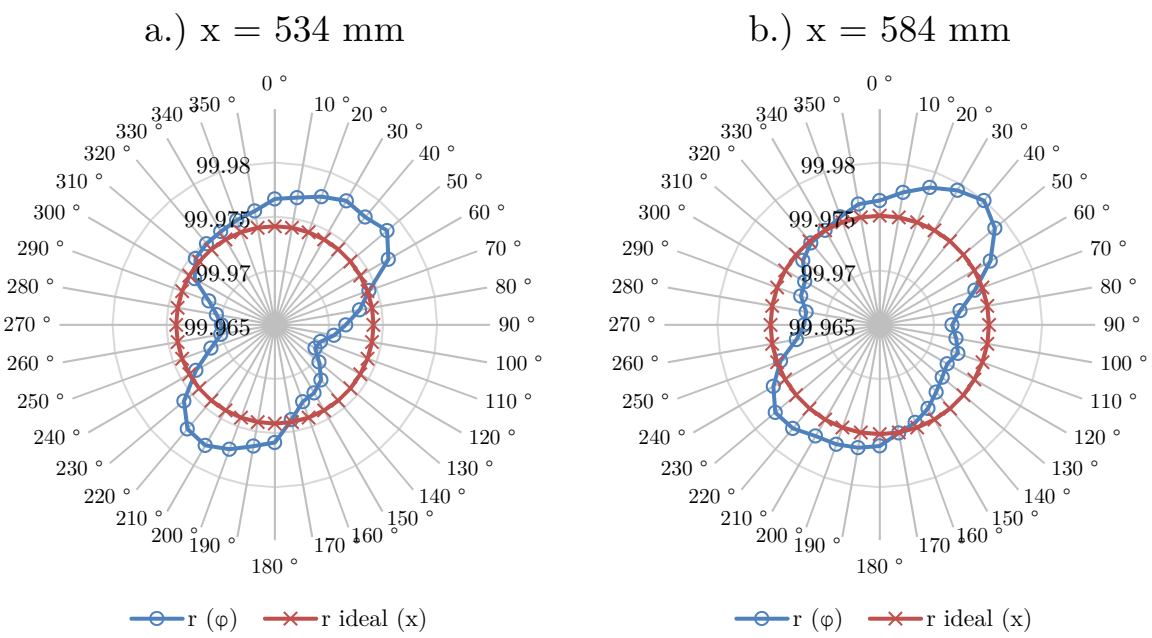

Figure 4.7: Comparison of the LSC radius (red crosses) to radii calculated from raw data (blue circles) for two measuring planes (a.) x=534 mm and b.) x=584 mm)); scaled ~5000:1

Note, that positively and negatively deviating radii for a certain angular position φ_i between the circle shape according to raw data (blue dots) and the circle shape according to the LSC (red crosses) approximately erase each other if the whole angular range of 360 ° and its centre shift are considered. For example, the raw data's cross-sectional area approximately equals the

LSC cross-sectional area (differences lower than 0.03 ppm for any measuring plane) while radius differences of ± 50 ppm occur. The factor of reducing form errors is important when it comes to measurement uncertainty influences arising from form errors. The 12 calculated LSC diameters D_{Pl_i} for each measuring plane are averaged to gain the Piston diameter $D_p = 199.952$.

As mentioned above, the measurement uncertainty of the piston diameter D_P depends on a few individual influences, mainly coming from the measuring system and the shape of the piston.

$$D_P = \frac{1}{12}\sum D_{Pl\_i} \tag{47}$$

The uncertainty arising from the standard deviation of the mean of all measuring plane diameters uD_{Geo} (0.64 µm) and the uncertainty of the respective measuring plane's diameter affect the uncertainty of D_P. The combined uncertainty of D_{Pl_i} includes the CMM's measurement uncertainty for the measured value D_{CMM} (0.5 µm for distance measurements < 200 mm), the CMM's resolution uncertainty uD_{Res} (0.05 µm, as the resolution of the CMM is 0.1 µm), it's repeatability between set 1 and set 2, uD_{Rep} (maximum value of 0.67 µm), and form errors uD_{Sh} that affect the cross-sectional area of any plane (maximum value of 0.03 ppm or 0.006 µm). The extended measurement uncertainty for any measuring plane's diameter D_{Pl} is 1.7 µm (k=2). The extended measurement uncertainty (k=2) of the piston diameter D_p is calculated according to equation (47) to be 2.1 µm (cf. Table 4.1).

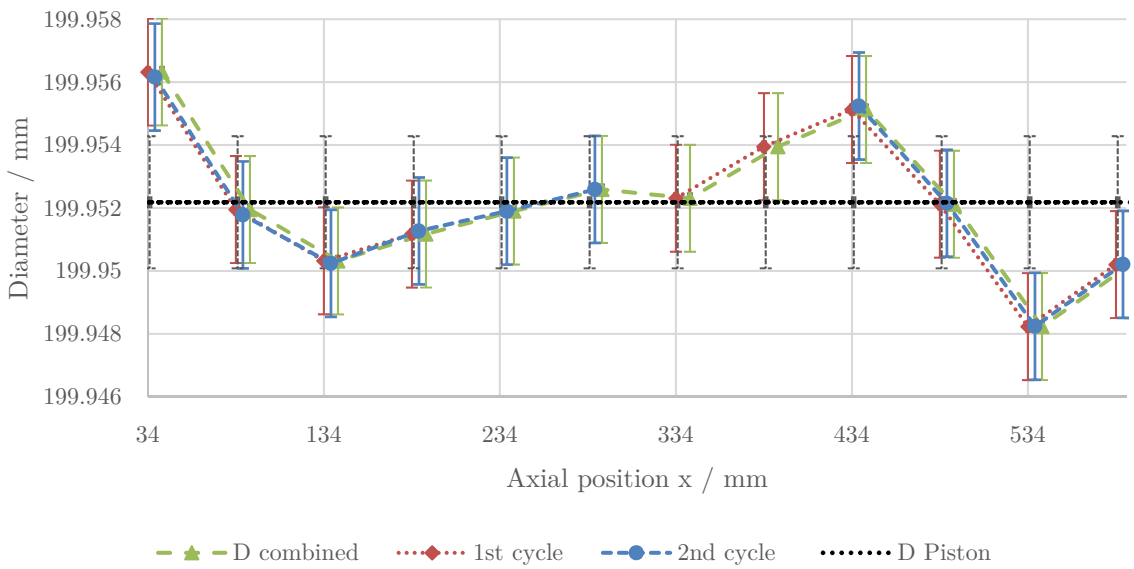

Figure 4.8: Diameter of displacer as a function of axial position

Figure 4.8 shows that the LSC diameters vary over the entire measuring range by a maximum of ~8 µm (between 199.956 and 199.948), whereby the repeatability of the first set of measurements (red diamonds) to the second set of measurements (blue balls) amounts to a maximum of 0.17 µm. Note that the measuring points are slightly shifted along the x-axis to make the specific measurement uncertainties more visible. Some measuring plane diameters differ from D_p by up to 4 µm, which is outside its measurement uncertainty of 2.1 µm. Thus,

the uncertainty of a measurement would increase if the piston wasn't displaced the whole distance but between inappropriate sections of the displacement range.

According to Table 4.1, the biggest contributions to the measurement uncertainty are related to the individual diameter repeatability (~41 %) the uncertainty of all plane diameters (~36 %), and the measurement system's uncertainty (~23 %).

Table 4.1: Uncertainty Budget for the Piston Diameter D_P

Quantity	Value [mm]	St. U. [mm] (*St. dev.)	Distr.	Sens. Coeff.	Contr. [mm]	Contr. [%]
Measured Diam. D_{CMM}	199.952	$0.5 \cdot 10^{-3}$ (*)	Norm.	1.0	$0.5 \cdot 10^{-3}$	22.80
Resolution uD_{Res}	0	$0.0289 \cdot 10^{-3}$	Rect.	1.0	$0.029 \cdot 10^{-3}$	0.08
Shape imperfections uD_{Sh}	0	$5.99 \cdot 10^{-6}$ (*)	Norm.	1.0	$6.0 \cdot 10^{-6}$	~0
Individual Diameter Repeatability uD_{Rep}	0	$0.67 \cdot 10^{-3}$ (*)	Norm.	1.0	$0.67 \cdot 10^{-3}$	40.93
Geometrical Deviation uD_{Geo}	0	$0.63 \cdot 10^{-3}$ (*)	Norm.	1.0	$0.63 \cdot 10^{-3}$	36.19
Comb. Uncertainty (k=1)					0.00105	

4.3.2.2 Distance Measurement

The test rig allows two methods to be used to determine the piston's travelled distance. The standard device is a linear scale measuring system. The measurement is performed by a measuring slide, which is connected to the piston and determines axial position changes on a scale according to the electromagnetic induction principle. According to the manufacturer's calibration certificate, the system has a standard measurement uncertainty of 7 µm+13(L/1000 mm) with the length L measured in mm. Thus, its uncertainty depends on the length of the piston stroke. The other uncertainty influences arising from its resolution (0.5 µm), possible angular errors (which is depending on the length of the piston stroke, too) and thermal instabilities are described in chapter 4.2.1. Combining equation (22) and equation (23) leads to equation (48).

$$s_{ref} = \left[s_0(1 - s_A)\left(1 + \alpha_{LM}\left(\vartheta_{amb} - \vartheta_{ref\_LM}\right)\right) + s_R\right] \tag{48}$$

For a measured value of s_0~500 mm, the standard uncertainty (k=1) of the distance measurement is calculated to be 14.7 µm. In this case, the respective expanded measurement uncertainty of s_{ref} amounts to 29.4 µm (k=2) or 58 ppm. According to Table 4.2, the biggest contributions to the measurement uncertainty of a distance measurement arise from the length measurement system's uncertainty (~84 %), temperature uncertainties during calibration (~10 %) and the alignment between piston and length measurement system (~3.5 %). It should be noted that the measurement uncertainty and its contributors depend on the measured distance. In chapter 4.3.2.3, the reference volume V_{ref} is introduced in dependence of the displacement distance. The travelled distance can also be indicated indirectly by using the incremental encoder of the servo motor with a resolution of 1024 increments per motor

revolution. With a ratio of 1:28 between spindle and motor rotation and a feed of 10 mm per spindle revolution, the length measurement resolution of this system amounts to 0.35 µm. However, external influences such as installation errors, angular errors, thermally induced changes in the measuring object, etc. are unknown. It is therefore not used for volume calculations but for control purposes.

Table 4.2: Uncertainty Budget for the distance measurement s_{ref} for s_0 = 0.504582 m

Quantity	Value	St. U. (*St. dev.)	Distr.	Sens. Coeff.	Contr. [mm]	Contr. [%]
s_0	0.504582 m	$0.0135 \cdot 10^{-3}$ m	Norm.	1.0	0.0135	83.9
α_{LM}	$8.00 \cdot 10^{-6}$ °C^{-1}	$1.00 \cdot 10^{-6}$ °C^{-1}	Rect.	$0.5 \cdot 10^{-12}$	$0.029 \cdot 10^{-15}$	~0
ϑ_{amb}	20.00 °C	1.15 °C	Rect.	$4.0 \cdot 10^{-6}$	$4.7 \cdot 10^{-6}$	10
$\vartheta_{ref\text{-}LM}$	20.00 °C	0.577 °C	Rect.	$-4.0 \cdot 10^{-6}$	$-2.3 \cdot 10^{-3}$	2.5
s_A	$9.50 \cdot 10^{-6}$ m	$5.48 \cdot 10^{-6}$ m	Rect.	-0.5	$-2.8 \cdot 10^{-6}$	3.5
s_R	0 m	$0.289 \cdot 10^{-6}$ m	Rect.	1.0	$0.29 \cdot 10^{-3}$	~0
Comb. Uncertainty (k=1)					0.0147	

4.3.2.3 Combined Reference Volume

The measurement uncertainty of the reference volume V_{ref} at ideal conditions is a function of its influence quantities s_{ref} and D_P multiplied by the constant $\pi/4$. As mentioned before, the uncertainties of both influence quantities depend on the distance of displacement. Thus, the uncertainty of the reference volume is directly influenced, too.

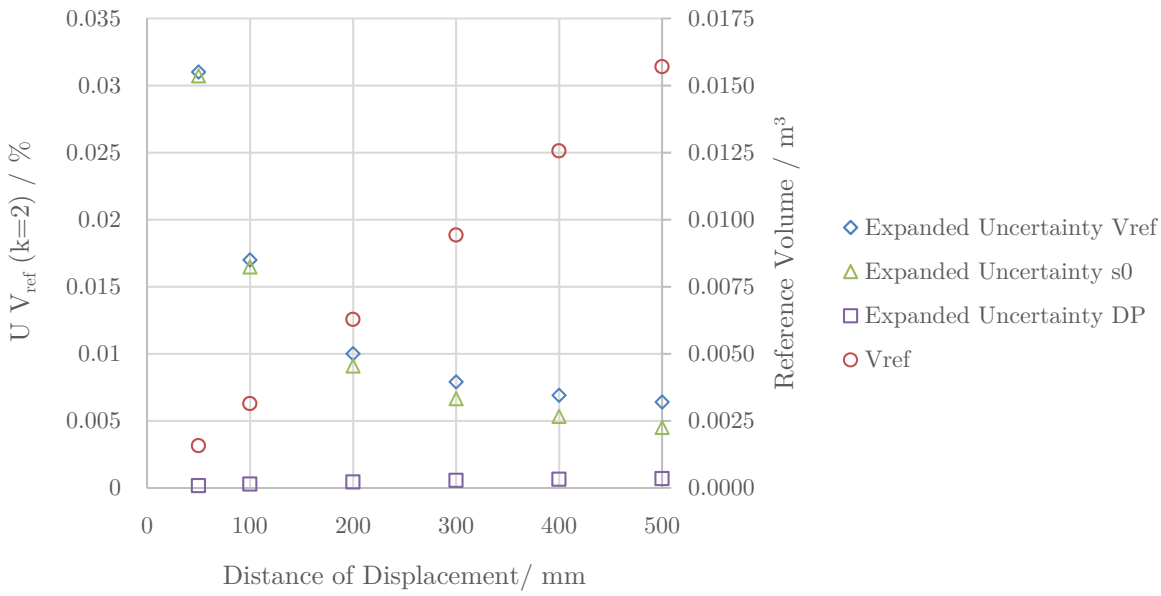

Figure 4.9: Influence of the distance of displacement on the Reference Volume and its uncertainty

Figure 4.9 shows the influence of the measured displacement distance on the reference volume V_{ref} (red balls) and its expanded uncertainty (blue diamonds). Furthermore, the influence of its biggest contributors s_0 (green triangles) and D_P (violet boxes) are included, too. While the expanded uncertainty (k=2) of V_{ref} is 0.0063 % or 63 ppm at a distance of 500 mm, it gradually increases with decreasing distances (0.031 % or 310 ppm for a distance of 50 mm). This behaviour can be traced back particularly to the uncertainty of the linear scale in use, as its influence on the uncertainty grows from 0.0042 % (~ 70 % of the expanded uncertainty of V_{ref}) at a distance of 500 mm to 0.03 % (~99 % of the expanded uncertainty of V_{ref}) at a distance of 50 mm. At the same time, the influence of the uncertainty of the piston diameter D_P on the expanded uncertainty of V_{ref} decreases from ~11 % to ~1 %. It should be noted that the scenario of shorter piston strokes is not theoretical but necessary to allow measurements at low flow rates and reasonable measurement times. In this case, the piston is displaced between axial positions where D_P is almost identical to the respective plane's diameter (between x=84 mm and x=384 mm; cf. Figure 4.8) to guarantee a measurement well within the piston diameter's expanded measurement uncertainty.

4.3.3 Cylinder Volume and Connecting Volume

The volumes of the cylinder V_C and the connecting piping between cylinder and MUT V_{CV} have been calculated theoretically based on CAD-based manufacturing drawings including tolerances according to standards DIN ISO 2768-1 [92] and DIN 2519 [93] for the respective parts. That partly leads to rather high relative uncertainties regarding the volume. Especially the volume of the connection piping is difficult to determine as production tolerances as well as unknown inner diameters of sensors, valves and other installations affect the volume. However, it should be noted that those volumes solely play a role for mass storage effects, which appear small compared to other effects as the temperature inside the cylinder is relatively stable and the connecting volume is small compared to the usually displaced volume (cf. 4.3.9).

Both uncertainties have been calculated according to following equations (49) and (50) with their respective uncertainties.

$$V_C = \tilde{s}_C \tilde{D}_C{}^2 \frac{\pi}{4} \tag{49}$$

The cylinder volume V_C is calculated to be 41.265 l with a standard uncertainty of 0.253 l.

$$V_{CV} = \tilde{s}_{CV} \tilde{D}_{CV}{}^2 \frac{\pi}{4} \tag{50}$$

The connecting volume V_{CV} is calculated to be 1.245 l with a standard uncertainty of 0.1 l.

The dead volume inside the cylinder is subject to the displaced volume subtracted from V_C during the measurement. For usual measurements, a displaced volume of ~16 l is employed. As mentioned in chapter 4.3.2.3, for low flow rates, the displaced volume can be chosen to be

smaller to save measuring time. In these cases, the dead volume inside the cylinder is larger (increasing its impact) and the ratio between connecting volume and displaced volume changes.

4.3.4 Temperature Measurements

To monitor the temperature of the measuring fluid, a total of 4 RTDs (Pt-100 resistance thermometers; 4-wired) are used at selected positions within the system (upper and lower areas of the container, inlet and outlet of the measuring section). Temperature readings affecting the model shown in equation (41) are the cylinder temperature at the start ϑ_C^i and end ϑ_C^f of a measurement, temperatures in the connecting volume at the start ϑ_{CV}^i and end ϑ_{CV}^f of the measurement and the average temperature at the MUT $\tilde{\vartheta}_{MUT}$. The two RTDs inside the cylinder are averaged to gain the cylinder temperature and two RTDs at the inlet and outlet of the measuring section are averaged to gain the connecting volume temperature. The averaged temperature at the MUT is also a function of the RTDs at the inlet and outlet, though averaged over the span of a measurement. According to [94], the uncertainty of a temperature measurement using a 4-wired RTD in this test rig can be expressed with:

$$\vartheta_i = \vartheta_m + U_F + U_C + U_{Th} + U_{\vartheta A} + U_{\vartheta w} + U_{LT} \tag{51}$$

where ϑ_i is the temperature readout, ϑ_m is the measured temperature (resolution), U_F is the uncertainty associated with heat conduction errors, U_C is the uncertainty of the calibration, U_{Th} is the uncertainty caused by thermoelectric voltage, $U_{\vartheta A}$ is the uncertainty due to ambient temperature, $U_{\vartheta w}$ is the uncertainty caused by linearisation errors of the control unit and U_{LT} is the uncertainty due to long term behaviour of the sensor. Note, that this equation usually consists of more contents. Some uncertainties regarding resistance influences (insulation, input, lead), power supply or insufficient heating and self-tempering were found to be neglectable for this special application. Furthermore, the devices have been calibrated at PTB Working Group 7.42 (Temperature Sensor Technology) with a measurement uncertainty of 10 mK (k=2).

Table 4.3: Uncertainty Budget for a temperature measurement of 20 °C

Quantity	Value	St. U.	Distr.	Sens. Coeff.	Contr. [°C]	Contr. [%]
ϑ_m	20.000 °C	0.00289 °C	Rect.	1.0	0.00289	~0
U_F	0 °C	0.0346 °C	Rect.	1.0	0.0346	8.3
U_{Th}	0 °C	0.0306 °C	Rect.	1.0	0.0306	6.5
$U_{\vartheta A}$	0 °C	0.000577 °C	Rect.	1.0	0.000577	~0
$U_{\vartheta w}$	0 °C	0.0866 °C	Rect.	1.0	0.0866	51.9
U_{LT}	0 °C	0.0693 °C	Rect.	1.0	0.0693	33.2
Comb. Uncertainty (k=1)					0.12	

The standard uncertainty of the temperature measurement for a given RTD is estimated to be 0.12 °C (cf. Table 4.3). It should be added that the standard uncertainty for the averaged temperature at the MUT is subject to possible temperature changes during the measurement that affect the standard deviation. In this case, the square root of the sum of the squared standard uncertainty and the squared standard deviation of the mean temperature is calculated leading to a higher uncertainty. Thus, the higher the temperature change at the MUT, the larger its standard deviation and subsequently the uncertainty influence of this temperature on the cpmbined measurement uncertainty.

4.3.5 Pressure Measurements

Piezoresistive pressure sensors are used to measure the system's pressure at the outlet of the cylinder and the outlet of the measuring section. The sensors have been calibrated with an electric pressure calibrator at operating conditions between normal pressure and 0.6 Mpa. The calibration facility has an expanded uncertainty of 0.05 %. The long-term stability and uncertainty of the pressure sensor are unknown. However, since the deviations of the sensor without calibration showed maximum deviations of lower than 0.36 % in the pressure range and the influence of the pressure on the measurement uncertainty is low (due to the examined fluids low compressibility), the combined uncertainty of the pressure sensors is generously estimated to be 1.0 % (k=1).

4.3.6 Thermal Expansion Coefficients / Test Rig and Medium

The thermal expansion coefficients are needed to compensate for temperature effects in parts of the test rig including the piston, the piping of the connecting volume, the cylinder, the length measurement system and of the fluid in use. Most parts of the test rig are made of stainless steel (1.4571), where thermal expansion coefficients are found to be $16.5 \cdot 10^{-6}$ K^{-1} according to manufacturer data sheets. The thermal expansion coefficient could be confirmed for the piston material by measuring the piston length difference between 18 °C and 24 °C.

For the length measuring system, the manufacturer data states a value of $8.0 \cdot 10^{-6}$ K^{-1} for the thermal expansion coefficient.

Since the density $\rho(\Theta)$ of the media in use has been measured, the thermal expansion coefficients β_i can be derived with equation (30). Its uncertainty is directly depending on the uncertainty of the density measurements ($\sim 5 \cdot 10^{-5}$) and the temperature. If the value is calculated for the average of two or more temperatures, the finally applied expansion coefficient is linearly interpolated between the two or more temperature-based expansion coefficients. A possibly resulting increase of the standard deviation is included in the measurement uncertainty of the value.

4.3.7 Compressibility Factor of the Medium

The speed of sound $c(\Theta)$ and the density $\rho(\Theta)$ of the media in use have been measured, so the isothermal expansion factor κ_i can be derived with equations (18) and (19). That leads to values that, as expected, play a minor role in the pressure range of the test rig. Its uncertainty is a function of the uncertainty of the density measurements (~$5 \cdot 10^{-5}$) and the uncertainty of speed of sound measurements (~0.1 %). However, since the influence of the compressibility factor on the uncertainty of the whole system is low, its value for water is assumed to be $4.6 \cdot 10^{-10}$ Pa^{-1} with a standard uncertainty of $0.4 \cdot 10^{-10}$ Pa^{-1} throughout the whole temperature range. For the glycol-based fluids, a value of $3.5 \pm 0.5 \cdot 10^{-10}$ Pa^{-1} (k=1) is assumed.

4.3.8 Gas inside the System

The possibility of gaseous portions inside the relevant volume during a measurement is stated in 4.2.2. Accordingly, a volume of 0.3 ml is subject to three influential cases, which are triggered by pressure and temperature changes between filling and the start of the measurement and by pressure changes during a measurement. Equation (40) describes the volume change ΔV_G of the gaseous volume during a measurement. Usually, the initial operating pressure is ~100000 Pa above filling pressure (ambient pressure of ~101300 Pa). Thus, the volume decreases by ~ 50 % to ~0.15 ml during pressurisation. For a temperature of 80 °C (or 353.15 K) and a filling temperature of 20 °C (293.15 K), the volume V_G^i would increase to ~0.18 ml during tempering. For the pressure ratio of p_C^i/p_C^f being relatively constant at 0.9 throughout the measuring range, the initial gas volume decreases by ~10 % during a measurement. In the case of the initial gas volume V_G^i being ~0.18 ml, the final gas volume V_G^f amounts to ~0.16 ml (or 10 ppm for a displaced volume of 15.7 l). The volume change ΔV_G, however amounts to 0.02 ml or ~1.3 ppm. During a measurement, only ΔV_G directly contributes to the combined measurement uncertainty of the volume at the MUT. For a temperature range of ϑ_C^i between 3 °C and 90 °C and a pressure range of 100000 Pa and 400000 Pa for p_C^i, this uncertainty lies between 0.5 ppm to 1.3 ppm for a piston stroke of 500 mm and 2 ppm to 6 ppm for a piston stroke of 100 mm.

4.3.9 Combined Uncertainty of the Volume at the MUT

Based on equation (41) and the uncertainty influences discussed above, the uncertainty of the volume that passed the MUT can now be determined. To introduce the combined uncertainty, a typical flow measurement of 0.6 m³/h at 20 °C including its uncertainty components is shown in Table 4.4. The uncertainty budget states a standard uncertainty of $1.38 \cdot 10^{-6}$ m³ for the volume at the MUT V_{MUT} of 0.015843282 m³. This yields an expanded relative uncertainty of 0.017 % (k=2) for this flow measurement.

According to [95], the uncertainty framework according to GUM is supposed to be adequate in many circumstances. Performing a Monte Carlo method and comparing the results to the GUM uncertainty budget can validate cases of doubt. Figure 4.10 gives the results, determined with GUM Workbench Pro applying the OMCE V:1.2.14.1 Simulator using 2000000 iterations. It

states an average value of 0.0158433 m³ and a standard uncertainty of $1.4 \cdot 10^{-6}$ m³, which fits well to the standard uncertainty calculated according to GUM.

Table 4.4: Uncertainty Budget for the Volume at the MUT for water with a flow rate of 0.6 m³/h at ~20 °C

Quantity	Value	St. U. (*St. dev.)	Distr.	Sens. Coeff.	Contr. [m³]	Contr. [%]
p_C^f	$0.22896 \cdot 10^{-6}$ Pa	1320 Pa	Rect.	$-0.012 \cdot 10^{-9}$	$-0.015 \cdot 10^{-6}$	~0
p_C^i	$0.21451 \cdot 10^{-6}$ Pa	1240 Pa	Rect.	$0.019 \cdot 10^{-9}$	$0.024 \cdot 10^{-6}$	~0
p_{CV}^f	$0.22230 \cdot 10^{-6}$ Pa	1280 Pa	Rect.	$-0.57 \cdot 10^{-12}$	$-0.73 \cdot 10^{-9}$	~0
p_{CV}^i	$0.21330 \cdot 10^{-6}$ Pa	1230 Pa	Rect.	$0.57 \cdot 10^{-12}$	$0.71 \cdot 10^{-9}$	~0
$\tilde{p}_{MUT}$	$0.21830 \cdot 10^{-6}$ Pa	5140 Pa (*)	Norm.	$-7.3 \cdot 10^{-12}$	$-0.037 \cdot 10^{-6}$	~0
p_{ref}	$0.10130 \cdot 10^{-6}$ Pa	585 Pa	Rect.	$-0.41 \cdot 10^{-15}$	$-0.24 \cdot 10^{-12}$	~0
ϑ_{Amb}	20.00 °C	1.15 °C	Rect.	$0.13 \cdot 10^{-6}$	$0.15 \cdot 10^{-6}$	1.1
ϑ_C^f	20.00 °C	0.120 °C	Rect.	$5.4 \cdot 10^{-6}$	$0.65 \cdot 10^{-6}$	22.5
ϑ_C^i	19.99 °C	0.120 °C	Rect.	$-8.3 \cdot 10^{-6}$	$-1.0 \cdot 10^{-6}$	52.3
ϑ_{CV}^f	19.75 °C	0.120 °C	Rect.	$0.20 \cdot 10^{-6}$	$0.024 \cdot 10^{-6}$	~0
ϑ_{CV}^i	19.82 °C	0.120 °C	Rect.	$-0.20 \cdot 10^{-6}$	$-0.024 \cdot 10^{-6}$	~0
$\tilde{\vartheta}_{MUT}$	19.77 °C	0.128 °C (*)	Norm.	$3.4 \cdot 10^{-6}$	$0.43 \cdot 10^{-6}$	9.9
$\vartheta_{ref\ LM}$	20.00 °C	0.577 °C	Rect.	$-0.13 \cdot 10^{-6}$	$-0.073 \cdot 10^{-6}$	0.3
$\vartheta_{ref\ P}$	20.00 °C	0.115 °C	Rect.	$-0.52 \cdot 10^{-6}$	$-0.06 \cdot 10^{-6}$	0.2
V_C^i	0.041308 m³	$0.400 \cdot 10^{-3}$ m³ (*)	Norm.	$-4.5 \cdot 10^{-6}$	$-1.8 \cdot 10^{-9}$	~0
V_G^{fill}	$0.300 \cdot 10^{-6}$ m³	$0.173 \cdot 10^{-6}$ m³	Rect.	$0.47 \cdot 10^{-3}$	$0.082 \cdot 10^{-9}$	~0
V_{CV}	$1.2450 \cdot 10^{-3}$ m³	$0.100 \cdot 10^{-3}$ m³ (*)	Norm.	$-0.014 \cdot 10^{-3}$	$-1.4 \cdot 10^{-9}$	~0
V_{ref}	0.015844181 m³	$0.503 \cdot 10^{-6}$ m³ (*)	Norm.	1.0	$0.51 \cdot 10^{-6}$	13.6
α_{LM}	$8.00 \cdot 10^{-6}$ °C⁻¹	$0.577 \cdot 10^{-6}$ °C⁻¹	Rect.	$0.14 \cdot 10^{-6}$	$0.082 \cdot 10^{-9}$	~0
α_{CV}	$16.50 \cdot 10^{-6}$ °C⁻¹	$0.577 \cdot 10^{-6}$ °C⁻¹	Rect.	$0.24 \cdot 10^{-3}$	$0.14 \cdot 10^{-9}$	~0
α_P	$16.50 \cdot 10^{-6}$ °C⁻¹	$0.577 \cdot 10^{-6}$ °C⁻¹	Rect.	$-0.32 \cdot 10^{-3}$	$-0.18 \cdot 10^{-9}$	~0
β_{CV}	$0.2111 \cdot 10^{-3}$ °C⁻¹	$0.272 \cdot 10^{-6}$ °C⁻¹	Rect.	$-0.078 \cdot 10^{-3}$	$-0.021 \cdot 10^{-9}$	~0
β_C	$0.2133 \cdot 10^{-3}$ °C⁻¹	$3.08 \cdot 10^{-9}$ °C⁻¹	Rect.	$-3.2 \cdot 10^{-3}$	$-9.8 \cdot 10^{-12}$	~0
κ_C	$0.4600 \cdot 10^{-9}$ Pa⁻¹	$0.0231 \cdot 10^{-9}$ Pa⁻¹	Rect.	-440	$-0.01 \cdot 10^{-6}$	~0
V_{MUT}	0.015843282 m³				$1.38 \cdot 10^{-6}$ m³	

Considering the uncertainty budget, it becomes obvious that the biggest contributions for this specific measurement come from the temperature measurements inside the cylinder followed

by the reference volume and the temperature measurement at the MUT. The influence of pressure measurements could be neglected for this measurement as well as influences that arise from mass storage effects in the connecting volume or gaseous volume inside the test rig. It should be noted, that uncertainty contributions are subject to notable changes for conditions that differ from temperatures near the reference temperature of 20 °C and for flow rates, where the displacement distance of the piston is reduced due to reasonable measuring durations.

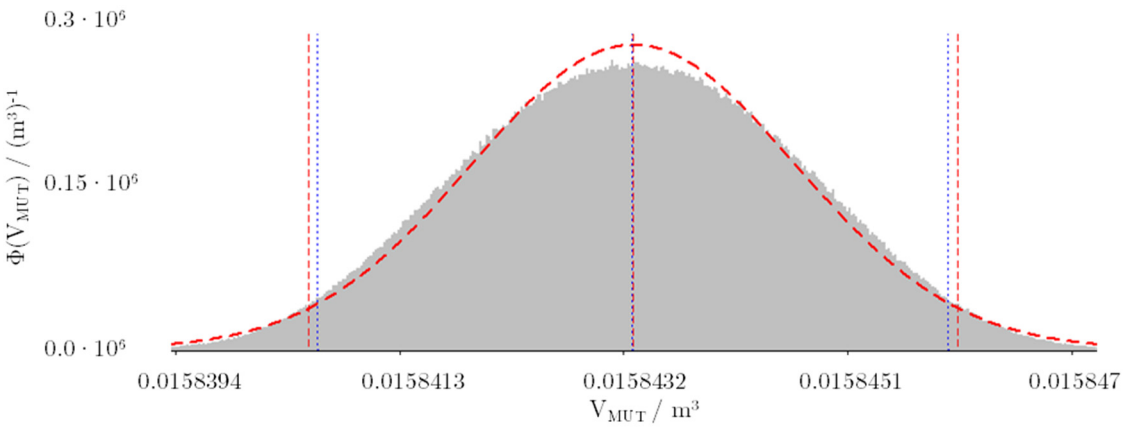

Figure 4.10: Results of the Monte Carlo Simulation for VMUT for 0.6 m³/h and 20 °C

To give an example, Figure 4.11 shows the uncertainty of V_{MUT} for different conditions and flow rates. These examples depict the rising influence of temperature-related contributions to the combined uncertainty of the test rig for temperatures diverging from reference temperature. The influence is not restricted to the measurement of the temperature but also to temperature control of the test rig. Especially for low flow rates combined with high temperatures, the temperature stability (affecting reference, gradient and mass storage effects) of the test rig shows room for improvements.

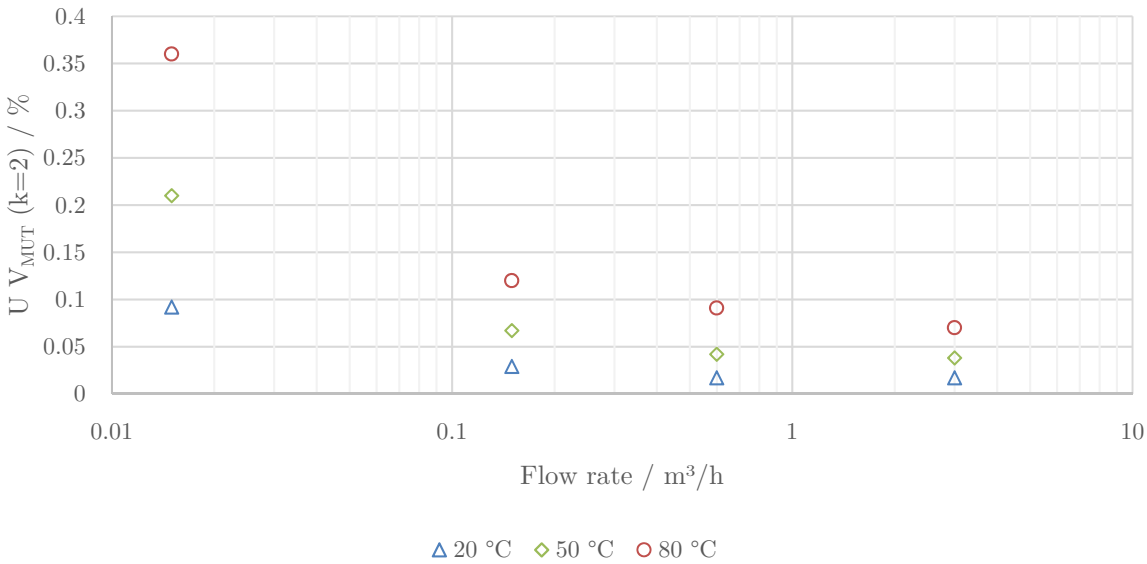

Figure 4.11: The expanded uncertainty of V_{MUT} for different flow rates and temperatures

4.4 Results of Intercomparison Measurements

As stated above, the volumetric test rig's volume measurement is based on traceable dimensional measurements of the displaced piston. However, the plausibility of the system should preferably be examined in order to detect obvious defects or deviations that are outside expected boundaries. In this case, the measurements were performed with the medium water and a calibrated EFM at six flow rates between 0.06 m³/h and ~2 m³/h and at medium temperatures of 20 °C, 50 °C and 80 °C. The comparison was carried out between the VGP and another PTB test rig, the "Haushaltszählerprüfstand" (HZP). The HZP, which is based on weighing, has an expanded measurement uncertainty of 0.1 % (k=2) for the examined flow rates and temperatures. The measurements at the VGP, originally done in 2015, were repeated in 2019 to check the system's long-term stability.

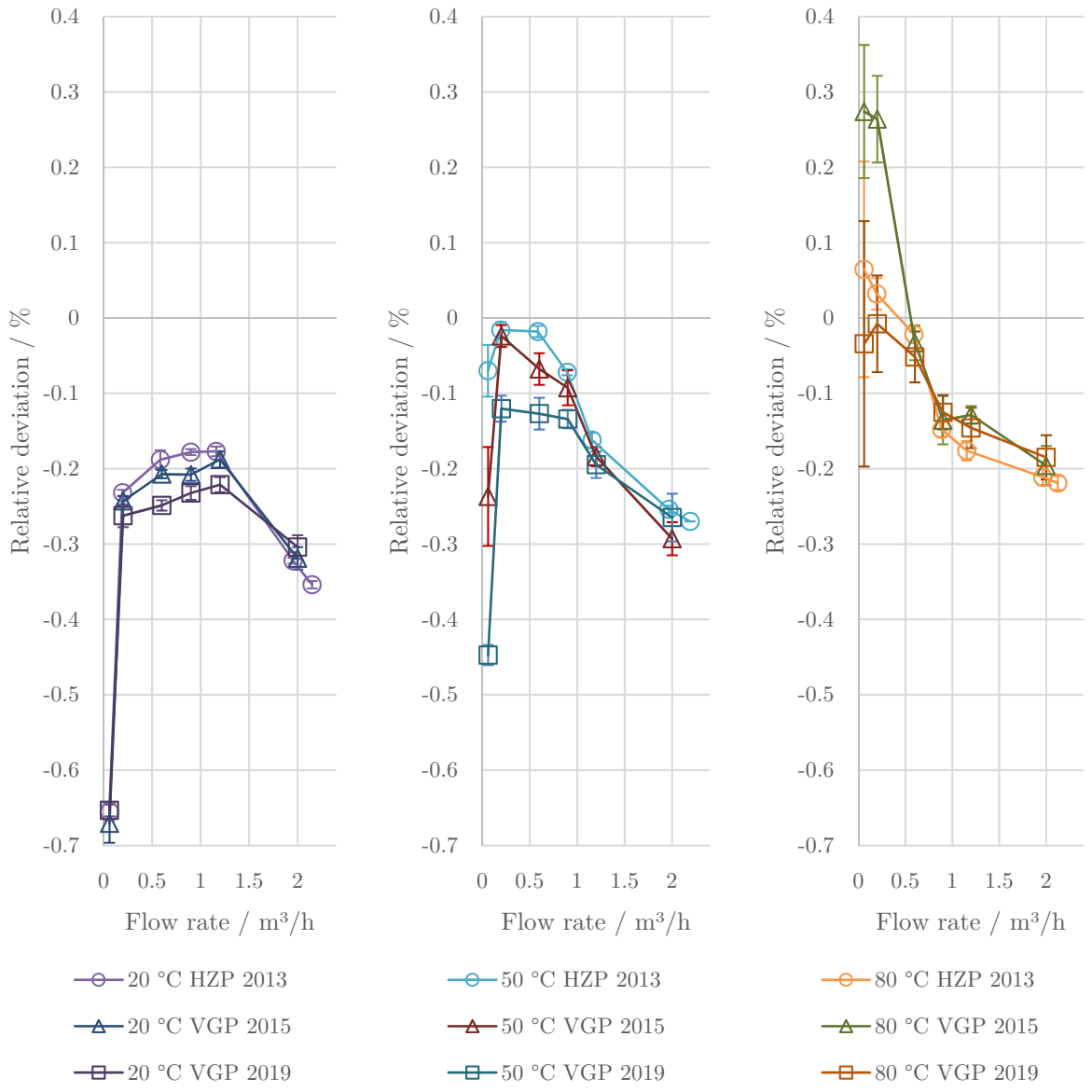

Figure 4.12: Results of Intercomparison Measurements between volumetric test rig and PTB's "Haushaltszählerprüfstand HZP"

The deviations of the EFM all lie within -0.67 % and 0.35 % throughout the whole measured range. At low flow rates of 0.2 m^3/h and below, the deviations and the standard deviations are higher compared to the flow rates above. Thus, the EFM's usablity for highest demands seems questionable at lower flow rates. At higher flow rates, however, all deviations lie within -0.35 % and -0.02 %.

For a temperature of 20 °C, the measurement deviations between HZP and VGP are within tolerable boundaries of ~0.05 % or lower (cf. Figure 4.12). The maximum deviations between any measurement of the VGP in 2015 and 2019 lie within 0.04 %. Note, that the error bars denote the EFM's standard deviation of the measurements.

For a temperature of 50 °C, the deviations between HZP and VGP are lower than ~0.1 %, apart from the flow rate of 0.06 m^3/h. Here, the deviations between HZP and VGP amount to ~0.4 %. The maximum deviations between any measurement of the VGP in 2015 and 2019 lie within ~0.1 % (apart from ~0.2 % at 0.06 m^3/h). The fluid temperature appears to have an influence on the relative deviations. Especially at low flow rates <0.6 m^3/h, the largest deviations occur while the repeatability declines. The deviations between HZP and VGP could be linked to slight condition-related differences between the test rigs, the measurement principle itself or the EFM's stability. The deviations between the measurements at the VGP in 2015 and 2019 could primarily be associated with the insulation of the VGP which was installed shortly after the measurements in 2015. The insulation's effect on the fluid temperature and stability during a measurement shows especially at low flow rates.

At 80 °C, the deviations between HZP and VGP are lower than 0.05 % at flow rates of 0.6 m^3/h and above. At lower flow rates, however, the deviations and the standard deviations are significantly larger (deviations up to ~0.2 %). The assumptions made for deviations of the measurements at 50 °C are adaptable to the measurements at 80 °C. In addition, the uncertainty of the VGP increases with rising temperature and decreasing flow rates (e.g. ~0.17 % at 0.06 m^3/h and 80 °C). That can also contribute to the deviation between VGP and HZP.

Overall, it can be stated that the plausibility of measurements is given even though there are differences between the test rigs and between the measurements of 2015 and 2019.

5. Results Flow Measurements

This chapter deals with the flow measurements, that have been performed. That includes tests with water and four glycol-based fluids. Most fluid/sensor combinations have been investigated at temperatures between 20 °C and 80 °C (Antifrogen N 40 % as a primary cooling fluid has been investigated at 6 °C and 12 °C, too). Usual flow points ranged from 6 l/h to 3000 l/h. Regarding the flow range of typical applications of glycol-based fluids as considered in chapter 2.2, flow points below 100 l/h appear unnecessary. However, investigated flow points below 100 l/h may allow to gather a deeper understanding of the fluid's flow behaviour.

When applicable, the investigated meters were corrected based on the results they produced and taken to test again with Tyfocor L 40 % and partly with other fluids; corrections ("calibrations") are common for fluids taken to test, since complex flow behaviour inside the measuring section of an individual meter requires empirical investigations.

Relative deviations E, given in %, are calculated according to:

$$E = \frac{V_M - V_C}{V_C} \cdot 100\ \%, \tag{52}$$

where V_M is the displayed measured value and V_C is the conventional true value.

The following graphs will show relative deviations, calculated from the average of five measurements including their standard deviation, in relation to the flow rate which is logarithmically scaled. Measured temperatures are shown in different colours and symbols. Further graphs are included to outline the behaviour of the sensors with regard to the Reynolds number or the speed of sound (based on the flow measurement principle, of course).

Following chapters are categorised according to flow measurement principles (ultrasonic flowmeters, impeller flowmeters, alternative principles). The respective chapters contain a short summary and the author's view on the behaviour.

5.1 Ultrasonic Flowmeter

5.1.1 Sensor I

5.1.1.1 Water

This ultrasonic q_p 1.5 flowmeter belongs to the accuracy class 2 according to DIN EN 1434. The lower limit of its flow rate q_i is 15 l/h; the heat meter shall operate at this flow rate without the maximum permissible error being exceeded. The permanent flow q_p is 1500 l/h and the upper limit of the flow rate q_s is 3000 l/h [10].

As Figure 5.1 shows, the meter performs according to its accuracy class with the measuring fluid water. Only at 6 l/h (which is below the sensor's lower flow limit) the meter is slightly outside the maximum permissible error (upper and lower permissible error is indicated by red-dotted line). The measurements show a good repeatability, especially inside the meter's flow

range between 15 l/h and 3000 l/h. Temperature dependency lies within narrow borders of about +/- 2 %.

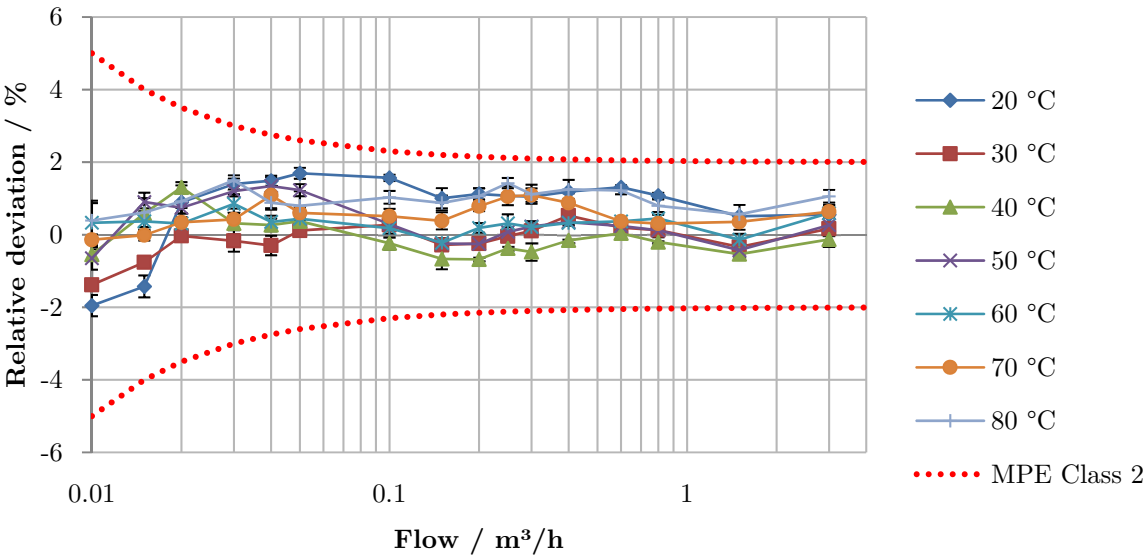

Figure 5.1: Results of flow measurements of Sensor 1 with water

5.1.1.2 Glycol-Water-Mixtures

Applied with different glycol water mixtures, the deviations of this ultrasonic flowmeter increase substantially depending on the fluids in use (cf. Figure 5.2). Noticeable are:

- the tendency to large positive deviations at low flow,
- the tendency to deviations around zero at high flow rates and
- a wide-spread temperature dependency, where lower temperatures can be associated with increasing deviations.

While fluids based on PG (Tyfocor L 40 % and Tyfocor LS) show relatively comparable deviations and a temperature dependency with maximum relative deviations around 55 %, the EG-based Antifrogen N 40 % shows lower maximum deviations of around 25 % and the higher-boiling PG-based Antifrogen Sol HT produces larger maximum deviations of 75 %. The spread of deviations in dependency of temperature is especially procounced with Antifrogen Sol HT and is significantly lower with Antifrogen N 40 %.

Usually, the Reynolds number Re can be used to analyse volume flow data. However, since the inner diameter of each specific flow sensor is different, the flow rate/kinematic viscosity ratio (FVR), which is proportional to Re, is used to compare the results. Figure 5.3 gives an overview of the five measured fluids. In order to keep the graph simple, each fluid is marked with one colour, respectively. The red-dotted area of the left part of the graph is magnified for better clarity. It shows the part of higher FVR values.

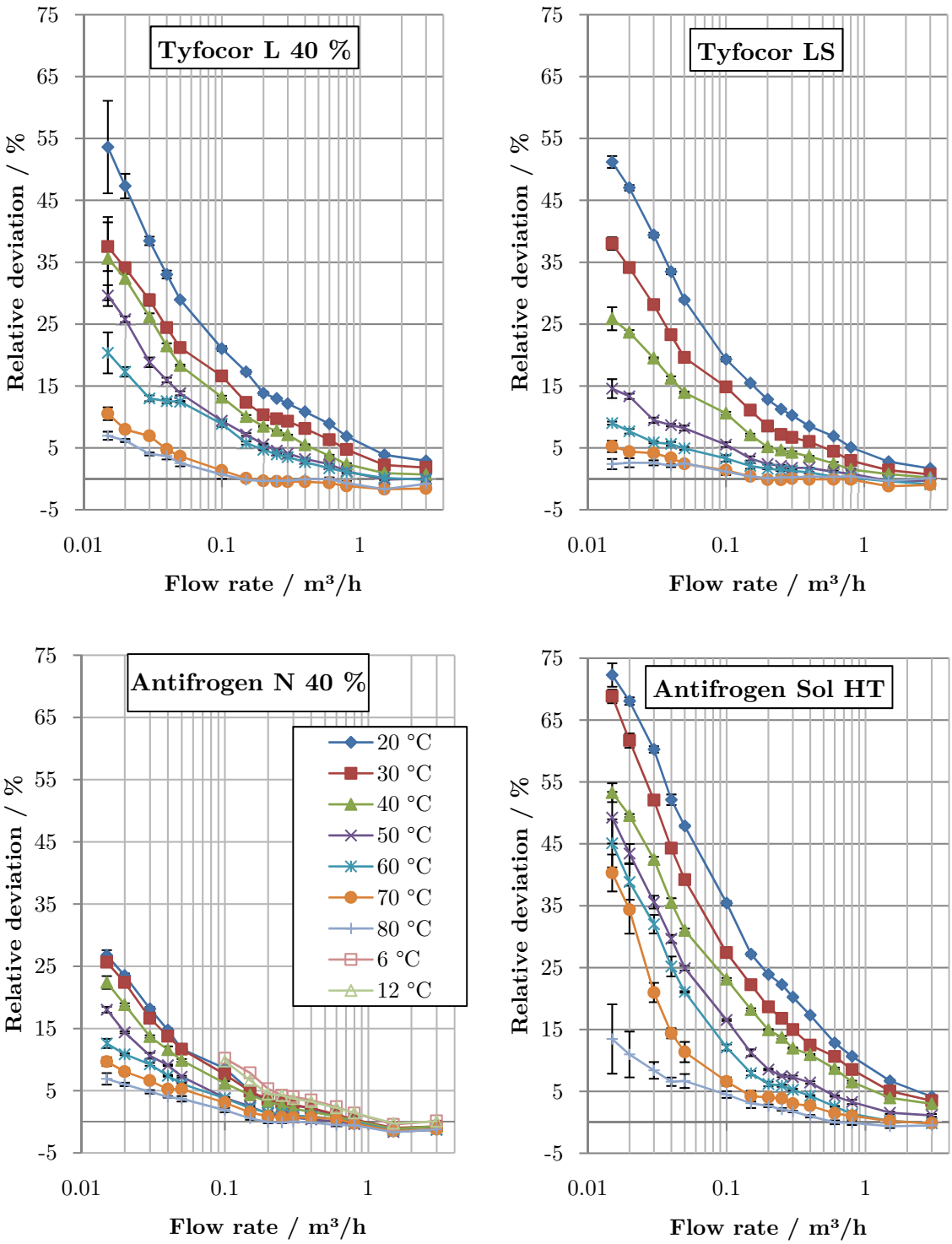

Figure 5.2: Results of flow measurements of Sensor I with glycol-water-mixtures

Obviously, water (grey) shows higher FVR values than the other fluids. While its lowest FVR value is around 0.006, Tyfocor L 40 % (blue) and Antifrogen N 40% (orange) show minimum values around 0.002, respectively, and Antifrogen Sol HT (green) and Tyfocor LS (red) show minimum values around 0.001. The maximum FVR values are at 8.409 (water), 3.233 (Tyfocor L 40 %), 1.942 (Antifrogen Sol HT), 3.045 (Tyfocor LS) and 3.717 (Antifrogen N 40 %). As FVR is proportional to Re, dependencies on Re can be derived from FVR, although a critical

shift range between laminar to turbulent flow isn't apparent. What is identifiable is the tendency to higher deviations as FVR decreases. Accordingly, relative deviations decrease as the FVR increases. At FVR above 0.500, all deviations lie between -2 % and 4 %.

The high deviations at low flow and lower temperatures are most likely a sign of flow profile influences (as described in chapter 3.5 and especially in Figure 3.10) on the sensor's ultrasonic path. This assumption would be backed up by the respective fluid's viscosity, which especially deviates from water at lower temperatures.

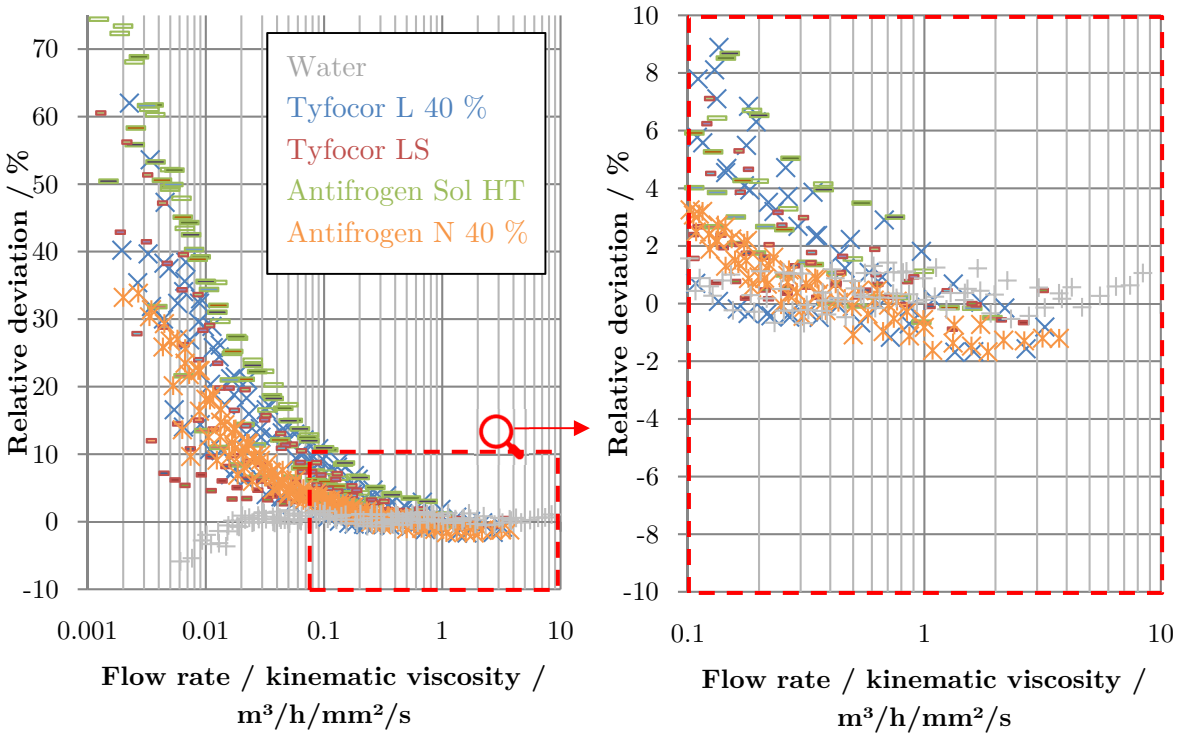

Figure 5.3: Flow rate/ kinematic viscosity ratio influence on Sensor I

5.1.1.3 Corrected Sensor Results

The sensor has been subject to corrections based on the measurement results with Tyfocor L 40 %. The corrections were done by the manufacturer's research and development department. Figure 5.4 shows results of the corrected sensor, measured with Tyfocor L 40 %, compared to the measurements with the uncorrected sensor. Obviously, relative deviations have been improved drastically, especially in regions of low flow. Temperature dependency is reduced by a big margin throughout the flow range, although it is still present at the minimum flow range. However, corrections have shifted the whole array a bit too far into negative relative deviations. Thus, for higher flow rates, the improvements appear only slight. At some temperatures and at maximum flow range, the results of the uncorrected sensor are even preferable. While the outcome of that first correction appears only partly beneficial, the repeatability of the measuring data and the improvements regarding temperature dependency presents a good base for further corrections on this specific sensor.

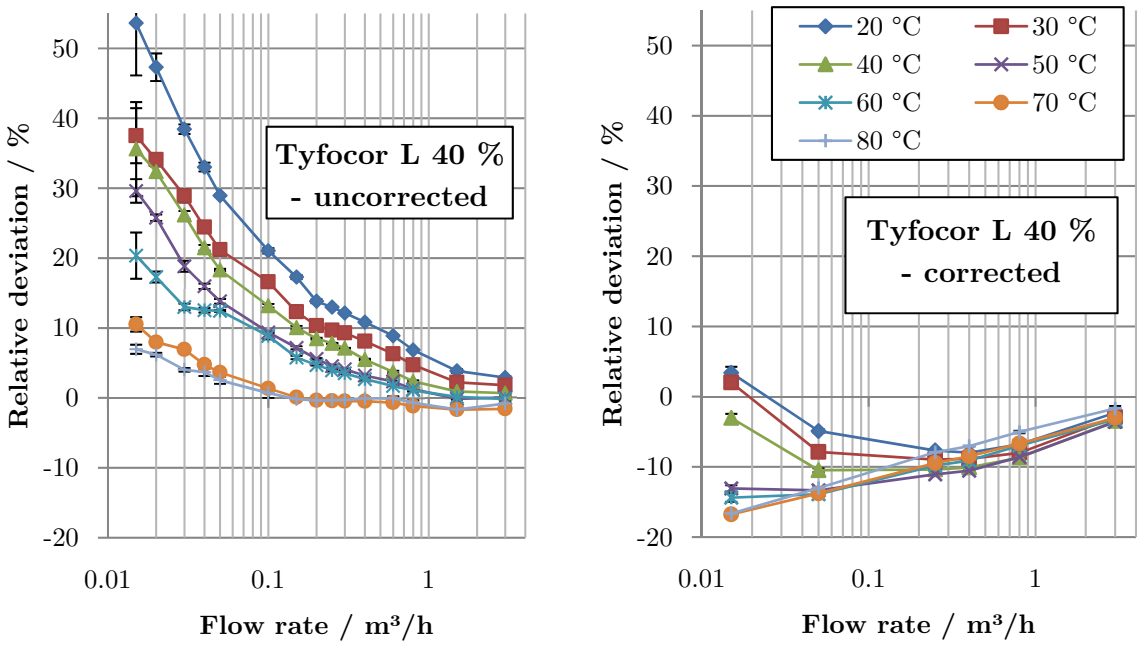

Figure 5.4: Comparison of results of corrected/uncorrected Sensor I with Tyfocor L 40 %

5.1.2 Sensor II

This ultrasonic q_p 1.5 flowmeter belongs to the accuracy class 2 according to DIN EN 1434. The lower limit of its flow rate q_i is 6 l/h; the heat meter shall operate at this flow rate without the maximum permissible error being exceeded. The permanent flow q_p is 1500 l/h and the upper limit of the flow rate q_s is 3000 l/h. This sensor is available for water and as a "Solar"-version for Tyfocor LS. Thus, the focus of measurements is put on glycol-based media.

5.1.2.1 Water

Measured with water, the flowmeter meets the requirements, as the measured relative deviations lie within permissible boundaries (cf. Figure 5.5). The sensor tends slightly to negative deviations while the repeatability is good, especially at flow rates of 0.05 m³/h and above. Note, that this sensor hasn't been measured extensively with water. The sensor was randomly checked for exceptional deviations at ~27 °C. Since there is already a "solar"-ready option of this sensor available, investigations focussed on glycol-based fluids.

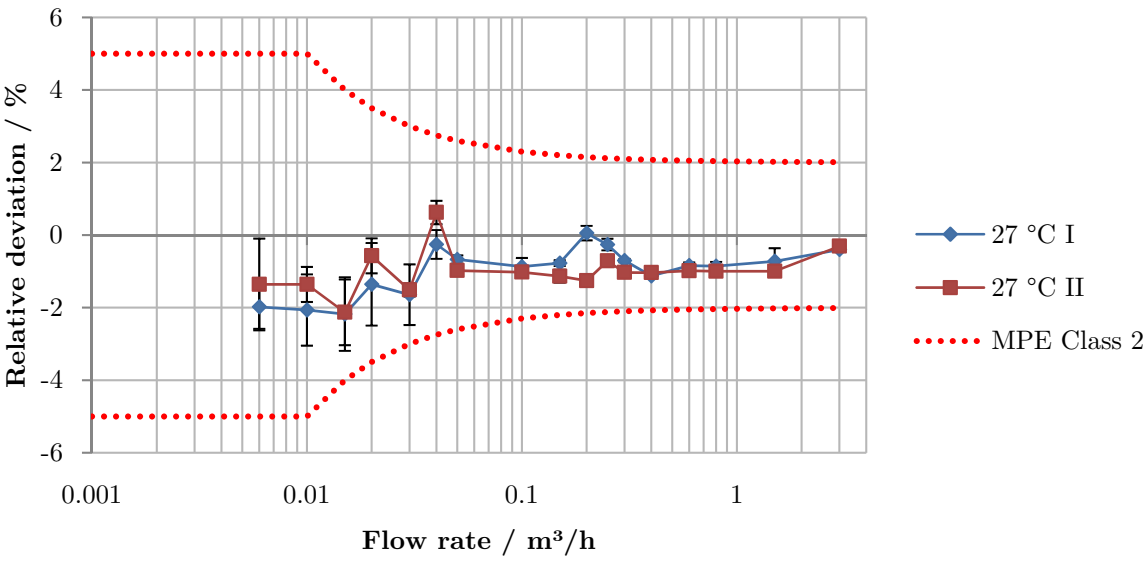

Figure 5.5: Results of flow measurements of Sensor II with water

5.1.2.2 Glycol-Water-Mixtures

As this sensor already offers the opportunity to examine a corrected version for glycol, the water version's results with glycol-water-mixtures are limited to two fluids, one based on PG and one based on EG, respectively. Figure 5.6 gives an overview of the results.

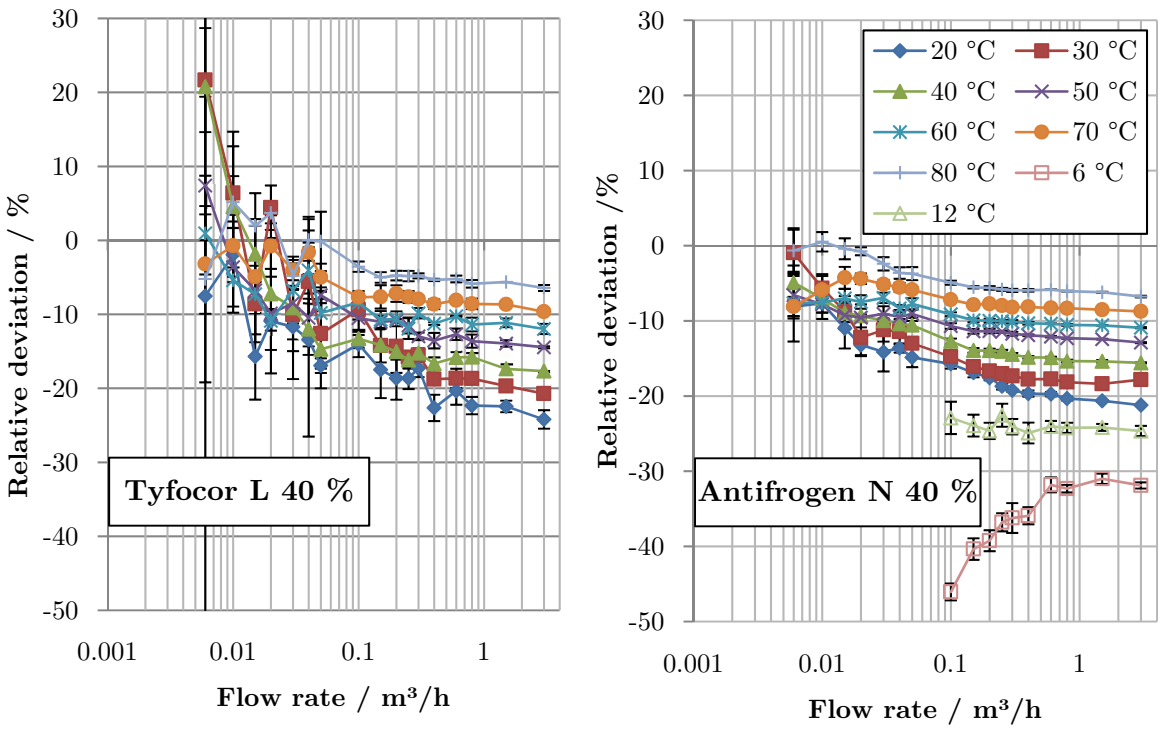

Figure 5.6: Results of flow measurements of Sensor II with PG and EG

Applied with two different glycol water mixtures, the deviations of this ultrasonic flowmeter increase substantially depending on the fluid in use. In general, the results tend to:

- large negative deviations at higher flow rates,
- whereas at low flow rates, the deviations tend to smaller negative deviations or positive deviations.
- A high temperature dependency can be observed, where lower temperatures can be associated with increased deviations.

Temperature dependency is bigger with Tyfocor L 40 % than with Antifrogen N 40 % at comparable temperatures. At flow rates above 0.05 m³/h, relative deviations are comparable for both fluids (maximum deviation with Tyfocor L 40 %: -24 %; maximum deviation with Antifrogen N 40 %: -21 %), while at flow rates below 100 l/h, the results as well as the repeatability differ from each other. Overall, repeatability is better with Antifrogen N 40 %; especially at low flow rates, the measurements with Tyfocor L 40 % show a chaotic pattern with worse repeatability. At higher flow rates, however, this behaviour improves drastically.

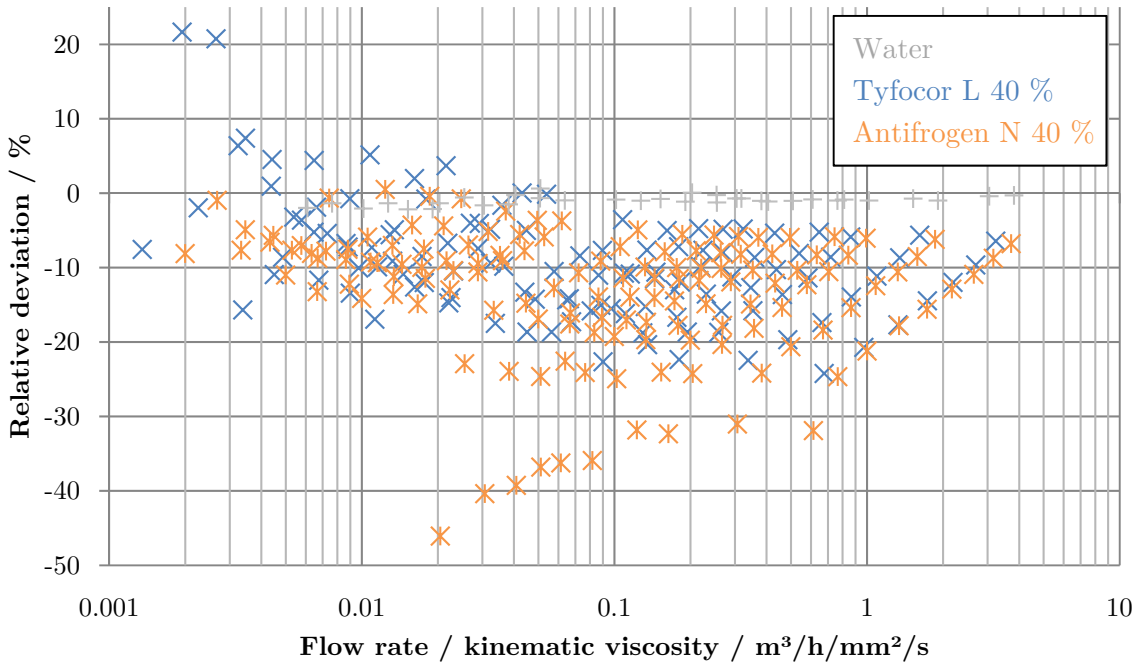

Figure 5.7: Flow rate / kinematic viscosity ratio influence on Sensor II

Figure 5.7 shows the Re-proportional flow rate/kinematic viscosity ratio. A tendency is hard to observe, as the deviations differ at comparable FVR values between water and both glycol-based fluids. At higher flow rates, a pattern becomes visible, though still not comparable to water. However, between Antifrogen N 40 % and Tyfocor L 40 %, relative deviations occur at almost similar FVRs.

Since this ultrasonic flowmeter works on the principle of phase shift (cf. 2.1.2.2), the speed of sound c is important to include, as it weighs in to the power of two. Thus, corrections have been applied on the measured results based on $c(T)$. Figure 5.8 shows the results of the sensor depending on the c-ratio without corrections (upper left) and with c^2-corrections (upper right)

and applied on measurements with Tyfocor L 40 % (bottom left) and Antifrogen N 40 % (bottom right).

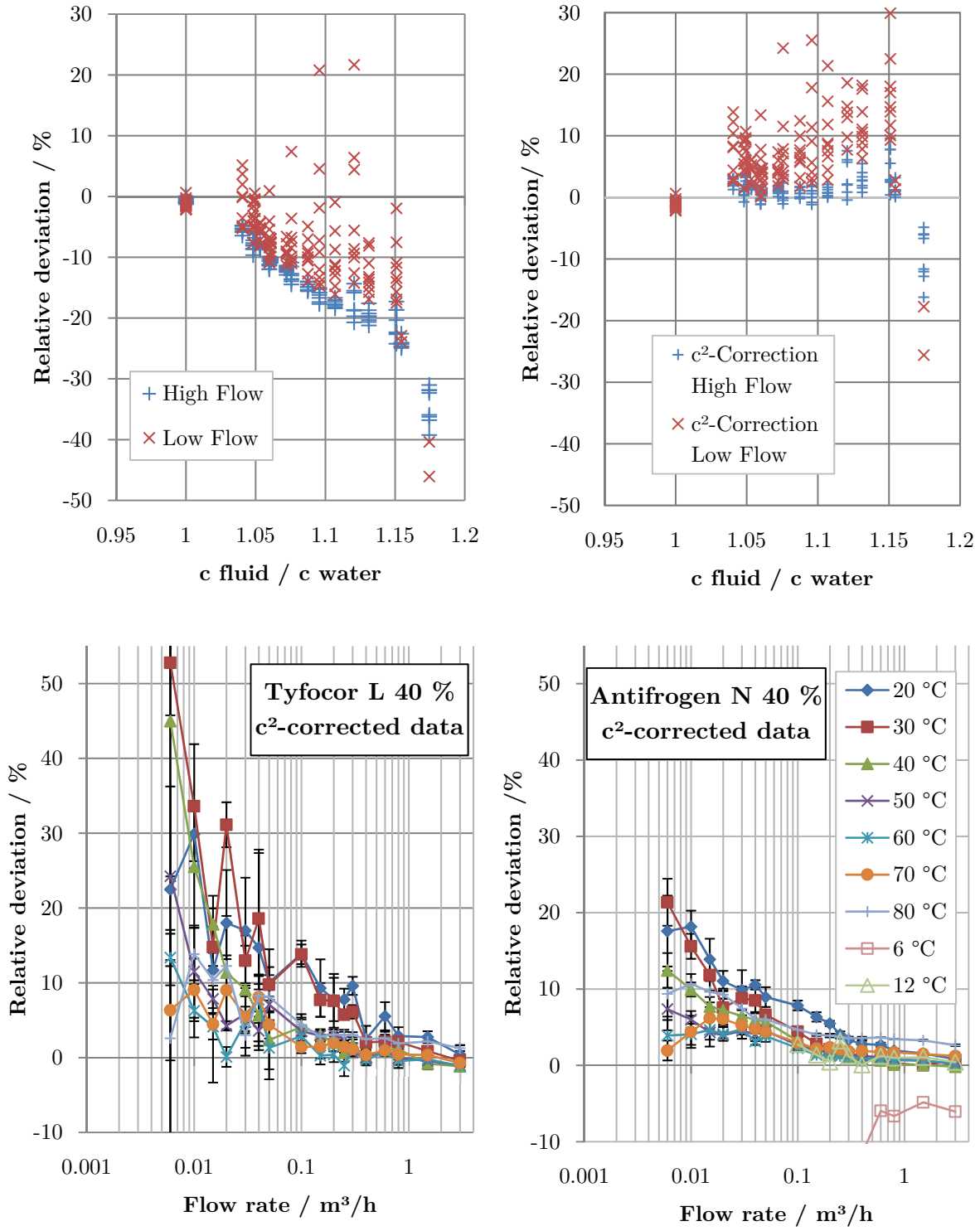

Figure 5.8: Influence of c-ratio on measurements

The flow range has been divided into two areas to look for patterns based on flow rate. Looking at the uncorrected results, the dependency appears clearly visible. Especially at high flow rates of 0.2 m³/h and above (blue crosses), the results are well in line between -5 % and -10 % at a

c-ratio of 1.05 and between -17 % and -24 % at a *c*-ratio of 1.15 indicating the tendency to drop to negative deviations at higher c-ratios. At low flow, the relative deviations are more widespread but with a clear tendency to negative deviations, as well.

The upper right side of the graph shows the volume measurements, which were simply multiplied with the respective c^2-ratio depending on the medium and temperature. The improvements are obvious, especially at high flow rates. Apart from measurements at 6 °C, relative deviations dropped to a span between -2 % and 6 %. At low flow rates, however, relative deviations switch to higher postive relative deviations of up to 50 %. Apart from measurements at 6 °C, this behaviour of high positive relative deviations at low flow and much improved relative deviations at low flow has been observed for the uncorrected version of Sensor I, too.

Further insights can be found bottom right and left, showing the c^2-ratio corrections applied to the measurements shown on page 84. The similarities to the measurements of the uncorrected Sensor I (cf. page 80f) are remarkable though the repeatability of Sensor II at low flow is comparatively worse.

5.1.2.3 Glycol-Water-Mixtures with "Solar"-Version

The manufacturer of Sensor II aimed into a new direction by providing a sensor for the medium Tyfocor LS (proclaimed with an extended maximum deviation of 10 %). The sensor was taken to test with Tyfocor LS but also with the remaining fluids to examine how the sensor would perform with related media (cf. Figure 5.9).

With Tyfocor LS the sensor shows comparatively low relative deviations between 7 % and -3 % throughout the whole flow range. Though the temperature dependency is visible, as largest deviations occur at lowest temperatures, it is less pronounced than experienced with other ultrasonic sensors. The tendency to pronounced positive deviations at low flow is lessened while the repeatability is better at high flow than at low flow. With Tyfocor L 40 %, a medium with comparable fluid properties (to Tyfocor LS), the deviations are slightly shifted to negative deviations at higher flow rates. In the low flow area, however, the deviations tend to positive deviations of up to 15 %. That pattern basically recurs for the remaining fluids, whereas the deviations and standard deviation at low flow appear slightly higher (up to ~22 %). For the EG-based Antifrogen N 40 % however, the temperature-dependent spread is more pronounced than for the other fluids (especially above 0.05 m^3/h).

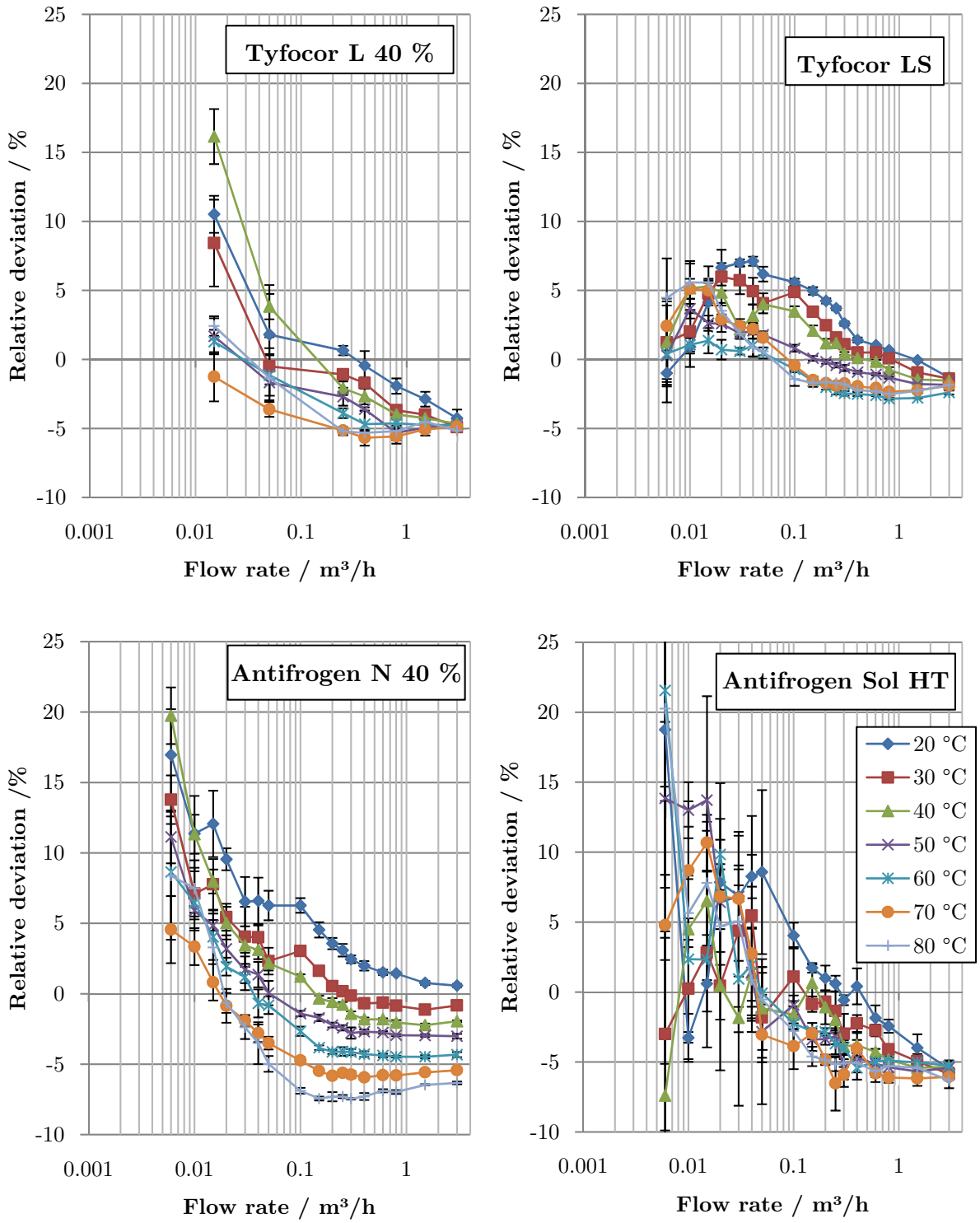

Figure 5.9: Results of flow measurements of Sensor II "Solar" with glycol-water-mixtures

Figure 5.10 shows the Re-proportional flow rate/kinematic viscosity ratio. Overall, a tendency of decreasing deviations with increasing FVR-values is observable. Above the FVR-value of 0.01, all deviations lie within a band of ~8 %, though Antifrogen N 40 % seems to be the main source of the spread. Thus, the speed of sound differences may be main source of deviations while the influence of viscosity is less influential.

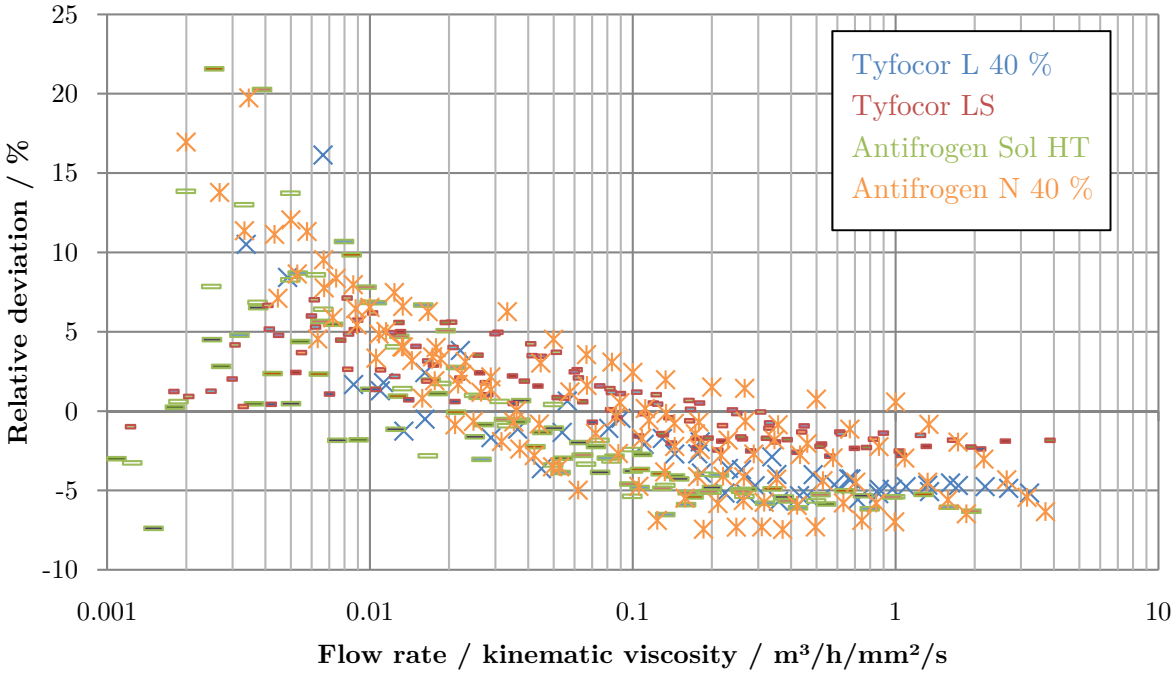

Figure 5.10: Flow rate/ kinematic viscosity ratio influence on Sensor II "Solar"-Version

Based on its measurement results, this type of sensor has been corrected for two fluids, Tyfocor L 40 % and Tyfocor LS. Both corrected versions have been measured with multiple fluids to examine the sensor's capability to measure a variety of glycol-based fluids.

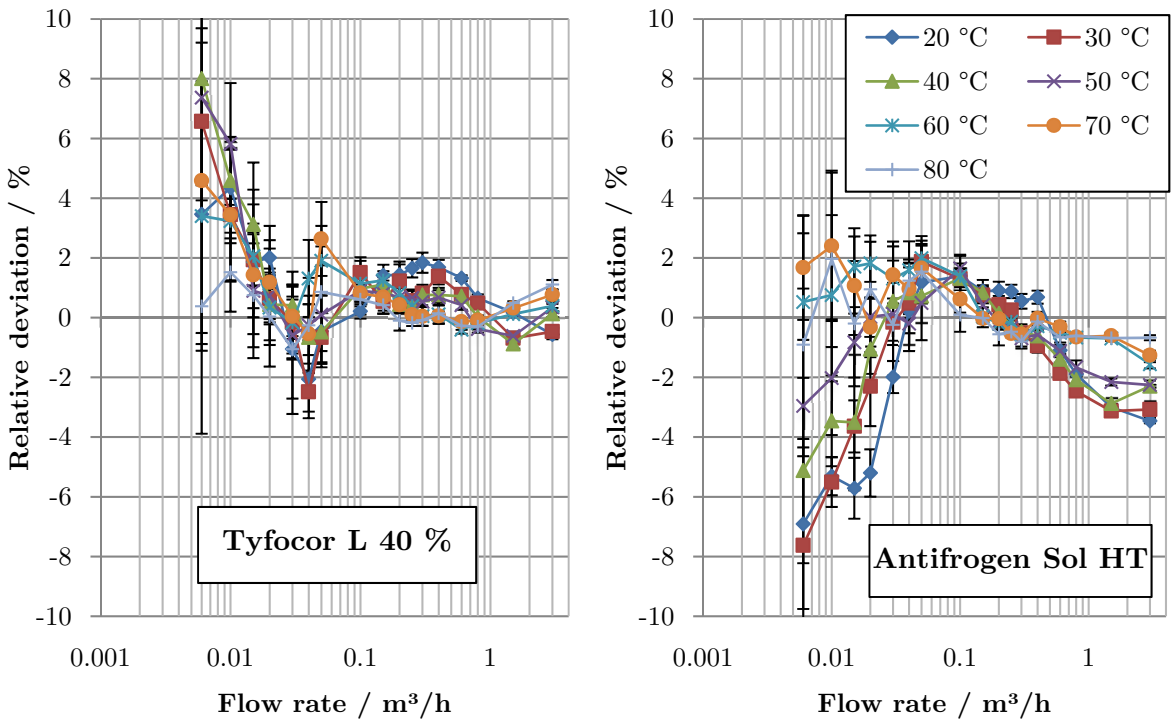

Figure 5.11: Corrected sensor for Tyfocor L 40 % with Tyfocor L 40 % and Antifrogen Sol HT

Figure 5.11 shows the results of the sensor, which was corrected for Tyfocor L 40 %, measured with Tyfocor L 40 % and Antifrogen Sol HT. The deviations and the temperature spread are

well corrected for the fluid the sensor is intended to measure. Above 15 l/h, all deviations lie within ± 3 %, from 100 l/h upwards, the deviations lie within ± 2 %. With Antifrogen Sol HT, however, deviations tend to be negative; especially at low flow and low temperatures (up to ~ -8 %) and at high flow rates (up to ~ -3.5 %).

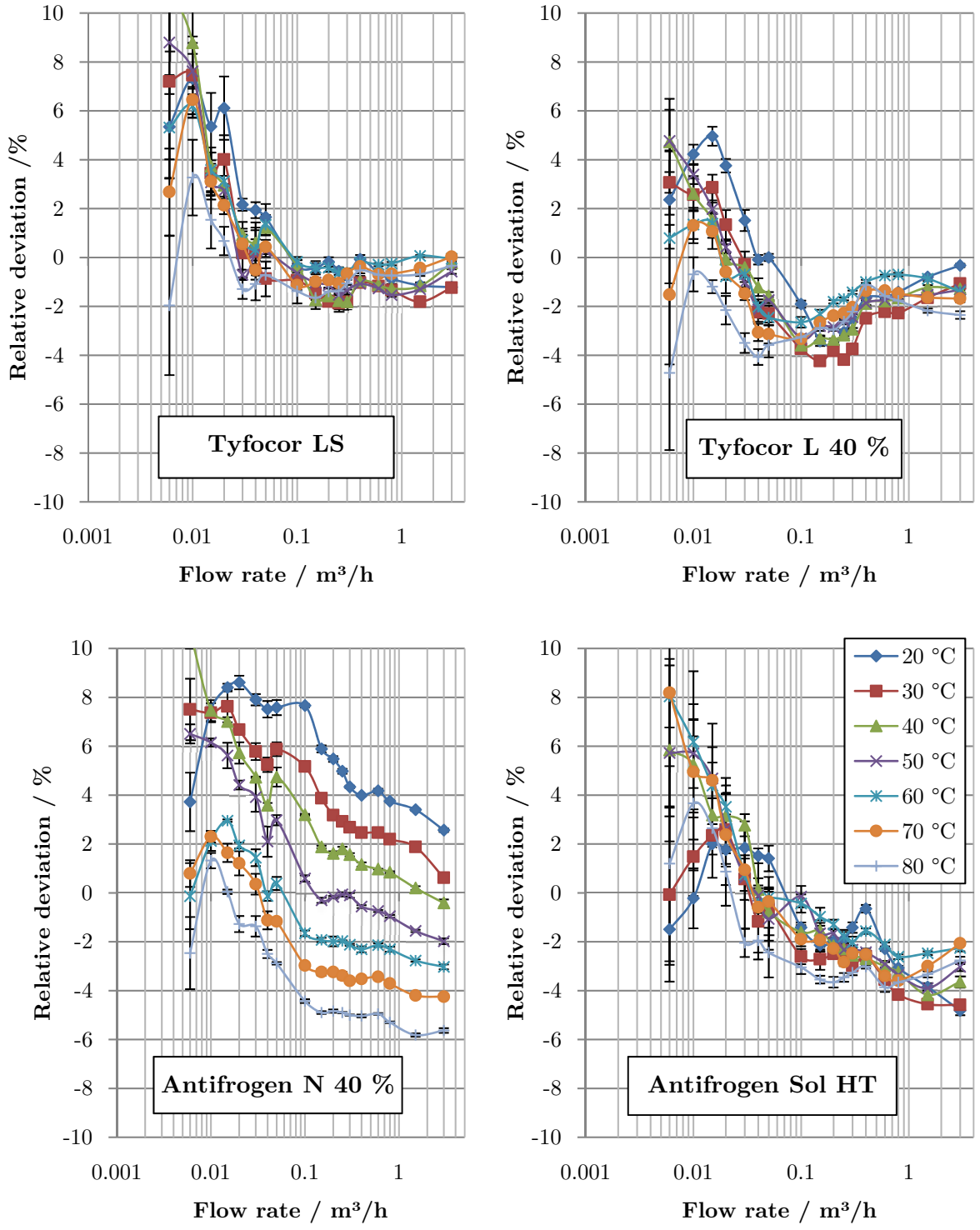

Figure 5.12: Corrected sensor for Tyfocor LS with several fluids

Figure 5.12 shows the measurement results with the sensor that has been corrected for Tyfocor LS. Measured with Tyfocor LS, the results lie between ± 2 % above 30 l/h. The temperature dependency is well corrected. Applied with Tyfocor L 40 %, the results are slightly shifted to negative deviations (~ -4 %) while the temperature dependency is comparable to the results with Tyfocor LS. All deviations lie within ± 5 %. With Antifrogen N 40 %, the temperature dependency is more pronounced, manifested in increasing deviations both in negative and positive direction (between ~10 % and ~ -6 %). In use with Antifrogen Sol HT, the overall temperature dependency is comparable to the results with the PG-based fluids, but the deviations tend to larger negative deviations at high flow (~ -5 %).

5.1.3 Sensor III

This ultrasonic q_p 1.5 flowmeter belongs to the accuracy class 2 according to DIN EN 1434. The lower limit of its flow rate q_i is 6 l/h; the heat meter shall operate at this flow rate without the maximum permissible error being exceeded. The permanent flow q_p is 1500 l/h and the upper limit of the flow rate q_s is 3000 l/h.

5.1.3.1 Water

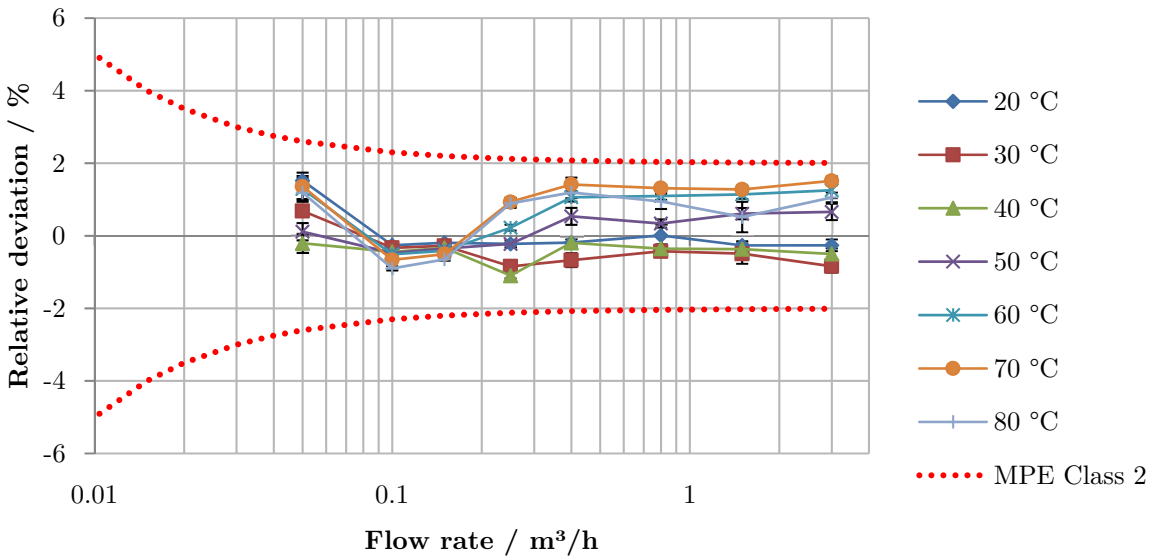

Figure 5.13: Results of flow measurements of Sensor III with water

Measured with water, the results lie well within its permissible limits (cf. Figure 5.13). The standard deviation is low throughout its flow range.

5.1.3.2 Glycol-Water-Mixtures

Figure 5.14 shows the results of Sensor III with glycol-based mixtures. Overall, relative deviations are clearly lower than the deviations that have been measured with the other US sensors. Apart from the low flow region, the temperature dependency is lower for all measurements. Above 100 l/h, the deviations measured with all examined fluids lie in a slightly

positive-orientated band within 6 % and -2 %. With Tyfocor L 40 % and Antifrogen N 40 %, even the low flow region can be measured with deviations below ~9 % and good repeatability. For these two fluids, all deviations above 100 l/h lie below 5 % and above 1 %.

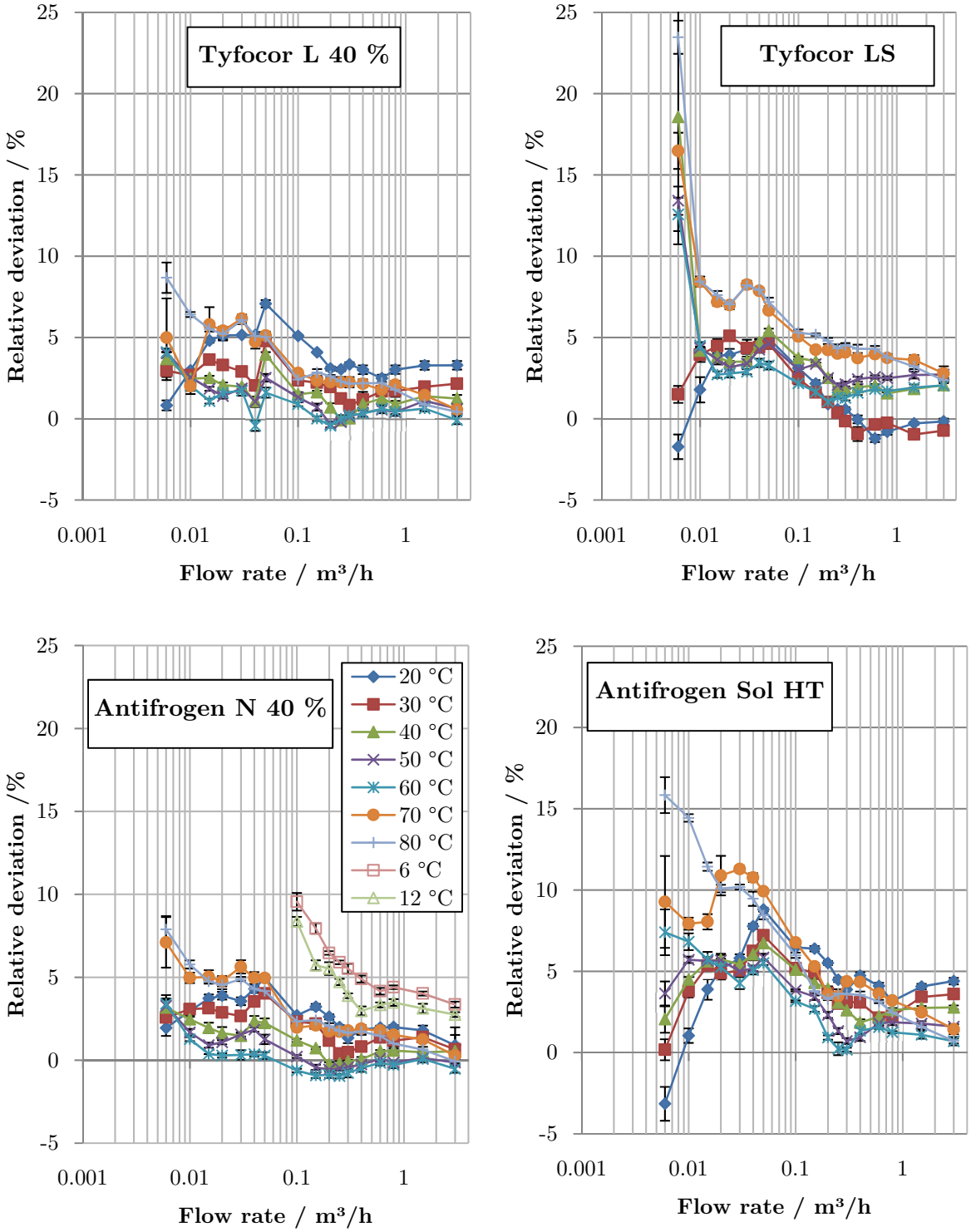

Figure 5.14: Results of flow measurements of Sensor III with glycol-water-mixtures

With Tyfocor LS and Antifrogen Sol HT, the deviations at low flow regions are larger, wide-spread and less repeatable (outlier with up to 23 %). Above 100 l/h, relative deviations are less temperature-dependent and lie within 7 % and ~ -1 % deviation.

Figure 5.15 shows the influence of the FVR on the deviations of Sensor III. In comparison to water, all deviations tend to positive deviations. Apart from some outliers for FVR values below 0.01, all deviations are below ~10 %. For FVR values above 0.1, all deviations are below ~5 %. Again, the influence of the flow conditions (triggered by viscosity influence) on the measurement result seems to be less pronounced for this US sensor compared to the other examined sensors.

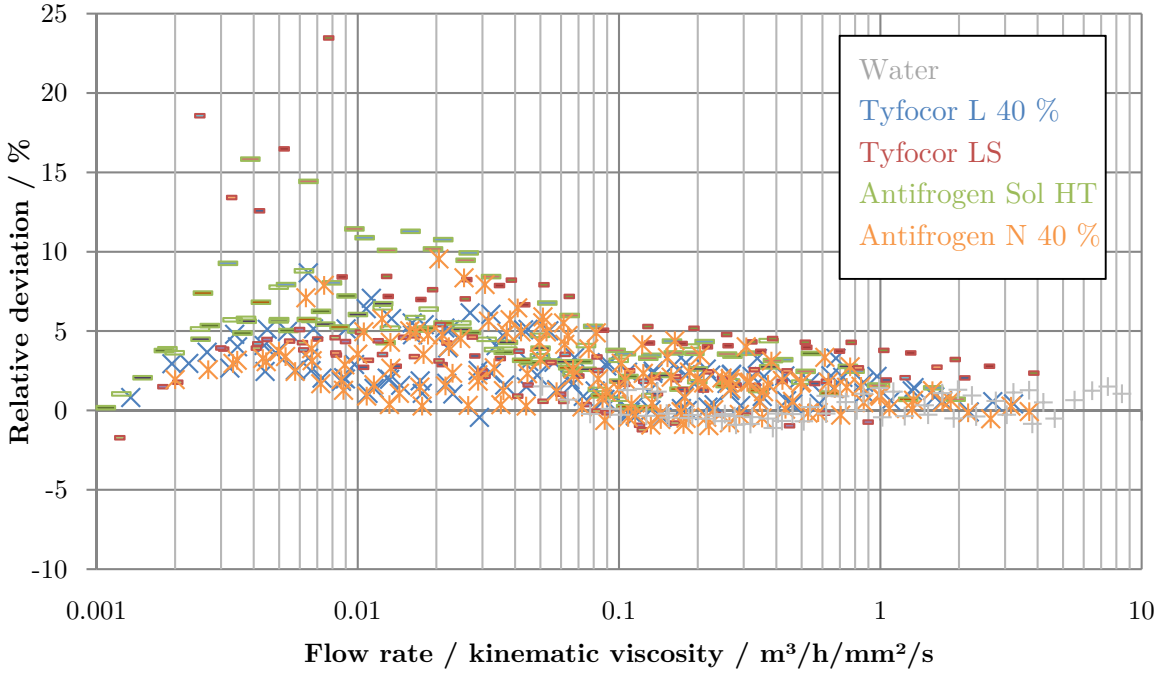

Figure 5.15: Flow rate/ kinematic viscosity ratio influence on Sensor III

5.1.3.3 Corrected Sensor Results

Though the results of this sensor with glycol-based fluids were better than the results experienced with the other (uncorrected) US sensors, corrections on the sensor have been applied to improve its performance for a special fluid.

Figure 5.16 shows the comparison between the uncorrected sensor measured with Tyfocor L 40 % (left) and the corrected version of the sensor (right). Main focus of the corrections has been the shift from slight positive deviations towards zero line. While that effect has been well-corrected (for all measurements starting from 15 l/h, its deviations are within ± 4 %), the temperature dependency could be subject to further improvements.

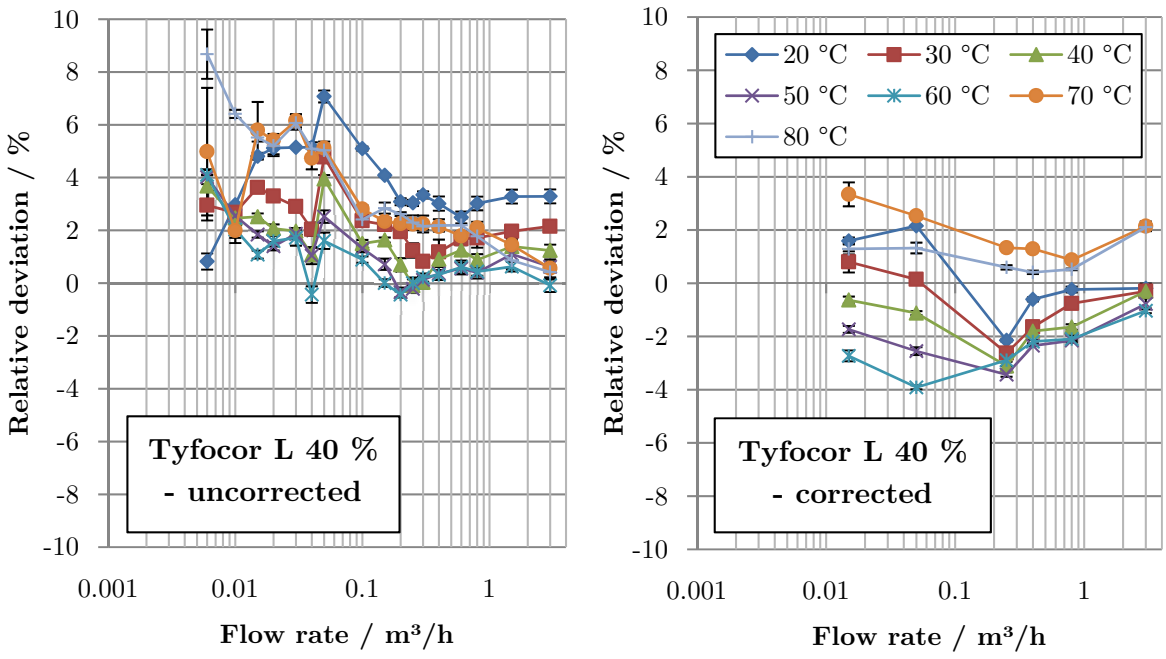

Figure 5.16: Corrected sensor III with Tyfocor L 40 %

5.1.4 Ultrasonic Flowmeters - Summary

This chapter aims at giving a summary on the results of three reasonably different US sensors.

The sensors based on the *phase difference* method (Sensor II for water and Tyfocor LS, respectively) are highly dependent on the speed of sound. For example:

- The water version produced an deviation of approx. -20 % at 20 °C for a flow rate of 150 l/h and above.
- As the speed of sound of observed fluids is a factor of ~1.1 higher than the speed of sound of water (cf. Figure 3.11: Comparison of $c(\Theta)$), its factor calculated to the power of two (approx. 1.21) directly influences the measurement
- It leads to corresponding deviations of around -20 % at 20 °C, at least for high flow rates.

While that factor has been expected, the simple approach to correct the sensor based on its speed of sound is not sufficient enough to push its deviations within usable boundaries over the entire flow range (cf. Figure 5.8: Influence of c-ratio on measurements). The influence of the flow profile on the measurement, especially at low flow rates, makes further adjustments (based on empirical methods) necessary. Otherwise, the results qualitatively correspond to the results of transit time difference-based Sensor I. Corrected sensors proved useful for measuring two special fluids (Tyfocor LS and Tyfocor L 40 %). Deviations with the respective fluid of use led to deviations comparable to an accuracy class 3 sensor, at least for flow rates of 30 l/h and higher. If those corrected sensors were used with related fluids (with comparable viscosity and speed of sound; Tyfocor LS, Tyfocor L 40 %, Antifrogen Sol HT), deviations below ± 5 % are achievable for flow rates of 30 l/h and above. Used with a fluid with a differing speed of sound-

temperature dependency (Antifrogen N 40 %), deviations increase to ± 8 % for flow rates of 30 l/h and above.

US sensors based on the principle of *transit time difference* are sensitive to flow state as deviations are shifted to more (Sensor I) or less (Sensor III) positive deviations which are highly temperature-dependent. This type of sensor isn't primarily depending on the measuring fluid's speed of sound but on the flow conditions. As the theoretic flow profile of water (the fluid, the sensors have originally been calibrated with) differs from the flow profile of glycol water mixtures, the flow rate is usually overestimated according to following assumption:

- During calibration/design process, the sensor is calibrated to measure water at designated flow rates and temperatures.
- Turbulent flow is desired as the velocity distribution inside the pipe is more even than at laminar flow state.
- Thus, the mean velocity is less sensitive to changing flow rates in turbulent flow state.
- But: at minimal flow rates of 6 l/h or 15 l/h, laminar flow rates can be assumed.
- Thus, the sensor's allowed flow range is assumed to include laminar, transient and turbulent flow.
- Calibration factors are determined empirical for the fluid water.

As the viscosity of glycol-based fluids is decisively higher than the viscosity of water, the Reynolds number of glycol-based fluids is shifted to higher flow rates compared to water. Thus, at flow rates where water is already in turbulent flow state, glycol-based fluids may still be in laminar or transient flow state (cf. Figure 3.10: Theoretical turbulent flow profile for water and other glycol-based fluids). Theoretically, laminar and transient flow state causes overestimation of flow velocity as velocity ratio between maximum and mean velocity is higher compared to turbulent flow. That leads to the case, that especially at lower flow rates, the mean velocity is overestimated which leads to positive deviations.

Theoretically, the adjustment of the Aichelen point for average flow velocity (0.71 R for laminar flow and 0.77 R for turbulent flow) could be an option to improve measurements at certain flow rates for a specific medium of known viscosity, at least under the assumption of an undisturbed flow profile. In practice, the flow conditions inside the measuring section of the sensor are highly complex and depending on the respective sensor design. That leads to disturbed flow profiles which make experimentally determined adjustments ("corrections") to the specific sensor to certain fluids, temperatures and flow velocities necessary.

Those corrections have been applied on both transit time difference sensors, though sensor III produced relatively good results right away. The corrections performed on sensor I improved the results dramatically but not satisfyingly for billing purposes. The corrections on sensor II enable the user of this sensor to gain results with relative deviations below ± 4 % throughout

the flow range between 15 l/ and 3000 l/h. It is agreed to perform further corrections on both sensors.

5.2 Impeller Flowmeter

5.2.1 Sensor IV

This impeller flowmeter in single-jet design belongs to the accuracy class 3 according to DIN EN 1434. The lower limit of its flow rate q_i is 30 l/h; the heat meter shall operate at this flow rate without the maximum permissible error being exceeded. The permanent flow q_p is 1500 l/h and the upper limit of the flow rate q_s is 3000 l/h.

5.2.1.1 Water

The measurement results with water (cf. Figure 5.17) are partly outside the upper limit of the flow sensor. Apart from that, the sensor shows the typical error curve of an impeller flowmeter. At low flow, the deviations are highly negative, which makes the sensor useless at those flow rates. At transient flow regime, the deviations are positive. At higher flow rates, the deviations tend towards zero. Repeatability is good, a distinct temperature dependency appears only at flow rates below the minimum usable flow rate of 30 l/h.

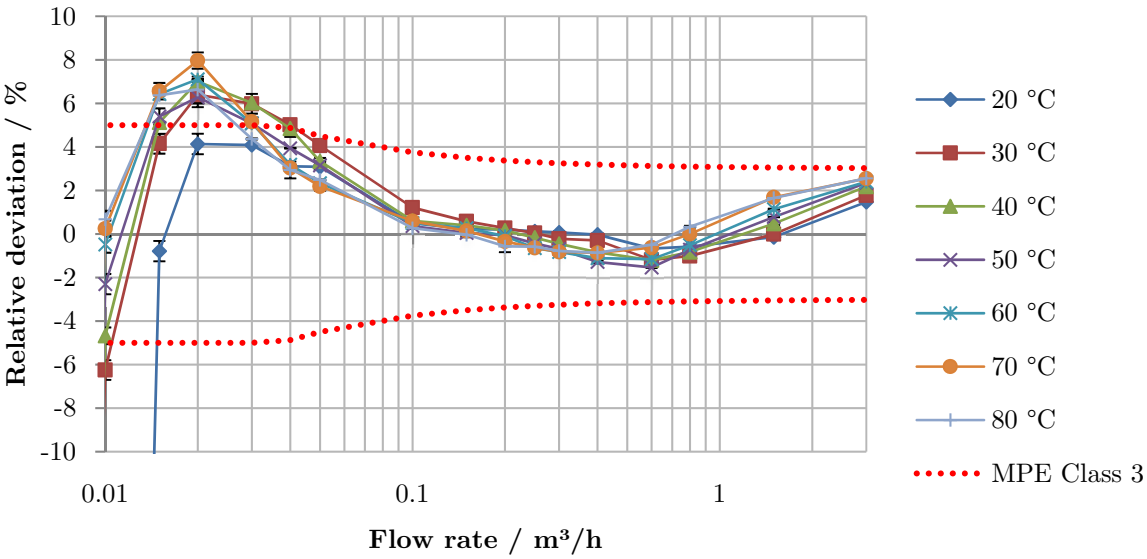

Figure 5.17: Results of flow measurements of Sensor IV with water

5.2.1.2 Glycol-Water-Mixtures

The results of the measurements with glycol-based fluids are shown in Figure 5.18. The results display the typical error curve of an impeller flowmeter. Compared to water, the maximum relative deviations of the characteristic overshoot towards positive deviations (~7 %) is not increased. The overshoot is shifted to higher flow rates in accordance to the specific medium's viscosity. Water, for example, has its highest deviation for 20 °C at 20 l/h while Antifrogen

Sol HT has this peak for the same temperature at 400 l/h. Apart from this shift to higher flow rates, the deviations show a good repeatability and a low temperature dependency.

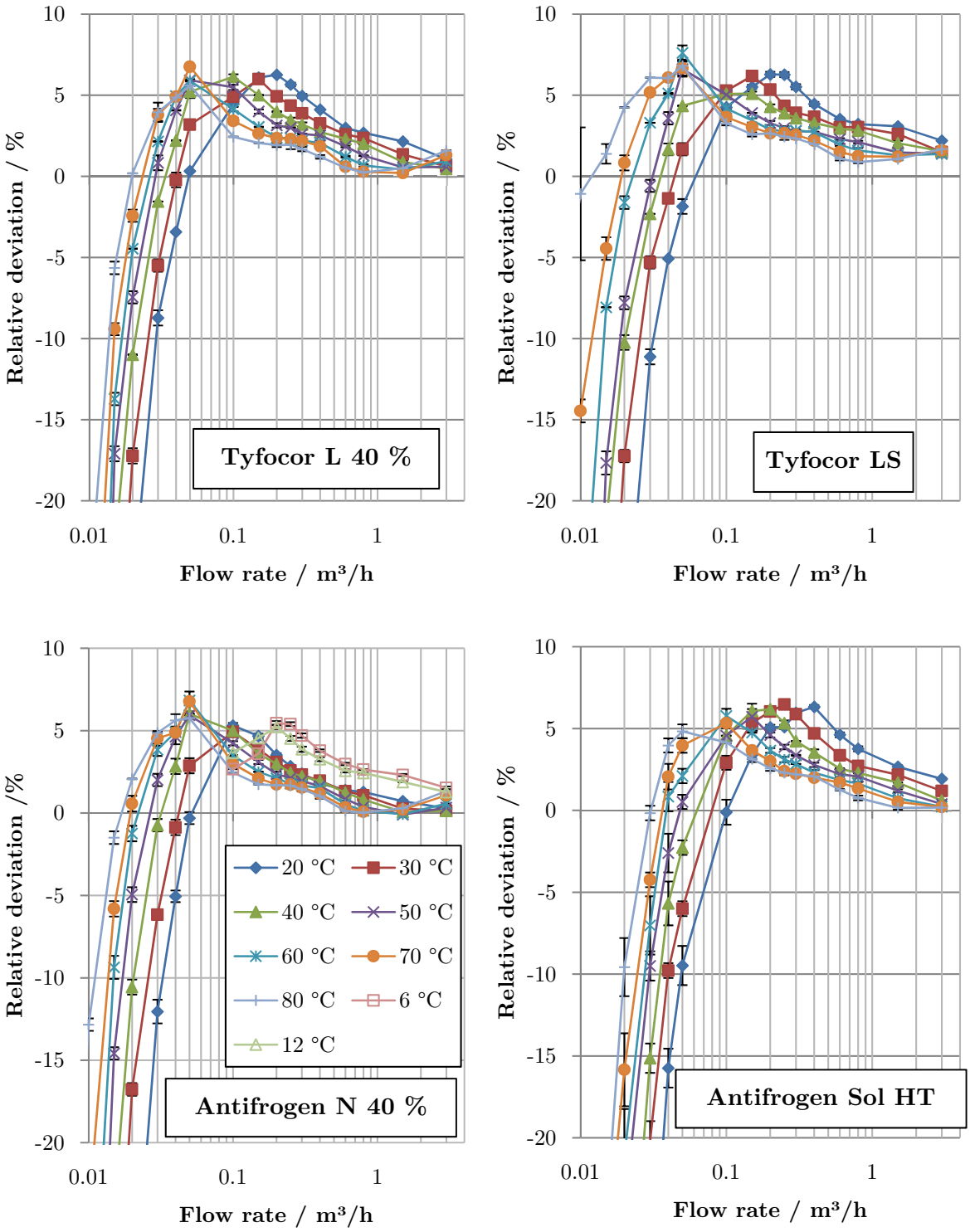

Figure 5.18: Results of flow measurements of Sensor IV with glycol-water-mixtures

The Re-dependency (or FVR influence) of this sensor is introduced in Figure 5.19. Apart from the low flow region, the deviations all lie within a narrow band of ~3 %, which is valid for FVR-values above 0.05.

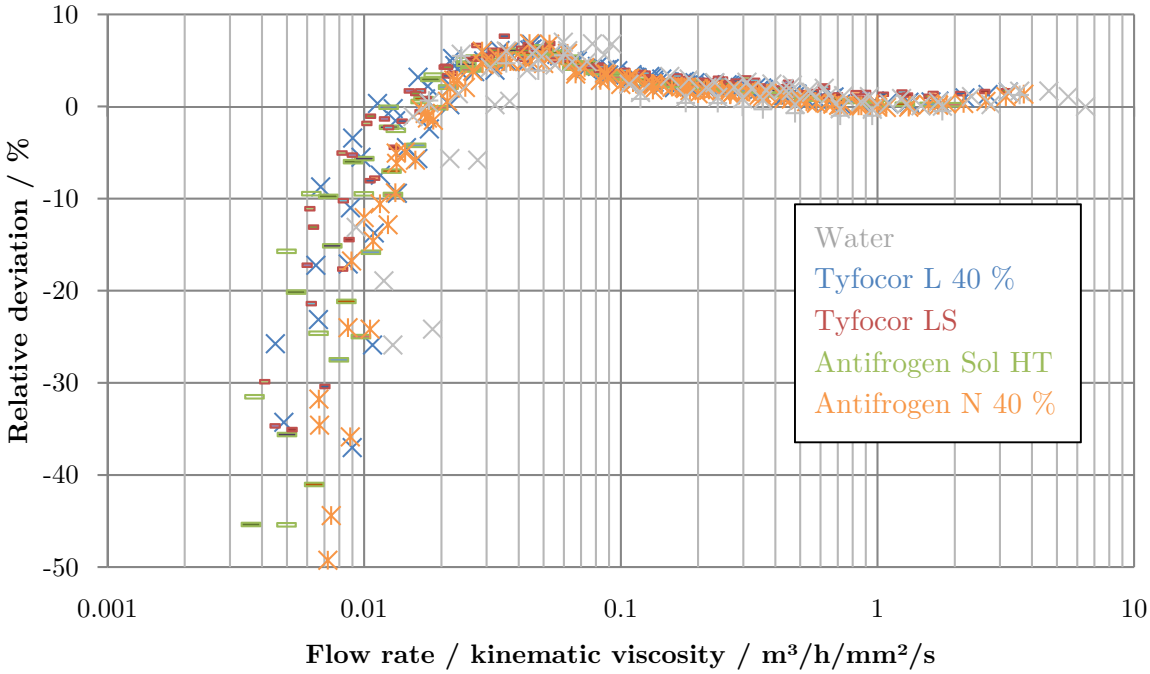

Figure 5.19: Flow rate/ kinematic viscosity ratio influence on Sensor IV

5.2.2 Sensor V

This impeller flowmeter belongs to the accuracy class 3 according to DIN EN 1434. The lower limit of its flow rate q_i is 30 l/h; the heat meter shall operate at this flow rate without the maximum permissible error being exceeded. The permanent flow q_p is 1500 l/h and the upper limit of the flow rate q_s is 3000 l/h.

5.2.2.1 Water

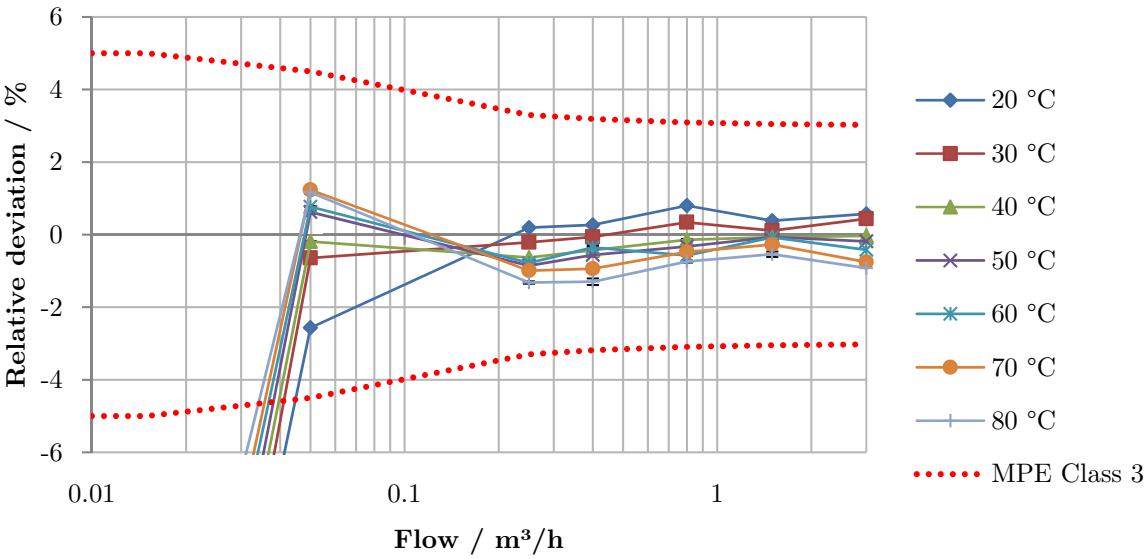

Figure 5.20: Results of flow measurements of Sensor V with water

The results with water (cf. Figure 5.20) are well within class 3 limits. Below the lower flow limit, deviations are negative. Positive overshooting is less pronounced than with Sensor IV. It

is assumed that those deviations at the transient area between lower flow rates and higher flow rates are internally corrected.

5.2.2.2 Glycol-Water-Mixtures

Figure 5.21 gives the results of Sensor V with glycol-based fluids. As observable with water, the positive overshooting is well controlled.

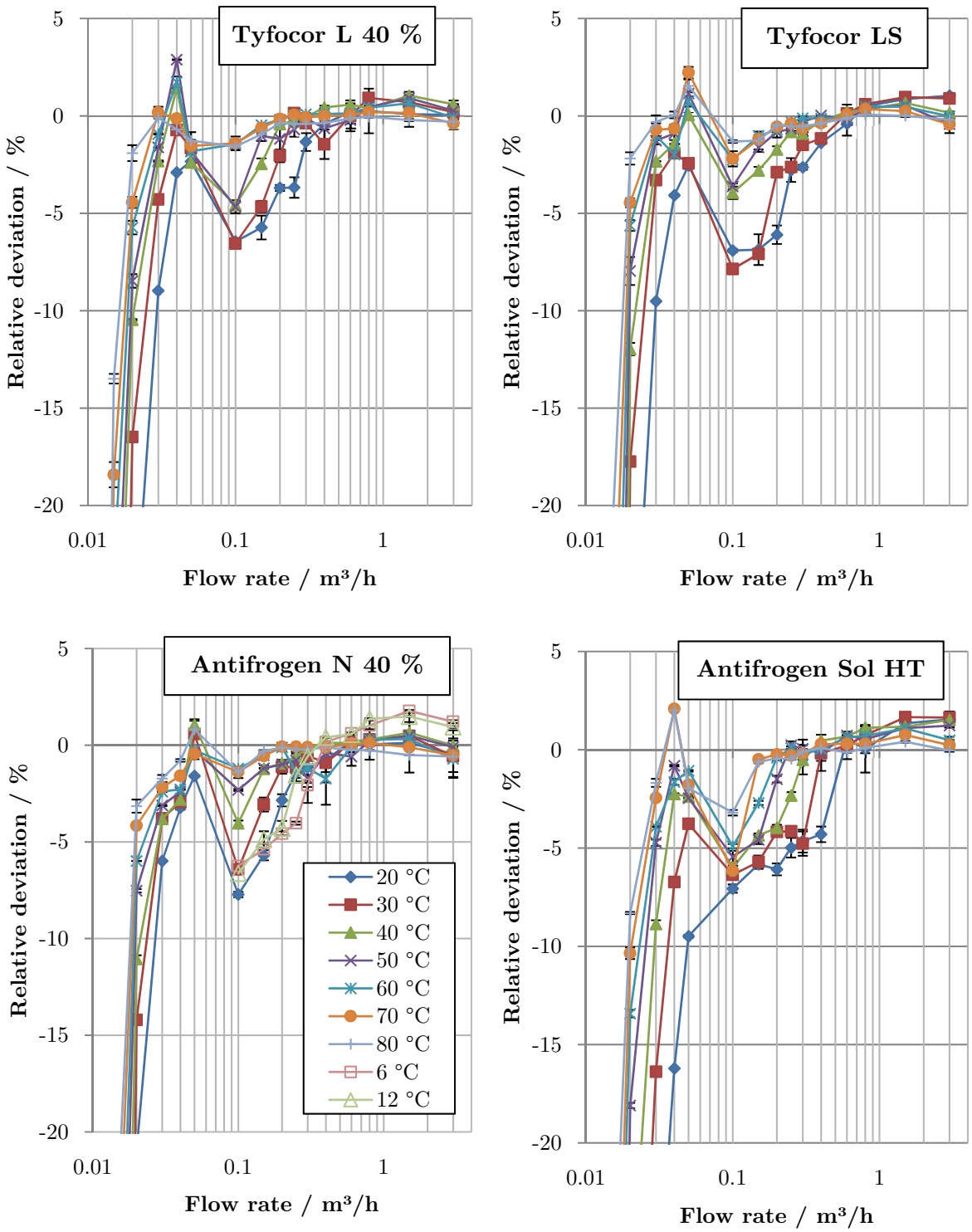

Figure 5.21: Results of flow measurements of Sensor V with glycol-water-mixtures

There is a secondary overshoot towards negative deviations, that may be resulting from the assumed internal corrections of the sensor regarding the measuring fluid water. These corrections could be an explanation for the Re-dependency (cf. Figure 5.22), which is less reasonable than experienced with Sensor IV. Above a FVR value of 0.1, all deviations lie within a narrow band of deviations of ~3 %. Below, the pattern is more chaotic and less predictable.

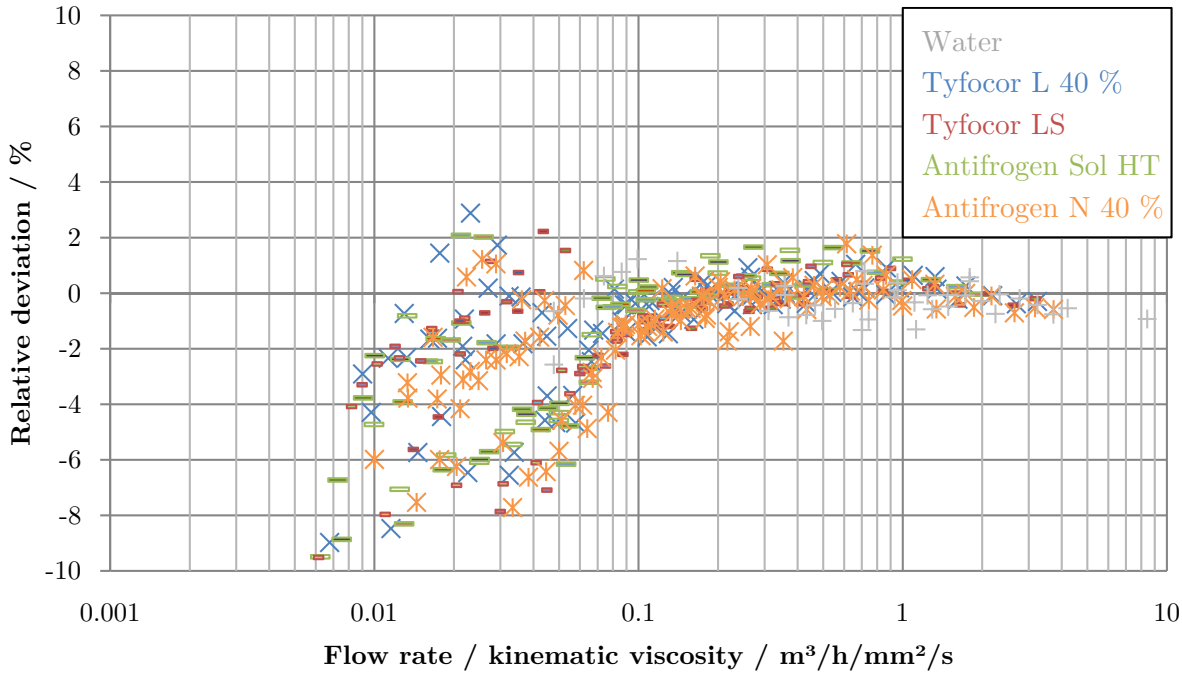

Figure 5.22: Flow rate/ kinematic viscosity ratio influence on Sensor V

5.2.2.3 Corrected sensor results

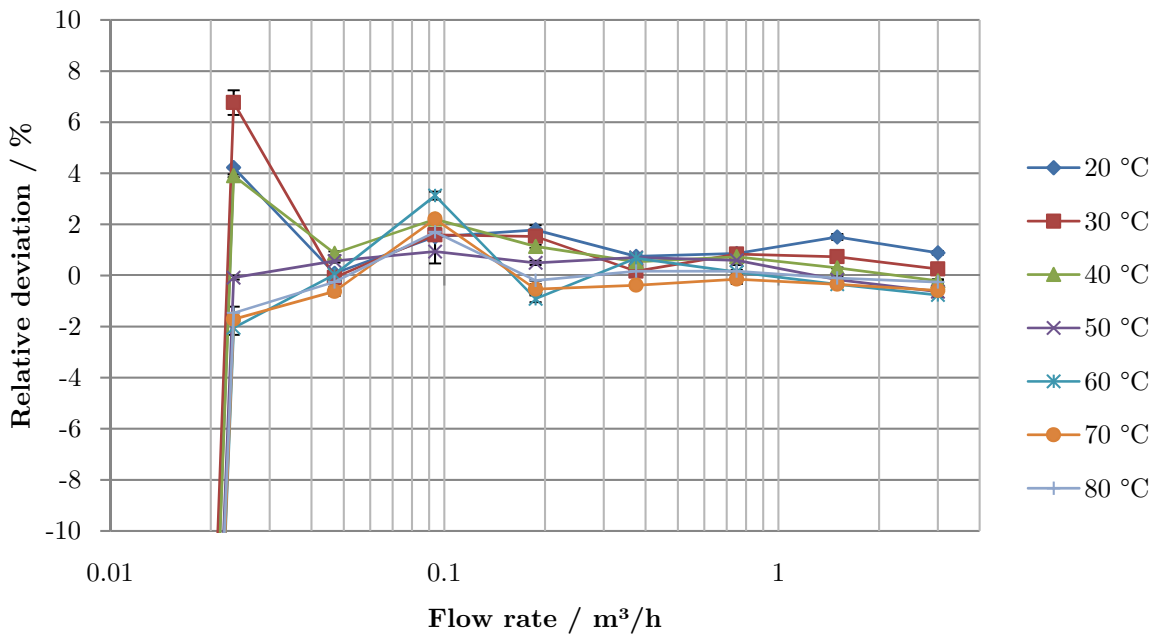

Figure 5.23: Corrected Sensor V with Tyfocor L 40 %

Sensor V has been corrected based on the flow measurements and put to test with the fluid Tyfocor L 40 % (cf. Figure 5.23). The corrections were performed according to the assumption that deviations at low flow (below 100 l/h) are negligible for the sensor's practical use. Thus, the corrected sensor shows large relative deviations at low flow (~6 % at 23.4 l/h; 3.1 % at 93.8 l) but is well corrected for flow rates above 100 l/h (±2 %).

5.2.3 Impeller Flowmeters - Summary

Overall, both impeller flow sensors tend to follow the Re-dependency with the typical error curve of impeller flow sensors:

1. Large negative deviations at low flow which makes the sensor useless at those flow rates.
2. Pronounced positive deviations at transient flow regime.
3. Tendency towards low deviations at high flow rates.

To be more exact, Sensor IV strictly follows Re-dependency while Sensor V seems to have internal corrections applied which lead to a "secondary overshooting" towards negative deviations. At higher flow rates, both sensors behave alike.

Sensor V has been corrected to a certain medium allowing deviations lower than ± ~3 % above 50 l/h or ±2 % above 100 l/h.

Real-life applications tend to work at higher flow rates (cooling: >1000 l/h) or at medium flow rates and higher temperatures (solar: > 100 l/h and > 70 °C). Thus, impeller flow sensors showed acceptable results for both applications (cooling: < 4 %; solar: < 6 %), regardless of possible corrections. If EG-based fluids are used for cooling purposes (which is reasonable due to its favourable viscosity), deviations lie within typical water meter class 2 limits. In this special case of high flow rates around 1000 l/h, corrections to the flow sensor are not necessary. However, if hardware corrections to a certain medium are planned, the sensor could be regulated by:

- Varying the flow channel angle on the impeller; a shift in direction of the rotation axis of the impeller leads to shorter lever and a later start-up of flow but also to less overshoot of the error curve towards negative deviations.
- A corresponding displacement of the angle in the opposite direction extends the lever of the impeller and improves the start-up behaviour, with the positive overshoot appearing more pronounced. (A combination of both may be possible.)
- In general, attempts should be made to generate turbulence to force a "steady flow" of the impeller [96].

5.3 Alternative Principles

The measurement results that have been presented so far, are related to sensors, which are mass products. For certain applications, more reliable alternatives to those economically

reasonable sensors might be necessary. This chapter deals with electromagnetic and Coriolis flowmeters and their measurement results with glycol-based fluids.

5.3.1 Electromagnetic Flowmeter

The investigated sensor is designed for batch metering. It is a small-scale device and certainly belongs to the more affordable electromagnetic flowmeters. Thus, there might be sensors with better accuracy which might accordingly be related to higher expenses.

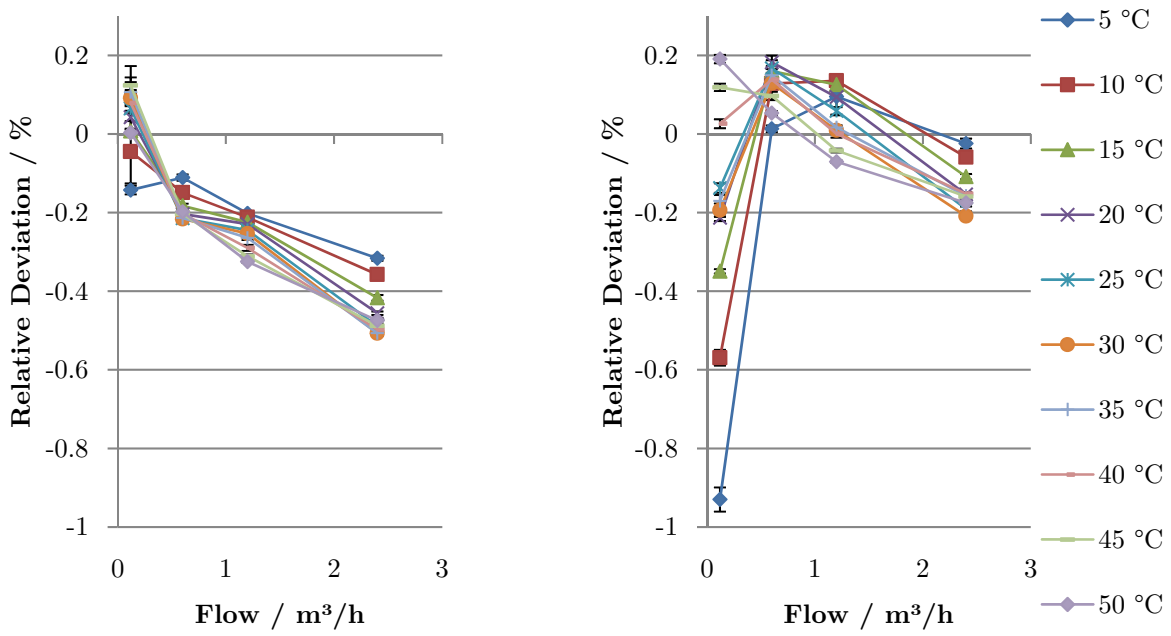

Figure 5.24: EFM measurements with water (left) and Tyfocor LS (right)

Figure 5.24 shows measurement results with the EFM measured with the measuring fluid water (left) and the measuring fluid Tyfocor LS (right), a PG-based fluid. With water the deviations of the measurements between 120 l/h and 2400 l/h are within -0.5 % and 0.2 %. There is little temperature dependency and a very good repeatability throughout the measured range. Measured with Tyfocor LS, the deviations appear more temperature-dependent, especially at the lower flow limit. At a flow of 120 l/h and a temperature of 5 °C, relative deviations are almost -1 %. With higher temperatures, the results improve drastically. Above 30 °C, all deviations are within ±0.2 % throughout the flow range. Interestingly, the maximum relative deviations at high flow are lower with Tyfocor LS than the maximum deviations with water. This case can be explained with the sensor's Reynolds-dependency (cf. Figure 5.25). At lowest Reynolds numbers of ~300, the deviations are negative. With increasing Reynolds numbers (up to ~4000), the deviations tend to zero. Above Re=4000, deviations tend to negative direction. In this area, deviations below -0.2 % occur at Re numbers above 40000. Those values are simply not reached with Tyfocor LS due to its higher viscosity.

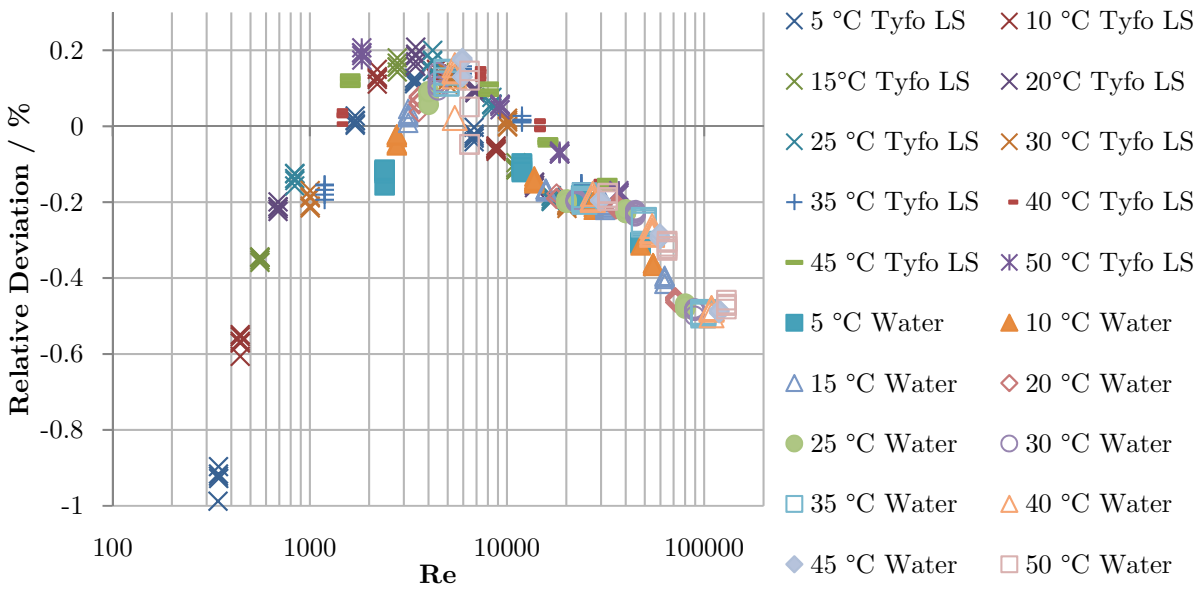

Figure 5.25: Relative deviations of the EFM sensor as a function of *Re*

Overall, the usability of the EFM in use with glycol-based fluids can be stated, though its flow range from lowest to highest flow might be limited to a factor of 1:20.

5.3.2 Coriolis Flowmeter

The Coriolis sensor is of interest for applications that require low deviations and/or a second measurement parameter (density). This sensor has been applied as best measuring device for most of the volumetric test rig's measurements. In addition, the included density measurements are used to control the respective fluid's stability during the flow investigations.

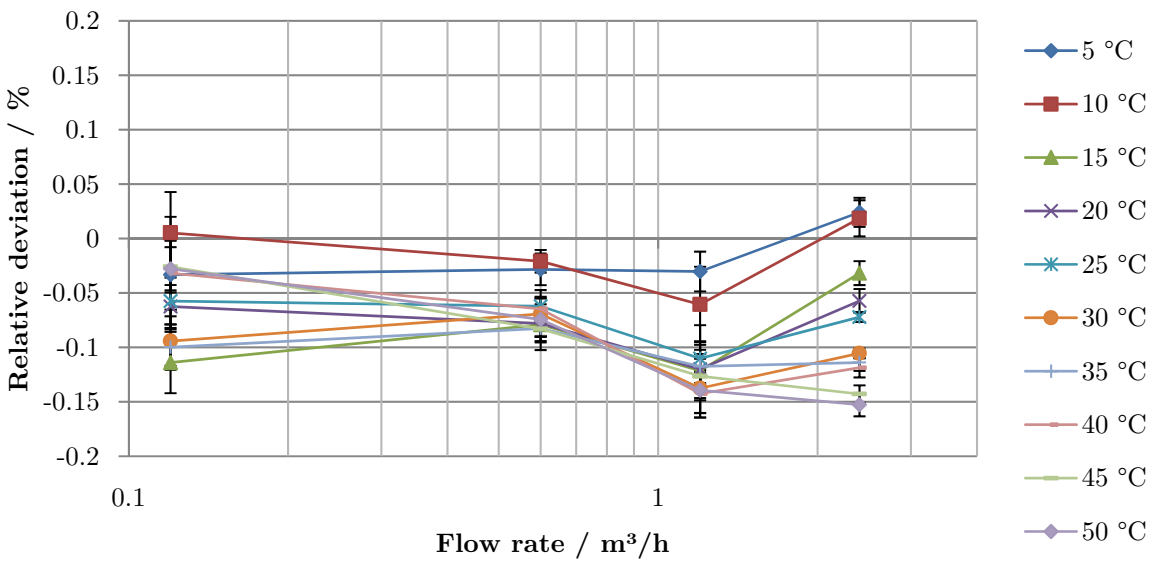

Figure 5.26: Measurement results of the Coriolis sensor with water

Thus, a lot of measurement data is available for all 4 glycol-based fluids and water. Figure 5.26 and Figure 5.27 show exemplary results with water and with glycol-based fluids, respectively.

Overall, for a flow range between 40 l/h and 3000 l/h, all deviations are within ~0.2 % and -0.4 %. A temperature dependency is observable, which associates increasing temperatures with slightly increasing negative deviations (at 3000 l/h, the deviations develop from ~0.1 % at 20 °C to -0.4 % at 80 °C).

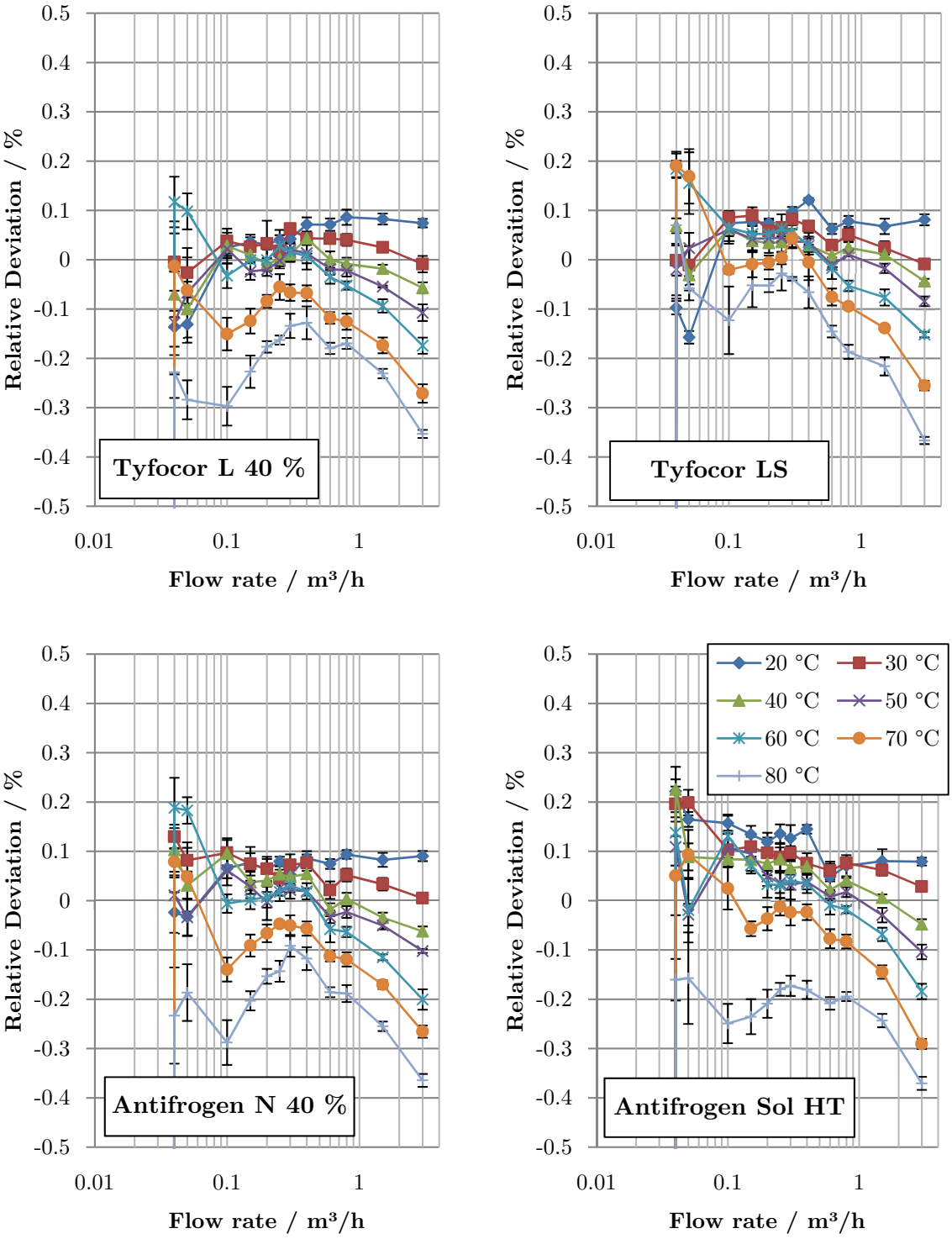

Figure 5.27: Results of flow measurements of the Coriolis sensor with glycol-water-mixtures

The temperature dependency can be corrected through internal zero-point adjustments of the sensor. Apart from its temperature dependency, the sensor shows little to no dependency to the specific fluid in use (slight deviations to the other fluids can be observed with Tyfocor LS at 80 °C). At lower flow rates (<100 l/h), the standard deviation is increased compared to measurements at higher flow rates.

As observable in Figure 5.28, the relative deviations all lie within a field of ±0.2 %. At lower FVR-values the centre of the field is approx. located at zero deviation while at higher FVR-values the field centre tends towards -0.2 %.

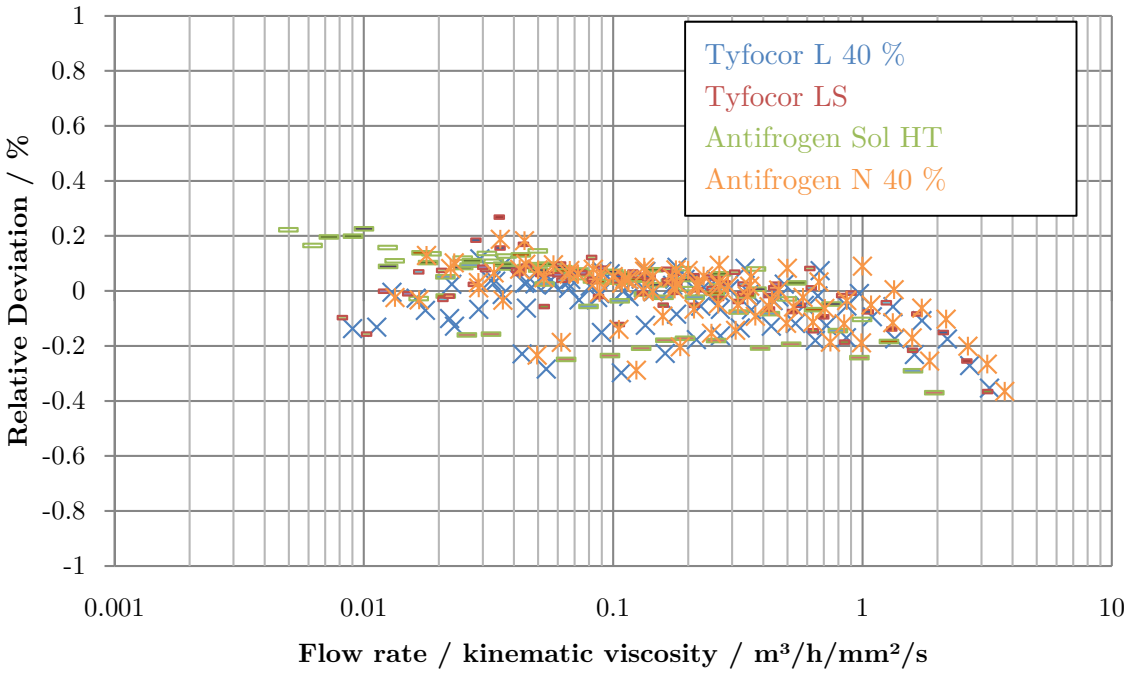

Figure 5.28: Flow rate/ kinematic viscosity ratio influence on Coriolis sensor

In summary, the Coriolis sensor is clearly capable of measuring each of the investigated fluids within narrow deviation limits. What's most beneficial compared to the other sensor types, is the potential to detect changes of the fluid through density changes. Although the flow measurement of this sensor isn't depending on the fluid's condition, a combined heat measurement certainly is dependent on the fluid's composition. Knowledge of the density depending on the temperature allows to draw conclusions on the fluid's composition (cf. 2.3.2) and subsequently on its stability in field/process.

6. Comments on Heat Metering with Glycol-Water-Mixtures

As the basic objective of this work is the introduction of glycol-water-mixtures into standardisation, the fundamental influence variables on heat metering are discussed in this chapter. While the measurement of temperature differences is supposed to have a minor influence when used with glycol (cf. 2.1.1), both the volume sensor (6.1) and the heat coefficient (6.2) results as well as their impact on heat metering (6.3) will be discussed in the following chapters. In chapter 6.4 the applicability of laboratory measurements to real-life field conditions is discussed. In chapter 6.5 options for standardisation are discussed.

6.1 Flow Measurement

The insights gained during flow measurements have been used to detect three basic possibilities to measure the flow of glycol-based fluids:

I. *Using the water-calibrated sensor for all fluids*: If no adjustments on the sensor for glycol-based media are performed, maximum deviations of around -45 % to 35 % can occur for typical applications. Those deviations are highly dependent on the flow measurement principle (cf. Figure 6.1) and the specific sensor. Obviously, the supplier and customer would have to negotiate a fair allocation of costs based on uncertain measurement data. Applying more sophisticated and expensive sensors like EFMs and Coriolis type sensors enables measurements of all the investigated fluids with deviations below 1 %. Economically, the use of those meter types is currently limited to large-scale systems.

II. *Adjustment to glycol, but not to certain medium*: If the sensor is adjusted to a certain medium but also used with other related media, deviations of around ±5 % and less are realistic (cf. Figure 5.12). That estimated value could probably be scaled-down if certain fluid groups would be used; for example, one group of EG-based fluids with 40 % glycol-fraction and a second group of PG-based fluids with 40 % glycol-fraction.

III. *Using the sensor for a certain fluid*: Adjusting the flow sensor to a certain glycol could lead to flow deviations below ±2 % to ±3 %, depending on the principle of flow measurement.

In addition to the three shown concepts of measuring with glycol-based fluids, one fundamental point should be discussed: The raise of lower flow limits of the flow sensor in use. Usual applications of glycol-water-mixtures are cooling systems with rather high flow rates of ~800 l/h and solar applications, where flow rates may be lower (min. ~100 l/h), but temperatures are higher (making the temperature-dependent viscosity less influential). Thus, a raise of q_i to reasonable values based on the sensor's application may be beneficial (in the author's opinion, a lower limit of 100 l/h would fit usual requirements). The measuring range where the largest relative deviations occur would be excluded.

6.2 Heat Coefficient

According to chapter 6.1, three basic ways to measure the flow rate of glycol-based fluids are introduced. The approach to employ three options of calculating the enthalpy change of the fluid in use corresponds.

I. *Employing the heat coefficient of water for all fluids*: No adjustments to glycol-based media leads to positive heat coefficient deviations of approx. 4 % to 18 % (for fluids and conditions that have been investigated in this work). Those deviations are highly depending both on operation conditions and the fluid in use.

II. *Adjustment of heat coefficient to glycol, but not to a certain medium*: If the heat coefficient is adjusted to a certain medium but also used with other related media, heat coefficient deviations of approx. ±1 % to ±10 % could occur, which are highly depending both on operation conditions and the fluid in use, too (cf. 3.4). The deviations may decrease to a maximum of ±3 %, if heat coefficients for certain fluid groups would be used; for example, one heat coefficient calculated for EG-based fluids with 40 % glycol-fraction and another heat coefficient calculated for PG-based fluids with 40 % glycol-fraction.

III. *Adjustment of heat coefficient to a certain medium*: If an adjustment to a certain medium was applied, the ideal heat coefficient would solely be depending on the uncertainty of its influencing parameters (measurement uncertainty of density and specific heat capacity (cf. 3.4) which is 1.5 % (k=2) for the measured fluid). Note, that real-life influences on the heat coefficient are discussed in 6.4.

6.3 Heat Metering

Both the measured volume and the heat coefficient are used to calculate the heat output of a heating system according to equation (3). Based on the assumptions made in 6.1, 6.2 and assuming, that for this simplistic way of qualitatetively determining the heat output, the temperature measurement influences are neglectable (cf. 2.1.1), the maximum range of deviations of the heat meter for a considered flow rate of 100 l/h and above are determined for two different cases (corrected and uncorrected).

Figure 6.1 gives a visual summary of all investigated sensors and the maximum boundaries of their theoretical heat metering capabilities, differentiating whether a correction to a certain fluid is applied (“C”-corrected) or not (“U”-uncorrected). Note, that relative deviations of the volume sensor (C: dark blue bars; U: bright blue bars) and relative deviations of the heat coefficient (C: dark green bars; U: bright green bars) are multiplied to obtain the relative heat output deviations (C: dark orange bars; U: bright orange bars).

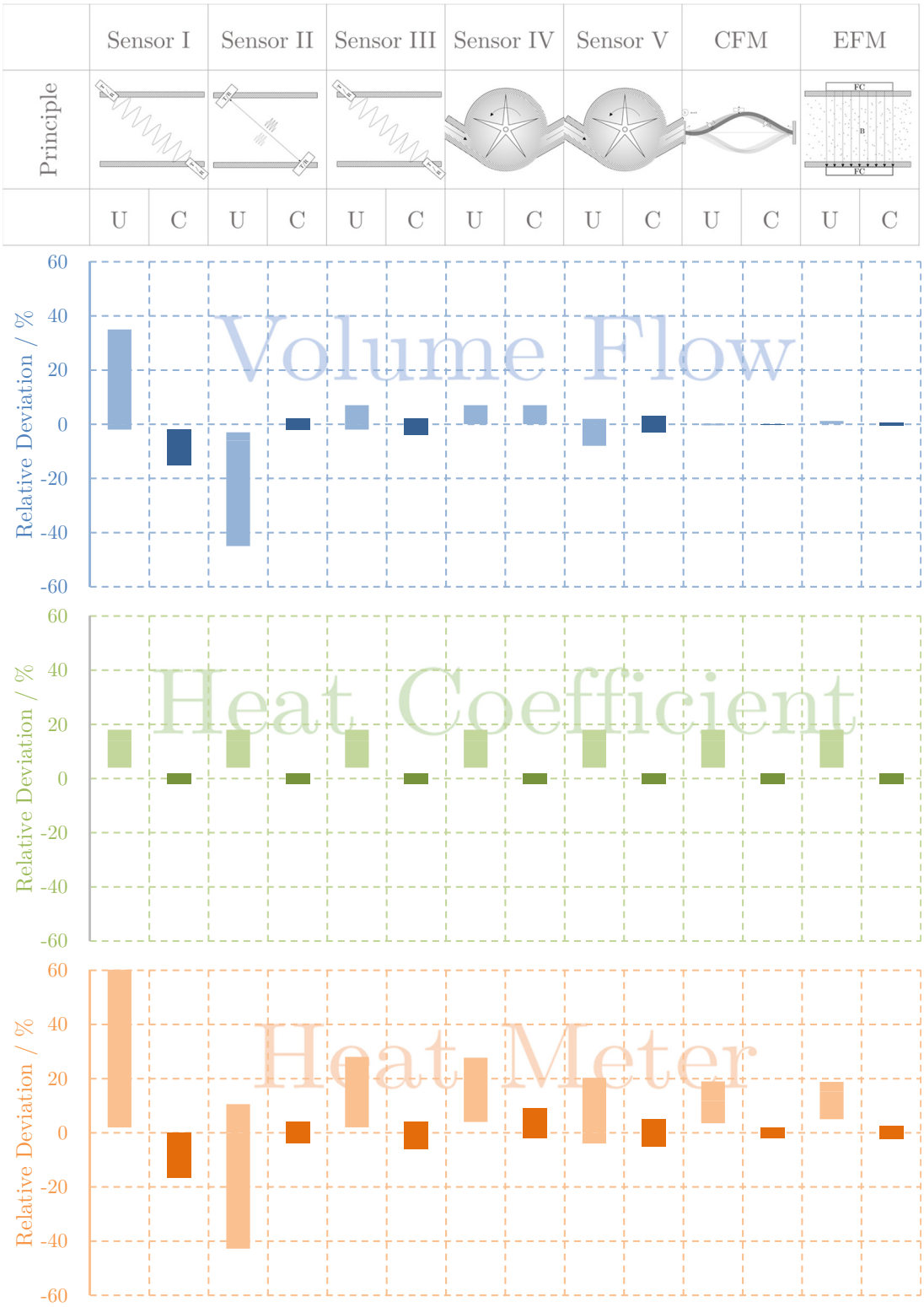

Figure 6.1: Summary of Heat Metering capabilities of investigated sensors

I. Approx. -42 % to 60 %, if *'the water heat meter for all glycol-based fluids'* is used. Note, that deviations are highly depending on the measurement principle and the fluid in use. The relative deviations of every single meter is lower than the maximum deviations of -42 % to 60 %. For example, maximum negative deviations of -42 % occur solely with the US sensor based on phase shift difference and the fluid Antifrogen N 40 % at 6 °C

and 100 l/h. US sensors based on transit time difference usually display positive volume flow deviations. Combined with heat coefficients that also display positive deviations, the respective influences can sum up, resulting in increased positive heat output deviations of up to ~60 %. Impeller flowmeters would induce deviations between -4 % and 26 %. Applying Coriolis or EFMs would lead to deviations between 4 % and approx. 18 %.

II. Approx. ± 15 %, if the heat meter is *'adjusted to glycol, but not to certain medium'*. Again, this estimate is highly depending on the fluid and sensor in use. For adjustments to certain fluid groups, the deviations could decrease to approx. ± 7 %.

III. Approx. ± 10 %, using the adjusted '*heat meter for a certain fluid'*. Note, that this value contains the combined possible deviations of all sensors; almost every single heat meter would cause lower deviations than ± 10 %. Sensor I, based on transit time difference, would cause deviations between -17 % and 0 %. Using Sensor III would lead to deviations between -6 % and 4 %. Sensor II based on phase shift difference could measure heat with deviations of approx. ± 4 %. Impeller flowmeters Sensors IV and V would lead to deviations between -2 % and 9 % or ± 5 %, respectively. Coriolis and electromagnetic flowmeters could measure the heat with deviations around ± 2 %.

6.4 Field Conditions

All results and considerations regarding the sensor's heat metering capabilities are so far based on investigations at laboratory conditions. Especially uncertainty influences regarding the fluid in real-life situations are unknown and can be seen critical. Influences of degradation, for example, are difficult to foresee, since the shown degradation experiments are not directly comparable to real solar system. Nevertheless, the author assumes neglectable changes in physical properties, if the technical system (solar heating flat plate collector) works according to its standard operation specifications. If overheating and stagnation takes place, the fluid is supposed to gradually degrade. This can lead to changes in fluid properties which may have an influence on enthalpy calculation but minor influences on the fluid's flow behaviour (although this assumption is based on results which cannot be fully linked back to "real" solar systems). Cooling applications are not supposed to be subject to degradation. Thus, no short-term changes in physical properties are expected.

Another critical point is linked to the condition of the fluid before it is deployed. Currently, the user of a typical heating or cooling system applying glycol-water-mixtures relies on manufacturer data of the fluids. That leads to at least two main problems.

1.) On the one hand, the manufacturer's published data sets of properties like density, specific heat capacity and viscosity are mainly not traceable. The reliability of those data sets is questionable, even for an unused medium. Furthermore, the composition of the fluids is subject to production-related uncertainties which may accumulate to

concentration deviations of ~1 % regarding glycol content. In this case, the uncertainties of fluid properties rise, manifesting in an influence on the heat metering's uncertainty (the viscosity affects the volume sensor indirectly; density and heat capacity affect the heat coefficient uncertainty (c.f. Appendix 10), U=1.8 % (k=2), and thus the calculation of enthalpy change directly).

2.) On the other hand, the stability of those fluids over a timespan of several years in use can cause problems. Environmental or maintenance influences may lead to changes in the fluid's content. Relevant physical properties may change accordingly. In field, the concentration change of the fluid should be monitored indirectly through reliable density or refraction index measurements. To gain consistent concentration measurements, the corresponding sensor must work within narrow uncertainty limits while great care has to be taken of environmental influences like temperature during measurement. In addition, the data sets of the fluid as well as its concentration must be reliable. Traceable measurements of relevant properties would be a solution. In practice, this procedure appears unlikely as it leads to higher investment costs in maintenance. Especially for small-scale thermal systems using glycol-water-mixtures, the effort may be non-profitable. Furthermore, once a change in concentration is detected, the question arises if the fluid in use should be brought to initial state by adding water or (the fitting) glycol concentrate. Alternatively, the change in concentration must be programmable inside the heat meter to prevent erroneous measurements. Both procedures come with rising uncertainties regarding heat metering.

It becomes obvious, that heat metering with glycol-water-mixtures includes not only effort prior to a measurement but especially during the lifespan of the respective technical system. Several influences have to be considered in order to produce reliable results.

6.5 Standardisation

Without going too much into detail it is obvious that heat metering for billing purposes requires standardisation. An accepted standard consists of general requirements and guidelines concerning the heat meter but also pattern approval and initial verification tests.

General requirements include maximum permissible errors of the heat meter and its sub-assemblies. For water, the flow sensor is categorised according to its accuracy class (Class 1: ~1 % permissible error; Class 2: ~2 % permissible error; Class 3: ~3 % permissible error). While permissible errors are depending on the flow rate q and its ratio to the permanent flow rate q_p, the maximum error needs to remain below 5 %. According to the results shown in chapter 5, there are corrected flow sensors which could satisfy Class 3 or even Class 2 error limits for a special fluid, at least if the lower limit of the flow rate is set to ~100 l/h. However, uncertainties regarding the measuring fluid and its stability may have an influence on the flow sensor,

although it is supposed to be small. The widening of existing accuracy classes or the establishment of a new accuracy class should be discussed.

For *the calculation unit* of a water heat meter, the maximum permissible error is 1.5 %. Currently, that limit cannot be satisfied. On the one hand, the expanded uncertainty (k=2) of the decisive heat coefficient is 1.5 % for the respective fluid tested in the laboratory. On the other hand, the fluid's composition may be subject to batch variation during production and field-conditions over a span of years. Based on the uncertainty of its glycol content, the uncertainty of the fluid's heat coefficient increases. For Tyfocor L, an error of 2.5 % in glycol content (e.g. 37.5 % instead of 40 %) leads to a heat coefficient with an expanded uncertainty of 3.4 % (k=2). Thus, the uncertainty that arises from the medium may be included to increase maximum permissible errors of the calculation unit.

Regarding *the testing of flow sensors*, it can be stated that calibration and testing facilities for water are common while corresponding facilities for glycol-based fluids are certainly rare. Furthermore, calibration of a sensor to a certain medium or even different media would preferably require the specific medium/media to be used as measuring fluid. Testing and calibrating the heat meter for glycol-based fluids *with the measuring fluid water* may be an authorisation requirement for the producer or the bureau of standards. The producer of the sensor could certainly use the calibration factors for water and apply them through Reynolds similarity to glycol-based fluids. Restrictions would arise from the specific fluid's viscosity which is higher than the viscosity of water (water at 20 °C has the same viscosity as Tyfocor L 40 % at 77 °C, Tyfocor LS at 82 °C, Antifrogen N 40 % at 68 °C and Antifrogen Sol HT at >100 °C). Thus, flow conditions should be comparable at those temperatures. However, reaching the lower flow limits at a low temperature and the respective Reynolds number with a glycol-based fluid may be a problem for a facility running with water.

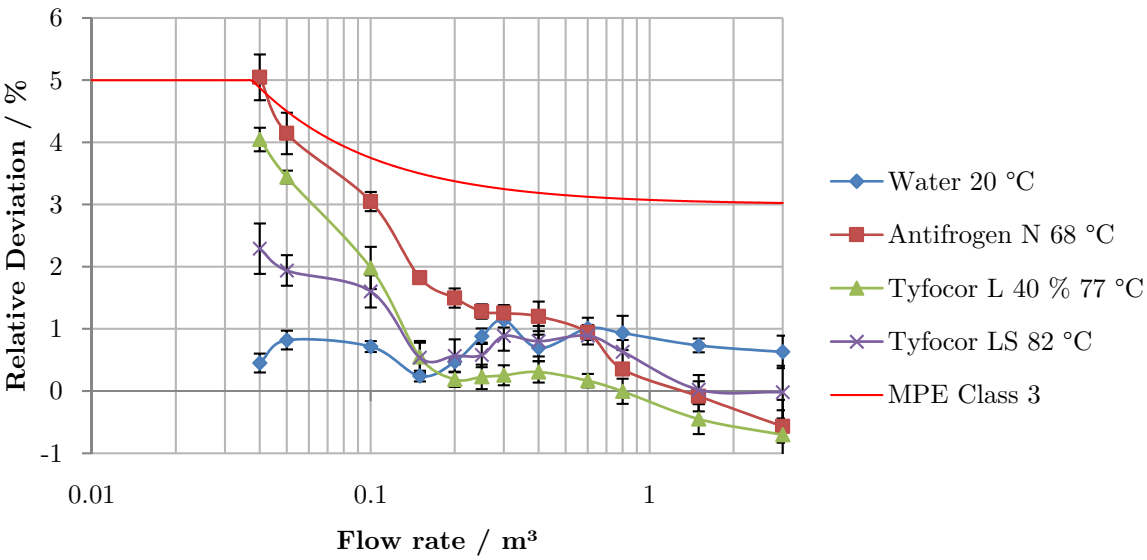

Figure 6.2: Relative Deviations of Sensor I under comparable flow conditions

Figure 6.2 shows the results of measurements done with uncorrected Sensor I and three glycol-based fluids and water. While deviations between the values are below 2 % at flow rates higher than 100 l/h, at lower flow rates the deviations rise. It is assumed, that temperature-dependent calibration factors of the sensor for water lead to larger deviations with the other fluids (the flow profile for a certain flow rate of water at 20 °C differs from the flow profile of water at 82 °C; a corresponding calibration factor corrects this difference, especially at laminar or transient flow regime). Thus, if the calibration factors for water at the respective flow rate and temperature were known, the results with glycol-based fluids could probably be improved. Obviously, this type of testing is reserved for the manufacturer of the sensor.

Testing the sensor in authorised laboratories would have to rely on another procedure. If the sensor has been tested with a specific glycol-based medium and the resulting deviations have been used to correct the sensor, the gained measurement data can be used. For example, if the water-calibrated sensor produces large negative deviations with glycol, the corrections to the sensor aim to shift the deviation in positive direction towards zero percent. Accordingly, if used in water, this specific sensor would show noticeable positive deviations depending on its correction factors. Those positive deviations of the corrected sensor with water can theoretically be derived from its uncorrected version's deviations with glycol.

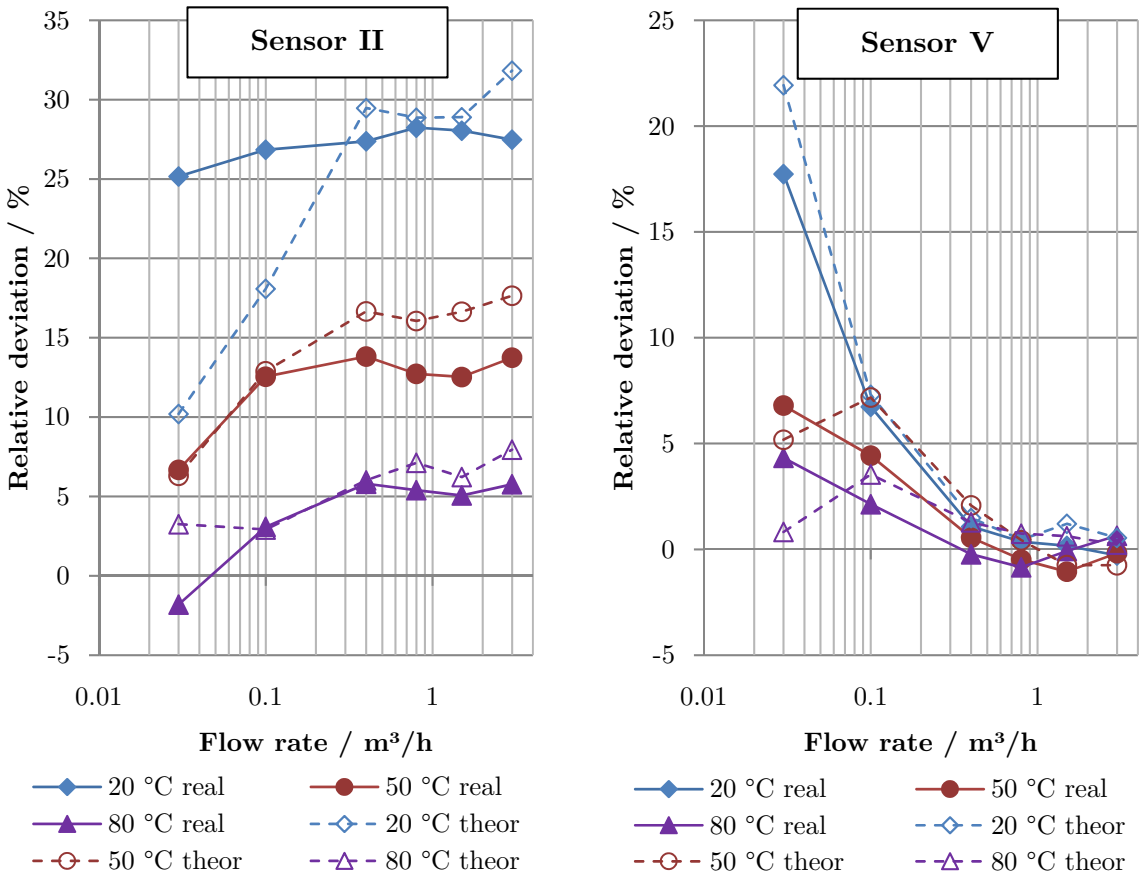

Figure 6.3: Theoretical and measured deviations of the corrected Sensors II and V with water

That case could be used for measurements with water. Basic requirements are previous measurements with the glycol-based medium and the knowledge of its results. Figure 6.3 shows the results of the corrected versions of Sensor II (left graph) and Sensor V (right graph) for Tyfocor L 40 %, but measured with water, as theoretically derived and practically measured. Measurements were performed at 20 °C, 50 °C and 80 °C at flow rates between 30 l/h and 3000 l/h. The results show that the principle works qualitatively while it should be noted that the standard deviation of the respective measurements with glycol and water directly influences the quality of the correction. Especially at higher flow rates, the results are promising while deviations and standard deviations at low flow rates tend to be less reliable. Currently, this procedure is performed for other sensors to gain further insights of its capabilities.

If this procedure was used, for example for initial verification tests, the corresponding maximum permissible error of the MUT would have to be based on a value, which probably isn't the value "0". For the example of Sensor II in Figure 6.3 and a flow rate of 1.5 m^3/h at 20 °C fluid temperature, the MUT would be approved if the measured value was within 28.9 ± 3 % (if the sensor would be declared a class 3 sensor). In this specific example and at this specific temperature and flow rate, the MUT would be approved as its relative deviation is at 28.0 %.

7. Summary/Outlook

Within the scope of this work data has been collected and procedures have been developed to enable the introduction of heat meters for glycol-water-mixtures into legal metrology. In a first step, the heat transfer and flow properties for a selection of 4 glycol-based media have been investigated. The second step included the determination of these fluids' influences on the flow measurement of heat meters. Therefore, a new volumetric testing facility at PTB's laboratories has been designed, built and validated.

Traceable investigations of the physical properties density $\rho(T)$, kinematic viscosity $\nu(T)$ and specific heat capacity $c_p(T)$ of the heat conveying fluids Tyfocor LS, Antifrogen Sol HT, Tyfocor L and Antifrogen N partially showed deviations of up to 18 % from the manufacturer's data. The gained data allows calculations of heat coefficients based on traceable measured values. Furthermore, preliminary investigations indicated that a review of the stability of the heat conveying medium under conditions of use (degradation) is necessary. Therefore, by means of two methods, aging effects on the above-described thermophysical properties of the heat carrier were investigated. Heat transfer properties partially changed to varying degrees depending on the glycol base, with Antifrogen Sol HT having an increase of its specific heat capacity by about 5 %. On the other hand, the influence of degradation on flow properties remained small as only slight changes in density and viscosity occurred. As the transferability to field conditions is currently not possible, further measurements with improved measuring instruments and in-field data acquisition are planned to confirm and further explore the field of degradation.

Furthermore, a new volumetric test rig was built to measure glycol-water-mixtures with an expanded uncertainty (k=2) between 0.017 % and 0.36 %, based on the flow rate and temperature. It currently allows temperatures between 3 °C and 90 °C (extendable to a range of -20 °C to 110 °C) and flow rates between 6 l/h and 3000 l/h, enabling a range of applications for the solar and cooling industry to be tested.

Test results of 5 mass-market suitable flowmeter types like ultrasonic and impeller flowmeters partially showed maximum deviations multiple times bigger than current maximum permitted deviations. The variety of deviations between the sensors was wide, regardless of similarities of the measurement principle. One ultrasonic sensor showed highly temperature-dependend positive-orientated deviations of up to 35 % for flow rates above 100 l/h. Another ultrasonic sensor measured the respective flow with highly temperature-depending negative deviations of up to -45 %. A third ultrasonic sensor appeared less fluid-depending showing deviations between -2 % and 7 % for any measured fluid. Deviations measured by impeller flow sensors appeared less pronounced. The first impeller flow sensor had deviations between 0 % and 7 % at flow rates of 100 l/h and above. The second impeller flow sensor showed deviations between -8 % and 2 %.

While total deviations differed from sensor to sensor, the results were well repeatable, and the specific deviations were comprehensible. After applying medium-specific corrections to the sensors, the results could mostly be improved drastically (±2 % deviations for Sensor II; ±3 % deviations for Sensor V) or improved considerably (deviations between -15 % and -2 % for Sensor I; deviations between -4 % and 2 % for Sensor III). Those improvements indicate that a legal use of those sensors in near future is possible. More sophisticated sensors like Coriolis or Electromagnetic flow sensors measured within a narrow deviation range below 1 %.

Further investigations included the evaluation of legal in-field use of glycol-based media, possible challenges and testing procedures. Restrictions may arise due to uncertainties in the specific fluid's composition as well as its stability in the field. Periodic or continuous testing of the fluid's composition may be appropable. Testing and calibration of glycol-applicable sensors with water as a basic requirement for legalisation appears feasible as experimentally shown by the author. However, further investigations with water will be done to gain deeper insights of the sensors' capabilities.

Future activities will focus on investigations regarding the fluid as well as the heat meter. That includes steps to gain a deeper understanding of the fluid and its behaviour in real-life installations. In-field data aquisition is planned to gain insights into possible fluid change processes with a statistically relevant base. Furthermore, the uncertainty of the heat coefficient could be drastically improved by applying more sophisticated measurement techniques to measure the fluid's heat capacity.

Investigations concerning the heat meter include flow measurements with slightly differing fluid concentrations to determine the fluid concentration influence on the flow sensor. Thus, the influence of fluid batch manufacturing uncertainties and the degradation of the fluid on the heat meter could be estimated more precisely. Furthermore, first accelerated long-term stability tests are currently performed. These consist of preliminary measurements of a batch of sensors with a glycol-based fluid. On a test stand which enables 4000 rapid temperature changes between 10 °C and 95 °C at a flow rate of 1.5 m^3/h, the sensors are put under thermal stress to simulate the sensor's lifetime in a glycol-based system. After simulation, the sensors are put to test again and compared to the preliminary measurements. First results are promising.

Flow-related investigations are currently restricted to small-scale sensors due to the capabilities of the current volumetric test rig. Thus, larger scale sensors are not tested yet. As larger scale applications for glycol-based media like solar district heating and cooling may become more and more relevant in today's growth-oriented society, measurements of the corresponding flow sensors may be necessary. Thus, test stands are needed, which can meet the requirements of those sensors in their respective applications.

8. References

[1] J. Rose, "Messtechnische Anwendungsfragen im Bereich EE-WärmeG," in *Technische Aspekte im EEG: Messung & Technik*, Landesvertretung Hessen, 2015, https://www.clearingstelle-eeg-kwkg.de/files/node/2684/Rose.pdf.

[2] F. Adunka and W. Kolaczia, "Zur Fehlerkurve der Flügelradzähler bei Flüssigkeiten mit hoher Viskosität," *Fernwärme international, FWI,* pp. 329-334, Heft 6, Jg. 13 1984.

[3] J.-F. March, "Der Einfluss von Glykol-Wasser-Gemischen auf die Messrichtigkeit von Wärmezählern für thermische Solaranlagen, PTB-Bericht ThEx-14," Wirtschaftsverlag NW, Bremerhaven, 2000, ISBN: 3897016397.

[4] J.-F. March, "Der Einfluss von Glykol-Wasser-Gemischen auf die Messrichtigkeit von Rechenwerken bei Wärmezählern für thermische Solaranlagen PTB-Bericht ThEx-24," Wirtschaftsverlag NW, Bremerhaven, 2002, ISBN: 3897018748, https://www.dbu.de/OPAC/ab/DBU-Abschlussbericht-AZ-16403.pdf.

[5] F. Adunka, Handbuch der Wärmeverbrauchsmessung, 4. Auflage, Essen: Vulkan Verlag, 2011, ISBN 3802723732, pp. 64-70.

[6] H. Spoor, "Enthalpie und k-Faktor bei Wasser-Glykolgemischen," in *European Metrology Association for Thermal Energy Measurement - Sommerschule*, Seeon, 2013.

[7] K. Lustig, "Experimentelle Untersuchungen zum Stillstandverhalten thermischer Solaranlagen," in *Experimentelle Untersuchungen zum Stillstandverhalten thermischer Solaranlagen*, Karlsruhe, Universität Karlsruhe, 2002, https://publikationen.bibliothek.kit.edu/2272002/1456, p. 118.

[8] J. Rose and T. Lederer, "Angewandte Wärmemengenmessung in strömenden Fluiden: Wärme- und Kältezähler," *PTBmitteilung, Amts- und Mitteilungsblatt der Physikalischen Deutschen Bundesanstalt Braunschweig und Berlin, 119. Jahrgang,* p. 32, March 2009, https://www.ptb.de/cms/fileadmin/internet/publikationen/ptb_mitteilungen/mitt2009/Heft1/PTB-Mitteilungen_2009_Heft_1.pdf.

[9] DIN Deutsches Institut für Normung, *DIN EN 60751:2009-05,* DIN Deutsches Institut für Normung, 2009, https://www.beuth.de/en/standard/din-en-60751/115799593.

[10] CEN - European Committee for Standardization, *DIN EN 1434-1:2015,* CEN - European Committee for Standardization, 2015, https://www.beuth.de/en/standard/din-en-1434-1/232361955.

[11] H. D. Eckert, in *Wärmezähler-Handbuch, 2. Auflage*, Frankfurt am Main, VWEW-Verlag, 1994, ISBN: 3802203909, p. 256.

[12] M. Nau and G. Leitgen, "Messunsicherheit bei der Temperaturmessung in strömenden Wasser-Glykol-Gemischen," in *European Metrology Association for Thermal Energy Measurement Summer School 2016*, Seeon, 2016.

[13] A. Brethauer, T. Fröhlich and E. Engels, "Vergleich von Wasser und Wasser-Glykol-Gemischen bei der Temperaturmessung," *tm - Technisches Messen,* pp. 635-643, 10 2018, https://doi.org/10.1515/teme-2018-0054.

[14] T. Boeckmann et al, "Long Term Stability of Coriolis Flow Meters: DESY experience," IOP Publishing, Bristol, 2017, https://iopscience.iop.org/article/10.1088/1757-899X/171/1/012140.

[15] European Solar Thermal Industry Federation, "Overview of the state of the art heat measurement technologies for larger solar thermal systems," ESTIF, -, 2007, http://www.estif.org/fileadmin/estif/content/policies/STAP/Measurement_state_of_the_art.pdf.

[16] U. Trenkner and P. Dias, "Technical study report on measuring, remote monitoring and remote controlling for solar thermal systems," United Nations Environment Programme, Paris, 2015, http://solarheateurope.eu/wp-content/uploads/2017/07/Technical-Study-Report-on-Measuring-Remote-Monitoring-and-Remote-controlling-for-Solar-Thermal-Systems.pdf.

[17] O. Fiedler, Strömungs- und Durchflußmeßtechnik, R. Oldenbourg Verlag GmbH, München, 1992, ISBN: 9783486221190.

[18] J. Hengstenberg, B. Sturm and O. Winkler, "Messen und Regeln in der chemischen Technik," in *Messen und Regeln in der chemischen Technik*, Berlin, Springer-Verlag Berlin Heidelberg GmbH, 1964, DOI: https://doi.org/10.1007/978-3-662-00100-4, p. 246.

[19] H.-C. Obst and I. Thomas Rogers.European Union Patent EP0407948 B1, 1995, https://patentimages.storage.googleapis.com/92/e9/b6/8c53868e3a2e86/EP0407948B1.pdf.

[20] R. C. Baker, An Introductory Guide to Flow Measurement, London: Professional Engineering Publishing Limited, 2002, ISBN 9780791801987.

[21] L. e. a. Dong-hui, “Investigation of the mixture flow rates of oil-water two-phase flow using the turbine flow meter,” in *The 6th International Symposium on Measurement Techniques for Multiphase Flows*, 2009, https://doi.org/10.1088/1742-6596/147/1/012062.

[22] K. Tawackolian, Fluiddynamische Auswirkungen auf die Messabweichung von Ultraschall-Durchflussmessgeräten, Berlin: Technische Universität Berlin, 2013, http://dx.doi.org/10.14279/depositonce-1141.

[23] R. W. Miller, Flow Measurement Engineering Handbook, New York: McGRAW-HILL BOOK COMPANY, 1983, ISBN: 9780070423664.

[24] Diehl Metering, “www.diehl.com,” 9 Januar 2018. [Online]. Available: https://www.diehl.com/cdn/files/pdb_files/882e8177-f7a5-11e8-96f1-00505683653e/SHARKY%20Solar%20775.pdf.

[25] J. L. Sorensen.European Union Patent EP2369305 A1, 2011, https://patentimages.storage.googleapis.com/1c/40/b6/4bbc500a5962e7/EP2369305A1.pdf.

[26] Diehl Metering, “www.diehl.com,” 9 January 2018. [Online]. Available: https://www.diehl.com/cdn/files/pdb_files/882e8177-f7a5-11e8-96f1-00505683653e/SHARKY%20Solar%20775.pdf. [Accessed 7 2 2019].

[27] Belimo, “www.belimo.ch,” 9 January 2018. [Online]. Available: http://www.belimo.ch/pdf/d/FM..R-SZ_datasheet_de-ch.pdf. [Accessed 7 2 2019].

[28] S. Baack, “Untersuchungen zur Messbeständigkeit, Messabweichung und Messunsicherheit von Wärmezählern beim Einsatz mit Glykol-Wasser-Lösungen,” in *European Metrology Association for Thermal Energy Measurement Summer School 2013*, Seeon, 2013.

[29] J. A. Shercliff, “Relation between the Velocity Profile and the Sensitivity of Electromagnetic Flowmeters,” *Journal of Applied Physics 25 (1954),* p. 817, 11 1 1954, https://doi.org/10.1063/1.1721749.

[30] C. Smyth, “Derivation of weight functions for the circular and rectangular channel magnetic flowmeters, by means of Green's theorem and conformal mapping.,” *Journal of Physics E: Scientific Instruments,* pp. 29-34, 24 10 1969, https://doi.org/10.1088/0022-3735/4/1/007.

[31] Physikalisch-Technische Bundesanstalt, *K 7.2,* Berlin, 2006, https://oar.ptb.de/files/download/56d6a9e8ab9f3f76468b4632.

[32] U. Endress, Durchflussfibel, Reinach: FLOWTEC AG, 1990, ISBN: 9783905615036.

[33] O. Büker, Untersuchungen zur Darstellung und Weitergabe der Skala 'Volumen von Wasser' mithilfe laseroptischer und konventioneller Messverfahren, Berlin: Technische Universität Berlin, 2010, http://dx.doi.org/10.14279/depositonce-2682.

[34] L. Cordova and T. Lederer, "Application of a novel method for validating the uncertainty estimation of a flow test facility," *tm - Technisches Messen, 81(9),* pp. 431-441, 2014, https://doi.org/10.1515/teme-2014-1039.

[35] M. Juling, Rückgeführte Volumenstrommessung mittels ortsaufgelöster Laser-Doppler-Anemometrie, Berlin: Technische Universität Berlin, 2016, http://dx.doi.org/10.14279/depositonce-5170.

[36] S. Raab, Simulation, Wirtschaftlichkeit und Auslegung solar unterstützter Nahwärmesysteme mit Heißwasser-Wärmespeicher, Stuttgart: CUVILLIER VERLAG, Göttingen, 2006, ISBN: 9783867270489, pp. 42-43.

[37] G. Wendt, "Analogiebetrachtungen zum Strömungsverhalten von Wasser, Gas und anderen Flüssigkeiten," in *European Metrology Association for Thermal Energy Measurement Summer School 2006*, Seeon, 2006.

[38] N. I. o. S. a. T. NIST, "NIST Chemistry WebBook, SRD 69," [Online]. Available: https://webbook.nist.gov/chemistry/fluid/. [Accessed 23 3 2018].

[39] W. Wagner and A. Pruß, "thermophysics.ru," 7 June 2002. [Online]. Available: http://thermophysics.ru/pdf_doc/IAPWS_1995.pdf. [Accessed 23 3 2018].

[40] W. Wagner and A. Kruse, Properties of Water and Steam: The Industrial Standard IAPWS-IF 97 for the Thermodynamic Properties and Supplementary Equations for Other Properties, Berlin; Heidelberg; New York; Barcelona; Budapest; Hongkong; London; Mailand; Paris; Santa Clara; Singapur; Tokio: Springer-Verlag, 1998, http://citeseerx.ist.psu.edu/viewdoc/download?doi=10.1.1.822.6326&rep=rep1&type=pdf.

[41] H. Spoor, "Enthalpie und k-Faktor bei Wasser-Glykolgemischen," in *European Metrology Association for Thermal Energy Measurement Summer School 2013*, Seeon, 2013.

[42] V. Quaschning, “Regenerative Energiesysteme, 8. Auflage,” in *Regenerative Energiesysteme, 8. Auflage*, München, Carl Hanser Verlag, 2013, ISBN 9783446442672, pp. 133-135.

[43] T. Frahm, “Solaranlagenportal,” 6 December 2017. [Online]. Available: https://www.solaranlagen-portal.com/solarthermie/lexikon/high-flow-solaranlage. [Accessed 6 12 2017].

[44] energie-experten.org, “energie-experten.org,” [Online]. Available: https://www.energie-experten.org/heizung/solarthermie/solarthermieanlage/high-flow-anlagen-und-low-flow-anlagen.html. [Accessed 6 12 2017].

[45] solarthermie.net, “solarthermie.net,” [Online]. Available: http://www.solarthermie.net/wissen/high-flow-und-low-flow-solaranlagen. [Accessed 6 12 2017].

[46] W. Rogatty, “www.ikz.de,” [Online]. Available: https://www.ikz.de/uploads/media/393--26.pdf. [Accessed 6 12 2017].

[47] W. Schenk, “Optimierung der Jahresarbeitszahl bei bestehenden Erdwärmesonden-Wärmepumpenanlagen - Strategie und Beispiele,” in *OTTI Oberflächennahe Geothermie*, Neumarkt, 2014, https://w3-mediapool.hm.edu/mediapool/media/fk05/fk05_lokal_1/fk05vs/forschung_und_entwicklung/publikationenprofschenk/OTTI_2014Optimierung_der_Jahresarbeitszahl_bei_bestehenden_Erd-waermesonden-Waermepumpenanlagen.pdf.

[48] M. e. a. Miara, “Wärmepumpen Effizienz - Messtechnische Untersuchungen von Wärmepumpenanlagen zur Analyse und Bewertung der Effizienz im realen Betrieb,” Freiburg, 2011, https://wp-monitoring.ise.fraunhofer.de/wp-effizienz//download/wp_effizienz_endbericht_langfassung.pdf.

[49] C. Lauterbach, *Potential, system analysis and preliminary design of low-temperature solar process heat systems,* Kassel: kassel university press GmbH, Kassel, 2014, ISBN: 9783862197422.

[50] O. e. a. Reul, “Coupling of borehole exchangers with solarthermal systems,” in *Proceedings of the 19th International Conference on Soil Mechanics and Geotechnical Engineering, Seoul 2017*, Seoul, 2017, https://www.issmge.org/uploads/publications/1/45/06-technical-committee-27-tc308-11.pdf.

[51] BASF - The Chemical Company, “1,2-Propylenglykol USP,” 2 2008. [Online]. Available: http://e-liquids.de/media/Zertifikate/101486.O.BASF.pdf. [Accessed 30 1 2019].

[52] Engineering ToolBox, “Ethylene Glycol Heat-Transfer Fluid,” 2003. [Online]. Available: https://www.engineeringtoolbox.com/ethylene-glycol-d_146.html. [Accessed 31 1 2019].

[53] E. Zorebski, M. Dzida and M. Piotrowska, “Study of the Acoustic and Thermodynamic Properties of 1,2- and 1,3-Propanediol by Means of High-Pressure Speed of Sound Measurements at Temperatures from (293 to 318) K and Pressures up to 101 MPa,” *Journal of Chemical & Engineering Data, Vol. 53,* pp. 136-144, 2018, DOI: 10.1021/je7004374.

[54] B. Whim, Johnson and P.G., Directory of Solvents, London Weinheim New York Tokyo Melbourne Madras: Blackie Academic & Professional, 1996, DOI: 10.1007/978-94-009-1549-7.

[55] D. Bohne, S. Fischer and E. Obermeier, “Thermal, Conductivity, Density, Viscosity, and Prandtl-Numbers of Ethylene Glycol-Water Mixtures,” *Berichte der Bunsengesellschaft,* pp. 739-742, 8 1984, https://doi.org/10.1002/bbpc.19840880813.

[56] H. Gedanitz, *Schallgeschwindigkeits- und Dichtemessungen in Fluiden,* Bochum: Ruhr-Universität Bochum, 2010, https://hss-opus.ub.ruhr-uni-bochum.de/opus4/frontdoor/deliver/index/docId/2374/file/diss.pdf.

[57] F. Hillerns and H. Schrimpf, “Korrosionsschutz und thermische Belastbarkeit,” *Sonnenenergie & Wärmetechnik,* 1999, ISSN 09448772.

[58] S. Sarge, Calorimetry - Fundamentals, Instrumentation and Applications, Weinheim: Wiley-VCH, 2014, DOI: 10.1002/9783527649365.

[59] M. Haller, A. Bohren and A. Reber, “Messung der Wärmekapazität von Solarfluiden,” Institut für Solartechnik, Rapperswil, 2017, http://www.spf.ch/fileadmin/user_upload/Forschung/Projekte/cpExakt_Schlussbericht-aR-cp_171201_oeffentlich.pdf.

[60] S. Kabelac, “Die Schallgeschwindigkeit als thermodynamische Zustandsgröße,” *Forschung im Ingenieuwesen,* no. 64, pp. 51-53, 1998, https://doi.org/10.1007/PL00010851.

[61] M. Haller and P. Vogelsanger, “WP4.D3 / Report on Corrosion and Lifetime Tests for Solar Fluids,” 2005,

https://www.researchgate.net/publication/242741766_WP4D3_REPORT_ON_CORROSION_AND_LIFETIME_TESTS_FOR_SOLAR_FLUIDS_FINAL_DRAFT.

[62] D. A. Stankowiak, “Vercracktes Glykol . ein unterschätztes Phänomen,” *SOLARTHERMIE,* p. 172, 2010, https://www.ihks-fachjournal.de/fachartikel/download.php?title=vercracktes-glykol-ein-unterschaetztes-phaenomen.

[63] R. Hausner and C. Fink, “Stagnation Behaviour of Thermal Solar Systems,” AEE INTEC, Arbeitsgemeinschaft ERNEUERBARE ENERGIEN, Institute for Sustainable Technologies, Gleisdorf, 2000, https://www.aee-intec.at/0uploads/dateien48.pdf.

[64] W. Rossiter, “The Determination of acidic Degradation Products in aqueous Ethylene Glycol and Propylene Glycol Solutions using Ion Chromatography,” *Solar Energy Materials, Volume 9, Issue 3,* pp. 267-279, October-December 1983, https://doi.org/10.1016/0165-1633(83)90049-7.

[65] W. Stichel, “Untersuchung der Korrosionsschutzwirkung von Wärmeträgern Teil 2, Chemische Korrosionsuntersuchungen mit dem Rotations-Zylinder und zum Schutz gegen Spaltkorrosion,” *Materials and Corrosion, Volume 48, Issue 10,* pp. 659-671, October 1997, https://doi.org/10.1002/maco.19970481002.

[66] J. Scheuren, Untersuchungen zum Stagnationsverhalten solarthermischer Kollektorfelder, Kassel: Unidruckerei der Universität Kassel, 2008, ISBN: 9783899584301.

[67] W. Stichel, “Einsatz von Frostschutzmitteln in Heizungsanlagen,” *IKZ-Haustechnik, 21/1997,* p. 32, 1997.

[68] I. Schmidt and W. Stichel, “Untersuchung der Korrosionsschutzwirkung von Wärmeträgern Teil 3, Elektrochemische Untersuchungen und Bewertungskriterien,” *Materials and Corrosion, Volume 49, Issue 8,* pp. 556-568, August 1998, https://doi.org/10.1002/(SICI)1521-4176(199808)49:8<556::AID-MACO556>3.0.CO;2-A.

[69] W. Stichel, “Untersuchung der Korrosionsschutzwirkung von Wärmeträgern Teil 1: Chemische Prüfungen, Screening- und Spezial-Tests,” *Materials and Corrosion,* pp. 576-578, 1997, https://doi.org/10.1002/maco.19970480904.

[70] M. Hafner, “Einsatz von Glykol-Wassergemischen in Solaranlagen aus Sicht des Herstellers,” in *Solar Combisystems, Task 26 - Industry Workshop*, Rapperswil, 2001, https://www.aee-intec.at/0uploads/dateien46.pdf.

[71] F. Hillerns, “Untersuchungen zur thermischen Dauerbelastbarkeit von Solarflüssigkeiten,” in *Solar Combisystems Task 26 - Industry Workshop - International Energy Agency Solar Heating & Cooling Programme*, Rapperswil, 2001, https://www.aee-intec.at/0uploads/dateien46.pdf.

[72] K. Dimitrova, Thermische Effekte im Kollektorfeld solarthermischer Anlagen, Chemnitz: TU Chemnitz, 2006, http://nbn-resolving.de/urn:nbn:de:swb:ch1-200601161.

[73] ASTM International, *Standard Test Method for Dynamic Viscosity and Density of Liquids by Stabinger Viscometer (and the Calculation of Kinematic Viscosity),* West Conshohocken: ASTM International, 2016, DOI: 10.1520/D7042-16E03.

[74] TUVNEL, “The Calibration of Flow Meters,” 15 November 2017. [Online]. Available: http://www.tuvnel.com/_x90lbm/The_Calibration_of_Flow_Meters.pdf. [Accessed 7 2 2019].

[75] H. E. Siekmann and P. U. Thamsen, Strömungslehre für den Maschinenbau - Technik und Beispiele, Berlin Heidelberg: Springer- Verlag, 2009, DOI: 10.1007/978-3-540-73990-6.

[76] W. Merzkirch, Fluid Mechanics of Flow Metering, Berlin-Heidelberg-New York: Springer Verlag, 2005, ISBN: 3540222421.

[77] H. J. Matthies and K. T. Renius, Einführung in die Ölhydraulik, Wiesbaden: Springer Vieweg, 2014, DOI: 10.1007/978-3-658-06715-1.

[78] ASTM International, *ASTM D1384-05(2012), Standard Test Method for Corrosion Test for Engine Coolants in Glassware,* West Conshohocken, 2012, DOI: 10.1520/D1384-05R12.

[79] A. Frick and C. Stern, DSC-Prüfung in der Anwendung, München: Carl Hanser Verlag, 2013, ISBN: 9783446436909.

[80] J. Steinbock, Aufbau und Validierung eines laseroptischen Normal-Durchfluss-Messgeräts für die metrologische Rückführung einer Hochtemperatur-Prüfanlage, Berlin: Technische Universität Berlin, 2017, http://dx.doi.org/10.14279/depositonce-5970.

[81] B. Mickan and R. Kramer, “PTB's Metrological Infrastructure for Gas Measurement,” *PTB Mitteilungen- Special Issue,* p. 5, 2009, https://www.ptb.de/cms/fileadmin/internet/publikationen/ptb_mitteilungen/mitt2009/Heft1/PTB-Mitteilungen_2009_Heft_1_en.pdf.

[82] W. Pöschel and R. Engel, “The Concept of a New Primary Standard for Liquid Flow Measurement at PTB Braunschweig,” in *The 9th International Conference on Flow Measurement FLOMEKO '98*, Lund, Sweden, 1998, https://www.ptb.de/cms/fileadmin/internet/fachabteilungen/abteilung_1/1.5_fluessigkeiten/1.52/flome_98.pdf.

[83] S. Baack, *Konstruktion und Auslegung einer volumetrischen Messanlage zur Bestimmung des Einflusses von Wasser-Glykol-Gemischen auf mechanische Wärmezähler,* Berlin, 2012, https://vzlbs.gbv.de/DB=24/XMLPRS=N/PPN?PPN=970227744.

[84] J. G. Pope, J. D. Wright, A. N. Johnson and C. J. Crowley, “NIST Special Publication 250-1039r1: Liquid Flow Meter Calibrations with the 0.1 L/s and the 2.5 L/s Piston Provers,” NIST, 2013, https://doi.org/10.6028/NIST.SP.250-1039r1.

[85] A. N. Johnson, T. Yeh and C. J. Crowley, “Uncertainty Analysis of NIST's 20 Liter Hydrocarbon Liquid Flow Standard,” *Mapan - Journal of Metrology Society of India, Vol. 26,* pp. 187-202, 1 9 2011, DOI: 10.1007/s12647-011-0018-1.

[86] Joint Committee for Guides in Metrology/Working Group 1, “Bureau International des Poids et Mesures,” 9 2008. [Online]. Available: https://www.bipm.org/utils/common/documents/jcgm/JCGM_100_2008_E.pdf. [Accessed 05 12 2018].

[87] Organisation International de Normalisation (ISO), “Organisation International de Normalisation (ISO),” [Online]. Available: https://www.iso.org/sites/JCGM/GUM/JCGM100/C045315e-html/C045315e_FILES/MAIN_C045315e/06_e.html. [Accessed 6 12 2018].

[88] G. E. Mattingly, “The characterization of a piston displacement-type flow meter calibration facility and the calibration and use of pulsed output type flow meters,” *Journal of Research of the National Institute of Standards and Technology,* 1992, DOI: 10.6028/jres.097.023.

[89] J. J. Aguilera and T. W. J. D. Yeh, “Inside diameter measurements for the cylinder of a 20 L piston prover,” in *Proceedings of 6th International Symposium for Fluid Flow Measurement*, Queretaro, Mexico, 2006, https://ws680.nist.gov/publication/get_pdf.cfm?pub_id=830966.

[90] H. Többen, “Kalibrierung einer Rohrprüfstrecke nach unterschiedlichen Verfahren,” [Online]. Available:

https://www.ptb.de/cms/fileadmin/internet/fachabteilungen/abteilung_1/1.5_fluessigkeiten/1.52/hdp_toebben.pdf. [Accessed 4 1 2019].

[91] R. Bullock, “Least-Squares Circle Fit,” 12 2 2017. [Online]. Available: https://dtcenter.org/met/users/docs/write_ups/circle_fit.pdf. [Accessed 13 12 2018].

[92] DIN, Deutsches Institut für Normung, *DIN ISO 2768-1:1991-06, General tolerances; tolerances for linear and angular dimensions without individual tolerance indications,* Berlin: Beuth Verlag, 1991, https://www.beuth.de/en/standard/din-iso-2768-1/1718351.

[93] DIN, Deutsches Institut für Normung, *DIN 2519:1966-08, Steel Flanges - Technical Conditions of Delivery,* Berlin: Beuth Verlag, 1966, https://www.beuth.de/en/standard/din-2519/692097.

[94] S. Krummeck and G. Scheller, Messunsicherheit einer Temperaturmesskette, Fulda: JUMO, 2018, https://www.jumo.net/attachments/JUMO/attachmentdownload?id=2870.

[95] JCGM, “Evaluation of measurement data - Supplement 1 to the "Guide to the expression of uncertainty in measurement" - Propagation of distributions using a Monte Carlot method,” 2008. [Online]. Available: https://www.bipm.org/utils/common/documents/jcgm/JCGM_101_2008_E.pdf. [Accessed 30 1 2019].

[96] H.-C. Obst and I. T. Rogers, “Turbine flowmeter for measuring fluid quantities”. European Patent Office Patent EP0407948B1, 13 7 1989, https://patentimages.storage.googleapis.com/92/e9/b6/8c53868e3a2e86/EP0407948B1.pdf.

[97] R. Stieglitz and V. Heinzel, “Solarthermische Niedertemperatursysteme,” in *Thermische Solaranlagen: Grundlagen, Technologie, Anwendungen*, Berlin, Springer-Verlag, 2013, p. 418.

[98] messtec GmbH, “messtec.ch,” [Online]. Available: http://www.messtec.ch/downloads/messunsicherheit.pdf. [Accessed 6 12 2018].

Appendix

A1 - Physical Properties

Appendix 1: Polynomial coefficients of the fluid's specific fluid properties

Property	Function	coeff	Tyfocor LS	Antifrogen Sol HT	Tyfocor L 25 %	Tyfocor L 30 %	Tyfocor L 35 %	Tyfocor L 40 %	Antifrogen N 20 %	Antifrogen N 25 %	Antifrogen N 30 %	Antifrogen N 35 %	Antifrogen N 40 %
spec. Heat Capacity	$cp(\Theta)= cp_0+c_1\Theta+c_2\Theta^2 +c_3\Theta^3$	cp_0	3.5233687	3.148892	3.9014405	3.8198562	3.728679	3.6063183	3.845405	3.7294445	3.602374	3.4941721	3.377743
		c_1	0.0079476	0.0071189	0.0038737	0.0053261	0.0062791	0.007077	0.003294	0.0042915	0.0056129	0.0061998	0.0067297
		c_2	-7.31E-05	-4.57E-05	-4.11E-05	-5.8E-05	-6.64E-05	-6.86E-05	-1.88E-05	-2.32E-05	-4.51E-05	-4.26E-05	-4.13E-05
		c_3	3.89E-07	1.96E-07	2.547E-07	3.366E-07	3.514E-07	3.521E-07	1.176E-07	1.326E-07	2.78E-07	1.996E-07	1.945E-07
Density	$\rho(\Theta)= \rho_0+b_1\Theta+b_2\Theta^2 +b_3\Theta^3+b_4\Theta^4 +b_5\Theta^5$	ρ_0	1045.146	1097.0087	1031.7197	1038.4448	1044.6204	1050.2465	1033.7568	1041.6043	1049.8737	1057.7023	1065.6119
		b_1	-0.516204	-0.613899	-0.259761	-0.340299	-0.414833	-0.480729	-0.201061	-0.263751	-0.327448	-0.384595	-0.437455
		b_2	-0.001769	-0.000808	-0.004038	-0.003204	-0.002458	-0.001842	-0.00437	-0.003533	-0.00282	-0.002298	-0.001774
		b_3	-8.57E-07	-6.19E-06	1.315E-05	6.818E-06	1.405E-06	-2.72E-06	1.781E-05	8.212E-06	4.136E-06	2.064E-06	-2.89E-06
		b_4	8.955E-09	3.018E-08	-3.22E-08	-8.9E-09	1.054E-08	2.49E-08	-6.58E-08	8.506E-09	-1.97E-21	-1.03E-20	4.297E-08
		b_5	4.63E-22	3.834E-22	5.416E-23	4.747E-22	-4.25E-24	3.727E-22	9.024E-11	-1.61E-10	2.018E-23	1.019E-22	-1.7E-10
dyn. Visc.	$n(\Theta)=A \exp[B/(\Theta+C)]$	A	0.032828	0.0406	0.0355287	0.0358	0.037	0.0366	0.0349	0.0322	0.0341	0.0337	0.033
		B	615.97961	702.9751	541.94974	556.576	565.3657	586.6417	550.3315	589.9173	598.9831	624.7879	654.4212
		C	101.31883	110.9366	105.96386	104.0289	101.8408	101.2447	119.3502	121.8475	121.0461	122.1239	123.3351
kin. Visc.	$v(\Theta)=A \exp[B/(\Theta+C)]$	A	0.0388409	0.0463	0.0417155	0.0421	0.0433	0.0427	0.0412	0.038	0.0401	0.0395	0.0386
		B	576.16925	658.37	502.55421	516.6379	527.1812	548.1675	503.7636	541.8151	550.9215	576.321	604.7115
		C	98.189115	107.6962	102.07695	100.3007	98.4843	98.0531	114.2217	116.9096	116.2889	117.5723	118.8975
Speed of Sound	$c(\Theta)=cO+c_1\Theta +c_2\Theta^2$	c_0	1738.5411	1780.025	1635	1672.2053	1703.4506	1728.7812	1556.7656	1592.0531	1624.5129	1654.1492	1680.5719
		c_1	-1.2989	-1.74151	0.90983	0.22523	-0.39779	-0.94836	2.13655	1.58753	1.02358	0.51578	0.05557
		c_2	-0.00789	-0.00516	-0.01757	-0.01427	-0.01132	-0.00888	-0.02224	-0.01984	-0.01661	-0.01408	-0.01178

Appendix 2: Heat capacity of investigated glycol-water-mixtures for different volume fractions [%]; deviations to manufacturer data

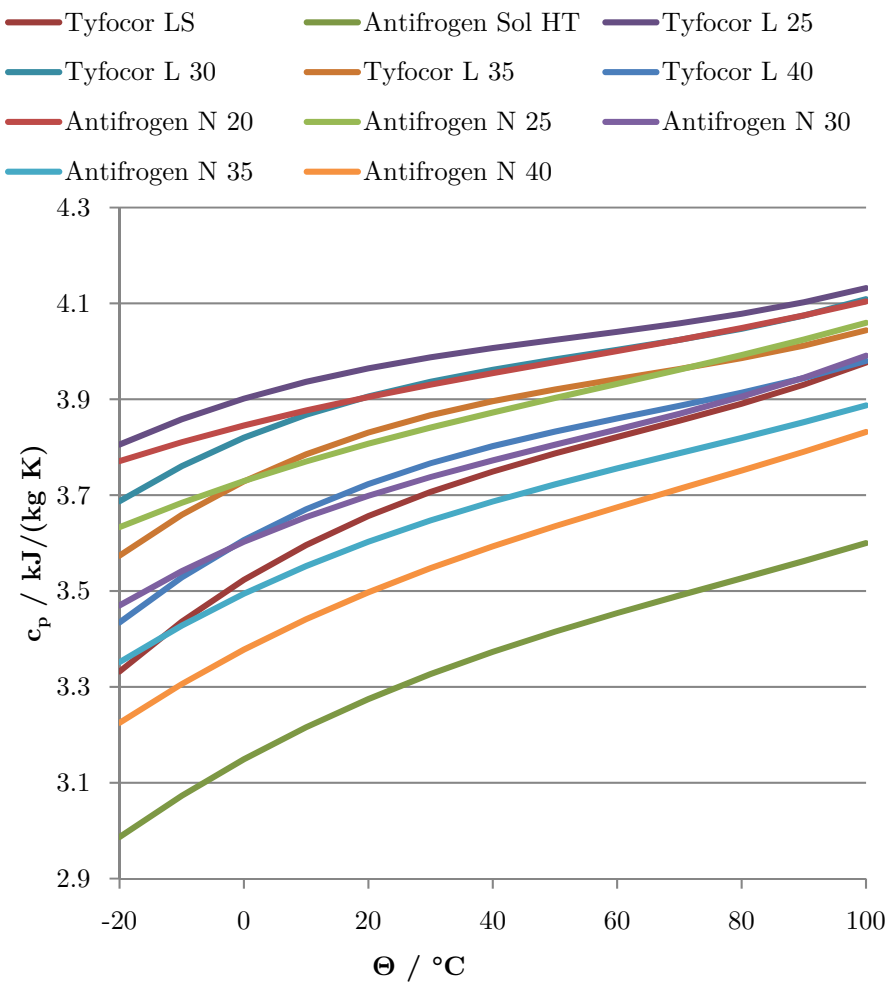

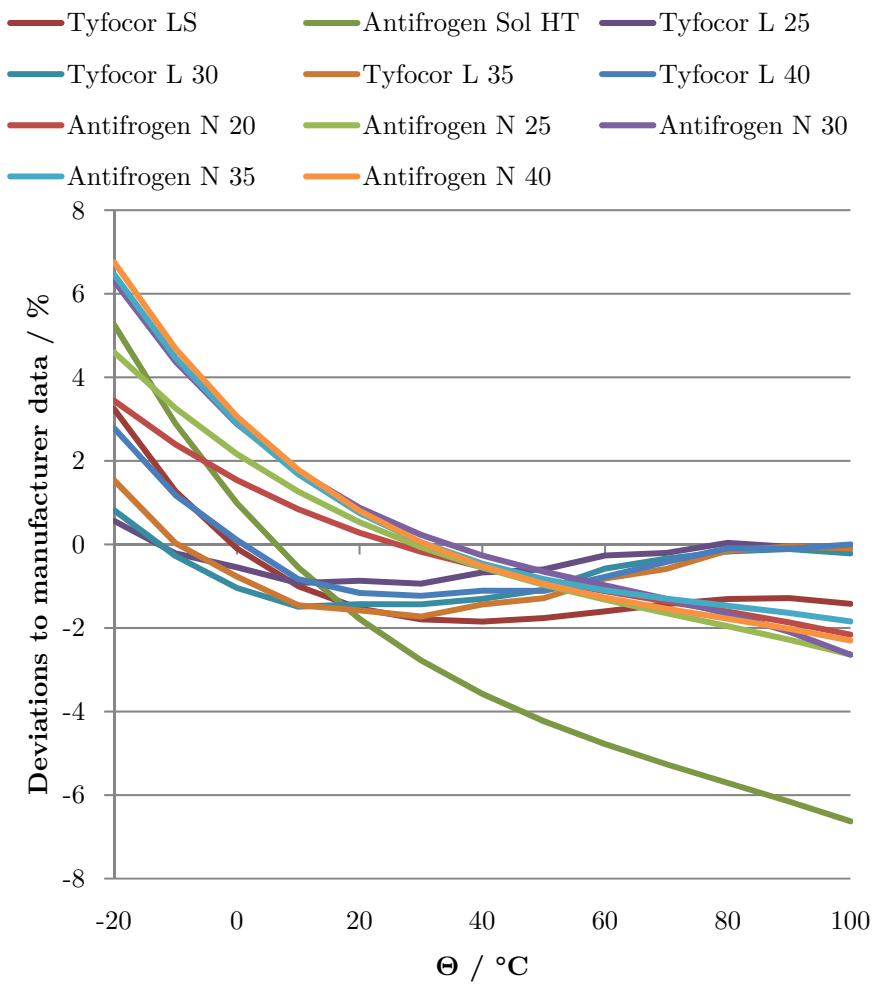

Appendix 3: Specific heat capacity of Tyfocor L (left) and Antifrogen N (right) for different volume fractions [%]

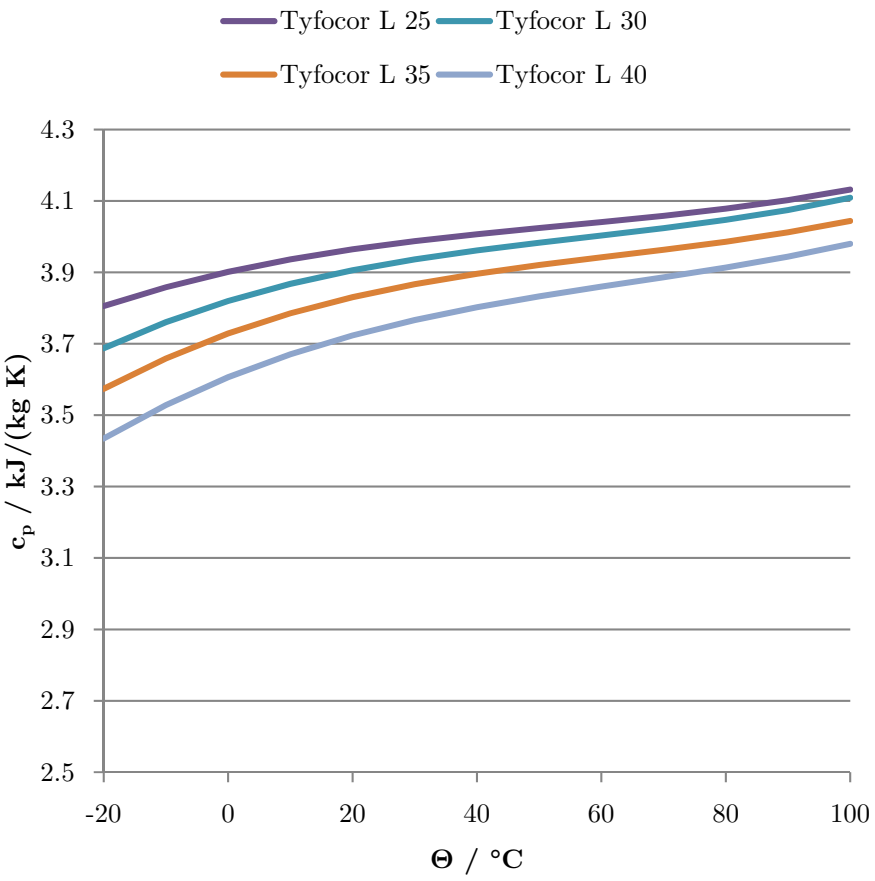

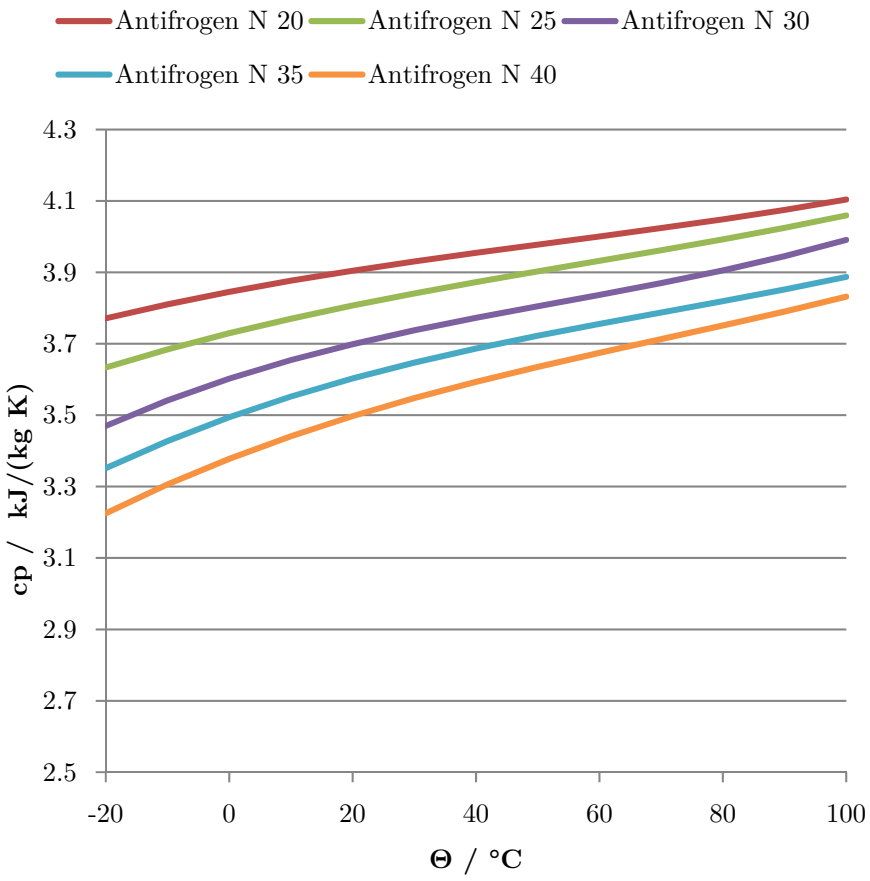

Appendix 4: Density of investigated fluids for different volume fractions [%]; deviations to manufacturer data

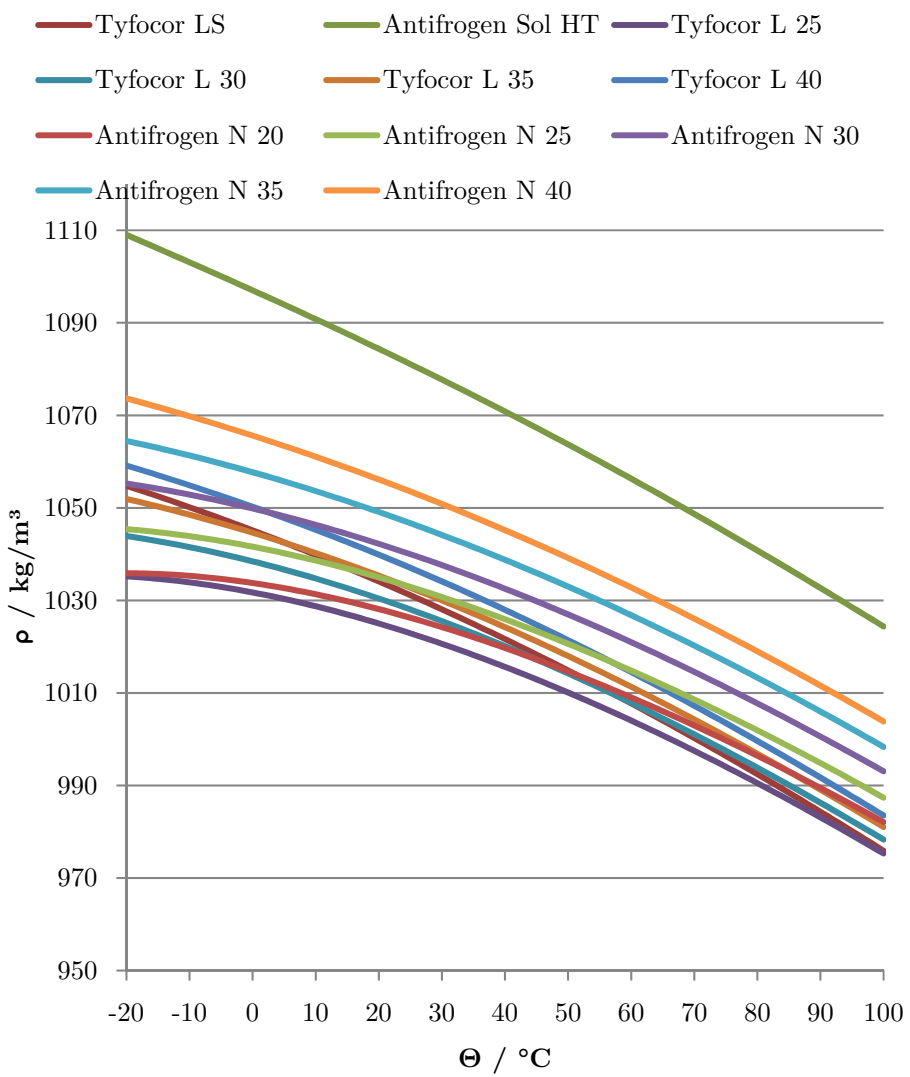

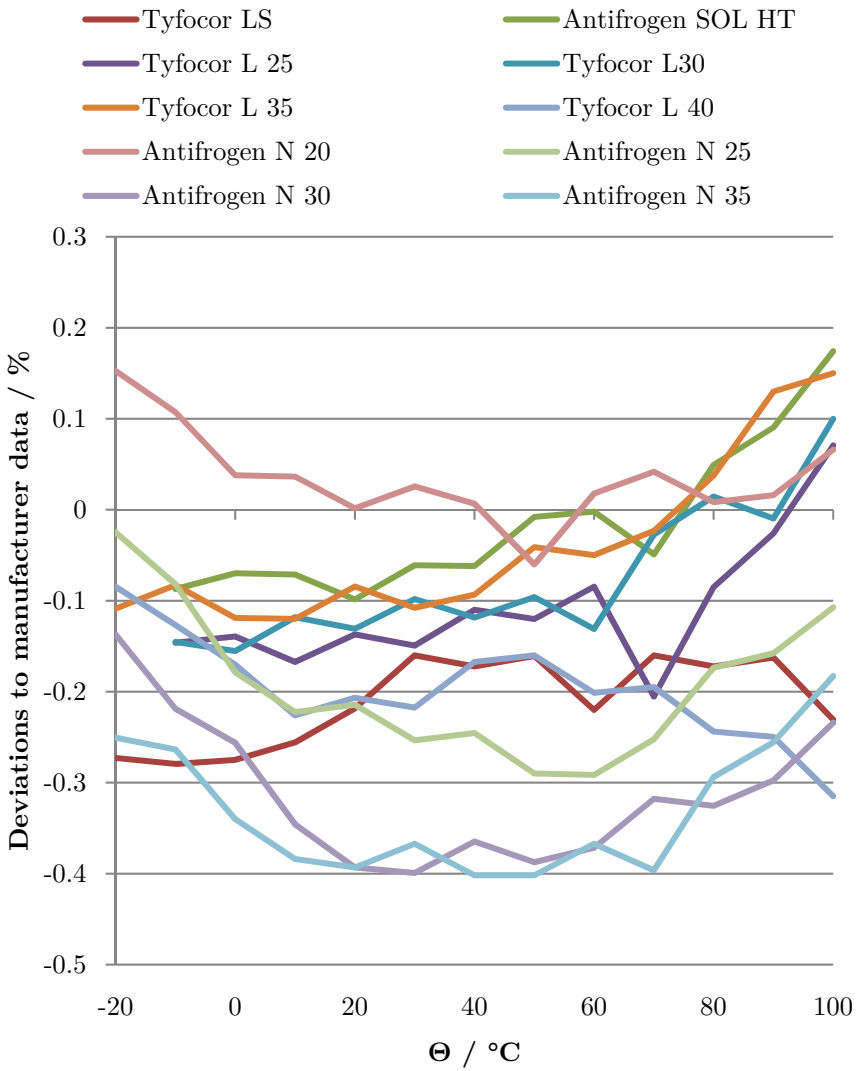

Appendix 5: Density of Tyfocor L (left) and Antifrogen N (right) for different volume fractions [%]

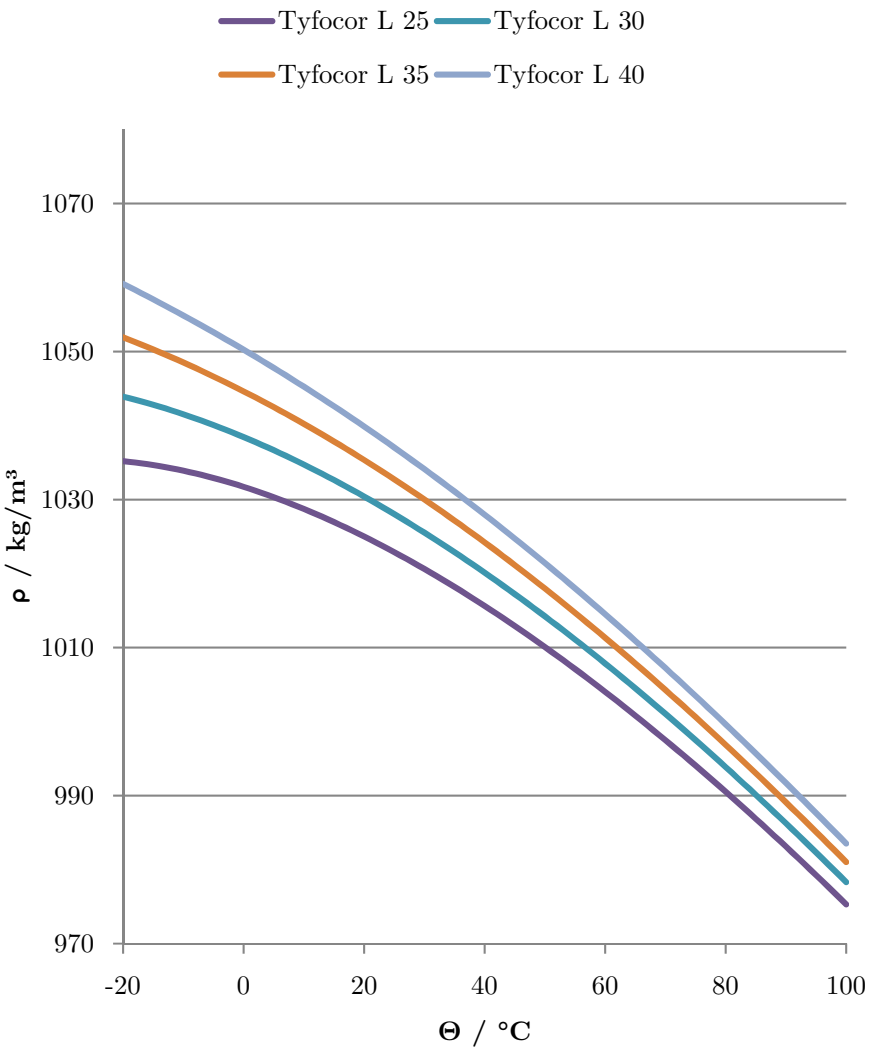

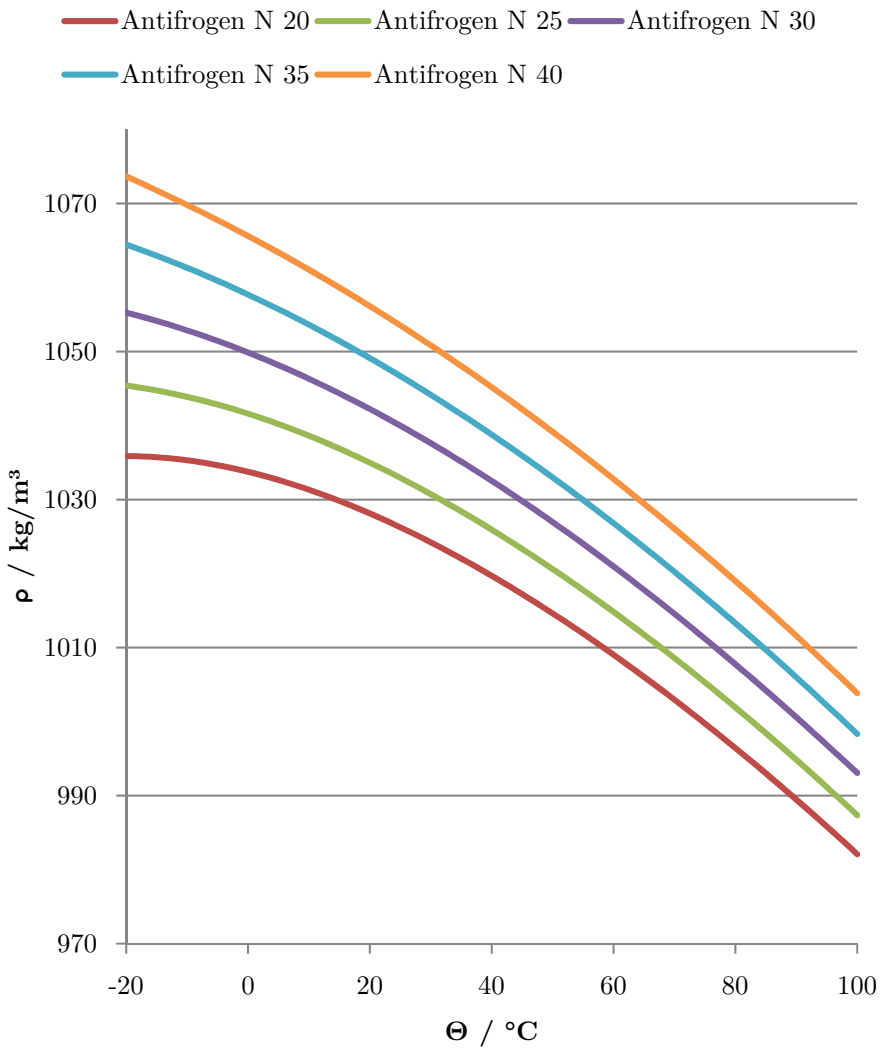

Appendix 6: Dynamic viscosity of investigated fluids for different volume fractions [%]; deviations to manufacturer data

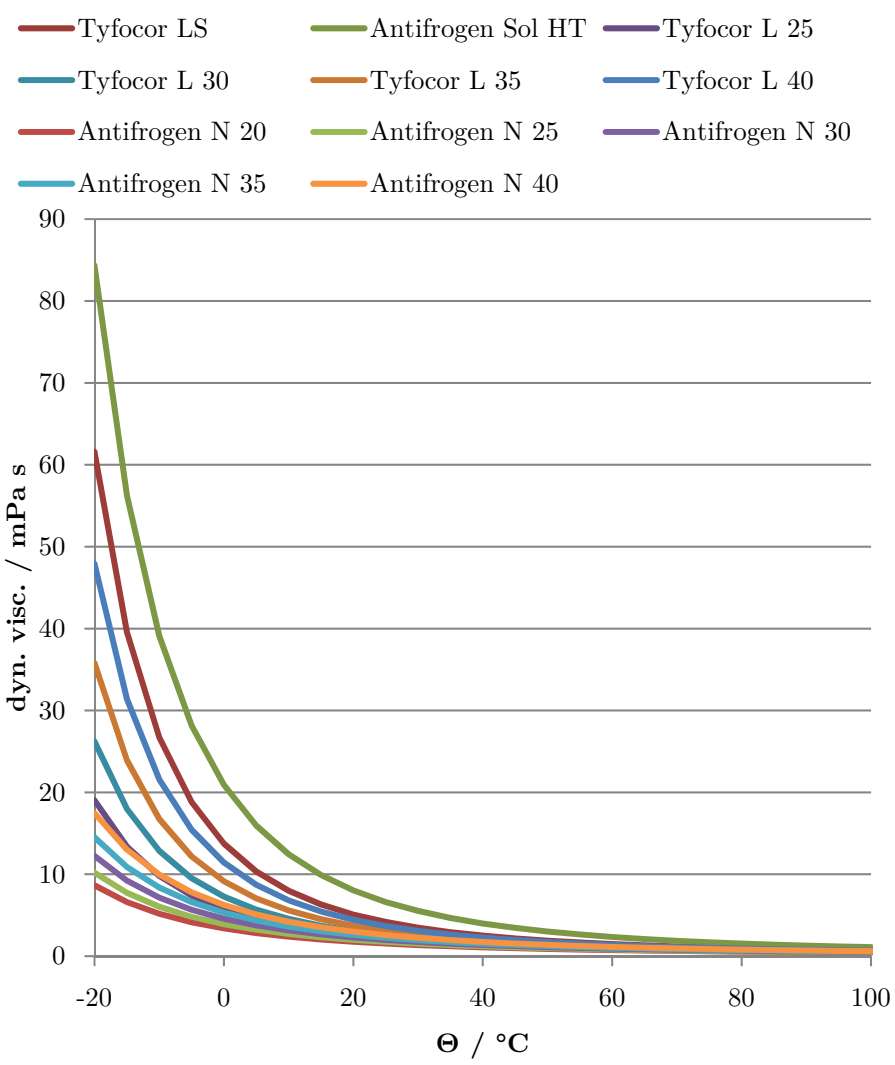

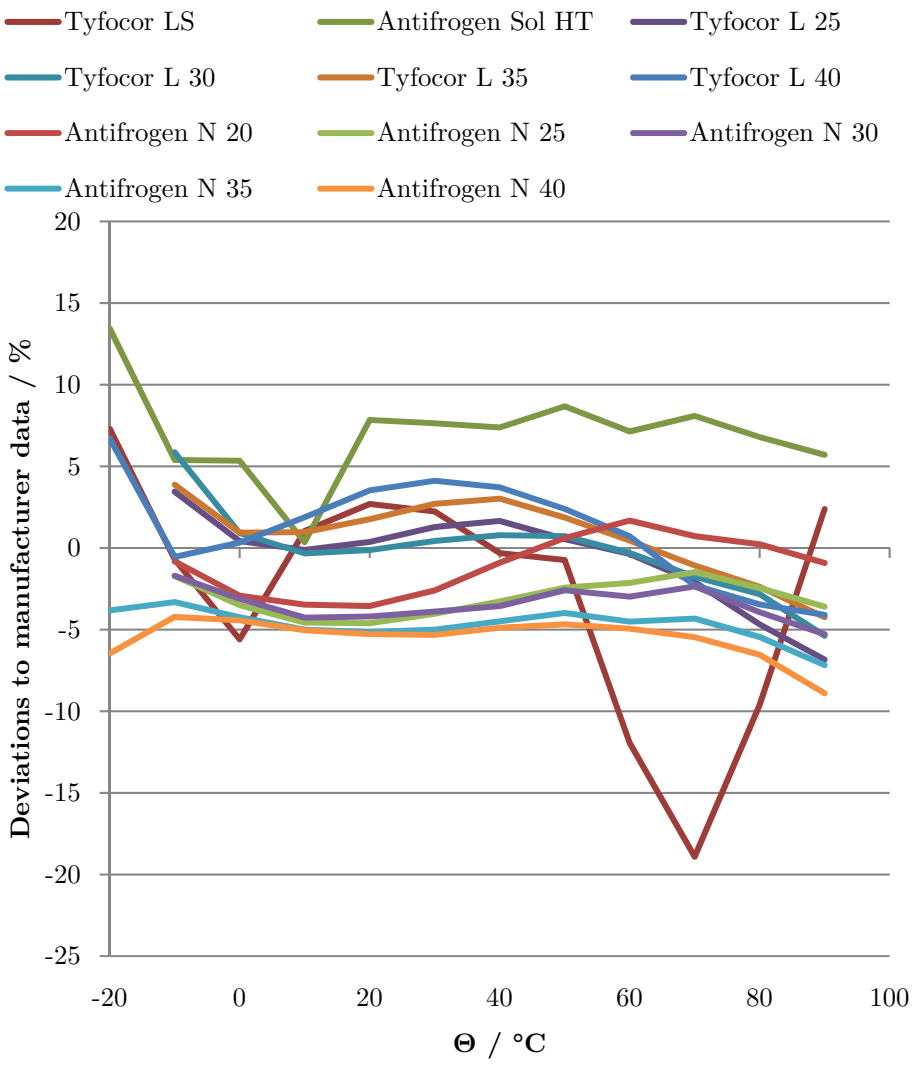

Appendix 7: Dynamic viscosity of Tyfocor L (left) and Antifrogen N (right) for different volume fractions [%]

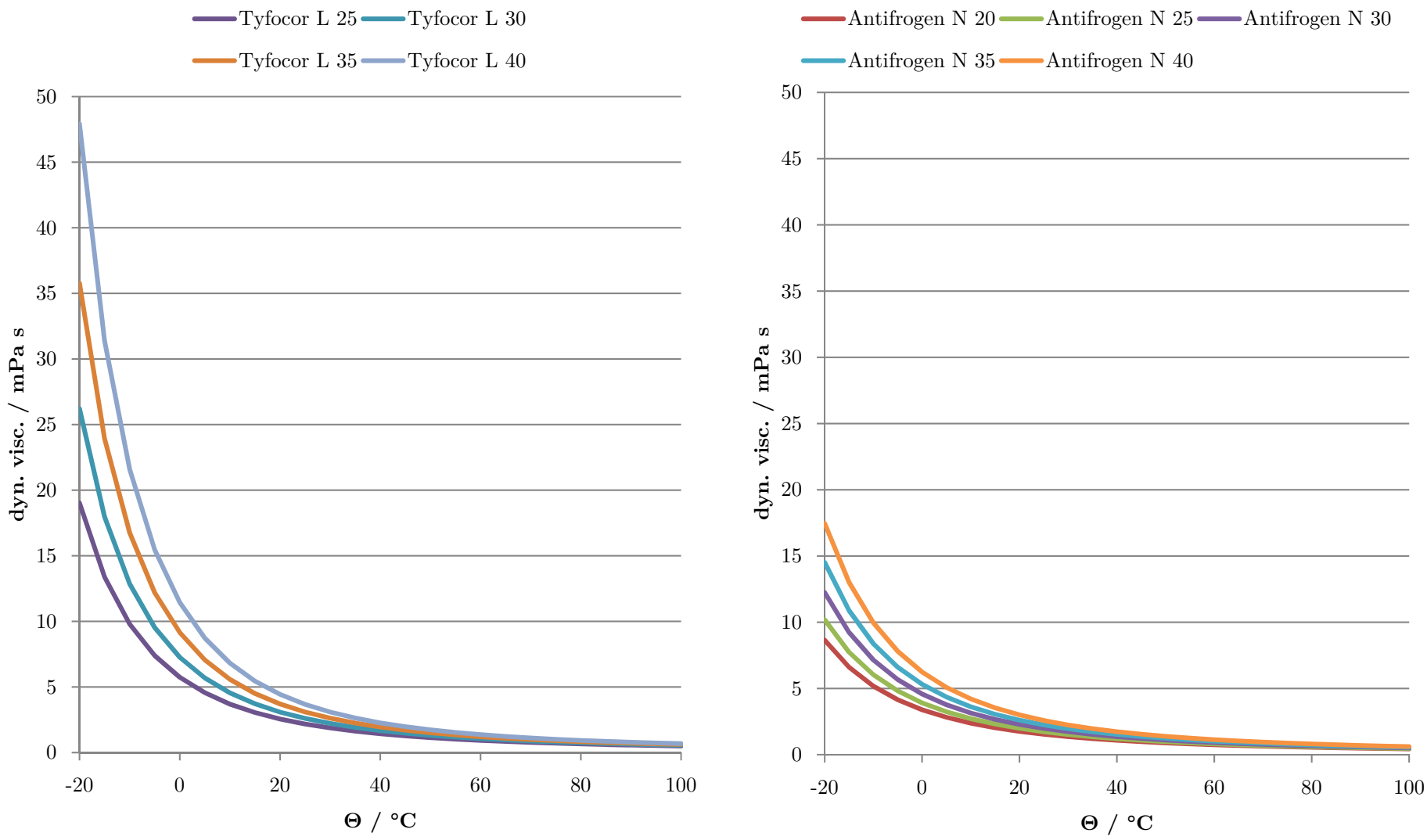

Appendix 8: Re differences between investigated fluids at the same flow rate

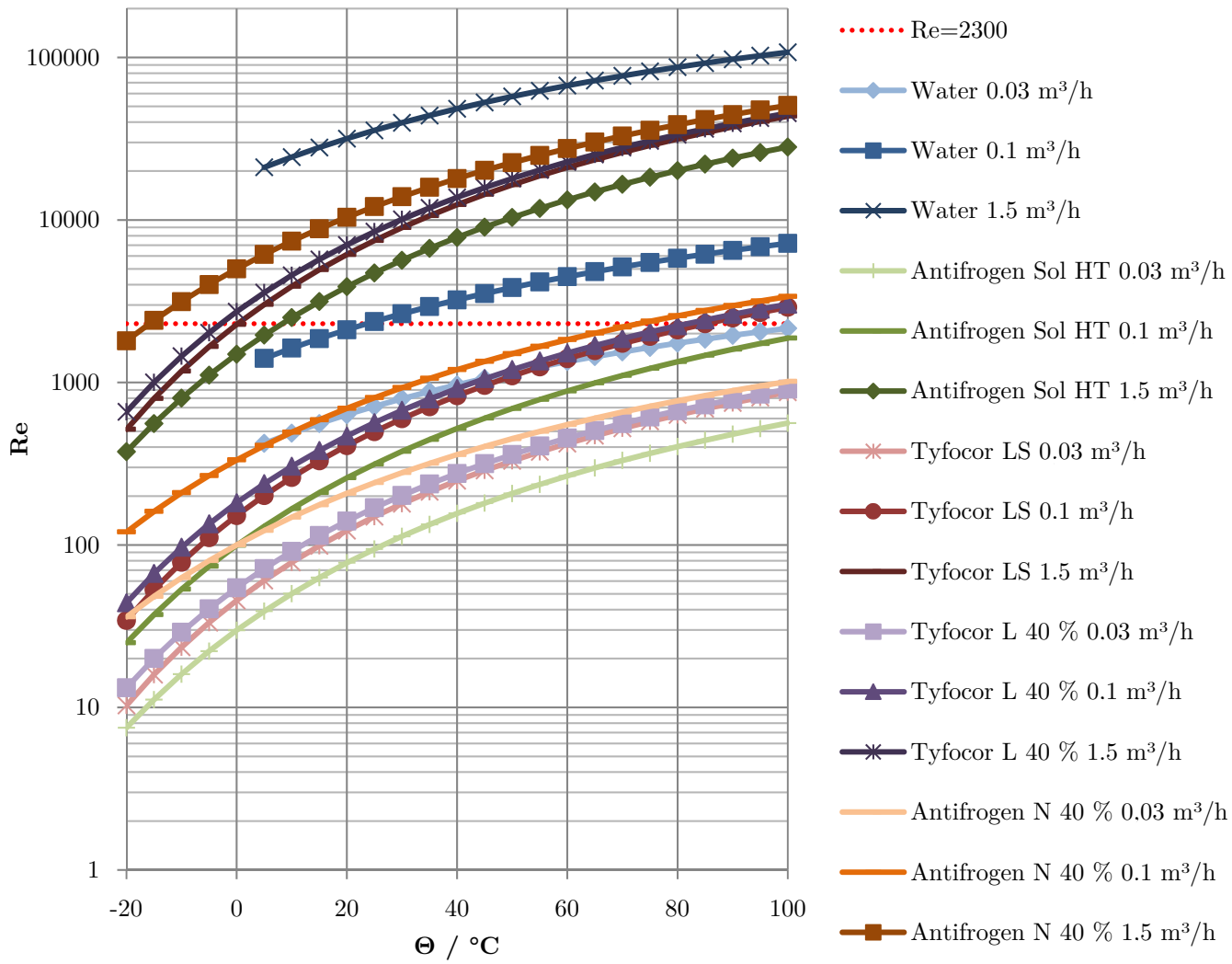

Appendix 9: Theoretic Flow profiles of investigated fluids for a pipe diameter of 8 mm

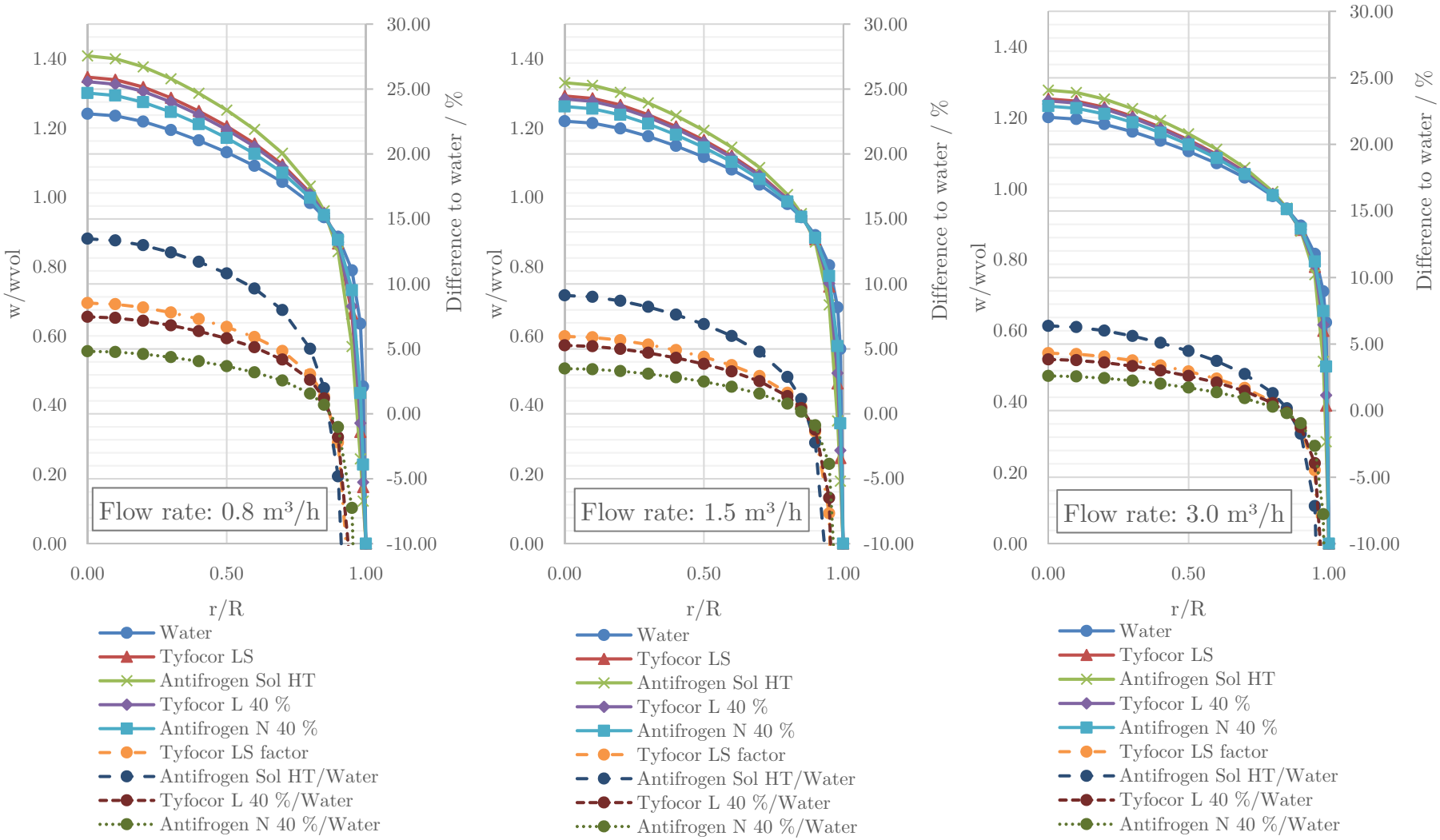

Appendix 10: Calculation of heat coefficient *k*

Following tables of heat coefficients k_i have been calculated according to:

$$k_f = \frac{\rho(\theta_f)}{\Delta\Theta} \cdot \int_{\theta_f}^{\theta_r} c_p(\Theta) d\Theta \tag{15}$$

$$k_r = \frac{\rho(\theta_r)}{\Delta\Theta} \cdot \int_{\theta_f}^{\theta_r} c_p(\Theta) d\Theta \tag{16}$$

The values of $\rho(\Theta)$ and $c_p(\Theta)$ are given as polynomial functions of the temperature Θ, calculated from the measured data (cf. Appendix 1: Polynomial coefficients of the fluid's specific fluid properties):

$\rho(\Theta)= \rho_0+b_1\Theta+ b_2\Theta^2+ b_3\Theta^3 +b_4\Theta^4 +b_5\Theta^5$

$c_p(\Theta)=c_{pO}+c_1\Theta+ c_2\Theta^2 c_3\Theta^3$

This results in the calculation of the ideal heat coefficients k_f and k_r in feed and return flow:

$$k_f = \frac{\rho_0 + b_1 \cdot \Theta_f + b_2 \cdot {\Theta_f}^2 + b_3 \cdot {\Theta_f}^3 + b_4 \cdot {\Theta_f}^4 + b_5 \cdot {\Theta_f}^5}{\Theta_f - \Theta_r} \cdot \left[\left(c_{p0} \cdot \Theta_f + \frac{c_1 \cdot {\Theta_f}^2}{2} + \frac{c_2 \cdot {\Theta_f}^3}{3} + \frac{c_3 \cdot {\Theta_f}^4}{4}\right) - \left(c_{p0} \cdot \Theta_r + \frac{c_1 \cdot {\Theta_r}^2}{2} + \frac{c_2 \cdot {\Theta_r}^3}{3} + \frac{c_3 \cdot {\Theta_r}^4}{4}\right)\right]$$

$$k_r = \frac{\rho_0 + b_1 \cdot \Theta_r + b_2 \cdot {\Theta_r}^2 + b_3 \cdot {\Theta_r}^3 + b_4 \cdot {\Theta_r}^4 + b_5 \cdot {\Theta_r}^5}{\Theta_f - \Theta_r} \cdot \left[\left(c_{p0} \cdot \Theta_f + \frac{c_1 \cdot {\Theta_f}^2}{2} + \frac{c_2 \cdot {\Theta_f}^3}{3} + \frac{c_3 \cdot {\Theta_f}^4}{4}\right) - \left(c_{p0} \cdot \Theta_r + \frac{c_1 \cdot {\Theta_r}^2}{2} + \frac{c_2 \cdot {\Theta_r}^3}{3} + \frac{c_3 \cdot {\Theta_r}^4}{4}\right)\right]$$

Regarding the measurement uncertainty of k_i, there are contributions coming from its measured input values $\rho(\Theta)$ and $c_p(\Theta)$ as well as the fluid's composition (affecting the values of $\rho(\Theta)$ and $c_p(\Theta)$) and the temperature measurement in feed and return. The expanded measurement uncertainties (k=2) of $\rho(\Theta)$ and $c_p(\Theta)$ are 0.005 % and 1.5 %, respectively. The uncertainty of the temperature measurement is depending on the temperature sensor's accuracy class. Uncertainty factors coming from composition errors can be estimated from the fluid's values of $\rho(\Theta)$ and $c_p(\Theta)$ at other compositions (e.g. linear interpolation between 40 % and 35 % glycol content). For the density of a mixture of Tyfocor L at a certain temperature,

the uncertainty factor $k_{\rho 1\_\%}$ (1.000 ± 0.086 %) that arises from an assumed fluid composition error of 1 % is multiple times more influential than the uncertainty of the density measurement (but still unsignificant compared the the measurement uncertainty of c_p). For c_p at a certain temperature, the uncertainty factor $k_{cp\_1\%}$ (1.00 ± 0.50 %) that arises from an assumed fluid composition error of 1 % is less influential than the uncertainty of the c_p measurement. By applying those uncertainty factors to the respective values of $\rho(\Theta)$ and $c_p(\Theta)$ in equations (15) and (16), the measurement uncertainty of k_i can be estimated. For a fluid composition error of 1 % for Tyfocor L 40 %, the biggest contribution to the expanded measurement uncertainty of k_i, U_k=1.8 % (k=2) comes from the measurement uncertainty of c_p (~68.6 %) and its uncertainty factor $k_{cp\_1\%}$ (~30.5 %). Note, that rising fluid composition uncertainties become significantly more influential on the uncertainty of k_i.

Appendix 11: Heat coefficient k of Tyfocor LS, measured in return [kWh/(m³K)]

k Return	Return temperature																								
Feed temperature	-20	-15	-10	-5	0	5	10	15	20	25	30	35	40	45	50	55	60	65	70	75	80	85	90	95	100
-20		0.982	0.988	0.992	0.997	1.001	1.004	1.007	1.009	1.011	1.013	1.014	1.015	1.016	1.016	1.016	1.016	1.016	1.015	1.014	1.013	1.012	1.011	1.009	1.008
-15	0.984		0.995	1.000	1.004	1.008	1.011	1.013	1.016	1.017	1.019	1.020	1.021	1.021	1.022	1.021	1.021	1.021	1.020	1.019	1.018	1.016	1.015	1.014	1.012
-10	0.992	0.997		1.007	1.011	1.014	1.017	1.019	1.022	1.023	1.025	1.026	1.026	1.026	1.027	1.026	1.026	1.025	1.024	1.023	1.022	1.021	1.019	1.018	1.016
-5	0.999	1.004	1.009		1.017	1.020	1.023	1.025	1.027	1.029	1.030	1.031	1.031	1.031	1.031	1.031	1.030	1.029	1.028	1.027	1.026	1.025	1.023	1.021	1.020
0	1.006	1.011	1.015	1.019		1.026	1.028	1.031	1.032	1.034	1.035	1.035	1.036	1.036	1.036	1.035	1.034	1.033	1.032	1.031	1.030	1.028	1.027	1.025	1.023
5	1.012	1.017	1.021	1.025	1.028		1.034	1.036	1.037	1.038	1.039	1.040	1.040	1.040	1.040	1.039	1.038	1.037	1.036	1.035	1.033	1.032	1.030	1.028	1.026
10	1.018	1.023	1.027	1.031	1.034	1.036		1.040	1.042	1.043	1.044	1.044	1.044	1.044	1.043	1.043	1.042	1.041	1.040	1.038	1.037	1.035	1.033	1.031	1.030
15	1.024	1.028	1.032	1.036	1.039	1.041	1.043		1.046	1.047	1.048	1.048	1.048	1.048	1.047	1.046	1.045	1.044	1.043	1.041	1.040	1.038	1.036	1.034	1.033
20	1.029	1.034	1.037	1.041	1.043	1.046	1.048	1.049		1.051	1.052	1.052	1.052	1.051	1.050	1.050	1.049	1.047	1.046	1.044	1.043	1.041	1.039	1.037	1.035
25	1.035	1.039	1.042	1.045	1.048	1.050	1.052	1.053	1.054		1.055	1.055	1.055	1.054	1.054	1.053	1.052	1.050	1.049	1.047	1.046	1.044	1.042	1.040	1.038
30	1.039	1.043	1.047	1.049	1.052	1.054	1.056	1.057	1.058	1.058		1.058	1.058	1.058	1.057	1.056	1.054	1.053	1.052	1.050	1.048	1.046	1.045	1.043	1.041
35	1.044	1.048	1.051	1.054	1.056	1.058	1.059	1.060	1.061	1.062	1.062		1.061	1.060	1.060	1.058	1.057	1.056	1.054	1.053	1.051	1.049	1.047	1.045	1.043
40	1.048	1.052	1.055	1.057	1.060	1.061	1.063	1.064	1.064	1.065	1.065	1.064		1.063	1.062	1.061	1.060	1.058	1.057	1.055	1.053	1.051	1.050	1.048	1.046
45	1.052	1.056	1.059	1.061	1.063	1.065	1.066	1.067	1.067	1.068	1.068	1.067	1.067		1.065	1.064	1.062	1.061	1.059	1.058	1.056	1.054	1.052	1.050	1.048
50	1.056	1.059	1.062	1.065	1.066	1.068	1.069	1.070	1.070	1.071	1.070	1.070	1.069	1.069		1.066	1.065	1.063	1.062	1.060	1.058	1.056	1.054	1.052	1.051
55	1.060	1.063	1.066	1.068	1.070	1.071	1.072	1.073	1.073	1.073	1.073	1.073	1.072	1.071	1.070		1.067	1.066	1.064	1.062	1.061	1.059	1.057	1.055	1.053
60	1.063	1.066	1.069	1.071	1.073	1.074	1.075	1.076	1.076	1.076	1.076	1.075	1.074	1.074	1.072	1.071		1.068	1.066	1.065	1.063	1.061	1.059	1.057	1.055
65	1.067	1.070	1.072	1.074	1.076	1.077	1.078	1.078	1.079	1.079	1.078	1.078	1.077	1.076	1.075	1.073	1.072		1.069	1.067	1.065	1.063	1.062	1.060	1.058
70	1.070	1.073	1.075	1.077	1.079	1.080	1.081	1.081	1.081	1.081	1.081	1.080	1.079	1.078	1.077	1.076	1.074	1.073		1.069	1.068	1.066	1.064	1.062	1.060
75	1.074	1.076	1.078	1.080	1.082	1.083	1.083	1.084	1.084	1.084	1.083	1.083	1.082	1.081	1.080	1.078	1.077	1.075	1.074		1.070	1.068	1.067	1.065	1.063
80	1.077	1.079	1.081	1.083	1.084	1.085	1.086	1.086	1.086	1.086	1.086	1.085	1.084	1.083	1.082	1.081	1.079	1.078	1.076	1.074		1.071	1.069	1.067	1.066
85	1.080	1.082	1.084	1.086	1.087	1.088	1.089	1.089	1.089	1.089	1.088	1.088	1.087	1.086	1.085	1.083	1.082	1.080	1.079	1.077	1.075		1.072	1.070	1.069
90	1.083	1.085	1.087	1.089	1.090	1.091	1.091	1.092	1.092	1.091	1.091	1.090	1.089	1.088	1.087	1.086	1.084	1.083	1.081	1.080	1.078	1.076		1.073	1.072
95	1.086	1.088	1.090	1.092	1.093	1.094	1.094	1.094	1.094	1.094	1.094	1.093	1.092	1.091	1.090	1.088	1.087	1.086	1.084	1.082	1.081	1.079	1.078		1.075
100	1.089	1.091	1.093	1.095	1.096	1.097	1.097	1.097	1.097	1.097	1.096	1.096	1.095	1.094	1.093	1.091	1.090	1.088	1.087	1.085	1.084	1.082	1.081	1.079	

Appendix 12: Heat coefficient k of Tyfocor LS, measured in feed [kWh/(m³K)]

k Feed	Return temperature																								
Feed temperature	-20	-15	-10	-5	0	5	10	15	20	25	30	35	40	45	50	55	60	65	70	75	80	85	90	95	100
-20		0.984	0.992	0.999	1.006	1.012	1.018	1.024	1.029	1.035	1.039	1.044	1.048	1.052	1.056	1.060	1.063	1.067	1.070	1.074	1.077	1.080	1.083	1.086	
-15	0.982		0.997	1.004	1.011	1.017	1.023	1.028	1.034	1.039	1.043	1.048	1.052	1.056	1.059	1.063	1.066	1.070	1.073	1.076	1.079	1.082	1.085	1.088	
-10	0.988	0.995		1.009	1.015	1.021	1.027	1.032	1.037	1.042	1.047	1.051	1.055	1.059	1.062	1.066	1.069	1.072	1.075	1.078	1.081	1.084	1.087	1.090	
-5	0.992	1.000	1.007		1.019	1.025	1.031	1.036	1.041	1.045	1.049	1.054	1.057	1.061	1.065	1.068	1.071	1.074	1.077	1.080	1.083	1.086	1.089	1.092	
0	0.997	1.004	1.011	1.017		1.028	1.034	1.039	1.043	1.048	1.052	1.056	1.060	1.063	1.066	1.070	1.073	1.076	1.079	1.082	1.084	1.087	1.090	1.093	
5	1.001	1.008	1.014	1.020	1.026		1.036	1.041	1.046	1.050	1.054	1.058	1.061	1.065	1.068	1.071	1.074	1.077	1.080	1.083	1.085	1.088	1.091	1.094	
10	1.004	1.011	1.017	1.023	1.028	1.034		1.043	1.048	1.052	1.056	1.059	1.063	1.066	1.069	1.072	1.075	1.078	1.081	1.083	1.086	1.089	1.091	1.094	
15	1.007	1.013	1.019	1.025	1.031	1.036	1.040		1.049	1.053	1.057	1.060	1.064	1.067	1.070	1.073	1.076	1.078	1.081	1.084	1.086	1.089	1.092	1.094	
20	1.009	1.016	1.022	1.027	1.032	1.037	1.042	1.046		1.054	1.058	1.061	1.064	1.067	1.070	1.073	1.076	1.079	1.081	1.084	1.086	1.089	1.092	1.094	
25	1.011	1.017	1.023	1.029	1.034	1.038	1.043	1.047	1.051		1.058	1.062	1.065	1.068	1.071	1.073	1.076	1.079	1.081	1.084	1.086	1.089	1.091	1.094	
30	1.013	1.019	1.025	1.030	1.035	1.039	1.044	1.048	1.052	1.055		1.062	1.065	1.068	1.070	1.073	1.076	1.078	1.081	1.083	1.086	1.088	1.091	1.094	
35	1.014	1.020	1.026	1.031	1.035	1.040	1.044	1.048	1.052	1.055	1.058		1.064	1.067	1.070	1.073	1.075	1.078	1.080	1.083	1.085	1.088	1.090	1.093	
40	1.015	1.021	1.026	1.031	1.036	1.040	1.044	1.048	1.052	1.055	1.058	1.061		1.067	1.069	1.072	1.074	1.077	1.079	1.082	1.084	1.087	1.089	1.092	
45	1.016	1.021	1.026	1.031	1.036	1.040	1.044	1.048	1.051	1.054	1.058	1.060	1.063		1.069	1.071	1.074	1.076	1.078	1.081	1.083	1.086	1.088	1.091	
50	1.016	1.022	1.027	1.031	1.036	1.040	1.043	1.047	1.050	1.054	1.057	1.060	1.062	1.065		1.070	1.072	1.075	1.077	1.080	1.082	1.085	1.087	1.090	
55	1.016	1.021	1.026	1.031	1.035	1.039	1.043	1.046	1.050	1.053	1.056	1.058	1.061	1.064	1.066		1.071	1.073	1.076	1.078	1.081	1.083	1.086	1.088	
60	1.016	1.021	1.026	1.030	1.034	1.038	1.042	1.045	1.049	1.052	1.054	1.057	1.060	1.062	1.065	1.067		1.072	1.074	1.077	1.079	1.082	1.084	1.087	
65	1.016	1.021	1.025	1.029	1.033	1.037	1.041	1.044	1.047	1.050	1.053	1.056	1.058	1.061	1.063	1.066	1.068		1.073	1.075	1.078	1.080	1.083	1.086	
70	1.015	1.020	1.024	1.028	1.032	1.036	1.040	1.043	1.046	1.049	1.052	1.054	1.057	1.059	1.062	1.064	1.066	1.069		1.074	1.076	1.079	1.081	1.084	
75	1.014	1.019	1.023	1.027	1.031	1.035	1.038	1.041	1.044	1.047	1.050	1.053	1.055	1.058	1.060	1.062	1.065	1.067	1.069		1.074	1.077	1.080	1.082	
80	1.013	1.018	1.022	1.026	1.030	1.033	1.037	1.040	1.043	1.046	1.048	1.051	1.053	1.056	1.058	1.061	1.063	1.065	1.068	1.070		1.075	1.078	1.081	
85	1.012	1.016	1.021	1.025	1.028	1.032	1.035	1.038	1.041	1.044	1.046	1.049	1.051	1.054	1.056	1.059	1.061	1.063	1.066	1.068	1.071		1.076	1.079	
90	1.011	1.015	1.019	1.023	1.027	1.030	1.033	1.036	1.039	1.042	1.045	1.047	1.050	1.052	1.054	1.057	1.059	1.062	1.064	1.067	1.069	1.072		1.078	
95	1.009	1.014	1.018	1.021	1.025	1.028	1.031	1.034	1.037	1.040	1.043	1.045	1.048	1.050	1.052	1.055	1.057	1.060	1.062	1.065	1.067	1.070	1.073		
100	1.008	1.012	1.016	1.020	1.023	1.026	1.030	1.033	1.035	1.038	1.041	1.043	1.046	1.048	1.051	1.053	1.055	1.058	1.060	1.063	1.066	1.069	1.072	1.075	

Appendix 13: Heat coefficient k of Antifrogen Sol HT, measured in return [kWh/(m³K)]

k Return	Return temperature																								
Feed temperature	-20	-15	-10	-5	0	5	10	15	20	25	30	35	40	45	50	55	60	65	70	75	80	85	90	95	100
-20		0.925	0.929	0.932	0.936	0.939	0.942	0.944	0.947	0.949	0.950	0.952	0.953	0.954	0.955	0.955	0.956	0.956	0.956	0.955	0.955	0.954	0.954	0.953	0.952
-15	0.927		0.935	0.939	0.942	0.945	0.948	0.950	0.952	0.954	0.956	0.957	0.958	0.959	0.960	0.960	0.960	0.960	0.960	0.960	0.959	0.959	0.958	0.957	0.956
-10	0.934	0.938		0.945	0.948	0.951	0.954	0.956	0.958	0.960	0.961	0.962	0.963	0.964	0.965	0.965	0.965	0.965	0.965	0.964	0.964	0.963	0.962	0.961	0.960
-5	0.940	0.944	0.948		0.954	0.957	0.959	0.961	0.963	0.965	0.966	0.967	0.968	0.969	0.969	0.969	0.969	0.969	0.969	0.968	0.968	0.967	0.966	0.965	0.964
0	0.946	0.950	0.953	0.957		0.962	0.964	0.966	0.968	0.970	0.971	0.972	0.973	0.973	0.974	0.974	0.974	0.973	0.973	0.972	0.972	0.971	0.970	0.969	0.968
5	0.952	0.956	0.959	0.962	0.965		0.969	0.971	0.973	0.974	0.976	0.976	0.977	0.978	0.978	0.978	0.978	0.977	0.977	0.976	0.976	0.975	0.974	0.973	0.971
10	0.958	0.961	0.964	0.967	0.970	0.972		0.976	0.978	0.979	0.980	0.981	0.981	0.982	0.982	0.982	0.982	0.981	0.981	0.980	0.979	0.978	0.977	0.976	0.975
15	0.963	0.966	0.970	0.972	0.975	0.977	0.979		0.982	0.983	0.984	0.985	0.985	0.986	0.986	0.986	0.985	0.985	0.984	0.983	0.983	0.982	0.980	0.979	0.978
20	0.968	0.971	0.974	0.977	0.980	0.982	0.983	0.985		0.987	0.988	0.989	0.989	0.989	0.989	0.989	0.989	0.988	0.988	0.987	0.986	0.985	0.984	0.982	0.981
25	0.973	0.976	0.979	0.982	0.984	0.986	0.988	0.989	0.990		0.992	0.993	0.993	0.993	0.993	0.993	0.992	0.992	0.991	0.990	0.989	0.988	0.987	0.986	0.984
30	0.978	0.981	0.984	0.986	0.988	0.990	0.992	0.993	0.994	0.995		0.996	0.997	0.997	0.996	0.996	0.996	0.995	0.994	0.993	0.992	0.991	0.990	0.989	0.987
35	0.983	0.985	0.988	0.990	0.992	0.994	0.996	0.997	0.998	0.999	0.999		1.000	1.000	1.000	0.999	0.999	0.998	0.997	0.996	0.995	0.994	0.993	0.991	0.990
40	0.987	0.990	0.992	0.995	0.996	0.998	1.000	1.001	1.002	1.002	1.003	1.003		1.003	1.003	1.003	1.002	1.001	1.000	0.999	0.998	0.997	0.996	0.994	0.993
45	0.991	0.994	0.996	0.998	1.000	1.002	1.003	1.004	1.005	1.006	1.006	1.007	1.007		1.006	1.006	1.005	1.004	1.003	1.002	1.001	1.000	0.998	0.997	0.996
50	0.995	0.998	1.000	1.002	1.004	1.006	1.007	1.008	1.009	1.009	1.010	1.010	1.010	1.009		1.009	1.008	1.007	1.006	1.005	1.004	1.002	1.001	1.000	0.998
55	0.999	1.002	1.004	1.006	1.008	1.009	1.010	1.011	1.012	1.012	1.013	1.013	1.013	1.012	1.012		1.011	1.010	1.009	1.008	1.006	1.005	1.004	1.002	1.001
60	1.003	1.006	1.008	1.010	1.011	1.012	1.014	1.014	1.015	1.016	1.016	1.016	1.016	1.015	1.015	1.014		1.013	1.011	1.010	1.009	1.008	1.006	1.005	1.003
65	1.007	1.009	1.011	1.013	1.015	1.016	1.017	1.018	1.018	1.019	1.019	1.019	1.019	1.018	1.018	1.017	1.016		1.014	1.013	1.012	1.010	1.009	1.008	1.006
70	1.011	1.013	1.015	1.016	1.018	1.019	1.020	1.021	1.021	1.022	1.022	1.022	1.021	1.021	1.020	1.020	1.019	1.018		1.016	1.014	1.013	1.012	1.010	1.009
75	1.014	1.016	1.018	1.020	1.021	1.022	1.023	1.024	1.024	1.025	1.025	1.024	1.024	1.024	1.023	1.022	1.022	1.021	1.019		1.017	1.016	1.014	1.013	1.011
80	1.018	1.020	1.021	1.023	1.024	1.025	1.026	1.027	1.027	1.027	1.027	1.027	1.027	1.026	1.026	1.025	1.024	1.023	1.022	1.021		1.018	1.017	1.015	1.014
85	1.021	1.023	1.025	1.026	1.027	1.028	1.029	1.030	1.030	1.030	1.030	1.030	1.030	1.029	1.029	1.028	1.027	1.026	1.025	1.023	1.022		1.019	1.018	1.016
90	1.024	1.026	1.028	1.029	1.030	1.031	1.032	1.033	1.033	1.033	1.033	1.033	1.032	1.032	1.031	1.030	1.029	1.028	1.027	1.026	1.025	1.023		1.020	1.019
95	1.028	1.029	1.031	1.032	1.034	1.034	1.035	1.036	1.036	1.036	1.036	1.036	1.035	1.035	1.034	1.033	1.032	1.031	1.030	1.029	1.027	1.026	1.025		1.022
100	1.031	1.033	1.034	1.035	1.037	1.037	1.038	1.038	1.039	1.039	1.039	1.038	1.038	1.037	1.037	1.036	1.035	1.034	1.033	1.031	1.030	1.029	1.027	1.026	

Appendix 14: Heat coefficient k of Antifrogen Sol HT, measured in feed [kWh/(m³K)]

k Feed	Return temperature																								
Feed temperature	-20	-15	-10	-5	0	5	10	15	20	25	30	35	40	45	50	55	60	65	70	75	80	85	90	95	100
-20		0.937	0.944	0.950	0.956	0.962	0.968	0.973	0.978	0.983	0.988	0.993	0.997	1.002	1.006	1.010	1.014	1.018	1.021	1.025	1.028	1.032	1.035	1.039	1.042
-15	0.934		0.948	0.954	0.960	0.966	0.971	0.977	0.982	0.987	0.991	0.996	1.000	1.004	1.009	1.012	1.016	1.020	1.024	1.027	1.030	1.034	1.037	1.040	1.044
-10	0.939	0.945		0.958	0.964	0.969	0.975	0.980	0.985	0.990	0.994	0.999	1.003	1.007	1.011	1.015	1.018	1.022	1.026	1.029	1.032	1.036	1.039	1.042	1.045
-5	0.943	0.949	0.955		0.967	0.973	0.978	0.983	0.988	0.992	0.997	1.001	1.005	1.009	1.013	1.017	1.020	1.024	1.027	1.031	1.034	1.037	1.040	1.044	1.047
0	0.946	0.952	0.959	0.964		0.975	0.981	0.985	0.990	0.995	0.999	1.003	1.007	1.011	1.015	1.019	1.022	1.026	1.029	1.032	1.035	1.039	1.042	1.045	1.048
5	0.949	0.956	0.962	0.967	0.973		0.983	0.988	0.993	0.997	1.001	1.005	1.009	1.013	1.017	1.020	1.024	1.027	1.030	1.034	1.037	1.040	1.043	1.046	1.049
10	0.952	0.959	0.964	0.970	0.975	0.980		0.990	0.995	0.999	1.003	1.007	1.011	1.015	1.018	1.022	1.025	1.028	1.032	1.035	1.038	1.041	1.044	1.047	1.050
15	0.955	0.961	0.967	0.972	0.978	0.983	0.987		0.996	1.001	1.005	1.008	1.012	1.016	1.019	1.023	1.026	1.029	1.032	1.036	1.039	1.042	1.044	1.047	1.050
20	0.958	0.964	0.969	0.974	0.980	0.984	0.989	0.994		1.002	1.006	1.010	1.013	1.017	1.020	1.024	1.027	1.030	1.033	1.036	1.039	1.042	1.045	1.048	1.051
25	0.960	0.966	0.971	0.976	0.981	0.986	0.991	0.995	0.999		1.007	1.011	1.014	1.018	1.021	1.024	1.028	1.031	1.034	1.037	1.040	1.043	1.045	1.048	1.051
30	0.962	0.967	0.973	0.978	0.983	0.987	0.992	0.996	1.000	1.004		1.012	1.015	1.019	1.022	1.025	1.028	1.031	1.034	1.037	1.040	1.043	1.046	1.048	1.051
35	0.964	0.969	0.974	0.979	0.984	0.989	0.993	0.997	1.001	1.005	1.009		1.016	1.019	1.022	1.025	1.028	1.031	1.034	1.037	1.040	1.043	1.046	1.048	1.051
40	0.965	0.970	0.975	0.980	0.985	0.989	0.994	0.998	1.002	1.006	1.009	1.013		1.019	1.022	1.026	1.029	1.031	1.034	1.037	1.040	1.043	1.045	1.048	1.051
45	0.966	0.971	0.976	0.981	0.986	0.990	0.994	0.998	1.002	1.006	1.009	1.013	1.016		1.022	1.026	1.028	1.031	1.034	1.037	1.040	1.042	1.045	1.048	1.051
50	0.967	0.972	0.977	0.982	0.986	0.991	0.995	0.999	1.002	1.006	1.010	1.013	1.016	1.019		1.025	1.028	1.031	1.034	1.037	1.039	1.042	1.045	1.047	1.050
55	0.968	0.973	0.978	0.982	0.987	0.991	0.995	0.999	1.003	1.006	1.010	1.013	1.016	1.019	1.022		1.028	1.031	1.033	1.036	1.039	1.042	1.044	1.047	1.050
60	0.969	0.974	0.978	0.983	0.987	0.991	0.995	0.999	1.002	1.006	1.009	1.013	1.016	1.019	1.022	1.025		1.030	1.033	1.036	1.038	1.041	1.044	1.046	1.049
65	0.969	0.974	0.978	0.983	0.987	0.991	0.995	0.999	1.002	1.006	1.009	1.012	1.015	1.018	1.021	1.024	1.027		1.032	1.035	1.038	1.040	1.043	1.045	1.048
70	0.969	0.974	0.979	0.983	0.987	0.991	0.995	0.998	1.002	1.005	1.008	1.012	1.015	1.018	1.020	1.023	1.026	1.029		1.034	1.037	1.039	1.042	1.045	1.047
75	0.969	0.974	0.978	0.983	0.987	0.991	0.994	0.998	1.001	1.005	1.008	1.011	1.014	1.017	1.020	1.022	1.025	1.028	1.030		1.036	1.038	1.041	1.044	1.046
80	0.969	0.974	0.978	0.982	0.986	0.990	0.994	0.997	1.001	1.004	1.007	1.010	1.013	1.016	1.019	1.021	1.024	1.027	1.029	1.032		1.037	1.040	1.043	1.045
85	0.969	0.973	0.978	0.982	0.986	0.989	0.993	0.997	1.000	1.003	1.006	1.009	1.012	1.015	1.018	1.020	1.023	1.026	1.028	1.031	1.034		1.039	1.042	1.044
90	0.969	0.973	0.977	0.981	0.985	0.989	0.992	0.996	0.999	1.002	1.005	1.008	1.011	1.014	1.017	1.019	1.022	1.025	1.027	1.030	1.032	1.035		1.040	1.043
95	0.968	0.972	0.977	0.980	0.984	0.988	0.991	0.995	0.998	1.001	1.004	1.007	1.010	1.013	1.015	1.018	1.021	1.023	1.026	1.029	1.031	1.034	1.037		1.042
100	0.967	0.972	0.976	0.980	0.983	0.987	0.990	0.994	0.997	1.000	1.003	1.006	1.009	1.012	1.014	1.017	1.020	1.022	1.025	1.027	1.030	1.033	1.035	1.038	

Appendix 15: Heat coefficient k of Tyfocor L 25 %, measured in return [kWh/(m³K)]

k Return	Return temperature																								
Feed temperature	-20	-15	-10	-5	0	5	10	15	20	25	30	35	40	45	50	55	60	65	70	75	80	85	90	95	100
-20		1.098	1.101	1.103	1.105	1.107	1.108	1.109	1.109	1.109	1.109	1.109	1.108	1.107	1.105	1.104	1.102	1.100	1.098	1.095	1.093	1.090	1.088	1.085	1.082
-15	1.098		1.105	1.107	1.109	1.110	1.111	1.112	1.112	1.112	1.112	1.111	1.110	1.109	1.108	1.106	1.104	1.102	1.100	1.098	1.095	1.093	1.090	1.087	1.084
-10	1.102	1.105		1.110	1.112	1.114	1.114	1.115	1.115	1.115	1.115	1.114	1.113	1.112	1.110	1.108	1.107	1.104	1.102	1.100	1.097	1.095	1.092	1.089	1.086
-5	1.106	1.109	1.111		1.115	1.116	1.117	1.118	1.118	1.118	1.117	1.116	1.115	1.114	1.112	1.111	1.109	1.106	1.104	1.102	1.099	1.096	1.094	1.091	1.088
0	1.109	1.112	1.114	1.117		1.119	1.120	1.120	1.120	1.120	1.120	1.119	1.117	1.116	1.114	1.113	1.111	1.108	1.106	1.104	1.101	1.098	1.095	1.092	1.090
5	1.112	1.115	1.117	1.119	1.121		1.123	1.123	1.123	1.122	1.122	1.121	1.120	1.118	1.116	1.114	1.112	1.110	1.108	1.105	1.103	1.100	1.097	1.094	1.091
10	1.115	1.118	1.120	1.122	1.123	1.124		1.125	1.125	1.124	1.124	1.123	1.121	1.120	1.118	1.116	1.114	1.112	1.109	1.107	1.104	1.101	1.098	1.096	1.093
15	1.118	1.120	1.123	1.124	1.126	1.126	1.127		1.127	1.126	1.126	1.124	1.123	1.122	1.120	1.118	1.116	1.113	1.111	1.108	1.106	1.103	1.100	1.097	1.094
20	1.120	1.123	1.125	1.127	1.128	1.129	1.129	1.129		1.128	1.127	1.126	1.125	1.123	1.121	1.119	1.117	1.115	1.112	1.110	1.107	1.104	1.101	1.098	1.095
25	1.123	1.125	1.127	1.129	1.130	1.131	1.131	1.131	1.131		1.129	1.128	1.126	1.125	1.123	1.121	1.118	1.116	1.114	1.111	1.108	1.105	1.103	1.100	1.097
30	1.125	1.127	1.129	1.131	1.132	1.132	1.133	1.133	1.132	1.131		1.129	1.128	1.126	1.124	1.122	1.120	1.117	1.115	1.112	1.110	1.107	1.104	1.101	1.098
35	1.127	1.129	1.131	1.133	1.134	1.134	1.134	1.134	1.134	1.133	1.132		1.129	1.127	1.125	1.123	1.121	1.119	1.116	1.113	1.111	1.108	1.105	1.102	1.099
40	1.129	1.131	1.133	1.134	1.135	1.136	1.136	1.136	1.135	1.134	1.133	1.132		1.129	1.127	1.125	1.122	1.120	1.117	1.115	1.112	1.109	1.106	1.103	1.100
45	1.131	1.133	1.135	1.136	1.137	1.137	1.137	1.137	1.137	1.136	1.135	1.133	1.132		1.128	1.126	1.123	1.121	1.118	1.116	1.113	1.110	1.108	1.105	1.102
50	1.133	1.135	1.136	1.138	1.138	1.139	1.139	1.138	1.138	1.137	1.136	1.134	1.133	1.131		1.127	1.125	1.122	1.120	1.117	1.114	1.112	1.109	1.106	1.103
55	1.134	1.136	1.138	1.139	1.140	1.140	1.140	1.140	1.139	1.138	1.137	1.136	1.134	1.132	1.130		1.126	1.123	1.121	1.118	1.116	1.113	1.110	1.107	1.104
60	1.136	1.138	1.139	1.141	1.141	1.142	1.141	1.141	1.140	1.140	1.138	1.137	1.135	1.133	1.131	1.129		1.125	1.122	1.119	1.117	1.114	1.111	1.108	1.106
65	1.138	1.140	1.141	1.142	1.143	1.143	1.143	1.142	1.142	1.141	1.140	1.138	1.136	1.135	1.133	1.130	1.128		1.123	1.121	1.118	1.115	1.113	1.110	1.107
70	1.139	1.141	1.142	1.143	1.144	1.144	1.144	1.144	1.143	1.142	1.141	1.139	1.138	1.136	1.134	1.132	1.129	1.127		1.122	1.119	1.117	1.114	1.111	1.108
75	1.141	1.142	1.144	1.145	1.145	1.146	1.145	1.145	1.144	1.143	1.142	1.141	1.139	1.137	1.135	1.133	1.131	1.128	1.126		1.121	1.118	1.115	1.113	1.110
80	1.142	1.144	1.145	1.146	1.147	1.147	1.147	1.146	1.146	1.145	1.143	1.142	1.140	1.138	1.136	1.134	1.132	1.130	1.127	1.125		1.120	1.117	1.114	1.112
85	1.144	1.145	1.147	1.148	1.148	1.148	1.148	1.148	1.147	1.146	1.145	1.143	1.141	1.140	1.138	1.136	1.133	1.131	1.129	1.126	1.124		1.119	1.116	1.113
90	1.145	1.147	1.148	1.149	1.150	1.150	1.149	1.149	1.148	1.147	1.146	1.145	1.143	1.141	1.139	1.137	1.135	1.133	1.130	1.128	1.125	1.123		1.118	1.115
95	1.147	1.149	1.150	1.151	1.151	1.151	1.151	1.150	1.150	1.149	1.147	1.146	1.144	1.143	1.141	1.139	1.136	1.134	1.132	1.130	1.127	1.125	1.122		1.117
100	1.149	1.150	1.151	1.152	1.153	1.153	1.152	1.152	1.151	1.150	1.149	1.148	1.146	1.144	1.142	1.140	1.138	1.136	1.134	1.131	1.129	1.127	1.124	1.122	

Appendix 16: Heat coefficient k of Tyfocor L 25 %, measured in feed [kWh/(m³K)]

k Feed	Return temperature																								
Feed temperature	-20	-15	-10	-5	0	5	10	15	20	25	30	35	40	45	50	55	60	65	70	75	80	85	90	95	100
-20		1.098	1.102	1.106	1.109	1.112	1.115	1.118	1.120	1.123	1.125	1.127	1.129	1.131	1.133	1.134	1.136	1.138	1.139	1.141	1.142	1.144	1.145	1.147	1.149
-15	1.098		1.105	1.109	1.112	1.115	1.118	1.120	1.123	1.125	1.127	1.129	1.131	1.133	1.135	1.136	1.138	1.140	1.141	1.142	1.144	1.145	1.147	1.149	1.150
-10	1.101	1.105		1.111	1.114	1.117	1.120	1.123	1.125	1.127	1.129	1.131	1.133	1.135	1.136	1.138	1.139	1.141	1.142	1.144	1.145	1.147	1.148	1.150	1.151
-5	1.103	1.107	1.110		1.117	1.119	1.122	1.124	1.127	1.129	1.131	1.133	1.134	1.136	1.138	1.139	1.141	1.142	1.143	1.145	1.146	1.148	1.149	1.151	1.152
0	1.105	1.109	1.112	1.115		1.121	1.123	1.126	1.128	1.130	1.132	1.134	1.135	1.137	1.138	1.140	1.141	1.143	1.144	1.145	1.147	1.148	1.150	1.151	1.153
5	1.107	1.110	1.114	1.116	1.119		1.124	1.126	1.129	1.131	1.132	1.134	1.136	1.137	1.139	1.140	1.142	1.143	1.144	1.146	1.147	1.148	1.150	1.151	1.153
10	1.108	1.111	1.114	1.117	1.120	1.123		1.127	1.129	1.131	1.133	1.134	1.136	1.137	1.139	1.140	1.141	1.143	1.144	1.145	1.147	1.148	1.149	1.151	1.152
15	1.109	1.112	1.115	1.118	1.120	1.123	1.125		1.129	1.131	1.133	1.134	1.136	1.137	1.138	1.140	1.141	1.142	1.144	1.145	1.146	1.148	1.149	1.150	1.152
20	1.109	1.112	1.115	1.118	1.120	1.123	1.125	1.127		1.131	1.132	1.134	1.135	1.137	1.138	1.139	1.140	1.142	1.143	1.144	1.146	1.147	1.148	1.150	1.151
25	1.109	1.112	1.115	1.118	1.120	1.122	1.124	1.126	1.128		1.131	1.133	1.134	1.136	1.137	1.138	1.140	1.141	1.142	1.143	1.145	1.146	1.147	1.149	1.150
30	1.109	1.112	1.115	1.117	1.120	1.122	1.124	1.126	1.127	1.129		1.132	1.133	1.135	1.136	1.137	1.138	1.140	1.141	1.142	1.143	1.145	1.146	1.147	1.149
35	1.109	1.111	1.114	1.116	1.119	1.121	1.123	1.124	1.126	1.128	1.129		1.132	1.133	1.134	1.136	1.137	1.138	1.139	1.141	1.142	1.143	1.145	1.146	1.148
40	1.108	1.110	1.113	1.115	1.117	1.120	1.121	1.123	1.125	1.126	1.128	1.129		1.132	1.133	1.134	1.135	1.136	1.138	1.139	1.140	1.141	1.143	1.144	1.146
45	1.107	1.109	1.112	1.114	1.116	1.118	1.120	1.122	1.123	1.125	1.126	1.127	1.129		1.131	1.132	1.133	1.135	1.136	1.137	1.138	1.140	1.141	1.143	1.144
50	1.105	1.108	1.110	1.112	1.114	1.116	1.118	1.120	1.121	1.123	1.124	1.125	1.127	1.128		1.130	1.131	1.133	1.134	1.135	1.136	1.138	1.139	1.141	1.142
55	1.104	1.106	1.108	1.111	1.113	1.114	1.116	1.118	1.119	1.121	1.122	1.123	1.125	1.126	1.127		1.129	1.130	1.132	1.133	1.134	1.136	1.137	1.139	1.140
60	1.102	1.104	1.107	1.109	1.111	1.112	1.114	1.116	1.117	1.118	1.120	1.121	1.122	1.123	1.125	1.126		1.128	1.129	1.131	1.132	1.133	1.135	1.136	1.138
65	1.100	1.102	1.104	1.106	1.108	1.110	1.112	1.113	1.115	1.116	1.117	1.119	1.120	1.121	1.122	1.123	1.125		1.127	1.128	1.130	1.131	1.133	1.134	1.136
70	1.098	1.100	1.102	1.104	1.106	1.108	1.109	1.111	1.112	1.114	1.115	1.116	1.117	1.118	1.120	1.121	1.122	1.123		1.126	1.127	1.129	1.130	1.132	1.134
75	1.095	1.098	1.100	1.102	1.104	1.105	1.107	1.108	1.110	1.111	1.112	1.113	1.115	1.116	1.117	1.118	1.119	1.121	1.122		1.125	1.126	1.128	1.130	1.131
80	1.093	1.095	1.097	1.099	1.101	1.103	1.104	1.106	1.107	1.108	1.110	1.111	1.112	1.113	1.114	1.116	1.117	1.118	1.119	1.121		1.124	1.125	1.127	1.129
85	1.090	1.093	1.095	1.096	1.098	1.100	1.101	1.103	1.104	1.105	1.107	1.108	1.109	1.110	1.112	1.113	1.114	1.115	1.117	1.118	1.120		1.123	1.125	1.127
90	1.088	1.090	1.092	1.094	1.095	1.097	1.098	1.100	1.101	1.103	1.104	1.105	1.106	1.108	1.109	1.110	1.111	1.113	1.114	1.115	1.117	1.119		1.122	1.124
95	1.085	1.087	1.089	1.091	1.092	1.094	1.096	1.097	1.098	1.100	1.101	1.102	1.103	1.105	1.106	1.107	1.108	1.110	1.111	1.113	1.114	1.116	1.118		1.122
100	1.082	1.084	1.086	1.088	1.090	1.091	1.093	1.094	1.095	1.097	1.098	1.099	1.100	1.102	1.103	1.104	1.106	1.107	1.108	1.110	1.112	1.113	1.115	1.117	

Appendix 17: Heat coefficient k of Tyfocor L 30 %, measured in return [kWh/(m³K)]

k Return	Return temperature																								
Feed temperature	-20	-15	-10	-5	0	5	10	15	20	25	30	35	40	45	50	55	60	65	70	75	80	85	90	95	100
-20		1.074	1.078	1.081	1.084	1.087	1.088	1.090	1.091	1.092	1.092	1.092	1.092	1.091	1.090	1.089	1.088	1.086	1.084	1.082	1.080	1.078	1.076	1.073	1.071
-15	1.075		1.083	1.086	1.089	1.091	1.093	1.094	1.095	1.096	1.096	1.096	1.096	1.095	1.094	1.093	1.091	1.089	1.088	1.086	1.083	1.081	1.079	1.076	1.074
-10	1.080	1.084		1.091	1.094	1.096	1.097	1.099	1.099	1.100	1.100	1.100	1.099	1.098	1.097	1.096	1.094	1.092	1.091	1.088	1.086	1.084	1.081	1.079	1.076
-5	1.085	1.089	1.093		1.098	1.100	1.101	1.102	1.103	1.103	1.103	1.103	1.102	1.101	1.100	1.099	1.097	1.095	1.093	1.091	1.089	1.086	1.084	1.081	1.079
0	1.090	1.094	1.097	1.100		1.104	1.105	1.106	1.107	1.107	1.107	1.106	1.105	1.104	1.103	1.101	1.100	1.098	1.096	1.093	1.091	1.089	1.086	1.083	1.081
5	1.094	1.098	1.101	1.103	1.106		1.108	1.109	1.110	1.110	1.110	1.109	1.108	1.107	1.106	1.104	1.102	1.100	1.098	1.096	1.093	1.091	1.088	1.085	1.083
10	1.098	1.102	1.105	1.107	1.109	1.111		1.112	1.113	1.113	1.112	1.112	1.111	1.109	1.108	1.106	1.104	1.102	1.100	1.098	1.095	1.093	1.090	1.087	1.085
15	1.102	1.105	1.108	1.110	1.112	1.114	1.115		1.115	1.115	1.115	1.114	1.113	1.112	1.110	1.108	1.106	1.104	1.102	1.100	1.097	1.095	1.092	1.089	1.087
20	1.105	1.109	1.111	1.113	1.115	1.116	1.117	1.118		1.118	1.117	1.116	1.115	1.114	1.112	1.110	1.108	1.106	1.104	1.102	1.099	1.096	1.094	1.091	1.088
25	1.109	1.112	1.114	1.116	1.118	1.119	1.120	1.120	1.120		1.119	1.118	1.117	1.116	1.114	1.112	1.110	1.108	1.106	1.103	1.101	1.098	1.095	1.093	1.090
30	1.112	1.115	1.117	1.119	1.121	1.122	1.122	1.123	1.122	1.122		1.120	1.119	1.118	1.116	1.114	1.112	1.110	1.107	1.105	1.102	1.100	1.097	1.094	1.091
35	1.115	1.117	1.120	1.122	1.123	1.124	1.124	1.125	1.125	1.124	1.123		1.121	1.119	1.118	1.116	1.114	1.111	1.109	1.106	1.104	1.101	1.098	1.096	1.093
40	1.117	1.120	1.122	1.124	1.125	1.126	1.127	1.127	1.126	1.126	1.125	1.124		1.121	1.119	1.117	1.115	1.113	1.110	1.108	1.105	1.103	1.100	1.097	1.095
45	1.120	1.122	1.125	1.126	1.127	1.128	1.129	1.129	1.128	1.128	1.127	1.126	1.124		1.121	1.119	1.117	1.114	1.112	1.109	1.107	1.104	1.101	1.099	1.096
50	1.122	1.125	1.127	1.128	1.129	1.130	1.130	1.130	1.130	1.129	1.128	1.127	1.126	1.124		1.120	1.118	1.116	1.113	1.111	1.108	1.105	1.103	1.100	1.097
55	1.125	1.127	1.129	1.130	1.131	1.132	1.132	1.132	1.132	1.131	1.130	1.129	1.127	1.125	1.124		1.119	1.117	1.115	1.112	1.110	1.107	1.104	1.102	1.099
60	1.127	1.129	1.131	1.132	1.133	1.134	1.134	1.134	1.133	1.132	1.131	1.130	1.129	1.127	1.125	1.123		1.118	1.116	1.114	1.111	1.108	1.106	1.103	1.101
65	1.129	1.131	1.133	1.134	1.135	1.135	1.136	1.135	1.135	1.134	1.133	1.132	1.130	1.128	1.126	1.124	1.122		1.117	1.115	1.112	1.110	1.107	1.105	1.102
70	1.131	1.133	1.135	1.136	1.137	1.137	1.137	1.137	1.136	1.135	1.134	1.133	1.132	1.130	1.128	1.126	1.124	1.121		1.116	1.114	1.111	1.109	1.106	1.104
75	1.133	1.135	1.136	1.138	1.138	1.139	1.139	1.138	1.138	1.137	1.136	1.135	1.133	1.131	1.129	1.127	1.125	1.123	1.120		1.116	1.113	1.111	1.108	1.106
80	1.135	1.137	1.138	1.139	1.140	1.140	1.140	1.140	1.139	1.139	1.137	1.136	1.134	1.133	1.131	1.129	1.127	1.124	1.122	1.120		1.115	1.112	1.110	1.108
85	1.137	1.139	1.140	1.141	1.142	1.142	1.142	1.142	1.141	1.140	1.139	1.138	1.136	1.134	1.132	1.130	1.128	1.126	1.124	1.121	1.119		1.114	1.112	1.110
90	1.139	1.140	1.142	1.143	1.144	1.144	1.144	1.143	1.143	1.142	1.141	1.139	1.138	1.136	1.134	1.132	1.130	1.128	1.126	1.123	1.121	1.119		1.114	1.112
95	1.141	1.142	1.144	1.145	1.145	1.146	1.145	1.145	1.144	1.143	1.142	1.141	1.139	1.138	1.136	1.134	1.132	1.130	1.127	1.125	1.123	1.121	1.118		1.114
100	1.143	1.144	1.146	1.147	1.147	1.147	1.147	1.147	1.146	1.145	1.144	1.143	1.141	1.140	1.138	1.136	1.134	1.132	1.130	1.127	1.125	1.123	1.121	1.119	

Appendix 18: Heat coefficient k of Tyfocor L 30 %, measured in feed [kWh/(m³K)]

k Feed	Return temperature																								
Feed temperature	-20	-15	-10	-5	0	5	10	15	20	25	30	35	40	45	50	55	60	65	70	75	80	85	90	95	100
-20		1.075	1.080	1.085	1.090	1.094	1.098	1.102	1.105	1.109	1.112	1.115	1.117	1.120	1.122	1.125	1.127	1.129	1.131	1.133	1.135	1.137	1.139	1.141	1.143
-15	1.074		1.084	1.089	1.094	1.098	1.102	1.105	1.109	1.112	1.115	1.117	1.120	1.122	1.125	1.127	1.129	1.131	1.133	1.135	1.137	1.139	1.140	1.142	1.144
-10	1.078	1.083		1.093	1.097	1.101	1.105	1.108	1.111	1.114	1.117	1.120	1.122	1.125	1.127	1.129	1.131	1.133	1.135	1.136	1.138	1.140	1.142	1.144	1.146
-5	1.081	1.086	1.091		1.100	1.103	1.107	1.110	1.113	1.116	1.119	1.122	1.124	1.126	1.128	1.130	1.132	1.134	1.136	1.138	1.139	1.141	1.143	1.145	1.147
0	1.084	1.089	1.094	1.098		1.106	1.109	1.112	1.115	1.118	1.121	1.123	1.125	1.127	1.129	1.131	1.133	1.135	1.137	1.138	1.140	1.142	1.144	1.145	1.147
5	1.087	1.091	1.096	1.100	1.104		1.111	1.114	1.116	1.119	1.122	1.124	1.126	1.128	1.130	1.132	1.134	1.135	1.137	1.139	1.140	1.142	1.144	1.146	1.147
10	1.088	1.093	1.097	1.101	1.105	1.108		1.115	1.117	1.120	1.122	1.124	1.127	1.129	1.130	1.132	1.134	1.136	1.137	1.139	1.140	1.142	1.144	1.145	1.147
15	1.090	1.094	1.099	1.102	1.106	1.109	1.112		1.118	1.120	1.123	1.125	1.127	1.129	1.130	1.132	1.134	1.135	1.137	1.138	1.140	1.142	1.143	1.145	1.147
20	1.091	1.095	1.099	1.103	1.107	1.110	1.113	1.115		1.120	1.122	1.125	1.126	1.128	1.130	1.132	1.133	1.135	1.136	1.138	1.139	1.141	1.143	1.144	1.146
25	1.092	1.096	1.100	1.103	1.107	1.110	1.113	1.115	1.118		1.122	1.124	1.126	1.128	1.129	1.131	1.132	1.134	1.135	1.137	1.139	1.140	1.142	1.143	1.145
30	1.092	1.096	1.100	1.103	1.107	1.110	1.112	1.115	1.117	1.119		1.123	1.125	1.127	1.128	1.130	1.131	1.133	1.134	1.136	1.137	1.139	1.141	1.142	1.144
35	1.092	1.096	1.100	1.103	1.106	1.109	1.112	1.114	1.116	1.118	1.120		1.124	1.126	1.127	1.129	1.130	1.132	1.133	1.135	1.136	1.138	1.139	1.141	1.143
40	1.092	1.096	1.099	1.102	1.105	1.108	1.111	1.113	1.115	1.117	1.119	1.121		1.124	1.126	1.127	1.129	1.130	1.132	1.133	1.134	1.136	1.138	1.139	1.141
45	1.091	1.095	1.098	1.101	1.104	1.107	1.109	1.112	1.114	1.116	1.118	1.119	1.121		1.124	1.125	1.127	1.128	1.130	1.131	1.133	1.134	1.136	1.138	1.140
50	1.090	1.094	1.097	1.100	1.103	1.106	1.108	1.110	1.112	1.114	1.116	1.118	1.119	1.121		1.124	1.125	1.126	1.128	1.129	1.131	1.132	1.134	1.136	1.138
55	1.089	1.093	1.096	1.099	1.101	1.104	1.106	1.108	1.110	1.112	1.114	1.116	1.117	1.119	1.120		1.123	1.124	1.126	1.127	1.129	1.130	1.132	1.134	1.136
60	1.088	1.091	1.094	1.097	1.100	1.102	1.104	1.106	1.108	1.110	1.112	1.114	1.115	1.117	1.118	1.119		1.122	1.124	1.125	1.127	1.128	1.130	1.132	1.134
65	1.086	1.089	1.092	1.095	1.098	1.100	1.102	1.104	1.106	1.108	1.110	1.111	1.113	1.114	1.116	1.117	1.118		1.121	1.123	1.124	1.126	1.128	1.130	1.132
70	1.084	1.088	1.091	1.093	1.096	1.098	1.100	1.102	1.104	1.106	1.107	1.109	1.110	1.112	1.113	1.115	1.116	1.117		1.120	1.122	1.124	1.126	1.127	1.130
75	1.082	1.086	1.088	1.091	1.093	1.096	1.098	1.100	1.102	1.103	1.105	1.106	1.108	1.109	1.111	1.112	1.114	1.115	1.116		1.120	1.121	1.123	1.125	1.127
80	1.080	1.083	1.086	1.089	1.091	1.093	1.095	1.097	1.099	1.101	1.102	1.104	1.105	1.107	1.108	1.110	1.111	1.112	1.114	1.116		1.119	1.121	1.123	1.125
85	1.078	1.081	1.084	1.086	1.089	1.091	1.093	1.095	1.096	1.098	1.100	1.101	1.103	1.104	1.105	1.107	1.108	1.110	1.111	1.113	1.115		1.119	1.121	1.123
90	1.076	1.079	1.081	1.084	1.086	1.088	1.090	1.092	1.094	1.095	1.097	1.098	1.100	1.101	1.103	1.104	1.106	1.107	1.109	1.111	1.112	1.114		1.118	1.121
95	1.073	1.076	1.079	1.081	1.083	1.085	1.087	1.089	1.091	1.093	1.094	1.096	1.097	1.099	1.100	1.102	1.103	1.105	1.106	1.108	1.110	1.112	1.114		1.119
100	1.071	1.074	1.076	1.079	1.081	1.083	1.085	1.087	1.088	1.090	1.091	1.093	1.095	1.096	1.097	1.099	1.101	1.102	1.104	1.106	1.108	1.110	1.112	1.114	

Appendix 19: Heat coefficient k of Tyfocor L 35 %, measured in return [kWh/(m³K)]

k Return	Return temperature																								
Feed temperature	-20	-15	-10	-5	0	5	10	15	20	25	30	35	40	45	50	55	60	65	70	75	80	85	90	95	100
-20		1.049	1.054	1.058	1.061	1.064	1.066	1.068	1.070	1.071	1.072	1.072	1.072	1.072	1.071	1.070	1.069	1.068	1.066	1.065	1.063	1.061	1.058	1.056	1.054
-15	1.051		1.060	1.064	1.067	1.069	1.072	1.074	1.075	1.076	1.076	1.077	1.077	1.076	1.075	1.074	1.073	1.072	1.070	1.068	1.066	1.064	1.062	1.059	1.057
-10	1.057	1.062		1.069	1.072	1.075	1.077	1.078	1.080	1.080	1.081	1.081	1.081	1.080	1.079	1.078	1.077	1.075	1.074	1.072	1.069	1.067	1.065	1.062	1.060
-5	1.063	1.067	1.071		1.077	1.080	1.081	1.083	1.084	1.085	1.085	1.085	1.085	1.084	1.083	1.082	1.080	1.079	1.077	1.075	1.072	1.070	1.068	1.065	1.063
0	1.068	1.073	1.076	1.079		1.084	1.086	1.087	1.088	1.089	1.089	1.089	1.088	1.087	1.086	1.085	1.083	1.082	1.080	1.078	1.075	1.073	1.070	1.068	1.065
5	1.073	1.077	1.081	1.084	1.086		1.090	1.091	1.092	1.092	1.092	1.092	1.091	1.090	1.089	1.088	1.086	1.084	1.082	1.080	1.078	1.075	1.073	1.070	1.068
10	1.078	1.082	1.085	1.088	1.090	1.092		1.095	1.095	1.096	1.096	1.095	1.094	1.093	1.092	1.091	1.089	1.087	1.085	1.083	1.080	1.078	1.075	1.073	1.070
15	1.083	1.086	1.089	1.092	1.094	1.096	1.097		1.099	1.099	1.099	1.098	1.097	1.096	1.095	1.093	1.091	1.089	1.087	1.085	1.082	1.080	1.077	1.075	1.072
20	1.087	1.090	1.093	1.096	1.098	1.099	1.101	1.101		1.102	1.101	1.101	1.100	1.099	1.097	1.095	1.094	1.092	1.089	1.087	1.084	1.082	1.079	1.077	1.074
25	1.091	1.094	1.097	1.099	1.101	1.103	1.104	1.104	1.104		1.104	1.103	1.102	1.101	1.099	1.098	1.096	1.094	1.091	1.089	1.086	1.084	1.081	1.078	1.076
30	1.095	1.098	1.100	1.102	1.104	1.105	1.106	1.107	1.107	1.107		1.106	1.104	1.103	1.101	1.100	1.098	1.095	1.093	1.091	1.088	1.086	1.083	1.080	1.077
35	1.098	1.101	1.103	1.105	1.107	1.108	1.109	1.109	1.109	1.109	1.109		1.106	1.105	1.103	1.102	1.100	1.097	1.095	1.092	1.090	1.087	1.085	1.082	1.079
40	1.101	1.104	1.106	1.108	1.110	1.111	1.111	1.112	1.112	1.111	1.111	1.110		1.107	1.105	1.103	1.101	1.099	1.097	1.094	1.092	1.089	1.086	1.083	1.081
45	1.104	1.107	1.109	1.111	1.112	1.113	1.114	1.114	1.114	1.113	1.113	1.112	1.110		1.107	1.105	1.103	1.101	1.098	1.096	1.093	1.090	1.088	1.085	1.082
50	1.107	1.110	1.112	1.113	1.115	1.115	1.116	1.116	1.116	1.115	1.114	1.113	1.112	1.110		1.107	1.104	1.102	1.100	1.097	1.095	1.092	1.089	1.086	1.084
55	1.110	1.112	1.114	1.116	1.117	1.118	1.118	1.118	1.118	1.117	1.116	1.115	1.114	1.112	1.110		1.106	1.104	1.101	1.099	1.096	1.093	1.091	1.088	1.085
60	1.112	1.115	1.116	1.118	1.119	1.120	1.120	1.120	1.120	1.119	1.118	1.117	1.115	1.114	1.112	1.110		1.105	1.103	1.100	1.098	1.095	1.092	1.089	1.087
65	1.115	1.117	1.119	1.120	1.121	1.122	1.122	1.122	1.121	1.121	1.120	1.118	1.117	1.115	1.113	1.111	1.109		1.104	1.102	1.099	1.096	1.094	1.091	1.088
70	1.117	1.119	1.121	1.122	1.123	1.124	1.124	1.124	1.123	1.122	1.121	1.120	1.118	1.117	1.115	1.113	1.110	1.108		1.103	1.101	1.098	1.095	1.093	1.090
75	1.119	1.121	1.123	1.124	1.125	1.125	1.125	1.125	1.125	1.124	1.123	1.121	1.120	1.118	1.116	1.114	1.112	1.110	1.107		1.102	1.099	1.097	1.094	1.092
80	1.121	1.123	1.125	1.126	1.127	1.127	1.127	1.127	1.126	1.125	1.124	1.123	1.121	1.120	1.118	1.116	1.113	1.111	1.109	1.106		1.101	1.099	1.096	1.094
85	1.124	1.125	1.127	1.128	1.129	1.129	1.129	1.129	1.128	1.127	1.126	1.125	1.123	1.121	1.119	1.117	1.115	1.113	1.110	1.108	1.105		1.100	1.098	1.095
90	1.126	1.127	1.129	1.130	1.131	1.131	1.131	1.130	1.130	1.129	1.128	1.126	1.125	1.123	1.121	1.119	1.117	1.114	1.112	1.110	1.107	1.105		1.100	1.097
95	1.128	1.130	1.131	1.132	1.132	1.133	1.133	1.132	1.131	1.131	1.129	1.128	1.126	1.125	1.123	1.121	1.119	1.116	1.114	1.112	1.109	1.107	1.104		1.100
100	1.130	1.132	1.133	1.134	1.134	1.135	1.134	1.134	1.133	1.132	1.131	1.130	1.128	1.126	1.125	1.123	1.120	1.118	1.116	1.114	1.111	1.109	1.107	1.104	

Appendix 20: Heat coefficient k of Tyfocor L 35 %, measured in feed [kWh/(m³K)]

k Feed	Return temperature																								
Feed temperature	-20	-15	-10	-5	0	5	10	15	20	25	30	35	40	45	50	55	60	65	70	75	80	85	90	95	100
-20		1.051	1.057	1.063	1.068	1.073	1.078	1.083	1.087	1.091	1.095	1.098	1.101	1.104	1.107	1.110	1.112	1.115	1.117	1.119	1.121	1.124	1.126	1.128	1.130
-15	1.049		1.062	1.067	1.073	1.077	1.082	1.086	1.090	1.094	1.098	1.101	1.104	1.107	1.110	1.112	1.115	1.117	1.119	1.121	1.123	1.125	1.127	1.130	1.132
-10	1.054	1.060		1.071	1.076	1.081	1.085	1.089	1.093	1.097	1.100	1.103	1.106	1.109	1.112	1.114	1.116	1.119	1.121	1.123	1.125	1.127	1.129	1.131	1.133
-5	1.058	1.064	1.069		1.079	1.084	1.088	1.092	1.096	1.099	1.102	1.105	1.108	1.111	1.113	1.116	1.118	1.120	1.122	1.124	1.126	1.128	1.130	1.132	1.134
0	1.061	1.067	1.072	1.077		1.086	1.090	1.094	1.098	1.101	1.104	1.107	1.110	1.112	1.115	1.117	1.119	1.121	1.123	1.125	1.127	1.129	1.131	1.132	1.134
5	1.064	1.069	1.075	1.080	1.084		1.092	1.096	1.099	1.103	1.105	1.108	1.111	1.113	1.115	1.118	1.120	1.122	1.124	1.125	1.127	1.129	1.131	1.133	1.135
10	1.066	1.072	1.077	1.081	1.086	1.090		1.097	1.101	1.104	1.106	1.109	1.111	1.114	1.116	1.118	1.120	1.122	1.124	1.125	1.127	1.129	1.131	1.133	1.134
15	1.068	1.074	1.078	1.083	1.087	1.091	1.095		1.101	1.104	1.107	1.109	1.112	1.114	1.116	1.118	1.120	1.122	1.124	1.125	1.127	1.129	1.130	1.132	1.134
20	1.070	1.075	1.080	1.084	1.088	1.092	1.095	1.099		1.104	1.107	1.109	1.112	1.114	1.116	1.118	1.120	1.121	1.123	1.125	1.126	1.128	1.130	1.131	1.133
25	1.071	1.076	1.080	1.085	1.089	1.092	1.096	1.099	1.102		1.107	1.109	1.111	1.113	1.115	1.117	1.119	1.121	1.122	1.124	1.125	1.127	1.129	1.131	1.132
30	1.072	1.076	1.081	1.085	1.089	1.092	1.096	1.099	1.101	1.104		1.109	1.111	1.113	1.114	1.116	1.118	1.120	1.121	1.123	1.124	1.126	1.128	1.129	1.131
35	1.072	1.077	1.081	1.085	1.089	1.092	1.095	1.098	1.101	1.103	1.106		1.110	1.112	1.113	1.115	1.117	1.118	1.120	1.121	1.123	1.125	1.126	1.128	1.130
40	1.072	1.077	1.081	1.085	1.088	1.091	1.094	1.097	1.100	1.102	1.104	1.106		1.110	1.112	1.114	1.115	1.117	1.118	1.120	1.121	1.123	1.125	1.126	1.128
45	1.072	1.076	1.080	1.084	1.087	1.090	1.093	1.096	1.099	1.101	1.103	1.105	1.107		1.110	1.112	1.114	1.115	1.117	1.118	1.120	1.121	1.123	1.125	1.126
50	1.071	1.075	1.079	1.083	1.086	1.089	1.092	1.095	1.097	1.099	1.101	1.103	1.105	1.107		1.110	1.112	1.113	1.115	1.116	1.118	1.119	1.121	1.123	1.125
55	1.070	1.074	1.078	1.082	1.085	1.088	1.091	1.093	1.095	1.098	1.100	1.102	1.103	1.105	1.107		1.110	1.111	1.113	1.114	1.116	1.117	1.119	1.121	1.123
60	1.069	1.073	1.077	1.080	1.083	1.086	1.089	1.091	1.094	1.096	1.098	1.100	1.101	1.103	1.104	1.106		1.109	1.110	1.112	1.113	1.115	1.117	1.119	1.120
65	1.068	1.072	1.075	1.079	1.082	1.084	1.087	1.089	1.092	1.094	1.095	1.097	1.099	1.101	1.102	1.104	1.105		1.108	1.110	1.111	1.113	1.114	1.116	1.118
70	1.066	1.070	1.074	1.077	1.080	1.082	1.085	1.087	1.089	1.091	1.093	1.095	1.097	1.098	1.100	1.101	1.103	1.104		1.107	1.109	1.110	1.112	1.114	1.116
75	1.065	1.068	1.072	1.075	1.078	1.080	1.083	1.085	1.087	1.089	1.091	1.092	1.094	1.096	1.097	1.099	1.100	1.102	1.103		1.106	1.108	1.110	1.112	1.114
80	1.063	1.066	1.069	1.072	1.075	1.078	1.080	1.082	1.084	1.086	1.088	1.090	1.092	1.093	1.095	1.096	1.098	1.099	1.101	1.102		1.105	1.107	1.109	1.111
85	1.061	1.064	1.067	1.070	1.073	1.075	1.078	1.080	1.082	1.084	1.086	1.087	1.089	1.090	1.092	1.093	1.095	1.096	1.098	1.099	1.101		1.105	1.107	1.109
90	1.058	1.062	1.065	1.068	1.070	1.073	1.075	1.077	1.079	1.081	1.083	1.085	1.086	1.088	1.089	1.091	1.092	1.094	1.095	1.097	1.099	1.100		1.104	1.107
95	1.056	1.059	1.062	1.065	1.068	1.070	1.073	1.075	1.077	1.078	1.080	1.082	1.083	1.085	1.086	1.088	1.089	1.091	1.093	1.094	1.096	1.098	1.100		1.104
100	1.054	1.057	1.060	1.063	1.065	1.068	1.070	1.072	1.074	1.076	1.077	1.079	1.081	1.082	1.084	1.085	1.087	1.088	1.090	1.092	1.094	1.095	1.097	1.100	

Appendix 21: Heat coefficient k of Tyfocor L 40 %, measured in return [kWh/(m³K)]

k Return	Return temperature																								
Feed temperature	-20	-15	-10	-5	0	5	10	15	20	25	30	35	40	45	50	55	60	65	70	75	80	85	90	95	100
-20		1.016	1.021	1.025	1.029	1.032	1.035	1.037	1.039	1.041	1.042	1.043	1.043	1.043	1.043	1.043	1.042	1.041	1.040	1.039	1.037	1.036	1.034	1.032	1.030
-15	1.018		1.027	1.031	1.035	1.038	1.041	1.043	1.045	1.046	1.047	1.048	1.048	1.048	1.048	1.047	1.047	1.046	1.044	1.043	1.041	1.040	1.038	1.036	1.034
-10	1.025	1.030		1.038	1.041	1.044	1.046	1.048	1.050	1.051	1.052	1.053	1.053	1.053	1.052	1.052	1.051	1.050	1.048	1.047	1.045	1.043	1.041	1.039	1.037
-5	1.031	1.036	1.040		1.047	1.049	1.052	1.054	1.055	1.056	1.057	1.057	1.057	1.057	1.056	1.056	1.055	1.053	1.052	1.050	1.049	1.047	1.045	1.043	1.040
0	1.037	1.042	1.046	1.049		1.055	1.057	1.058	1.060	1.061	1.061	1.061	1.061	1.061	1.060	1.059	1.058	1.057	1.055	1.054	1.052	1.050	1.048	1.046	1.043
5	1.043	1.047	1.051	1.054	1.057		1.061	1.063	1.064	1.065	1.065	1.065	1.065	1.065	1.064	1.063	1.062	1.060	1.059	1.057	1.055	1.053	1.051	1.049	1.046
10	1.048	1.052	1.056	1.059	1.062	1.064		1.067	1.068	1.069	1.069	1.069	1.069	1.068	1.067	1.066	1.065	1.063	1.062	1.060	1.058	1.056	1.053	1.051	1.049
15	1.054	1.057	1.061	1.064	1.066	1.068	1.070		1.072	1.072	1.073	1.072	1.072	1.071	1.070	1.069	1.068	1.066	1.064	1.062	1.060	1.058	1.056	1.054	1.051
20	1.058	1.062	1.065	1.068	1.070	1.072	1.074	1.075		1.076	1.076	1.076	1.075	1.074	1.073	1.072	1.070	1.069	1.067	1.065	1.063	1.061	1.058	1.056	1.054
25	1.063	1.066	1.069	1.072	1.074	1.076	1.077	1.078	1.079		1.079	1.079	1.078	1.077	1.076	1.075	1.073	1.071	1.069	1.067	1.065	1.063	1.061	1.058	1.056
30	1.067	1.070	1.073	1.076	1.078	1.079	1.081	1.081	1.082	1.082		1.081	1.081	1.080	1.079	1.077	1.075	1.074	1.072	1.070	1.067	1.065	1.063	1.061	1.058
35	1.071	1.074	1.077	1.079	1.081	1.083	1.084	1.084	1.085	1.085	1.085		1.083	1.082	1.081	1.079	1.078	1.076	1.074	1.072	1.070	1.067	1.065	1.063	1.060
40	1.075	1.078	1.080	1.083	1.084	1.086	1.087	1.087	1.088	1.088	1.087	1.087		1.085	1.083	1.082	1.080	1.078	1.076	1.074	1.072	1.069	1.067	1.065	1.062
45	1.078	1.081	1.084	1.086	1.087	1.089	1.089	1.090	1.090	1.090	1.090	1.089	1.088		1.085	1.084	1.082	1.080	1.078	1.076	1.074	1.071	1.069	1.066	1.064
50	1.082	1.084	1.087	1.089	1.090	1.091	1.092	1.093	1.093	1.092	1.092	1.091	1.090	1.089		1.086	1.084	1.082	1.080	1.078	1.075	1.073	1.071	1.068	1.066
55	1.085	1.088	1.090	1.092	1.093	1.094	1.095	1.095	1.095	1.095	1.094	1.093	1.092	1.091	1.089		1.086	1.084	1.082	1.080	1.077	1.075	1.073	1.070	1.068
60	1.088	1.090	1.093	1.094	1.096	1.096	1.097	1.097	1.097	1.097	1.096	1.095	1.094	1.093	1.091	1.090		1.086	1.084	1.081	1.079	1.077	1.074	1.072	1.070
65	1.091	1.093	1.095	1.097	1.098	1.099	1.099	1.100	1.099	1.099	1.098	1.097	1.096	1.095	1.093	1.092	1.090		1.085	1.083	1.081	1.079	1.076	1.074	1.072
70	1.094	1.096	1.098	1.099	1.100	1.101	1.102	1.102	1.102	1.101	1.100	1.099	1.098	1.097	1.095	1.093	1.091	1.089		1.085	1.083	1.081	1.078	1.076	1.074
75	1.096	1.099	1.100	1.102	1.103	1.103	1.104	1.104	1.104	1.103	1.102	1.101	1.100	1.099	1.097	1.095	1.093	1.091	1.089		1.085	1.082	1.080	1.078	1.076
80	1.099	1.101	1.103	1.104	1.105	1.106	1.106	1.106	1.106	1.105	1.104	1.103	1.102	1.101	1.099	1.097	1.095	1.093	1.091	1.089		1.084	1.082	1.080	1.078
85	1.102	1.104	1.105	1.107	1.107	1.108	1.108	1.108	1.108	1.107	1.106	1.105	1.104	1.102	1.101	1.099	1.097	1.095	1.093	1.091	1.089		1.084	1.082	1.080
90	1.104	1.106	1.108	1.109	1.110	1.110	1.110	1.110	1.110	1.109	1.108	1.107	1.106	1.104	1.103	1.101	1.099	1.097	1.095	1.093	1.091	1.089		1.084	1.082
95	1.107	1.109	1.110	1.111	1.112	1.112	1.113	1.112	1.112	1.111	1.110	1.109	1.108	1.107	1.105	1.103	1.101	1.099	1.097	1.095	1.093	1.091	1.089		1.085
100	1.109	1.111	1.112	1.114	1.114	1.115	1.115	1.115	1.114	1.113	1.113	1.111	1.110	1.109	1.107	1.105	1.103	1.102	1.100	1.097	1.095	1.093	1.091	1.089	

Appendix 22: Heat coefficient k of Tyfocor L 40 %, measured in feed [kWh/(m³K)]

k Feed	Return temperature																								
Feed temperature	-20	-15	-10	-5	0	5	10	15	20	25	30	35	40	45	50	55	60	65	70	75	80	85	90	95	100
-20		1.018	1.025	1.031	1.037	1.043	1.048	1.054	1.058	1.063	1.067	1.071	1.075	1.078	1.082	1.085	1.088	1.091	1.094	1.096	1.099	1.102	1.104	1.107	1.109
-15	1.016		1.030	1.036	1.042	1.047	1.052	1.057	1.062	1.066	1.070	1.074	1.078	1.081	1.084	1.088	1.090	1.093	1.096	1.099	1.101	1.104	1.106	1.109	1.111
-10	1.021	1.027		1.040	1.046	1.051	1.056	1.061	1.065	1.069	1.073	1.077	1.080	1.084	1.087	1.090	1.093	1.095	1.098	1.100	1.103	1.105	1.108	1.110	1.112
-5	1.025	1.031	1.038		1.049	1.054	1.059	1.064	1.068	1.072	1.076	1.079	1.083	1.086	1.089	1.092	1.094	1.097	1.099	1.102	1.104	1.107	1.109	1.111	1.114
0	1.029	1.035	1.041	1.047		1.057	1.062	1.066	1.070	1.074	1.078	1.081	1.084	1.087	1.090	1.093	1.096	1.098	1.100	1.103	1.105	1.107	1.110	1.112	1.114
5	1.032	1.038	1.044	1.049	1.055		1.064	1.068	1.072	1.076	1.079	1.083	1.086	1.089	1.091	1.094	1.096	1.099	1.101	1.103	1.106	1.108	1.110	1.112	1.115
10	1.035	1.041	1.046	1.052	1.057	1.061		1.070	1.074	1.077	1.081	1.084	1.087	1.089	1.092	1.095	1.097	1.099	1.102	1.104	1.106	1.108	1.110	1.113	1.115
15	1.037	1.043	1.048	1.054	1.058	1.063	1.067		1.075	1.078	1.081	1.084	1.087	1.090	1.093	1.095	1.097	1.100	1.102	1.104	1.106	1.108	1.110	1.112	1.115
20	1.039	1.045	1.050	1.055	1.060	1.064	1.068	1.072		1.079	1.082	1.085	1.088	1.090	1.093	1.095	1.097	1.099	1.102	1.104	1.106	1.108	1.110	1.112	1.114
25	1.041	1.046	1.051	1.056	1.061	1.065	1.069	1.072	1.076		1.082	1.085	1.088	1.090	1.092	1.095	1.097	1.099	1.101	1.103	1.105	1.107	1.109	1.111	1.113
30	1.042	1.047	1.052	1.057	1.061	1.065	1.069	1.073	1.076	1.079		1.085	1.087	1.090	1.092	1.094	1.096	1.098	1.100	1.102	1.104	1.106	1.108	1.110	1.113
35	1.043	1.048	1.053	1.057	1.061	1.065	1.069	1.072	1.076	1.079	1.081		1.087	1.089	1.091	1.093	1.095	1.097	1.099	1.101	1.103	1.105	1.107	1.109	1.111
40	1.043	1.048	1.053	1.057	1.061	1.065	1.069	1.072	1.075	1.078	1.081	1.083		1.088	1.090	1.092	1.094	1.096	1.098	1.100	1.102	1.104	1.106	1.108	1.110
45	1.043	1.048	1.053	1.057	1.061	1.065	1.068	1.071	1.074	1.077	1.080	1.082	1.085		1.089	1.091	1.093	1.095	1.097	1.099	1.101	1.102	1.104	1.107	1.109
50	1.043	1.048	1.052	1.056	1.060	1.064	1.067	1.070	1.073	1.076	1.079	1.081	1.083	1.085		1.089	1.091	1.093	1.095	1.097	1.099	1.101	1.103	1.105	1.107
55	1.043	1.047	1.052	1.056	1.059	1.063	1.066	1.069	1.072	1.075	1.077	1.079	1.082	1.084	1.086		1.090	1.092	1.093	1.095	1.097	1.099	1.101	1.103	1.105
60	1.042	1.047	1.051	1.055	1.058	1.062	1.065	1.068	1.070	1.073	1.075	1.078	1.080	1.082	1.084	1.086		1.090	1.091	1.093	1.095	1.097	1.099	1.101	1.103
65	1.041	1.046	1.050	1.053	1.057	1.060	1.063	1.066	1.069	1.071	1.074	1.076	1.078	1.080	1.082	1.084	1.086		1.089	1.091	1.093	1.095	1.097	1.099	1.102
70	1.040	1.044	1.048	1.052	1.055	1.059	1.062	1.064	1.067	1.069	1.072	1.074	1.076	1.078	1.080	1.082	1.084	1.085		1.089	1.091	1.093	1.095	1.097	1.100
75	1.039	1.043	1.047	1.050	1.054	1.057	1.060	1.062	1.065	1.067	1.070	1.072	1.074	1.076	1.078	1.080	1.081	1.083	1.085		1.089	1.091	1.093	1.095	1.097
80	1.037	1.041	1.045	1.049	1.052	1.055	1.058	1.060	1.063	1.065	1.067	1.070	1.072	1.074	1.075	1.077	1.079	1.081	1.083	1.085		1.089	1.091	1.093	1.095
85	1.036	1.040	1.043	1.047	1.050	1.053	1.056	1.058	1.061	1.063	1.065	1.067	1.069	1.071	1.073	1.075	1.077	1.079	1.081	1.082	1.084		1.089	1.091	1.093
90	1.034	1.038	1.041	1.045	1.048	1.051	1.053	1.056	1.058	1.061	1.063	1.065	1.067	1.069	1.071	1.073	1.074	1.076	1.078	1.080	1.082	1.084		1.089	1.091
95	1.032	1.036	1.039	1.043	1.046	1.049	1.051	1.054	1.056	1.058	1.061	1.063	1.065	1.066	1.068	1.070	1.072	1.074	1.076	1.078	1.080	1.082	1.084		1.089
100	1.030	1.034	1.037	1.040	1.043	1.046	1.049	1.051	1.054	1.056	1.058	1.060	1.062	1.064	1.066	1.068	1.070	1.072	1.074	1.076	1.078	1.080	1.082	1.085	

Appendix 23: Heat coefficient k of Antifrogen N 20 %, measured in return [kWh/(m³K)]

k Return	Return temperature																								
Feed temperature	-20	-15	-10	-5	0	5	10	15	20	25	30	35	40	45	50	55	60	65	70	75	80	85	90	95	100
-20		1.088	1.090	1.092	1.094	1.095	1.096	1.097	1.097	1.098	1.098	1.097	1.097	1.096	1.095	1.094	1.093	1.091	1.090	1.088	1.086	1.084	1.082	1.080	1.077
-15	1.088		1.093	1.095	1.097	1.098	1.099	1.100	1.100	1.100	1.100	1.100	1.099	1.098	1.097	1.096	1.095	1.093	1.092	1.090	1.088	1.086	1.084	1.082	1.079
-10	1.091	1.094		1.098	1.099	1.101	1.101	1.102	1.102	1.102	1.102	1.102	1.101	1.101	1.099	1.098	1.097	1.095	1.094	1.092	1.090	1.088	1.086	1.084	1.081
-5	1.094	1.096	1.098		1.102	1.103	1.104	1.104	1.105	1.105	1.105	1.104	1.103	1.103	1.102	1.100	1.099	1.097	1.096	1.094	1.092	1.090	1.088	1.085	1.083
0	1.096	1.099	1.101	1.103		1.105	1.106	1.107	1.107	1.107	1.107	1.106	1.106	1.105	1.104	1.102	1.101	1.099	1.098	1.096	1.094	1.092	1.090	1.087	1.085
5	1.099	1.101	1.103	1.105	1.107		1.108	1.109	1.109	1.109	1.109	1.108	1.108	1.107	1.106	1.104	1.103	1.101	1.100	1.098	1.096	1.094	1.091	1.089	1.087
10	1.101	1.104	1.106	1.107	1.109	1.110		1.111	1.111	1.111	1.111	1.110	1.110	1.109	1.107	1.106	1.105	1.103	1.101	1.099	1.097	1.095	1.093	1.091	1.088
15	1.104	1.106	1.108	1.110	1.111	1.112	1.113		1.113	1.113	1.113	1.112	1.111	1.110	1.109	1.108	1.106	1.105	1.103	1.101	1.099	1.097	1.095	1.092	1.090
20	1.106	1.108	1.110	1.112	1.113	1.114	1.115	1.115		1.115	1.115	1.114	1.113	1.112	1.111	1.110	1.108	1.107	1.105	1.103	1.101	1.099	1.096	1.094	1.092
25	1.108	1.110	1.112	1.114	1.115	1.116	1.117	1.117	1.117		1.116	1.116	1.115	1.114	1.113	1.111	1.110	1.108	1.106	1.105	1.103	1.100	1.098	1.096	1.093
30	1.110	1.112	1.114	1.116	1.117	1.118	1.119	1.119	1.119	1.119		1.118	1.117	1.116	1.115	1.113	1.112	1.110	1.108	1.106	1.104	1.102	1.100	1.097	1.095
35	1.112	1.114	1.116	1.118	1.119	1.120	1.120	1.121	1.121	1.120	1.120		1.118	1.117	1.116	1.115	1.113	1.112	1.110	1.108	1.106	1.104	1.101	1.099	1.097
40	1.114	1.116	1.118	1.120	1.121	1.122	1.122	1.122	1.122	1.122	1.122	1.121		1.119	1.118	1.116	1.115	1.113	1.111	1.109	1.107	1.105	1.103	1.101	1.098
45	1.116	1.118	1.120	1.122	1.123	1.123	1.124	1.124	1.124	1.124	1.123	1.123	1.122		1.119	1.118	1.116	1.115	1.113	1.111	1.109	1.107	1.105	1.102	1.100
50	1.118	1.120	1.122	1.123	1.124	1.125	1.126	1.126	1.126	1.126	1.125	1.124	1.123	1.122		1.120	1.118	1.116	1.115	1.113	1.111	1.108	1.106	1.104	1.101
55	1.120	1.122	1.124	1.125	1.126	1.127	1.127	1.128	1.128	1.127	1.127	1.126	1.125	1.124	1.123		1.120	1.118	1.116	1.114	1.112	1.110	1.108	1.106	1.103
60	1.122	1.124	1.126	1.127	1.128	1.129	1.129	1.129	1.129	1.129	1.128	1.128	1.127	1.126	1.124	1.123		1.120	1.118	1.116	1.114	1.112	1.109	1.107	1.105
65	1.124	1.126	1.127	1.129	1.130	1.130	1.131	1.131	1.131	1.131	1.130	1.129	1.128	1.127	1.126	1.124	1.123		1.119	1.118	1.115	1.113	1.111	1.109	1.106
70	1.125	1.127	1.129	1.130	1.131	1.132	1.132	1.133	1.133	1.132	1.132	1.131	1.130	1.129	1.128	1.126	1.125	1.123		1.119	1.117	1.115	1.113	1.111	1.108
75	1.127	1.129	1.131	1.132	1.133	1.134	1.134	1.134	1.134	1.134	1.133	1.133	1.132	1.130	1.129	1.128	1.126	1.125	1.123		1.119	1.117	1.115	1.112	1.110
80	1.129	1.131	1.133	1.134	1.135	1.136	1.136	1.136	1.136	1.136	1.135	1.134	1.133	1.132	1.131	1.129	1.128	1.126	1.124	1.123		1.118	1.116	1.114	1.112
85	1.131	1.133	1.134	1.136	1.137	1.137	1.138	1.138	1.138	1.137	1.137	1.136	1.135	1.134	1.133	1.131	1.130	1.128	1.126	1.124	1.122		1.118	1.116	1.114
90	1.133	1.135	1.136	1.137	1.138	1.139	1.139	1.139	1.139	1.139	1.138	1.138	1.137	1.136	1.134	1.133	1.131	1.130	1.128	1.126	1.124	1.122		1.118	1.116
95	1.134	1.136	1.138	1.139	1.140	1.141	1.141	1.141	1.141	1.141	1.140	1.139	1.138	1.137	1.136	1.135	1.133	1.132	1.130	1.128	1.126	1.124	1.122		1.118
100	1.136	1.138	1.140	1.141	1.142	1.143	1.143	1.143	1.143	1.143	1.142	1.141	1.140	1.139	1.138	1.137	1.135	1.133	1.132	1.130	1.128	1.126	1.124	1.122	

Appendix 24: Heat coefficient k of Antifrogen N 20 %, measured in feed [kWh/(m³K)]

k Feed	Return temperature																								
Feed temperature	-20	-15	-10	-5	0	5	10	15	20	25	30	35	40	45	50	55	60	65	70	75	80	85	90	95	100
-20		1.088	1.091	1.094	1.096	1.099	1.101	1.104	1.106	1.108	1.110	1.112	1.114	1.116	1.118	1.120	1.122	1.124	1.125	1.127	1.129	1.131	1.133	1.134	1.136
-15	1.088		1.094	1.096	1.099	1.101	1.104	1.106	1.108	1.110	1.112	1.114	1.116	1.118	1.120	1.122	1.124	1.126	1.127	1.129	1.131	1.133	1.135	1.136	1.138
-10	1.090	1.093		1.098	1.101	1.103	1.106	1.108	1.110	1.112	1.114	1.116	1.118	1.120	1.122	1.124	1.126	1.127	1.129	1.131	1.133	1.134	1.136	1.138	1.140
-5	1.092	1.095	1.098		1.103	1.105	1.107	1.110	1.112	1.114	1.116	1.118	1.120	1.122	1.123	1.125	1.127	1.129	1.130	1.132	1.134	1.136	1.137	1.139	1.141
0	1.094	1.097	1.099	1.102		1.107	1.109	1.111	1.113	1.115	1.117	1.119	1.121	1.123	1.124	1.126	1.128	1.130	1.131	1.133	1.135	1.137	1.138	1.140	1.142
5	1.095	1.098	1.101	1.103	1.105		1.110	1.112	1.114	1.116	1.118	1.120	1.122	1.123	1.125	1.127	1.129	1.130	1.132	1.134	1.136	1.137	1.139	1.141	1.143
10	1.096	1.099	1.101	1.104	1.106	1.108		1.113	1.115	1.117	1.119	1.120	1.122	1.124	1.126	1.127	1.129	1.131	1.132	1.134	1.136	1.138	1.139	1.141	1.143
15	1.097	1.100	1.102	1.104	1.107	1.109	1.111		1.115	1.117	1.119	1.121	1.122	1.124	1.126	1.128	1.129	1.131	1.133	1.134	1.136	1.138	1.139	1.141	1.143
20	1.097	1.100	1.102	1.105	1.107	1.109	1.111	1.113		1.117	1.119	1.121	1.122	1.124	1.126	1.128	1.129	1.131	1.133	1.134	1.136	1.138	1.139	1.141	1.143
25	1.098	1.100	1.102	1.105	1.107	1.109	1.111	1.113	1.115		1.119	1.120	1.122	1.124	1.126	1.127	1.129	1.131	1.132	1.134	1.136	1.137	1.139	1.141	1.143
30	1.098	1.100	1.102	1.105	1.107	1.109	1.111	1.113	1.115	1.116		1.120	1.122	1.123	1.125	1.127	1.128	1.130	1.132	1.133	1.135	1.137	1.138	1.140	1.142
35	1.097	1.100	1.102	1.104	1.106	1.108	1.110	1.112	1.114	1.116	1.118		1.121	1.123	1.124	1.126	1.128	1.129	1.131	1.133	1.134	1.136	1.138	1.139	1.141
40	1.097	1.099	1.101	1.103	1.106	1.108	1.110	1.111	1.113	1.115	1.117	1.118		1.122	1.123	1.125	1.127	1.128	1.130	1.132	1.133	1.135	1.137	1.138	1.140
45	1.096	1.098	1.101	1.103	1.105	1.107	1.109	1.110	1.112	1.114	1.116	1.117	1.119		1.122	1.124	1.126	1.127	1.129	1.130	1.132	1.134	1.136	1.137	1.139
50	1.095	1.097	1.099	1.102	1.104	1.106	1.107	1.109	1.111	1.113	1.115	1.116	1.118	1.119		1.123	1.124	1.126	1.128	1.129	1.131	1.133	1.134	1.136	1.138
55	1.094	1.096	1.098	1.100	1.102	1.104	1.106	1.108	1.110	1.111	1.113	1.115	1.116	1.118	1.120		1.123	1.124	1.126	1.128	1.129	1.131	1.133	1.135	1.137
60	1.093	1.095	1.097	1.099	1.101	1.103	1.105	1.106	1.108	1.110	1.112	1.113	1.115	1.116	1.118	1.120		1.123	1.125	1.126	1.128	1.130	1.131	1.133	1.135
65	1.091	1.093	1.095	1.097	1.099	1.101	1.103	1.105	1.107	1.108	1.110	1.112	1.113	1.115	1.116	1.118	1.120		1.123	1.125	1.126	1.128	1.130	1.132	1.133
70	1.090	1.092	1.094	1.096	1.098	1.100	1.101	1.103	1.105	1.106	1.108	1.110	1.111	1.113	1.115	1.116	1.118	1.119		1.123	1.124	1.126	1.128	1.130	1.132
75	1.088	1.090	1.092	1.094	1.096	1.098	1.099	1.101	1.103	1.105	1.106	1.108	1.109	1.111	1.113	1.114	1.116	1.118	1.119		1.123	1.124	1.126	1.128	1.130
80	1.086	1.088	1.090	1.092	1.094	1.096	1.097	1.099	1.101	1.103	1.104	1.106	1.107	1.109	1.111	1.112	1.114	1.115	1.117	1.119		1.122	1.124	1.126	1.128
85	1.084	1.086	1.088	1.090	1.092	1.094	1.095	1.097	1.099	1.100	1.102	1.104	1.105	1.107	1.108	1.110	1.112	1.113	1.115	1.117	1.118		1.122	1.124	1.126
90	1.082	1.084	1.086	1.088	1.090	1.091	1.093	1.095	1.096	1.098	1.100	1.101	1.103	1.105	1.106	1.108	1.109	1.111	1.113	1.115	1.116	1.118		1.122	1.124
95	1.080	1.082	1.084	1.085	1.087	1.089	1.091	1.092	1.094	1.096	1.097	1.099	1.101	1.102	1.104	1.106	1.107	1.109	1.111	1.112	1.114	1.116	1.118		1.122
100	1.077	1.079	1.081	1.083	1.085	1.087	1.088	1.090	1.092	1.093	1.095	1.097	1.098	1.100	1.101	1.103	1.105	1.106	1.108	1.110	1.112	1.114	1.116	1.118	

Appendix 25: Heat coefficient k of Antifrogen N 25 %, measured in return [kWh/(m³K)]

k Return	Return temperature																								
Feed temperature	-20	-15	-10	-5	0	5	10	15	20	25	30	35	40	45	50	55	60	65	70	75	80	85	90	95	100
-20		1.058	1.061	1.064	1.066	1.068	1.069	1.070	1.071	1.072	1.073	1.073	1.073	1.073	1.072	1.072	1.071	1.070	1.069	1.068	1.066	1.065	1.063	1.062	1.060
-15	1.059		1.065	1.067	1.069	1.071	1.072	1.074	1.075	1.075	1.076	1.076	1.076	1.076	1.075	1.075	1.074	1.073	1.072	1.070	1.069	1.068	1.066	1.064	1.062
-10	1.063	1.066		1.071	1.073	1.074	1.076	1.077	1.078	1.078	1.079	1.079	1.079	1.079	1.078	1.077	1.077	1.076	1.074	1.073	1.072	1.070	1.068	1.067	1.065
-5	1.066	1.069	1.072		1.076	1.078	1.079	1.080	1.081	1.081	1.082	1.082	1.082	1.081	1.081	1.080	1.079	1.078	1.077	1.076	1.074	1.073	1.071	1.069	1.067
0	1.070	1.072	1.075	1.077		1.081	1.082	1.083	1.084	1.084	1.084	1.085	1.084	1.084	1.083	1.083	1.082	1.081	1.080	1.078	1.077	1.075	1.073	1.072	1.070
5	1.073	1.076	1.078	1.080	1.082		1.085	1.086	1.087	1.087	1.087	1.087	1.087	1.087	1.086	1.085	1.084	1.083	1.082	1.081	1.079	1.077	1.076	1.074	1.072
10	1.076	1.079	1.081	1.083	1.085	1.087		1.089	1.089	1.090	1.090	1.090	1.090	1.089	1.088	1.088	1.087	1.086	1.084	1.083	1.081	1.080	1.078	1.076	1.074
15	1.079	1.082	1.084	1.086	1.088	1.089	1.090		1.092	1.092	1.092	1.092	1.092	1.092	1.091	1.090	1.089	1.088	1.087	1.085	1.084	1.082	1.080	1.078	1.076
20	1.082	1.085	1.087	1.089	1.091	1.092	1.093	1.094		1.095	1.095	1.095	1.094	1.094	1.093	1.092	1.091	1.090	1.089	1.087	1.086	1.084	1.082	1.081	1.079
25	1.085	1.088	1.090	1.092	1.093	1.095	1.096	1.096	1.097		1.097	1.097	1.097	1.096	1.096	1.095	1.094	1.092	1.091	1.090	1.088	1.086	1.085	1.083	1.081
30	1.088	1.090	1.092	1.094	1.096	1.097	1.098	1.099	1.099	1.100		1.100	1.099	1.099	1.098	1.097	1.096	1.095	1.093	1.092	1.090	1.088	1.087	1.085	1.083
35	1.090	1.093	1.095	1.097	1.098	1.100	1.101	1.101	1.102	1.102	1.102		1.101	1.101	1.100	1.099	1.098	1.097	1.095	1.094	1.092	1.091	1.089	1.087	1.085
40	1.093	1.096	1.098	1.099	1.101	1.102	1.103	1.104	1.104	1.104	1.104	1.104		1.103	1.102	1.101	1.100	1.099	1.097	1.096	1.094	1.093	1.091	1.089	1.087
45	1.096	1.098	1.100	1.102	1.103	1.105	1.105	1.106	1.106	1.107	1.107	1.106	1.106		1.104	1.103	1.102	1.101	1.100	1.098	1.096	1.095	1.093	1.091	1.089
50	1.098	1.101	1.103	1.104	1.106	1.107	1.108	1.108	1.109	1.109	1.109	1.108	1.108	1.107		1.105	1.104	1.103	1.102	1.100	1.099	1.097	1.095	1.093	1.091
55	1.101	1.103	1.105	1.107	1.108	1.109	1.110	1.111	1.111	1.111	1.111	1.111	1.110	1.109	1.109		1.106	1.105	1.104	1.102	1.101	1.099	1.097	1.095	1.093
60	1.103	1.105	1.107	1.109	1.110	1.111	1.112	1.113	1.113	1.113	1.113	1.113	1.112	1.111	1.111	1.110		1.107	1.106	1.104	1.103	1.101	1.099	1.097	1.095
65	1.106	1.108	1.110	1.111	1.113	1.114	1.114	1.115	1.115	1.115	1.115	1.115	1.114	1.114	1.113	1.112	1.111		1.108	1.106	1.105	1.103	1.101	1.099	1.097
70	1.108	1.110	1.112	1.114	1.115	1.116	1.117	1.117	1.117	1.117	1.117	1.117	1.116	1.116	1.115	1.114	1.113	1.111		1.108	1.107	1.105	1.103	1.101	1.100
75	1.110	1.112	1.114	1.116	1.117	1.118	1.119	1.119	1.120	1.120	1.119	1.119	1.118	1.118	1.117	1.116	1.115	1.113	1.112		1.109	1.107	1.105	1.104	1.102
80	1.113	1.115	1.117	1.118	1.119	1.120	1.121	1.121	1.122	1.122	1.122	1.121	1.121	1.120	1.119	1.118	1.117	1.116	1.114	1.113		1.109	1.108	1.106	1.104
85	1.115	1.117	1.119	1.120	1.122	1.123	1.123	1.124	1.124	1.124	1.124	1.123	1.123	1.122	1.121	1.120	1.119	1.118	1.116	1.115	1.113		1.110	1.108	1.106
90	1.117	1.119	1.121	1.123	1.124	1.125	1.125	1.126	1.126	1.126	1.126	1.126	1.125	1.124	1.123	1.122	1.121	1.120	1.119	1.117	1.116	1.114		1.110	1.109
95	1.120	1.122	1.123	1.125	1.126	1.127	1.128	1.128	1.128	1.128	1.128	1.128	1.127	1.126	1.126	1.125	1.123	1.122	1.121	1.119	1.118	1.116	1.115		1.111
100	1.122	1.124	1.126	1.127	1.128	1.129	1.130	1.130	1.131	1.131	1.130	1.130	1.129	1.129	1.128	1.127	1.126	1.125	1.123	1.122	1.120	1.119	1.117	1.115	

Appendix 26: Heat coefficient k of Antifrogen N 25 %, measured in feed [kWh/(m³K)]

k Feed	Return temperature																								
Feed temperature	-20	-15	-10	-5	0	5	10	15	20	25	30	35	40	45	50	55	60	65	70	75	80	85	90	95	100
-20		1.059	1.063	1.066	1.070	1.073	1.076	1.079	1.082	1.085	1.088	1.090	1.093	1.096	1.098	1.101	1.103	1.106	1.108	1.110	1.113	1.115	1.117	1.120	1.122
-15	1.058		1.066	1.069	1.072	1.076	1.079	1.082	1.085	1.088	1.090	1.093	1.096	1.098	1.101	1.103	1.105	1.108	1.110	1.112	1.115	1.117	1.119	1.122	1.124
-10	1.061	1.065		1.072	1.075	1.078	1.081	1.084	1.087	1.090	1.092	1.095	1.098	1.100	1.103	1.105	1.107	1.110	1.112	1.114	1.117	1.119	1.121	1.123	1.126
-5	1.064	1.067	1.071		1.077	1.080	1.083	1.086	1.089	1.092	1.094	1.097	1.099	1.102	1.104	1.107	1.109	1.111	1.114	1.116	1.118	1.120	1.123	1.125	1.127
0	1.066	1.069	1.073	1.076		1.082	1.085	1.088	1.091	1.093	1.096	1.098	1.101	1.103	1.106	1.108	1.110	1.113	1.115	1.117	1.119	1.122	1.124	1.126	1.128
5	1.068	1.071	1.074	1.078	1.081		1.087	1.089	1.092	1.095	1.097	1.100	1.102	1.105	1.107	1.109	1.111	1.114	1.116	1.118	1.120	1.123	1.125	1.127	1.129
10	1.069	1.072	1.076	1.079	1.082	1.085		1.090	1.093	1.096	1.098	1.101	1.103	1.105	1.108	1.110	1.112	1.114	1.117	1.119	1.121	1.123	1.125	1.128	1.130
15	1.070	1.074	1.077	1.080	1.083	1.086	1.089		1.094	1.096	1.099	1.101	1.104	1.106	1.108	1.111	1.113	1.115	1.117	1.119	1.121	1.124	1.126	1.128	1.130
20	1.071	1.075	1.078	1.081	1.084	1.087	1.089	1.092		1.097	1.099	1.102	1.104	1.106	1.109	1.111	1.113	1.115	1.117	1.120	1.122	1.124	1.126	1.128	1.131
25	1.072	1.075	1.078	1.081	1.084	1.087	1.090	1.092	1.095		1.100	1.102	1.104	1.107	1.109	1.111	1.113	1.115	1.117	1.120	1.122	1.124	1.126	1.128	1.131
30	1.073	1.076	1.079	1.082	1.084	1.087	1.090	1.092	1.095	1.097		1.102	1.104	1.107	1.109	1.111	1.113	1.115	1.117	1.119	1.122	1.124	1.126	1.128	1.130
35	1.073	1.076	1.079	1.082	1.085	1.087	1.090	1.092	1.095	1.097	1.100		1.104	1.106	1.108	1.111	1.113	1.115	1.117	1.119	1.121	1.123	1.126	1.128	1.130
40	1.073	1.076	1.079	1.082	1.084	1.087	1.090	1.092	1.094	1.097	1.099	1.101		1.106	1.108	1.110	1.112	1.114	1.116	1.118	1.121	1.123	1.125	1.127	1.129
45	1.073	1.076	1.079	1.081	1.084	1.087	1.089	1.092	1.094	1.096	1.099	1.101	1.103		1.107	1.109	1.111	1.114	1.116	1.118	1.120	1.122	1.124	1.126	1.129
50	1.072	1.075	1.078	1.081	1.083	1.086	1.088	1.091	1.093	1.096	1.098	1.100	1.102	1.104		1.109	1.111	1.113	1.115	1.117	1.119	1.121	1.123	1.126	1.128
55	1.072	1.075	1.077	1.080	1.083	1.085	1.088	1.090	1.092	1.095	1.097	1.099	1.101	1.103	1.105		1.110	1.112	1.114	1.116	1.118	1.120	1.122	1.125	1.127
60	1.071	1.074	1.077	1.079	1.082	1.084	1.087	1.089	1.091	1.094	1.096	1.098	1.100	1.102	1.104	1.106		1.111	1.113	1.115	1.117	1.119	1.121	1.123	1.126
65	1.070	1.073	1.076	1.078	1.081	1.083	1.086	1.088	1.090	1.092	1.095	1.097	1.099	1.101	1.103	1.105	1.107		1.111	1.113	1.116	1.118	1.120	1.122	1.125
70	1.069	1.072	1.074	1.077	1.080	1.082	1.084	1.087	1.089	1.091	1.093	1.095	1.097	1.100	1.102	1.104	1.106	1.108		1.112	1.114	1.116	1.119	1.121	1.123
75	1.068	1.070	1.073	1.076	1.078	1.081	1.083	1.085	1.087	1.090	1.092	1.094	1.096	1.098	1.100	1.102	1.104	1.106	1.108		1.113	1.115	1.117	1.119	1.122
80	1.066	1.069	1.072	1.074	1.077	1.079	1.081	1.084	1.086	1.088	1.090	1.092	1.094	1.096	1.099	1.101	1.103	1.105	1.107	1.109		1.113	1.116	1.118	1.120
85	1.065	1.068	1.070	1.073	1.075	1.077	1.080	1.082	1.084	1.086	1.088	1.091	1.093	1.095	1.097	1.099	1.101	1.103	1.105	1.107	1.109		1.114	1.116	1.119
90	1.063	1.066	1.068	1.071	1.073	1.076	1.078	1.080	1.082	1.085	1.087	1.089	1.091	1.093	1.095	1.097	1.099	1.101	1.103	1.105	1.108	1.110		1.115	1.117
95	1.062	1.064	1.067	1.069	1.072	1.074	1.076	1.078	1.081	1.083	1.085	1.087	1.089	1.091	1.093	1.095	1.097	1.099	1.101	1.104	1.106	1.108	1.110		1.115
100	1.060	1.062	1.065	1.067	1.070	1.072	1.074	1.076	1.079	1.081	1.083	1.085	1.087	1.089	1.091	1.093	1.095	1.097	1.100	1.102	1.104	1.106	1.109	1.111	

Appendix 27: Heat coefficient k of Antifrogen N 30 %, measured in return [kWh/(m³K)]

k Return	Return temperature																								
Feed temperature	-20	-15	-10	-5	0	5	10	15	20	25	30	35	40	45	50	55	60	65	70	75	80	85	90	95	100
-20		1.022	1.026	1.029	1.032	1.035	1.037	1.039	1.041	1.043	1.044	1.044	1.045	1.045	1.045	1.045	1.045	1.044	1.043	1.043	1.042	1.041	1.039	1.038	1.037
-15	1.023		1.031	1.034	1.037	1.040	1.042	1.044	1.046	1.047	1.048	1.049	1.049	1.049	1.049	1.049	1.048	1.048	1.047	1.046	1.045	1.044	1.043	1.041	1.040
-10	1.028	1.032		1.039	1.042	1.044	1.047	1.048	1.050	1.051	1.052	1.052	1.053	1.053	1.053	1.052	1.052	1.051	1.050	1.049	1.048	1.047	1.046	1.044	1.043
-5	1.033	1.037	1.040		1.046	1.049	1.051	1.052	1.054	1.055	1.056	1.056	1.056	1.056	1.056	1.056	1.055	1.054	1.054	1.053	1.051	1.050	1.049	1.047	1.046
0	1.038	1.041	1.045	1.048		1.053	1.055	1.056	1.058	1.059	1.059	1.060	1.060	1.060	1.059	1.059	1.058	1.058	1.057	1.055	1.054	1.053	1.052	1.050	1.049
5	1.042	1.046	1.049	1.052	1.055		1.059	1.060	1.061	1.062	1.063	1.063	1.063	1.063	1.063	1.062	1.061	1.060	1.059	1.058	1.057	1.056	1.054	1.053	1.052
10	1.046	1.050	1.053	1.056	1.058	1.060		1.063	1.065	1.065	1.066	1.066	1.066	1.066	1.065	1.065	1.064	1.063	1.062	1.061	1.060	1.058	1.057	1.056	1.054
15	1.050	1.054	1.057	1.060	1.062	1.064	1.065		1.068	1.068	1.069	1.069	1.069	1.069	1.068	1.068	1.067	1.066	1.065	1.064	1.062	1.061	1.060	1.058	1.057
20	1.054	1.058	1.061	1.063	1.065	1.067	1.069	1.070		1.071	1.072	1.072	1.072	1.072	1.071	1.070	1.069	1.068	1.067	1.066	1.065	1.064	1.062	1.061	1.059
25	1.058	1.061	1.064	1.066	1.069	1.070	1.072	1.073	1.074		1.075	1.075	1.075	1.074	1.074	1.073	1.072	1.071	1.070	1.069	1.067	1.066	1.064	1.063	1.062
30	1.061	1.065	1.067	1.070	1.072	1.073	1.075	1.076	1.077	1.077		1.077	1.077	1.077	1.076	1.075	1.074	1.073	1.072	1.071	1.070	1.068	1.067	1.065	1.064
35	1.065	1.068	1.070	1.073	1.075	1.076	1.078	1.079	1.079	1.080	1.080		1.080	1.079	1.079	1.078	1.077	1.076	1.075	1.073	1.072	1.071	1.069	1.068	1.066
40	1.068	1.071	1.074	1.076	1.078	1.079	1.080	1.081	1.082	1.082	1.082	1.082		1.082	1.081	1.080	1.079	1.078	1.077	1.076	1.074	1.073	1.071	1.070	1.069
45	1.071	1.074	1.076	1.079	1.080	1.082	1.083	1.084	1.084	1.085	1.085	1.085	1.084		1.083	1.082	1.081	1.080	1.079	1.078	1.077	1.075	1.074	1.072	1.071
50	1.074	1.077	1.079	1.081	1.083	1.084	1.086	1.086	1.087	1.087	1.087	1.087	1.087	1.086		1.085	1.084	1.083	1.081	1.080	1.079	1.077	1.076	1.075	1.073
55	1.077	1.080	1.082	1.084	1.086	1.087	1.088	1.089	1.089	1.090	1.090	1.089	1.089	1.088	1.088		1.086	1.085	1.084	1.082	1.081	1.080	1.078	1.077	1.076
60	1.080	1.082	1.085	1.087	1.088	1.090	1.091	1.091	1.092	1.092	1.092	1.092	1.091	1.091	1.090	1.089		1.087	1.086	1.085	1.083	1.082	1.081	1.079	1.078
65	1.083	1.085	1.087	1.089	1.091	1.092	1.093	1.094	1.094	1.094	1.094	1.094	1.094	1.093	1.092	1.091	1.090		1.088	1.087	1.086	1.084	1.083	1.082	1.081
70	1.085	1.088	1.090	1.092	1.093	1.095	1.095	1.096	1.096	1.097	1.097	1.096	1.096	1.095	1.095	1.094	1.093	1.092		1.089	1.088	1.087	1.086	1.084	1.083
75	1.088	1.090	1.093	1.094	1.096	1.097	1.098	1.099	1.099	1.099	1.099	1.099	1.098	1.098	1.097	1.096	1.095	1.094	1.093		1.091	1.089	1.088	1.087	1.086
80	1.091	1.093	1.095	1.097	1.098	1.100	1.100	1.101	1.101	1.101	1.101	1.101	1.101	1.100	1.099	1.099	1.098	1.097	1.095	1.094		1.092	1.091	1.090	1.089
85	1.093	1.096	1.098	1.100	1.101	1.102	1.103	1.103	1.104	1.104	1.104	1.104	1.103	1.103	1.102	1.101	1.100	1.099	1.098	1.097	1.096		1.094	1.092	1.091
90	1.096	1.098	1.100	1.102	1.104	1.105	1.105	1.106	1.106	1.106	1.106	1.106	1.106	1.105	1.104	1.104	1.103	1.102	1.101	1.100	1.099	1.098		1.095	1.094
95	1.099	1.101	1.103	1.105	1.106	1.107	1.108	1.109	1.109	1.109	1.109	1.109	1.108	1.108	1.107	1.106	1.105	1.105	1.104	1.103	1.102	1.101	1.100		1.098
100	1.102	1.104	1.106	1.108	1.109	1.110	1.111	1.111	1.112	1.112	1.112	1.111	1.111	1.111	1.110	1.109	1.108	1.107	1.107	1.106	1.105	1.104	1.103	1.102	

Appendix 28: Heat coefficient k of Antifrogen N 30 %, measured in feed [kWh/(m³K)]

k Feed	Return temperature																								
Feed temperature	-20	-15	-10	-5	0	5	10	15	20	25	30	35	40	45	50	55	60	65	70	75	80	85	90	95	100
-20		1.023	1.028	1.033	1.038	1.042	1.046	1.050	1.054	1.058	1.061	1.065	1.068	1.071	1.074	1.077	1.080	1.083	1.085	1.088	1.091	1.093	1.096	1.099	1.102
-15	1.022		1.032	1.037	1.041	1.046	1.050	1.054	1.058	1.061	1.065	1.068	1.071	1.074	1.077	1.080	1.082	1.085	1.088	1.090	1.093	1.096	1.098	1.101	1.104
-10	1.026	1.031		1.040	1.045	1.049	1.053	1.057	1.061	1.064	1.067	1.070	1.074	1.076	1.079	1.082	1.085	1.087	1.090	1.093	1.095	1.098	1.100	1.103	1.106
-5	1.029	1.034	1.039		1.048	1.052	1.056	1.060	1.063	1.066	1.070	1.073	1.076	1.079	1.081	1.084	1.087	1.089	1.092	1.094	1.097	1.100	1.102	1.105	1.108
0	1.032	1.037	1.042	1.046		1.055	1.058	1.062	1.065	1.069	1.072	1.075	1.078	1.080	1.083	1.086	1.088	1.091	1.093	1.096	1.098	1.101	1.104	1.106	1.109
5	1.035	1.040	1.044	1.049	1.053		1.060	1.064	1.067	1.070	1.073	1.076	1.079	1.082	1.084	1.087	1.090	1.092	1.095	1.097	1.100	1.102	1.105	1.107	1.110
10	1.037	1.042	1.047	1.051	1.055	1.059		1.065	1.069	1.072	1.075	1.078	1.080	1.083	1.086	1.088	1.091	1.093	1.095	1.098	1.100	1.103	1.105	1.108	1.111
15	1.039	1.044	1.048	1.052	1.056	1.060	1.063		1.070	1.073	1.076	1.079	1.081	1.084	1.086	1.089	1.091	1.094	1.096	1.099	1.101	1.103	1.106	1.109	1.111
20	1.041	1.046	1.050	1.054	1.058	1.061	1.065	1.068		1.074	1.077	1.079	1.082	1.084	1.087	1.089	1.092	1.094	1.096	1.099	1.101	1.104	1.106	1.109	1.112
25	1.043	1.047	1.051	1.055	1.059	1.062	1.065	1.068	1.071		1.077	1.080	1.082	1.085	1.087	1.090	1.092	1.094	1.097	1.099	1.101	1.104	1.106	1.109	1.112
30	1.044	1.048	1.052	1.056	1.059	1.063	1.066	1.069	1.072	1.075		1.080	1.082	1.085	1.087	1.090	1.092	1.094	1.097	1.099	1.101	1.104	1.106	1.109	1.112
35	1.044	1.049	1.052	1.056	1.060	1.063	1.066	1.069	1.072	1.075	1.077		1.082	1.085	1.087	1.089	1.092	1.094	1.096	1.099	1.101	1.104	1.106	1.109	1.111
40	1.045	1.049	1.053	1.056	1.060	1.063	1.066	1.069	1.072	1.075	1.077	1.080		1.084	1.087	1.089	1.091	1.094	1.096	1.098	1.101	1.103	1.106	1.108	1.111
45	1.045	1.049	1.053	1.056	1.060	1.063	1.066	1.069	1.072	1.074	1.077	1.079	1.082		1.086	1.088	1.091	1.093	1.095	1.098	1.100	1.103	1.105	1.108	1.111
50	1.045	1.049	1.053	1.056	1.059	1.063	1.065	1.068	1.071	1.074	1.076	1.079	1.081	1.083		1.088	1.090	1.092	1.095	1.097	1.099	1.102	1.104	1.107	1.110
55	1.045	1.049	1.052	1.056	1.059	1.062	1.065	1.068	1.070	1.073	1.075	1.078	1.080	1.082	1.085		1.089	1.091	1.094	1.096	1.099	1.101	1.104	1.106	1.109
60	1.045	1.048	1.052	1.055	1.058	1.061	1.064	1.067	1.069	1.072	1.074	1.077	1.079	1.081	1.084	1.086		1.090	1.093	1.095	1.098	1.100	1.103	1.105	1.108
65	1.044	1.048	1.051	1.054	1.058	1.060	1.063	1.066	1.068	1.071	1.073	1.076	1.078	1.080	1.083	1.085	1.087		1.092	1.094	1.097	1.099	1.102	1.105	1.107
70	1.043	1.047	1.050	1.054	1.057	1.059	1.062	1.065	1.067	1.070	1.072	1.075	1.077	1.079	1.081	1.084	1.086	1.088		1.093	1.095	1.098	1.101	1.104	1.107
75	1.043	1.046	1.049	1.053	1.055	1.058	1.061	1.064	1.066	1.069	1.071	1.073	1.076	1.078	1.080	1.082	1.085	1.087	1.089		1.094	1.097	1.100	1.103	1.106
80	1.042	1.045	1.048	1.051	1.054	1.057	1.060	1.062	1.065	1.067	1.070	1.072	1.074	1.077	1.079	1.081	1.083	1.086	1.088	1.091		1.096	1.099	1.102	1.105
85	1.041	1.044	1.047	1.050	1.053	1.056	1.058	1.061	1.064	1.066	1.068	1.071	1.073	1.075	1.077	1.080	1.082	1.084	1.087	1.089	1.092		1.098	1.101	1.104
90	1.039	1.043	1.046	1.049	1.052	1.054	1.057	1.060	1.062	1.064	1.067	1.069	1.071	1.074	1.076	1.078	1.081	1.083	1.086	1.088	1.091	1.094		1.100	1.103
95	1.038	1.041	1.044	1.047	1.050	1.053	1.056	1.058	1.061	1.063	1.065	1.068	1.070	1.072	1.075	1.077	1.079	1.082	1.084	1.087	1.090	1.092	1.095		1.102
100	1.037	1.040	1.043	1.046	1.049	1.052	1.054	1.057	1.059	1.062	1.064	1.066	1.069	1.071	1.073	1.076	1.078	1.081	1.083	1.086	1.089	1.091	1.094	1.098	

Appendix 29: Heat coefficient k of Antifrogen N 35 %, measured in return [kWh/(m³K)]

k Return	Return temperature																								
Feed temperature	-20	-15	-10	-5	0	5	10	15	20	25	30	35	40	45	50	55	60	65	70	75	80	85	90	95	100
-20		0.995	1.000	1.003	1.007	1.010	1.012	1.015	1.017	1.018	1.020	1.021	1.022	1.022	1.023	1.023	1.023	1.023	1.022	1.022	1.021	1.020	1.019	1.018	1.016
-15	0.997		1.005	1.009	1.012	1.015	1.017	1.020	1.021	1.023	1.024	1.025	1.026	1.027	1.027	1.027	1.027	1.027	1.026	1.025	1.025	1.024	1.022	1.021	1.020
-10	1.003	1.007		1.014	1.017	1.020	1.022	1.024	1.026	1.028	1.029	1.030	1.030	1.031	1.031	1.031	1.031	1.030	1.030	1.029	1.028	1.027	1.026	1.025	1.023
-5	1.008	1.012	1.016		1.022	1.025	1.027	1.029	1.031	1.032	1.033	1.034	1.035	1.035	1.035	1.035	1.035	1.034	1.033	1.033	1.032	1.030	1.029	1.028	1.026
0	1.013	1.017	1.021	1.024		1.029	1.031	1.033	1.035	1.036	1.037	1.038	1.038	1.039	1.039	1.039	1.038	1.038	1.037	1.036	1.035	1.034	1.032	1.031	1.029
5	1.018	1.022	1.025	1.028	1.031		1.036	1.037	1.039	1.040	1.041	1.042	1.042	1.042	1.042	1.042	1.042	1.041	1.040	1.039	1.038	1.037	1.035	1.034	1.032
10	1.023	1.026	1.030	1.033	1.035	1.038		1.041	1.043	1.044	1.045	1.045	1.046	1.046	1.046	1.045	1.045	1.044	1.043	1.042	1.041	1.040	1.038	1.037	1.035
15	1.027	1.031	1.034	1.037	1.039	1.042	1.043		1.046	1.047	1.048	1.049	1.049	1.049	1.049	1.048	1.048	1.047	1.046	1.045	1.044	1.043	1.041	1.040	1.038
20	1.031	1.035	1.038	1.041	1.043	1.045	1.047	1.049		1.051	1.052	1.052	1.052	1.052	1.052	1.051	1.051	1.050	1.049	1.048	1.047	1.045	1.044	1.042	1.041
25	1.036	1.039	1.042	1.045	1.047	1.049	1.051	1.052	1.053		1.055	1.055	1.055	1.055	1.055	1.054	1.054	1.053	1.052	1.051	1.049	1.048	1.046	1.045	1.043
30	1.040	1.043	1.046	1.048	1.051	1.052	1.054	1.055	1.057	1.057		1.058	1.058	1.058	1.058	1.057	1.056	1.056	1.054	1.053	1.052	1.050	1.049	1.047	1.046
35	1.043	1.047	1.049	1.052	1.054	1.056	1.057	1.059	1.060	1.060	1.061		1.061	1.061	1.060	1.060	1.059	1.058	1.057	1.056	1.054	1.053	1.051	1.050	1.048
40	1.047	1.050	1.053	1.055	1.057	1.059	1.061	1.062	1.063	1.063	1.064	1.064		1.064	1.063	1.062	1.062	1.061	1.060	1.058	1.057	1.055	1.054	1.052	1.050
45	1.051	1.054	1.056	1.058	1.060	1.062	1.064	1.065	1.066	1.066	1.066	1.067	1.066		1.066	1.065	1.064	1.063	1.062	1.061	1.059	1.058	1.056	1.054	1.053
50	1.054	1.057	1.059	1.062	1.064	1.065	1.066	1.068	1.068	1.069	1.069	1.069	1.069	1.069		1.067	1.067	1.065	1.064	1.063	1.062	1.060	1.058	1.057	1.055
55	1.057	1.060	1.063	1.065	1.067	1.068	1.069	1.070	1.071	1.071	1.072	1.072	1.072	1.071	1.071		1.069	1.068	1.067	1.065	1.064	1.062	1.061	1.059	1.057
60	1.060	1.063	1.066	1.068	1.069	1.071	1.072	1.073	1.074	1.074	1.074	1.074	1.074	1.074	1.073	1.072		1.070	1.069	1.068	1.066	1.065	1.063	1.061	1.059
65	1.064	1.066	1.068	1.070	1.072	1.074	1.075	1.076	1.076	1.077	1.077	1.077	1.076	1.076	1.075	1.074	1.074		1.071	1.070	1.068	1.067	1.065	1.063	1.062
70	1.067	1.069	1.071	1.073	1.075	1.076	1.077	1.078	1.079	1.079	1.079	1.079	1.079	1.078	1.078	1.077	1.076	1.075		1.072	1.071	1.069	1.067	1.066	1.064
75	1.069	1.072	1.074	1.076	1.078	1.079	1.080	1.081	1.081	1.082	1.082	1.081	1.081	1.081	1.080	1.079	1.078	1.077	1.076		1.073	1.071	1.070	1.068	1.066
80	1.072	1.075	1.077	1.079	1.080	1.081	1.082	1.083	1.084	1.084	1.084	1.084	1.083	1.083	1.082	1.081	1.080	1.079	1.078	1.077		1.073	1.072	1.070	1.068
85	1.075	1.078	1.080	1.081	1.083	1.084	1.085	1.086	1.086	1.086	1.086	1.086	1.086	1.085	1.084	1.084	1.083	1.081	1.080	1.079	1.077		1.074	1.072	1.071
90	1.078	1.080	1.082	1.084	1.085	1.087	1.087	1.088	1.089	1.089	1.089	1.089	1.088	1.088	1.087	1.086	1.085	1.084	1.082	1.081	1.080	1.078		1.075	1.073
95	1.081	1.083	1.085	1.087	1.088	1.089	1.090	1.091	1.091	1.091	1.091	1.091	1.090	1.090	1.089	1.088	1.087	1.086	1.085	1.083	1.082	1.080	1.079		1.075
100	1.083	1.086	1.088	1.089	1.091	1.092	1.092	1.093	1.093	1.094	1.094	1.093	1.093	1.092	1.092	1.091	1.090	1.088	1.087	1.086	1.084	1.083	1.081	1.080	

Appendix 30: Heat coefficient k of Antifrogen N 35 %, measured in feed [kWh/(m³K)]

k Feed	Return temperature																								
Feed temperature	-20	-15	-10	-5	0	5	10	15	20	25	30	35	40	45	50	55	60	65	70	75	80	85	90	95	100
-20		0.997	1.003	1.008	1.013	1.018	1.023	1.027	1.031	1.036	1.040	1.043	1.047	1.051	1.054	1.057	1.060	1.064	1.067	1.069	1.072	1.075	1.078	1.081	1.083
-15	0.995		1.007	1.012	1.017	1.022	1.026	1.031	1.035	1.039	1.043	1.047	1.050	1.054	1.057	1.060	1.063	1.066	1.069	1.072	1.075	1.078	1.080	1.083	1.086
-10	1.000	1.005		1.016	1.021	1.025	1.030	1.034	1.038	1.042	1.046	1.049	1.053	1.056	1.059	1.063	1.066	1.068	1.071	1.074	1.077	1.080	1.082	1.085	1.088
-5	1.003	1.009	1.014		1.024	1.028	1.033	1.037	1.041	1.045	1.048	1.052	1.055	1.058	1.062	1.065	1.068	1.070	1.073	1.076	1.079	1.081	1.084	1.087	1.089
0	1.007	1.012	1.017	1.022		1.031	1.035	1.039	1.043	1.047	1.051	1.054	1.057	1.060	1.064	1.067	1.069	1.072	1.075	1.078	1.080	1.083	1.085	1.088	1.091
5	1.010	1.015	1.020	1.025	1.029		1.038	1.042	1.045	1.049	1.052	1.056	1.059	1.062	1.065	1.068	1.071	1.074	1.076	1.079	1.081	1.084	1.087	1.089	1.092
10	1.012	1.017	1.022	1.027	1.031	1.036		1.043	1.047	1.051	1.054	1.057	1.061	1.064	1.066	1.069	1.072	1.075	1.077	1.080	1.082	1.085	1.087	1.090	1.092
15	1.015	1.020	1.024	1.029	1.033	1.037	1.041		1.049	1.052	1.055	1.059	1.062	1.065	1.068	1.070	1.073	1.076	1.078	1.081	1.083	1.086	1.088	1.091	1.093
20	1.017	1.021	1.026	1.031	1.035	1.039	1.043	1.046		1.053	1.057	1.060	1.063	1.066	1.068	1.071	1.074	1.076	1.079	1.081	1.084	1.086	1.089	1.091	1.093
25	1.018	1.023	1.028	1.032	1.036	1.040	1.044	1.047	1.051		1.057	1.060	1.063	1.066	1.069	1.071	1.074	1.077	1.079	1.082	1.084	1.086	1.089	1.091	1.094
30	1.020	1.024	1.029	1.033	1.037	1.041	1.045	1.048	1.052	1.055		1.061	1.064	1.066	1.069	1.072	1.074	1.077	1.079	1.082	1.084	1.086	1.089	1.091	1.094
35	1.021	1.025	1.030	1.034	1.038	1.042	1.045	1.049	1.052	1.055	1.058		1.064	1.067	1.069	1.072	1.074	1.077	1.079	1.081	1.084	1.086	1.089	1.091	1.093
40	1.022	1.026	1.030	1.035	1.038	1.042	1.046	1.049	1.052	1.055	1.058	1.061		1.066	1.069	1.072	1.074	1.076	1.079	1.081	1.083	1.086	1.088	1.090	1.093
45	1.022	1.027	1.031	1.035	1.039	1.042	1.046	1.049	1.052	1.055	1.058	1.061	1.064		1.069	1.071	1.074	1.076	1.078	1.081	1.083	1.085	1.088	1.090	1.092
50	1.023	1.027	1.031	1.035	1.039	1.042	1.046	1.049	1.052	1.055	1.058	1.060	1.063	1.066		1.071	1.073	1.075	1.078	1.080	1.082	1.084	1.087	1.089	1.092
55	1.023	1.027	1.031	1.035	1.039	1.042	1.045	1.048	1.051	1.054	1.057	1.060	1.062	1.065	1.067		1.072	1.074	1.077	1.079	1.081	1.084	1.086	1.088	1.091
60	1.023	1.027	1.031	1.035	1.038	1.042	1.045	1.048	1.051	1.054	1.056	1.059	1.062	1.064	1.067	1.069		1.074	1.076	1.078	1.080	1.083	1.085	1.087	1.090
65	1.023	1.027	1.030	1.034	1.038	1.041	1.044	1.047	1.050	1.053	1.056	1.058	1.061	1.063	1.065	1.068	1.070		1.075	1.077	1.079	1.081	1.084	1.086	1.088
70	1.022	1.026	1.030	1.033	1.037	1.040	1.043	1.046	1.049	1.052	1.054	1.057	1.060	1.062	1.064	1.067	1.069	1.071		1.076	1.078	1.080	1.082	1.085	1.087
75	1.022	1.025	1.029	1.033	1.036	1.039	1.042	1.045	1.048	1.051	1.053	1.056	1.058	1.061	1.063	1.065	1.068	1.070	1.072		1.077	1.079	1.081	1.083	1.086
80	1.021	1.025	1.028	1.032	1.035	1.038	1.041	1.044	1.047	1.049	1.052	1.054	1.057	1.059	1.062	1.064	1.066	1.068	1.071	1.073		1.077	1.080	1.082	1.084
85	1.020	1.024	1.027	1.030	1.034	1.037	1.040	1.043	1.045	1.048	1.050	1.053	1.055	1.058	1.060	1.062	1.065	1.067	1.069	1.071	1.073		1.078	1.080	1.083
90	1.019	1.022	1.026	1.029	1.032	1.035	1.038	1.041	1.044	1.046	1.049	1.051	1.054	1.056	1.058	1.061	1.063	1.065	1.067	1.070	1.072	1.074		1.079	1.081
95	1.018	1.021	1.025	1.028	1.031	1.034	1.037	1.040	1.042	1.045	1.047	1.050	1.052	1.054	1.057	1.059	1.061	1.063	1.066	1.068	1.070	1.072	1.075		1.080
100	1.016	1.020	1.023	1.026	1.029	1.032	1.035	1.038	1.041	1.043	1.046	1.048	1.050	1.053	1.055	1.057	1.059	1.062	1.064	1.066	1.068	1.071	1.073	1.075	

Appendix 31: Heat coefficient k of Antifrogen N 40 %, measured in return [kWh/(m³K)]

k Return	Return temperature																								
Feed temperature	-20	-15	-10	-5	0	5	10	15	20	25	30	35	40	45	50	55	60	65	70	75	80	85	90	95	100
-20		0.966	0.971	0.975	0.978	0.981	0.984	0.987	0.989	0.991	0.993	0.995	0.996	0.997	0.998	0.998	0.999	0.999	0.999	0.999	0.999	0.998	0.997	0.997	0.996
-15	0.968		0.977	0.980	0.984	0.987	0.990	0.992	0.995	0.997	0.998	1.000	1.001	1.002	1.002	1.003	1.003	1.003	1.003	1.003	1.003	1.002	1.002	1.001	1.000
-10	0.974	0.979		0.986	0.989	0.992	0.995	0.998	1.000	1.002	1.003	1.004	1.005	1.006	1.007	1.007	1.008	1.008	1.008	1.007	1.007	1.006	1.005	1.005	1.004
-5	0.980	0.984	0.988		0.995	0.998	1.000	1.003	1.005	1.006	1.008	1.009	1.010	1.011	1.011	1.012	1.012	1.012	1.012	1.011	1.011	1.010	1.009	1.008	1.007
0	0.986	0.990	0.993	0.997		1.003	1.005	1.007	1.009	1.011	1.012	1.013	1.014	1.015	1.015	1.016	1.016	1.016	1.015	1.015	1.014	1.014	1.013	1.012	1.011
5	0.991	0.995	0.998	1.002	1.005		1.010	1.012	1.014	1.015	1.016	1.018	1.018	1.019	1.019	1.020	1.020	1.019	1.019	1.019	1.018	1.017	1.016	1.015	1.014
10	0.996	1.000	1.003	1.007	1.009	1.012		1.016	1.018	1.019	1.021	1.022	1.022	1.023	1.023	1.023	1.023	1.023	1.023	1.022	1.021	1.021	1.020	1.019	1.017
15	1.001	1.005	1.008	1.011	1.014	1.016	1.019		1.022	1.023	1.025	1.025	1.026	1.027	1.027	1.027	1.027	1.026	1.026	1.025	1.025	1.024	1.023	1.022	1.021
20	1.006	1.009	1.013	1.016	1.018	1.021	1.023	1.024		1.027	1.028	1.029	1.030	1.030	1.030	1.030	1.030	1.030	1.029	1.029	1.028	1.027	1.026	1.025	1.024
25	1.010	1.014	1.017	1.020	1.022	1.025	1.027	1.028	1.030		1.032	1.033	1.033	1.034	1.034	1.034	1.033	1.033	1.033	1.032	1.031	1.030	1.029	1.028	1.027
30	1.015	1.018	1.021	1.024	1.026	1.029	1.031	1.032	1.034	1.035		1.036	1.037	1.037	1.037	1.037	1.037	1.036	1.036	1.035	1.034	1.033	1.032	1.031	1.030
35	1.019	1.022	1.025	1.028	1.030	1.032	1.034	1.036	1.037	1.038	1.039		1.040	1.040	1.040	1.040	1.040	1.039	1.039	1.038	1.037	1.036	1.035	1.034	1.032
40	1.023	1.026	1.029	1.032	1.034	1.036	1.038	1.039	1.041	1.042	1.042	1.043		1.043	1.043	1.043	1.043	1.042	1.042	1.041	1.040	1.039	1.038	1.037	1.035
45	1.027	1.030	1.033	1.035	1.038	1.040	1.041	1.043	1.044	1.045	1.046	1.046	1.046		1.046	1.046	1.046	1.045	1.044	1.044	1.043	1.042	1.041	1.039	1.038
50	1.031	1.034	1.037	1.039	1.041	1.043	1.045	1.046	1.047	1.048	1.049	1.049	1.049	1.049		1.049	1.049	1.048	1.047	1.046	1.045	1.044	1.043	1.042	1.041
55	1.035	1.038	1.040	1.043	1.045	1.046	1.048	1.049	1.050	1.051	1.052	1.052	1.052	1.052	1.052		1.051	1.051	1.050	1.049	1.048	1.047	1.046	1.045	1.043
60	1.038	1.041	1.044	1.046	1.048	1.050	1.051	1.052	1.053	1.054	1.055	1.055	1.055	1.055	1.055	1.055		1.054	1.053	1.052	1.051	1.050	1.049	1.047	1.046
65	1.042	1.045	1.047	1.049	1.051	1.053	1.054	1.056	1.056	1.057	1.058	1.058	1.058	1.058	1.058	1.057	1.057		1.056	1.055	1.054	1.053	1.051	1.050	1.049
70	1.045	1.048	1.050	1.053	1.054	1.056	1.057	1.059	1.059	1.060	1.061	1.061	1.061	1.061	1.061	1.060	1.060	1.059		1.057	1.056	1.055	1.054	1.053	1.052
75	1.049	1.051	1.054	1.056	1.058	1.059	1.061	1.062	1.062	1.063	1.064	1.064	1.064	1.064	1.063	1.063	1.062	1.062	1.061		1.059	1.058	1.057	1.056	1.054
80	1.052	1.055	1.057	1.059	1.061	1.062	1.064	1.065	1.065	1.066	1.066	1.067	1.067	1.066	1.066	1.066	1.065	1.064	1.064	1.063		1.061	1.060	1.058	1.057
85	1.055	1.058	1.060	1.062	1.064	1.065	1.067	1.068	1.068	1.069	1.069	1.069	1.069	1.069	1.069	1.069	1.068	1.067	1.066	1.066	1.065		1.062	1.061	1.060
90	1.059	1.061	1.063	1.065	1.067	1.068	1.070	1.070	1.071	1.072	1.072	1.072	1.072	1.072	1.072	1.071	1.071	1.070	1.069	1.068	1.067	1.066		1.064	1.063
95	1.062	1.064	1.066	1.068	1.070	1.071	1.072	1.073	1.074	1.075	1.075	1.075	1.075	1.075	1.075	1.074	1.073	1.073	1.072	1.071	1.070	1.069	1.068		1.066
100	1.065	1.068	1.070	1.071	1.073	1.074	1.075	1.076	1.077	1.078	1.078	1.078	1.078	1.078	1.077	1.077	1.076	1.076	1.075	1.074	1.073	1.072	1.071	1.070	

Appendix 32: Heat coefficient k of Antifrogen N 40 %, measured in feed [kWh/(m³K)]

k Feed	Return temperature																								
Feed temperature	-20	-15	-10	-5	0	5	10	15	20	25	30	35	40	45	50	55	60	65	70	75	80	85	90	95	100
-20		0.968	0.974	0.980	0.986	0.991	0.996	1.001	1.006	1.010	1.015	1.019	1.023	1.027	1.031	1.035	1.038	1.042	1.045	1.049	1.052	1.055	1.059	1.062	1.065
-15	0.966		0.979	0.984	0.990	0.995	1.000	1.005	1.009	1.014	1.018	1.022	1.026	1.030	1.034	1.038	1.041	1.045	1.048	1.051	1.055	1.058	1.061	1.064	1.068
-10	0.971	0.977		0.988	0.993	0.998	1.003	1.008	1.013	1.017	1.021	1.025	1.029	1.033	1.037	1.040	1.044	1.047	1.050	1.054	1.057	1.060	1.063	1.066	1.070
-5	0.975	0.980	0.986		0.997	1.002	1.007	1.011	1.016	1.020	1.024	1.028	1.032	1.035	1.039	1.043	1.046	1.049	1.053	1.056	1.059	1.062	1.065	1.068	1.071
0	0.978	0.984	0.989	0.995		1.005	1.009	1.014	1.018	1.022	1.026	1.030	1.034	1.038	1.041	1.045	1.048	1.051	1.054	1.058	1.061	1.064	1.067	1.070	1.073
5	0.981	0.987	0.992	0.998	1.003		1.012	1.016	1.021	1.025	1.029	1.032	1.036	1.040	1.043	1.046	1.050	1.053	1.056	1.059	1.062	1.065	1.068	1.071	1.074
10	0.984	0.990	0.995	1.000	1.005	1.010		1.019	1.023	1.027	1.031	1.034	1.038	1.041	1.045	1.048	1.051	1.054	1.057	1.061	1.064	1.067	1.070	1.072	1.075
15	0.987	0.992	0.998	1.003	1.007	1.012	1.016		1.024	1.028	1.032	1.036	1.039	1.043	1.046	1.049	1.052	1.056	1.059	1.062	1.065	1.068	1.070	1.073	1.076
20	0.989	0.995	1.000	1.005	1.009	1.014	1.018	1.022		1.030	1.034	1.037	1.041	1.044	1.047	1.050	1.053	1.056	1.059	1.062	1.065	1.068	1.071	1.074	1.077
25	0.991	0.997	1.002	1.006	1.011	1.015	1.019	1.023	1.027		1.035	1.038	1.042	1.045	1.048	1.051	1.054	1.057	1.060	1.063	1.066	1.069	1.072	1.075	1.078
30	0.993	0.998	1.003	1.008	1.012	1.016	1.021	1.025	1.028	1.032		1.039	1.042	1.046	1.049	1.052	1.055	1.058	1.061	1.064	1.066	1.069	1.072	1.075	1.078
35	0.995	1.000	1.004	1.009	1.013	1.018	1.022	1.025	1.029	1.033	1.036		1.043	1.046	1.049	1.052	1.055	1.058	1.061	1.064	1.067	1.069	1.072	1.075	1.078
40	0.996	1.001	1.005	1.010	1.014	1.018	1.022	1.026	1.030	1.033	1.037	1.040		1.046	1.049	1.052	1.055	1.058	1.061	1.064	1.067	1.069	1.072	1.075	1.078
45	0.997	1.002	1.006	1.011	1.015	1.019	1.023	1.027	1.030	1.034	1.037	1.040	1.043		1.049	1.052	1.055	1.058	1.061	1.064	1.066	1.069	1.072	1.075	1.078
50	0.998	1.002	1.007	1.011	1.015	1.019	1.023	1.027	1.030	1.034	1.037	1.040	1.043	1.046		1.052	1.055	1.058	1.061	1.063	1.066	1.069	1.072	1.075	1.077
55	0.998	1.003	1.007	1.012	1.016	1.020	1.023	1.027	1.030	1.034	1.037	1.040	1.043	1.046	1.049		1.055	1.057	1.060	1.063	1.066	1.069	1.071	1.074	1.077
60	0.999	1.003	1.008	1.012	1.016	1.020	1.023	1.027	1.030	1.033	1.037	1.040	1.043	1.046	1.049	1.051		1.057	1.060	1.062	1.065	1.068	1.071	1.073	1.076
65	0.999	1.003	1.008	1.012	1.016	1.019	1.023	1.026	1.030	1.033	1.036	1.039	1.042	1.045	1.048	1.051	1.054		1.059	1.062	1.064	1.067	1.070	1.073	1.076
70	0.999	1.003	1.008	1.012	1.015	1.019	1.023	1.026	1.029	1.033	1.036	1.039	1.042	1.044	1.047	1.050	1.053	1.056		1.061	1.064	1.066	1.069	1.072	1.075
75	0.999	1.003	1.007	1.011	1.015	1.019	1.022	1.025	1.029	1.032	1.035	1.038	1.041	1.044	1.046	1.049	1.052	1.055	1.057		1.063	1.066	1.068	1.071	1.074
80	0.999	1.003	1.007	1.011	1.014	1.018	1.021	1.025	1.028	1.031	1.034	1.037	1.040	1.043	1.045	1.048	1.051	1.054	1.056	1.059		1.065	1.067	1.070	1.073
85	0.998	1.002	1.006	1.010	1.014	1.017	1.021	1.024	1.027	1.030	1.033	1.036	1.039	1.042	1.044	1.047	1.050	1.053	1.055	1.058	1.061		1.066	1.069	1.072
90	0.997	1.002	1.005	1.009	1.013	1.016	1.020	1.023	1.026	1.029	1.032	1.035	1.038	1.041	1.043	1.046	1.049	1.051	1.054	1.057	1.060	1.062		1.068	1.071
95	0.997	1.001	1.005	1.008	1.012	1.015	1.019	1.022	1.025	1.028	1.031	1.034	1.037	1.039	1.042	1.045	1.047	1.050	1.053	1.056	1.058	1.061	1.064		1.070
100	0.996	1.000	1.004	1.007	1.011	1.014	1.017	1.021	1.024	1.027	1.030	1.032	1.035	1.038	1.041	1.043	1.046	1.049	1.052	1.054	1.057	1.060	1.063	1.066	

A2 - Degradation

Appendix 33: Polynomial coefficients of degraded fluid's specific fluid properties

Größe	Function	const.	Tyfocor LS degr.	Antifrogen Sol HT degr.	Tyfocor L 40 degr.	Antifrogen N 40 degr.
cp	$c_p(T)=cpO+c1T+ c2T^2 c3T^3$	cp0	3.5454558	3.2861384	3.6198091	3.3959497
		c1	0.0072873	0.0066067	0.0065895	0.0059021
		c2	-6.74E-05	-4.13E-05	-6.49E-05	-3.23E-05
		c3	3.235E-07	1.566E-07	3.168E-07	1.08E-07
ρ	$\rho(T)= \rho0+b1T+ b2T^2+ b3T^3 +b4T4 +b5T5$	ρ0	1045.1808	1096.3702	1049.8448	1064.4367
		b1	-0.513374	-0.605165	-0.470644	-0.427334
		b2	-0.001698	-0.00103	-0.002074	-0.001916
		b3	-5.4E-06	-3.53E-06	-1.55E-06	-1.41E-06
		b4	7.339E-08	2.425E-08	5.518E-08	3.207E-08
		b5	-2.95E-10	-7.26E-11	-2.99E-10	-1.37E-10
dyn. Visc	n= A exp[B/(t+C)]	A	0.0330434	0.040417	0.0369089	0.0327368
		B	614.07015	702.77534	58276275	652.70429
		C	101.08904	110.92551	100.9032	123.3005
c	$c(T)=cO+c1T+ c2T^2$	c0	n.d.	n.d.	n.d.	n.d.
		c1	n.d.	n.d.	n.d.	n.d.
		c2	n.d.	n.d.	n.d.	n.d.